1-22-2018

Modulation of the Hedgehog Signaling Pathway by Sterol-based Small Molecules

Chad Maschinot
University of Connecticut - Storrs, chad.maschinot@uconn.edu

Modulation of the Hedgehog Signaling Pathway by Sterol-based Small Molecules

Chad Anthony Maschinot, PhD

University of Connecticut, 2018

The Hedgehog (Hh) pathway is a development pathway with therapeutic potential as a target for treatment of cancers and degenerative disorders. Multiple agonists of Hh signaling have been investigated to treat degenerative disorders, oxysterols (OHCs) have been the most well studied. Previous studies have shown OHCs to bind directly to the cysteine-rich domain of Smoothened in a regio- and stereoselective manner. A series of OHC analogues were synthesized with modifications at the C-20 position to further study binding. Combined with modeling studies, inverting the C-20 stereochemistry was determined to switch the activity of the analogues from agonist to antagonists. Additional studies suggested that inversion rigidified the alkyl side chain to increase interactions leading to the activity change. Among the scaffolds under investigation as anti-cancer chemotherapeutics and antagonists of Hh signaling is vitamin D3 (VD3). Previous structure-activity relationship studies contained both modified A- and *seco*-B ring motifs, and provided potent and selective analogues for Hh signaling. To continue studies on this scaffold, new series of compounds were synthesized to explore additional interactions and spatial constraints. While continuing to evaluate the usefulness of amine-based *seco*-B ring motifs, these compounds incorporate functional groups of varying size and hydrophobicity at the C-11 position of the C-ring as well as hydroxylations at the C-25 position of the alkyl side chain. While large hydrophobic moieties at the C-11 position resulted in significant loss of Hh inhibition, smaller or more flexible moieties maintained anti-Hh activity. Hydroxylation at the C-25 position significantly increased VDR activation while also increasing anti-Hh potency for most analogues. Masking the hydroxyl group as a methyl ether could regain selectivity for Hh signaling with minor losses in anti-Hh activity. Mechanism of action studies have been contradictory, but suggest the vitamin D receptor (VDR) plays a role in inhibiting Hh signaling. These results call for additional and continued studies to identify the binding target and pocket to better understand these structure-activity relationships.

Modulation of the Hedgehog Signaling Pathway by Sterol-based Small Molecules

Chad Anthony Maschinot

B.S., Northern Kentucky University, **2013**

A Dissertation

Submitted in Partial Fulfillment of the

Requirements for the Degree of

Doctor of Philosophy

at the

University of Connecticut

2018

APPROVAL PAGE

Doctor of Philosophy Dissertation

Modulation of the Hedgehog Signaling Pathway by Sterol-based Small Molecules

Presented by

Chad Anthony Maschinot, B.S.

Major Advisor _____
M. Kyle Hadden

Associate Advisor _____
Andrew Wiemer

Associate Advisor _____
Brian Aneskievich

Associate Advisor _____
Dennis Wright

Associate Advisor _____
Mark Peczuh

University of Connecticut
2018

TABLE OF CONTENTS

Doctor of Philosophy Dissertation

Modulation of the Hedgehog Signaling Pathway by Sterol-based Small Molecules

TABLE OF CONTENTS

Doctor of Philosophy Dissertation

Modulation of the Hedgehog Signaling Pathway by Sterol-based Small Molecules

Modulation of the Hedgehog Signaling Pathway by Sterol-based Small Molecules

Chad Anthony Maschinot

Chapter 1:

The Therapeutic Potential of Hedgehog Signaling

Introduction

The Hedgehog (Hh) signaling pathway plays a crucial role in the embryonic development of many tissues and organs. In adult tissues, the pathway is significantly less active with the primary function of maintaining homeostasis of stem cell populations, primarily in the skin and central nervous system.[1] Abnormal regulation of the pathway, specifically constitutive activation, through mutations or irregular expression, has been linked to a variety of cancers, most notably basal cell carcinoma (BCC) and medulloblastoma (MB). Additionally, Hh signaling has been linked to a number of conditions from obesity to neurodegenerative disorders.

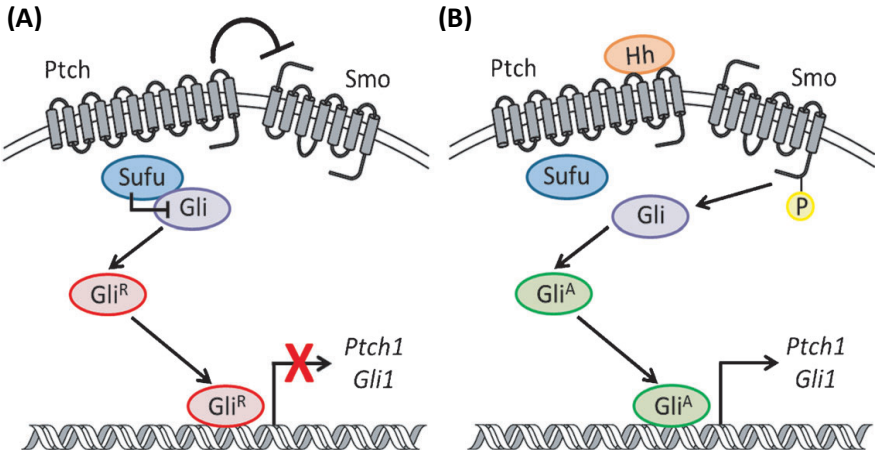

Figure 1. Simplified representation of the Hedgehog signaling pathway in (A) inactive and (B) active states.[2]

I. Canonical Hedgehog Signaling (Figure 1)

The Hh pathway is primarily regulated by the glioma-associated oncogene (Gli) family of zinc-finger transcription factors (Gli1-3) along with two trans-membrane receptor proteins: Patched (Ptch), a 12 trans-membrane (TM) domain surface receptor, and Smoothened (Smo), a 7TM membrane GPCR-like receptor. In mammalian cells, canonical signaling is initiated by binding of one of the Hh ligands – Desert (DHh), Indian (IHh) and Sonic (SHh) – to Ptch.

Before binding occurs, immature Hh proteins undergo multiple post-transcriptional modifications to regulate activity and Hh protein dispersion. The immature proteins first undergo autoproteolytic cleavage

allowing for covalent addition of a cholesterol moiety to the N-terminal peptide. Additionally, a palmitic acid moiety is attached to the most N-terminal cysteine residue solubilizing the protein and aiding in its translocalization and attachment to the cell membrane.[3] The mature proteins are secreted as a monomer by the transmembrane protein Dispatched (Disp) and the secreted glycoprotein, Scube2.

Following secretion, Hh ligands spread to target cells. In the absence of these ligands, Ptch is localized near and on the primary cilia. This suppresses Hh signaling by inhibiting downstream Smo activity through a poorly understood mechanism. A major downstream regulator of Hh signaling is the tumor suppressor protein, Suppressor of Fused (SuFu). The primary function of SuFu is the sequestering of Gli proteins in the cytoplasm to prevent their translocation to the nucleus.[4] Inhibition of Smo prevents the dissociation and accumulation of this Gli-SuFu complex in the primary cilium. Accumulation allows for hyper-phosphorylation of Gli to occur by protein kinase A (PKA), casein kinase 1α (CK1α) and glycogen synthase kinase 3β (GSK3β). Phosphorylated Gli then undergoes site specific ubiquitination resulting in partial proteasomal degradation of Gli to form repressor Gli (Gli_R). The proteasome removes the C-terminus allowing the N-terminal and DNA binding domain to translocate to the nucleus and repress transcription.[3]

Binding of Hh ligands to Ptch activates the signaling cascade. Upon binding, Ptch and the Hh ligand are internalized and degraded. Removal of Ptch from the primary cilium allows Smo to localize at the primary cilia, a critical component of Hh signaling.[5] Smo is then phosphorylated by CK1 and G-protein coupled receptor kinase 2 (GRK2) to form the active conformation.[6] Kinase protein Kif7, another major downstream component, moves to the tip of the primary cilium following pathway activation. Kif7 is then able to increase the trafficking of SuFu and Gli proteins to the cilium for the cascade to continue.[7] Additionally, Kif7 has been proposed to control cilium architecture and length, ensuring proper formation of functional primary cilium required for Hh signaling.[8] The increased accumulation of Hh components promotes the dissociation of SuFu and Gli resulting in full length Gli, or activated Gli (Gli_A). This dissociation allows for Gli_A to translocate to the nucleus and activate the transcription of Hh target genes, such as: *Ptch1*, *Gli1*, and *Gli2*.

II. Hh Signaling and Cancer

As previously mentioned, Hh signaling is primarily inactive in adults; however, mutations within the pathway may arise over time leading to dysregulation and constitutive activation. This dysregulation can ultimately lead to the development of cancers, most notably basal cell carcinoma (BCC) and medulloblastoma (MB).

In 1996, a link between cancer and Hh signaling was discovered where a familial loss-of-function mutation in *Ptch1* was responsible for the development of Gorlin's syndrome (nevoid BCC syndrome).[9] Gorlin's syndrome is an autosomal dominant disease characterized by predisposition to BCCs, medulloblastomas and ovarian fibromas.[10] Similarly, the most common human cancer, sporadic BCC, is driven by aberrant regulation of Hh signaling. This aberrant regulation is associated with UV exposure and a high frequency of loss of Ptch function. In total, 85% of BCC cases showed Hh pathway mutations. These mutations included inactivating *Ptch1* (75%) and *SuFu* (8%) mutations, and activating mutations in *Smo* (~20%).[11]

Another connection between Hh signaling and cancer has been described with MB where approximately 30% of cases can be characterized by activating mutations of Hh signaling.[12] Constitutive activation in granule neuron progenitors in the developing cerebellum leads to proliferation beyond the normal development period and the formation of MB.[13-14] Mutations of Hh components in MB can be broken down into ~45% *Ptch1*, ~14% *Smo* and ~14% *SuFu*. Interestingly, these mutations are attributed to disease progression at different stages with *Smo* mutations highly enriched in adults, and the majority of *SuFu* mutations found in infants (0 - 3 years old).[15-16]

Additionally, neuroblastoma (NB) has received attention as another form of cancer where Hh signaling plays an important role in disease progression. Neuroblastoma, like medulloblastoma, is a common pediatric cancer of the nervous system, specifically the sympathetic nervous system. In 2009, it was shown that Hh signaling maintained tumorigenicity of neuroblastoma cells.[17] In those studies, inhibition of Hh signaling by cyclopamine, a known natural product Smo inhibitor, resulted in apoptosis and cell cycle arrest in multiple NB cell lines. An additional study utilized a Gli1 inhibitor, to target downstream of Smo. In this

study, treatment of NB cell lines with the inhibitor resulted in down-regulation of *Gli1*, as well as *c-MYC* and *MYCN,* and induced apoptosis.[18]

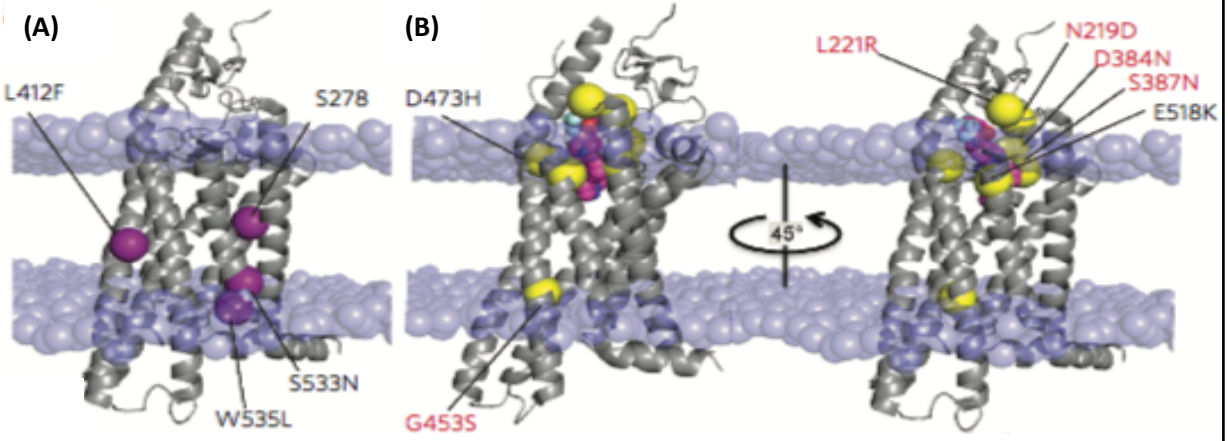

Figure 2. Mutations in Smo found in cancer.[12] (A) Mutations in the TM region thought to be oncogenic. (B) Mutations in the TM region associated with resistance to small-molecule Smo inhibitors GDC-0449 (**2,** black residues) and LDE225 (**3**, red residues). Reprinted by permission from Macmillan Publishers Ltd: Sharpe, H. J.; et al. *Nat. Chem. Biol.* **2015**, *11*, 246-255.

To date, multiple specific Smo mutations have been identified through genomic analysis of Hh-driven cancers.[12] These mutations were further characterized as oncogenic or resistance conferring (**Figure 2**, 2a and 2b respectively). The majority of these mutations are located within the TM region of Smo with the exception of a single mutation in the cytostolic tail, R562Q. The most studied oncogenic mutations, W535L, is located at at the end of the 7th TM-helix and thought to alter contacts with the extracellular loops to confer constitutive activation of Hh signaling.[12] Among the resistance driven mutations, D473H was identified in a biopsy from a relapsed MB patient, and remains the major functional characterized resistance mechanism.[12, 19-20] Under normal conditions, the Asp473 residue participates in the formation of a water network while also interacting directly with small molecules. Interestingly, it was shown that D473H mutant Smo was still susceptible to Ptch inhibition indicating it is a non-oncogenic mutation.[19] Follow-up studies revealed that any mutation of Asp473 conferred resistance and changing Asp473 to a basic residue resulted in constitutive activation.[20]

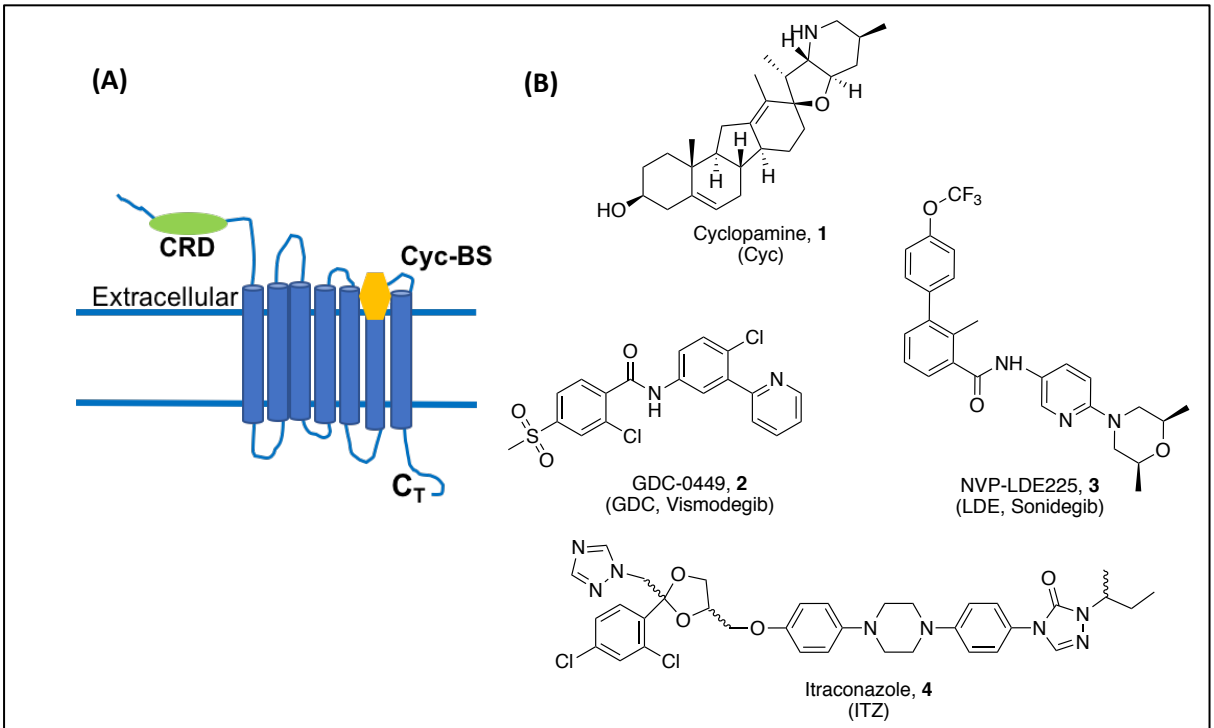

Figure 3. (A) 2D representation of Smo with key domains targeted by small molecules indicated, Green = Cysteine rich domain (CRD) and Yellow = Cyclopamine binding site (Cyc-BS); (B) Representative small molecule Smo inhibitors.

III. Small Molecule Antagonists of Hh Signaling

A. Smoothened (Traditional) Inhibitors

With the vast majority of Hh activating mutations observed in cancers being *Ptch* inactivating, or loss-of-function, mutations, much of small molecule development has focused on targeting the downstream component, Smo (**Figure 3**). The first small molecule inhibitor of Smo discovered was the naturally occurring alkaloid, cyclopamine (Cyc, **1**), that inhibited Hh signaling by direct binding to Smo. Even though Cyc has a poor pharmacokinetic profile, it has been utilized to further explore Hh pathway function and more specifically, the importance of Smo in tumor growth and progression.[21-22] These studies also supported the potential for small molecule modulation of Hh signaling as anticancer chemotherapeutics. In recent years, two Smo inhibitors have received approval from the Food and Drug Administration (FDA): GDC-0449 (Vismodegib, **2**) and NVP-LDE225 (Sonidegib, **3**).

Genentech first reported GDC-0449 as a potent inhibitor of Hh signaling in 2009, and it received FDA approval for the treatment of advanced BCC in 2012.[23-24] Unfortunately, the point mutation previously mentioned, D473H, developed and decreased GDC-0449's binding affinity by 100-fold.[19-20] Since then, additional point mutations have been identified that reduce the binding affinity in the TM region. This observation highlights a need for further therapeutic development capable of inhibiting wild-type and mutant Smo. In 2010, Novartis Institute of Biomedical Research first reported NVP-LDE225, a biphenyl carboxamide. LDE225 quickly became a clinical candidate due to its selectivity, potency against Smo, and ability to penetrate the blood brain barrier.[25] In 2015, LDE225 became the second Hh inhibitor to receive FDA approval specifically for locally advanced BCC. Unfortunately, several point mutations in conserved Smo residues have been identified in mouse models of MB that confer resistance.[12]

Multiple other small molecules are currently undergoing preclinical and clinical development.[1, 21] Among those small molecules, itraconazole (ITZ, **4**) has emerged as a potent lead candidate following high-throughput screening (HTS) of over 2,000 approved FDA and phase 1 compounds for anti-Hh activity.[26] As a commonly used antifungal agent, ITZ has been studied for many years and has a well-known safety profile making it a promising drug candidate. Perhaps more importantly, ITZ was shown to inhibit wild type and mutant D473H Smo by direct binding to Smo in a distinct manner from cyclopamine and other Smo antagonists.[21]

Additional small molecule Smo inhibitors (**Figure 4**) currently in clinical trials include compounds from Lilly (LY2940680, taladegib, **5**), Pfizer (PF-04449913, glasdegib, **6**), and Bristol-Myer Squibb (BMS-

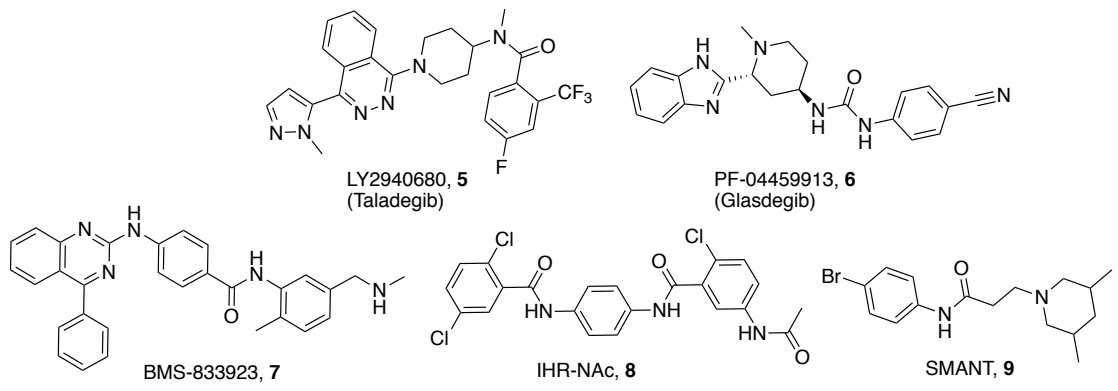

Figure 4. Additional Smo inhibitors in clinical and pre-clinical development.

833923, **5**).[21] Multiple other novel scaffolds are under development that directly displace BODIPY-Cyc, such as IHR-NAc(**8**), as well as inhibitors of Smo translocation/accumulation in the primary cilium, such as SMANT (**9**).[21]

B. Non-traditional Inhibitors

Multiple components of Hh signaling have been shown to be major contributors or critical for proper pathway function. These components include: (1) upstream components, such as Ptch and Kif7, (2) the TM-protein Smo, and (3) downstream components, such as Gli and PKA.[16] Approaches have been taken to target components upstream of Smo,[1] but the emergence of Smo mutations and resistance to Smo inhibitors has led to a focus of targeting downstream components (**Figure 5**). The advantage to this approach is not only bypassing the level of resistance but the ability to regulate signaling via agonists or antagonists exists. An additional advantage to these targets is to bypass SuFu mutations that have been observed. The major focus to date has been to target the Gli transcription factors, or the final-step of the signaling cascade.

In 2007, the first Gli inhibitors, including GANT61 (**10**), were discovered during a screening assay reported at the Karolinska Institutet in Huddinge, Sweden.[27] Importantly, GANT61 was able to reduce both Gli1 and Hip1 mRNA in SuFu$^{-/-}$ cells whereas traditional Smo inhibitors could not. Characterization of GANT61's mechanism of action in HEK293 cells revealed accumulation of transfected Gli suggesting

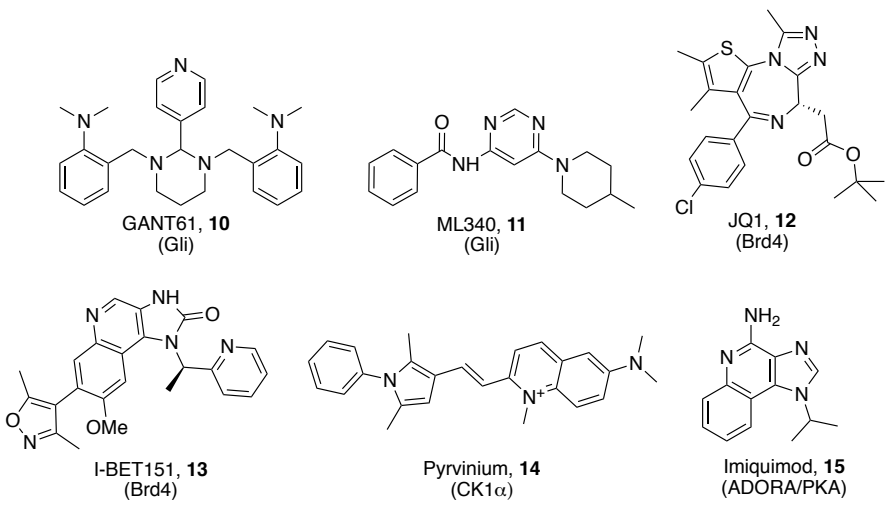

Figure 5. Hh inhibitors acting downstream of Smo.

inhibition of nuclear Gli, confirmed by electrophoretic mobility shift assays where pretreatment with GANT61 reduced the Gli-DNA binding band.[27] As the first reported Gli inhibitor, GANT61 has been extensively studied and shown to induce growth arrest leading to cell death,[28] and evaluated outside of traditional Hh-dependent cancers.[29]

Following these reports, the Sanford-Burnham Center for Chemical Genomics at Sanford-Burnham Medical Research Institute in collaboration with Stanford University reported another Gli specific inhibitor, ML340 (**11**) in 2012.[30] ML-340 provided a novel scaffold for Gli inhibitor development with promising characteristics, such as potency, reduced non-specific cytotoxic, high permeability and selectivity. However, ML-340 showed high plasma protein binding of ~99% in both mice and humans. Overall, ML340 could be useful as a selective probe to target downstream of Smo, but additional medicinal chemistry efforts are required to improve the preclinical pharmacokinetic properties.

In a similar approach to the inhibition of Hh signaling at the transcriptional level by Gli inhibitors, researchers at Stanford University School of Medicine showed that Hh signaling was modulated by a specific bromodomain protein, BRD4, that regulated *Gli* transcription downstream of Smo and SuFu by occupying the *Gli1* and *Gli2* promoters.[31] Additionally, shRNA knockdown of Brd4 resulted in decreased Gli1 and Gli2 mRNA levels that could be successfully rescued by the addition of full length Gli. Similarly, treatment of both wild type and *SuFu*$^{-/-}$ mouse embryonic fibroblast (MEF) cells with a known small molecule inhibitor of Brd4 (JQ1, **12**) could reduce Gli1 and Gli2 expression.[31] Inhibition of Brd4 also showed promise in combating Smo-inhibitor resistant tumors in cellular and mouse models.

A cell-based screening effort at the University of Miami for epigenetic modulators of Hh signaling identified I-BET151 (**13**), an inhibitor of several bromodomain containing proteins (BRD2-4).[32] Similar to JQ1, I-BET151 maintained potent inhibition in SuFu$^{-/-}$ MEFs and decreased the occupancy of BRD4 at the *Gli1* transcriptional start site. Additional, I-BET151 was able to reduce both tumor volume and tumor associated Gli1 expression in *in vivo* models of Hh-dependent MB.[32]

Additional strategies to target Hh activity exist by activating negative regulators downstream of Smo, such as CK1α or adenosine receptor/protein kinase A (ADORA/PKA). As previously mentioned, CK1α

Table 1. Anti-Hh activity of small-molecules targeting Hh components.

Compound	Target	IC_{50} Wild-type Smo	IC_{50} D473H Smo	Status	Reference
GDC-0449	Smo	3-22 nM	Loss of activity	Clinically approved	22
NVP-LDE225	Smo	2.5 nM	Loss of activity	Clinically approved	25
Itraconazole	Smo	270-690 nM	500 nM	Phase 1	26
GANT61	Gli	5 μM	ND	Preclinical	27
ML340	Gli	34 nM	ND	Preclinical	30
JQ1	Brd4	50 – 150 nM	Active[a]	Preclinical	31
I-BET151	Brd4	31 nM	ND	Preclinical	32
Pyrvinium	CK1α	~10 nM	Active[a]	Preclinical	33
Imiquimod	ADORA	Actvie[a]	ND	Preclinical	38

[a]Active = Specific IC_{50} value not reported. ND = No data reported.

and PKA serve as negative regulators of Hh signaling by phosphorylating and destabilizing Gli proteins. This destabilization leads to their proteasomal degradation and Hh antagonism. Therefore, activation of these negative regulators increases Gli phosphorylation to inhibit Hh signaling. Recently, an anti-pinworm compound, pyrvinium (**14**), was identified as a potent allosteric agonist of CK1α and subsequently evaluated for anti-Hh activity.[33-35] Pyrvinium could attenutate Hh activity in Hh-dependent MEFs and maintained activity in *SuFu*$^{-/-}$ cells, indicating the ability to inhibit downstream of Smo and SuFu.[33] Mechanistic studies indicated that inhibition was dependent on CK1α and direct interactions between Gli1 and CK1α promoted proteasomal degradation of Gli1. Furthermore, pyrvinium maintained anti-Hh activity in the presence of D473H mutant Smo.

Previous studies in *Drosophila* suggested that the nucleoside adenosine and its receptors (ADORAs) may serve as negative regulators of Hh signaling by promoting the proteolytic cleavage of Gli to Gli^R.[36] Imquimod (IMQ, **15**) is an adenosine analogue developed by Medicis Pharmaceuticals approved by the FDA for the topical treatment of a variety of skin disorders, including superficial BCC.[21] Multiple mechanisms have been implicated as mediators of the biological activity of IMQ, including toll-like receptors (TLR7 and TLR8) and several ADORAs.[37] Based on connections between its use as a treatment option for BCC and its ability to modulate ADORAs, researchers at the University of Salzburg evaluated its ability to regulate Hh signaling.[38] At higher concentration (42 μM), IMQ decreased Gli1 protein levels in Hh-dependent murine BCC cells. Additional studies indicated that the anti-Hh activity was a result of

PKA phosphorylation of Gli enhancing the proteolytic process to Gli^R, mediated through ADORA activation.[38]

To date, the Hh signaling pathway has been implicated as an anti-cancer target for a variety of human cancers, but recent evidence has shown that only BCC and MB are truly dependent on Hh signaling for oncogenic transformation and tumor growth. These findings have greatly reduced the therapeutic scope of Hh pathway inhibitors. Pathway inhibitors still have the potential to treat a large number of people with BCC being the most common human cancer and no targeted therapy existing for MB. The FDA approval of GDC-0449 (**2**) and LDE225 (**3**) and additional success in clinical and preclinical settings confirmed the validity of Smo, and Hh signaling, as a drug target. Taken together with the rise of resistance to GDC-0449 (**2**) and other Smo antagonists, the development of Hh pathway inhibitors targeting Smo and downstream components continues in both academic and industry settings. As the complexity of Hh signaling continues to grow and come into view, reports of enzymes and receptors indirectly regulating Gli expression have emerged as potential targets. The complexity of Hh signaling and the promise of Hh inhibitors ensures that development of small molecule Hh inhibitors will continue for the purpose of anti-cancer agents and chemical probes to further study the Hh pathway and indirect regulation of signaling.

IV. Hh Signaling and Degenerative Disorders

As previously mentioned, the evolutionarily conserved Hh pathway is one of the major pathways involved during embryonic development. Disruption of Hh signaling has been shown to be an underlying contributor to a variety of developmental disorders such as holoprosencephaly and limb abnormalities.[16] Holoprosencephaly is characterized by failure of the embryonic forebrain to sufficiently divide in the two lobes of the cerebral hemisphere. Additionally, specific Hh proteins are expressed throughout embryonic development controlling everything from hair follicle and eye development to bone growth and smooth muscle patterning.[39] With this in mind, Hh agonism has been studied for therapeutic potential in a variety of disease states. To date, the therapeutic areas that have been studied the most are neuro- and osteodegenerative diseases. Signaling in these tissues appears to be primarily regulated by specific Hh

protein isoforms with IHh in cartilage and bone, DHh in the peripheral nervous system (PNS) and SHh in a variety of cell types.[2, 39-40]

A. Hh Signaling and Neurodegenerative Disorder

Overall, Hh proteins act as morphogens, or agents that induce morphogenesis, by regulating the expression of families of transcription factors, such as the Gli family that Hh signaling targets, to ensure proper development and function. In the nervous system for example, DHh is secreted by Schwann cells, which are responsible for the formation of the myelin sheath around neuronal axons. Mice lacking DHh develop an abnormal nerve sheath, a leaky blood-nerve barrier, low action-potential conduction rates, and behavioral changes.[41] These results are suggested to be due to indirect mechanisms by which DHh regulates Hh signaling in perineurial cells leading to the secretion of neurotrophic, angiogenic, and growth factors that ensure proper development.[41-43]

To date, much of the therapeutic strategy for Hh pathway agonism is based on central nervous system (CNS) disorders, such as Parkinson's disease (PD). In the adult nervous system, Hh proteins and signaling components are present but the magnitude of signaling appears to be lower and more restricted.[44-45] It has also been shown that Hh signaling can be reactivated following tissue damage in adults. Reactivation in perineurial cells following sciatic nerve damage significantly increased Schwann cell production of SHh and DHh mRNA leading to increased Hh response.[39] Additionally, viral overexpression of SHh has been shown to stimulate neural stem cell proliferation in the hippocampus. Taken together, it has been suggested that activation or stimulation of Hh signaling may promote a functional neuroprotective and regenerative role in neurodegenerative diseases.

Parkinson's disease is a neurodegenerative disorder characterized by the loss of dopaminergic neurons in the substantia nigra, where it is known that SHh is involved in the differentiation of these neurons during embryonic development.[46] Most animal models of Parkinson's Disease are generated using 6-hydroxydopamine (6-OHDA), which is taken up by dopaminergic neurons resulting in decreased dopaminergic innervation and loss of function in the substantia nigra.[39] In multiple animal models using

this method, direct administration of SHh resulted in improved motor function and protected against drug-induced neurotoxicity.[47] Transplantation of SHh-secreting neural progenitor cells into 6-OHDA rat models was shown to improve motor function and behavior,[48] providing further evidence that Hh stimulation can be neuroprotective.

B. Hh signaling and Osteodegenerative Disorders

The other major area of study for therapeutic activation of Hh signaling is osteodegenerative disorders, such as osteoporosis. Osteoporosis is characterized by a decline in bone mass beyond what is expected as a function of various factors, such as age and sex, and typically leads to reduced bone strength and higher probability of fractures.[48] Normal bone remodeling follows a time sequence (~6 months) where demineralized space is filled with new bone. During this process, activation of osteoclast precursors ultimately leads to the formation of new bone and mature osteoblasts fill the resorption cavity.[49]

IHh is expressed in the growth plate and osteoblasts in postnatal humans and rodents, and was shown to be involved in limb patterning, intramembranous ossification, and endochondral ossification.[50] In one study using adult mice,[51] it was determined that Hh signaling indirectly induced osteoclast maturation to promote bone resorption, where increased Hh activity in the mature osteoblasts upregulated parathyroid hormone-related peptide expression promoting RANKL expression. Additional studies have shown that *IHh* and *Ptch1* are upregulated during the initial stage of fracture repair,[52] and SHh is activated at the remodeling site of fractures to regulate osteoblasts and osteoclast formation.[53] Similarly, both *Ptch1*-deficient mice and osteoblast precursor cells showed increased bone mass and differentiation to osteoblasts at accelerated rates as a result of an enhanced response runt-related transcription factor 2 (Runx2) and decreased Gli^R.[54] Evidence also suggests that terminal osteoblastic cell fate is determined by canonical Wnt/b-catenin signaling induced by IHh signaling.[55]

Overall, activation of Hh signaling shows promise as a therapeutic strategy for osteodegenerative disorders; however, contradictory evidence has shown that prolonged pathway activation may lead to detrimental side effects, including an increased risk of osteoporosis. In one study, activation of Hh signaling

in mature osteoblasts of adult mice led to reduced bone density and fragile long bones.[50] This evidence adds to a role of Hh signaling in bone formation and regulation, but suggests that a fine balance would be required.

V. Small Molecule Agonists of Hh signaling

Development of small molecules targeting the Hh pathway has primarily focused on the development of antagonists as anti-cancer chemotherapeutics, but multiple scaffolds have been studied as Hh agonists. These scaffolds can be divided into two major classes: (1) non-sterol and (2) sterol-based compounds (**Figure 6**).

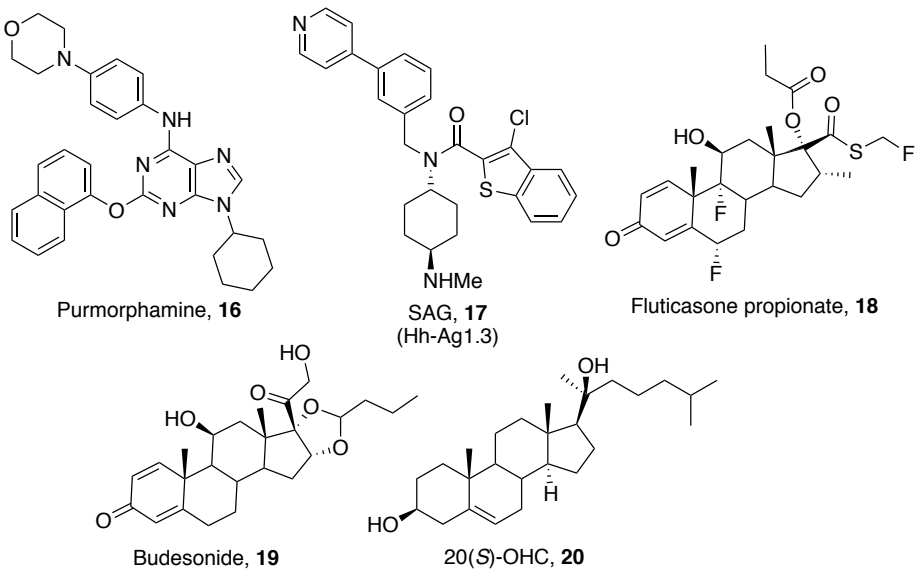

Figure 6. Small molecule modulators of Hh signaling; 16 – 17, 20 = agonists, 19 = antagonist.

A. Non-Sterol-Based Agonists

Purmorphamine (**16**), and tri-substituted purine derivatives, were discovered following an HTS assay to identify inducers of osteogenesis in C3H10T1/2 (C3H) MEFs, a cell line commonly used as a cellular model of osteoblast differentiation.[56] Additional studies indicated that purmorphamine's osteoinductive effects could be negated by administration of Cyc indicating its effects were a result of Hh activation.[57] Follow-up studies demonstrated that purmorphamine displaced BODIPY-Cyc showing that it directly

targeted Smo.[58] Multiple other studies have been performed to evaluate the therapeutic potential of purmorphamine. In one study, purmorphamine was part of a chemical system capable of promoting formation of forebrain GABA interneurons from induced pluripotent stem cells (iPSC).[59] Another study using iPSCs utilized purmorphamine as part of a four-step protocol to generate spinal motor neurons.[60] Taken together, these experiments demonstrated the therapeutic potential of small molecule Hh agonists for neurodegenerative disorders. More importantly, small molecule activation of Smo showed similar effects to external administration of Hh protein.

A second non-sterol series was discovered through an HTS assay in C3H cells stably expressing a luciferase reporter plasmid downstream of the *Gli1* promoter. This series is the biaryl benzothiophenes, such as SAG (**17**, Smoothened agonist).[61] These compounds were shown to potently activate Hh signaling following oral administration through direct binding to the transmembrane region of Smo, similar to Cyc.[19] Additional structure-activity relationship (SAR) studies have further increased the potency of this series to low nanomolar EC_{50} values.[62] The majority of therapeutic studies with this series have utilized SAG. These studies have shown promising results for neurodegenerative disorders as well as diabetes and obesity, where Hh signaling has been reported to block or inhibit the formation of fat, specifically white adipose tissue.[63] Treatment of C57BL/6J mice, which are susceptible to diet induced obesity and type-2 diabetes, with SAG stimulated insulin-dependent glucose uptake in muscle and brown adipose tissue preventing storage in white adipose tissue and fat formation.[64] Combination studies with retinoic acid in mouse embryonic stem cells induced differentiation of spinal progenitor cells and formation of functional motor neurons.[65]

Table 2. Representative Hh pathway agonists.

Compound	EC_{50} (μM)	Reference
Purmorphamine (**16**)	0.5	56
SAG (**17**)	0.01	61
Fluticasone propionate (**18**)	0.1	66
20(*S*)-OHC (**20**)	0.1	71

B. Sterol-Based Agonists

The majority of endogenous and synthetic Hh pathway agonists are sterol like small molecules. The first of these scaffolds are the glucocorticoids, including FDA approved glucocorticoids (GCs), such as

fluticasone propionate (**18**, Flonase). These compounds were initially identified as Hh pathway agonists using a U2OS cell model where overexpressing Smo resulted in β-arrestin2-GFP aggregation.[66] The GCs identified were able to upregulate Hh signaling at moderate levels by increasing the ciliary accumulation of Smo,[67] and were able to displace BODIPY-Cyc in a dose-dependent manner, although BODIPY-Cyc was not completely displaced (~20% displacement at 10 μM).[66] It is important to note that structurally related GCs, such as budesonide (**19**) inhibited Hh signaling at high concentration (IC_{50} of 40 μM) suggesting that this scaffold could provide both agonists and antagonists of Hh signaling.[67]

Perhaps the most well studied scaffold of Hh agonists are oxysterols (OHCs), or hydroxylated metabolites of cholesterol. Evidence first pointed to the importance of endogenous sterols for Hh signaling after the discovery that the covalent linking of a cholesterol moiety to the C-terminus of Hh proteins is essential for proper Hh signaling.[68] Adding to the importance of sterols, recent studies attempting to answer how Ptch endogenously regulates Smo activity suggested that Ptch influences intracellular cholesterol levels by contributing to cholesterol efflux.[69] Cholesterol itself has recently been proposed to be the natural ligand of Smo to activate downstream Hh signaling.[70] These two observations will be discussed in the following chapter.

Both natural and synthetic OHCs, such as 20(*S*)-OHC (**20**), have also been shown to activate Hh signaling via direct interactions with Smo.[71-73] In a study using M2-10B4 cells, pluripotent mesenchymal stem cells and osteogenic progenitor cells, OHCs demonstrated osteoinductive effects while also inhibiting adipogenic differentiation further demonstrating therapeutic potential for obesity and osteodegenerative disorders.[72, 74] The usefulness and potential of endogenous and synthetic OHCs as modulators of Hh signaling with be further discussed in the following chapter.

Summary

As one of the primary embryonic developmental pathways, the Hh signaling pathway has been linked to a variety of diseases and disorders from cancer to obesity. With cancers such as BCC and MB resulting

directly from constitutive activation of Hh signaling, much of small molecule development has focused on the development of inhibitors as anti-cancer chemotherapeutics. The complexity of Hh signaling provides multiple potential targets and mechanisms to regulate signaling. To date, the primary target investigated is the GPCR-like receptor Smo. Two small molecule inhibitors targeting Smo have received FDA approval, GDC-0449 (**2**) and LDE225 (**3**), for BCC treatment; however, resistance has emerged due to a specific point-mutation in Smo (D473H).[22-25] Additional Smo inhibitors are currently being investigated in clinical and preclinical settings that show activity against mutant Smo.[1,21] As another means to bypass mutant Smo, Hh components downstream of Smo are being investigated, such as Gli and Brd4. Compounds targeting downstream of Smo, such as **10** – **15**, have shown great potential so far and remain in preclinical development. Small molecule agonists of Hh signaling have also been developed and explored as means to treat a variety of diseases with the majority focusing on degenerative disorders, such as Parkinsons's disease and osteoporosis. Multiple scaffolds have emerged as potent agonists of Hh signaling, but the vast majority have been sterol-based small molecules such as glucocorticoids and oxysterols. These compounds have shown potent activation of Hh signaling and hold promise as preventative and post-treatment options for neurodegenerative and osteodegenerative disorders.

Modulation of the Hedgehog Signaling Pathway by Sterol-based Small Molecules

Chad Anthony Maschinot

Chapter 2:

Modulation of Hedgehog Signaling by Oxysterols

Introduction

Cholesterol is one of the most abundant and important small molecules in the human body. It makes up nearly half of the lipid molecules in the plasma membrane,[76] and serves as the precursor for steroidal hormones and bile acid.[77] As trans-membrane receptors, GPCRs are naturally embedded in cholesterol rich environments and therefore always in close proximity to cholesterol. It is not surprising that as the role and functions of GPCRs has become clearer, cholesterol binding motifs have been identified, and the biological functions of cholesterol have grown. As the proposed roles for cholesterol have grown, the roles and functions of oxysterols, cholesterol metabolites, have come into view.

I. Endogenous Oxysterols

Oxysterols can generally be defined as oxygenated derivatives of cholesterol, containing additional carbonyls, alcohols, or epoxide groups. Interest in oxysterols has been renewed in recent years as the additional evidence for the importance of cellular cholesterol has come into view.[78] Oxysterols in general are generated through non-enzymatic [reactive oxygen species (ROS)] and enzymatic oxidation reactions [cytochrome p450 (Cyp) enzymes]. With multiple endogenous OHCs identified, their specific functions appear to fall under two categories: (1) regulation of cholesterol homeostasis and/or (2) interference with normal cellular functions of cholesterol.[78] Additional roles have recently been proposed including the regulation of immune function.[79]

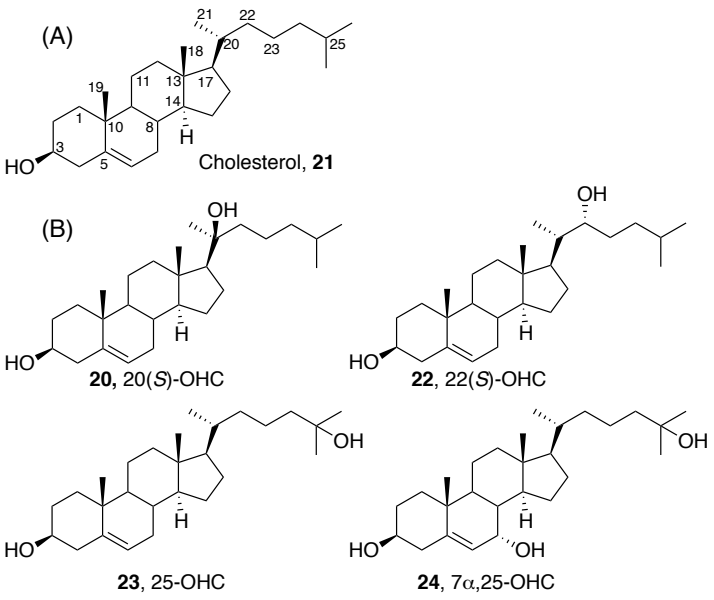

Figure 7. (A) The cholesterol numbering system and (B) representative endogenous oxysterols.

Regulation of cholesterol homeostasis by OHCs was first proposed in 1973 when impure cholesterol was able to inhibit cholesterol synthesis while purified cholesterol did not have this ability.[80] This was later attributed to small amounts of OHCs present, such as 20(*S*)- (**20**), 22(*S*)- (**21**), and 25-OHC (**22**), which showed the greatest inhibitory potency in subsequent studies.[81] Additional studies have shown that cholesterol does not need to be hydroxylated or metabolized to suppress its own synthesis.[70] Since the first isolation of the sterol receptor element binding protein (SREBP) transcription factors in 1993,[82] aspects of these contradictory studies have been clarified.

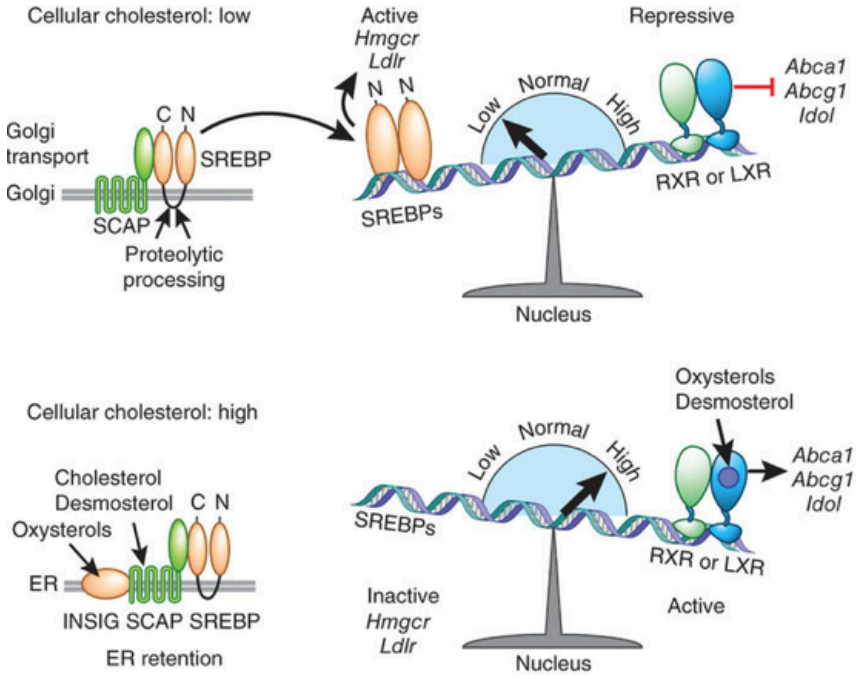

Figure 8. The effect of overall sterol status on the SREBP pathway of cholesterol homeostasis.[88] Low cholesterol levels are sensed by SCAP which escorts SREBP for cleavage and activation of SREBP gene activation via a sterol response element (SRE). OHCs bind to Insig to trigger the same effect. When sterol levels are sufficient, the SREBP/SCAP complex remains tethered to the ER by Insig preventing gene expression. Reprinted by permission from Macmillan Publishers Ltd: Nature Immunology. Spann, N. J.; Glass, C. K. Sterols and oxysterols in immune cell function. *Nat. Immunol.* **2013**, *14*, 893-900.

SREBPs are made as membrane-bound precursors in the endoplasmic reticulum (ER) bound to the SREBP-cleavage activating protein (SCAP). When cholesterol levels are low in the ER, SCAP guides SREBP to the Golgi, where the two proteins are cleaved (**Figure 8**). This releases SREBP into the nucleus to activate gene transcription via binding to sterol response elements (SRE). Interestingly, cholesterol and not oxysterols were shown to bind to the membrane region of SCAP, which upon cholesterol binding results

in the binding of SCAP to Insig.[83] It was later determined that OHCs regulate cholesterol synthesis by direct binding to Insig.[84] These two studies showed that the binding properties of SCAP and Insig were reciprocal, where the presence of a polar (hydroxylated) group on the alkyl-side chain resulted in a change in the binding target. Importantly, the overall net effect of reducing SREBP transcriptional activity was observed with administration of OHCs or cholesterol.[83-84]

OHCs have also been identified as natural ligands for the liver X receptors (LXRα and LXRβ), providing more evidence that they regulate cholesterol homeostasis. These receptors regulate genes that control whole body cholesterol and lipid homeostasis through a heterodimer formed with the retinoid X receptor (RXR). Target genes include the genes encoding for the ATP-binding cassette proteins ABCA1 and ABCG1, which both play an important role in cholesterol efflux.[85] Based on X-ray crystallography and murine studies, it appears that oxygenation at the 22-, 24-, and 27-positions of the cholesterol scaffold (**Figure 7**, **21**) are important for LXR binding.[86-87]

Endogenous OHCs have also been proposed to have functions within the immune system.[88] Studies have shown both LXRs and SREBPs play roles in immune response.[88-91] Besides regulating cholesterol and fatty acid homeostasis, LXRs regulate genes encoding for anti-inflammatory proteins or molecules that promote the synthesis of anti-inflammatory fatty acids, while also suppressing genes controlled by the pro-inflammatory transcription factors NF-κB and AP-1.[88] Studies in macrophages have also indicated that SREBPs, SREBP1a specifically, activates the *Nlrp1a* gene, which encodes a core component of the NLRP1 inflammasome.[92] Endogenous LXR ligands are expected to promote anti-inflammatory activities of LXRs while suppressing the processing of SREBPs to decreases the activation of genes involved in the inflammatory response.[88]

One specific OHC proposed to have immune functions is 25-OHC (**23**). In *in vitro* and *in vivo* studies, LXRs have been linked to innate immune responses to bacterial and protozoan pathogens, where increases in the production of 25-OHC were observed.[88] The treatment of macrophages with type 1 interferons to stimulate the immune response as well as viral infection itself, showed rapid upregulation of cholesterol

25-hydroxylase (CH25H), the enzyme responsible for 25-OHC production. In additional studies, 25-OHC showed broad inhibitory activity against enveloped viruses and CH25H-deficient mice were more susceptible to infection.[93]

Another proposed role of OHCs is the regulation of B cell functions. For example, stimulation of macrophage toll-like receptors (TLRs) induced CH25H expression and 25-OHC production. This resulted in a decrease in immunoglobulin A (IgA),[94] suggesting that 25-OHC suppresses immunoglobulin class switching of naïve B cells. Another oxysterol with the C25 hydroxylation, 7α,25-OHC (**24**) is a potent ligand with sub-nanomolar potency for the GPCR EBI2 (GPR183), which is required for B cell migration and differentiation into antibody-secreting plasma cells.[95-96] As other immune cells express EBI2, this suggests that local concentrations of oxysterols may coordinate the innate and adaptive immune responses via interactions with EBI2.

II. Endogenous Regulation of Smo

As previously mentioned, Smo is one of two trans-membrane receptors that regulate Hh signaling and is a member of the Frizzled class (class F) of G-protein coupled receptor (GPCR)-like proteins. Similar to other GPCRs, Smo possesses stereotypical structural features, including seven-TM domains, an amino-terminal cysteine rich domain (CRD), extra- and intracellular loops, and a carboxy-terminus tail (C_T) that can undergo a number of post-translational modifications (PTMs), including phosphorylation as previously discussed. The specific mechanism, or mechanisms, that lead to activation and inhibition of Smo by Ptch under natural conditions remains elusive, but multiple hypotheses do exist (**Figure 9**).[97]

These hypotheses are based on the significant evidence already presented on the inherent druggability and ability to regulate Smo by both synthetic and naturally occurring small molecules, such as Cyc and OHCs. It is known that inhibition, or repression, of Smo by Ptch is indirect with no evidence of direct contact,[98] but instead one Ptch molecule is estimated to regulate up to 50 Smo.[99] Additionally, Ptch shares homology with an ancient class of bacterial transporters that transports lipophilic toxins and contains a sterol sensing domain.[100] Combining these observations, it has been proposed that Ptch functions by

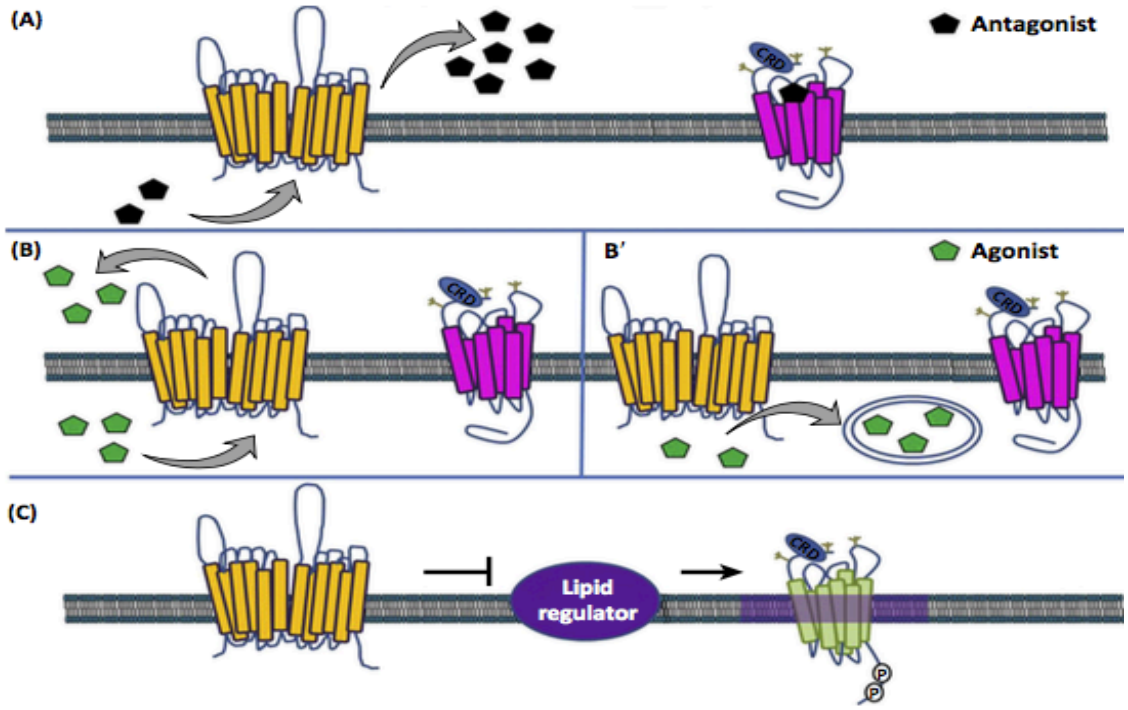

Figure 9. Models of Ptch regulation of Smo activity.[97] (A) Ptch (yellow) pumps-out an antagonistic small molecule that binds to Smo preventing accumulation and signaling. (B) Ptch pumps-out a Smo agonist out of the cell, or sequesters it (B'), where it is unable to activate Smo. (C) Ptch controls a lipid regulator that blocks the accumulation of lipid species in microdomains, such as the primary cilium, that regulate Smo accumulation. Models A and B can also be utilized for the opposite small molecule species where a theoretical agonist could be pumped out to activate Smo or an antagonist could be sequestered intracellularly to prevent signaling. Reprinted from Trends in Pharmacological Sciences, 37, Arnesdorf, A.; et al. Smoothened Regulation: A Tale of Two Signals, 62-72, 2016, with permission from Elsevier.

regulating the availability of a sterol-like Smo regulator,[100] such as OHCs.[71-73] One hypothesis is that Ptch pumps agonists outside of the cell to repress Smo activity. Binding of Hh protein to Ptch then: (1) prevents removal of the agonist from the cell, allowing the agonist to interact with Smo and initiate signaling, or (2) increases the extracellular concentration of the agonist which in turn binds to Smo upon its translocation to the primary cilium to initiate signaling. Contradictory evidence to this theory is that deletion or absence of Ptch results in constitutive activation of Hh signaling, suggesting that the small molecule regulated by Ptch is an antagonist.[101] In a similar matter, Ptch would then be able to sequester or efflux the antagonist.

As evident by these hypotheses, the endogenous small molecule that may regulate Smo remains in question. Recent evidence attempting to answer this question suggests that cholesterol itself regulates Smo.[70] Cholesterol is necessary for Hh signaling beyond the cholesterol modification of Hh proteins. Treatment of chick embryos with cyclodextrin, a cyclic oligosaccharide that forms non-covalent complexes with sterols, resulted in facial defects similar to those observed with a Hh pathway antagonist, and high concentrations of cyclodextrin decreased Hh activity to levels comparable to Cyc.[102] It was further determined that the decreased Hh response occurred at sterol levels sufficient for normal auto-processing and cholesterol modification of Hh protein. This suggests that cholesterol plays a role in regulating Hh signaling beyond the modification of Hh proteins.

III. Cholesterol Derivatives and Hh signaling

In the last few years, it has been proposed that cholesterol may be involved in Ptch regulation of Smo and may be the natural Smo ligand.[70] As a GPCR, it is not surprising that cholesterol and its derivatives have been shown to bind to Smo. The importance of cholesterol to GPCRs has become clear in recent years with multiple cholesterol sensing, or recognition, sites being identified in multiple GPCR familes.[77]

To date, multiple cholesterol binding motifs have been identified in GPCRs that show a range of one to six cholesterol molecules per binding interface and all were located within a trans-membrane domain with high preference and occurrence of hydrophobic residues.[77] In multiple cases, it was also shown that cholesterol aids in stabilizing the receptors against thermal, extreme pH, and proteolytic degradation.[103-104] Besides direct binding of cholesterol to GPCRs, the modulation of cholesterol concentrations can alter the physical properties of the membrane leading to conformational changes of the proteins and modified function.[105-106] Combining these studies on other GPCRs with the proposed methods for Smo regulation, it is not surprising that studies have shown direct interactions between cholesterol, and its oxysterol derivatives, and Smo.[70-73]

Oxysterols were first identified as agonists for Hh signaling in 2006,[71] but it was not until 2012 that their binding site was determined to be the Smo-CRD.[73,107] Comparing the naturally occurring 20(*S*)-OHC

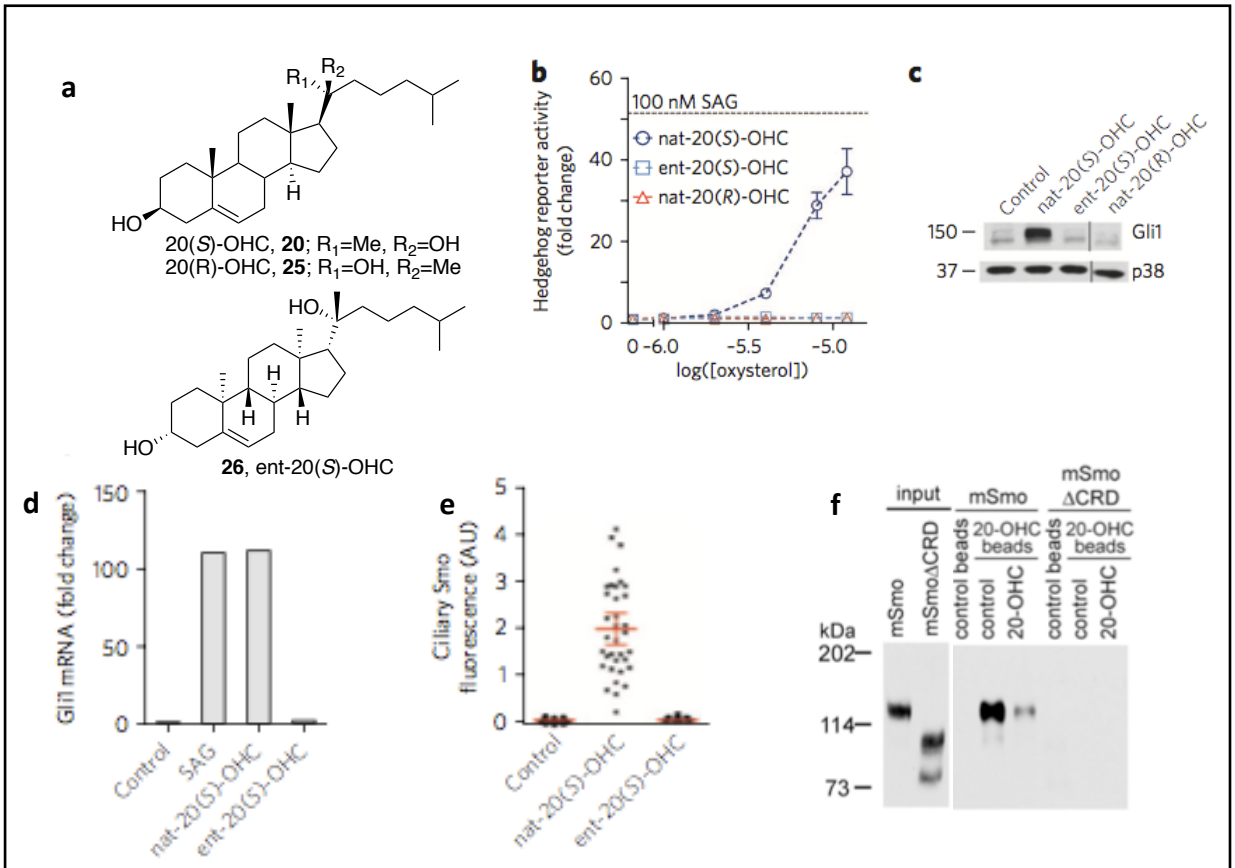

Figure 10.[73,107] Stereoselective activation of Hh signaling. (**a**) Structures of 20-OHCs. (**b**) Gli reporter activity in NIH 3T3 cells treated with OHCs as fold change relative to ethanol alone. (**c**) Immunoblotting results of Gli reporter assay. (**d**) Quantitative real-time PCR (qRT-PCR) analysis confirming immunoblotting and reporter activity. (**e**) Quantification of ciliary Smo fluorescence in NIH 3T3 cells with 10 μM OHC. (**f**) Binding of cherry-tagged mSmo and mSmoΔCRD to 20(S)-OHC beads indicates that the CRD region is required for binding. Reprinted by permission from Macmillan Publishers Ltd: Nachtergaele, S.; et al. *Nat. Chem. Biol*. **2012**, 8, 211-220; and Nedelcu, D.; et al. *Nat. Chem. Biol.* **2013**, 9, 557-564.

(**20**) with its diastereomer, 20(*R*)-OHC (**25**), and enantiomer (**26**), indicated that the OHC Smo-CRD binding interaction was stereoselective in nature. (**Figure 10**).[73] In these studies, **20** was the only compound of the three to potently activate Hh signaling and induce ciliary accumulation of Smo (**Figure 10e**). For follow-up studies, **20** was covalently attached to agarose beads via a polyethylene glycol (PEG) linker (**20**-beads). Binding of murine Smo (mSmo) to **20**-beads was observed while free **20** was capable of displacing mSmo from the beads.[107] In similar studies with the CRD region deleted (mSmoΔCRD), no binding of **20**-beads was observed indicating that the CRD region is required for OHC binding (**Figure 10f**).

Follow up studies performed in the Hadden lab further confirmed the stereoselective nature of the Smo-OHC interaction.[108] In these studies, a variety of OHCs with hydroxylated side chains were synthesized to study the regioselective nature of OHC binding (**Figure 11**) and evaluated in C3H MEFS (**Table 3**). The ability of the OHCs to activate Hh signaling was determined 24 h following administration to the cells. After 24 h of incubation, mRNA was collected from the cells using the commercially available Fast Taqman Cells-to-Ct Kit (ThermoScientific). The mRNA was quantified via quantitative real time-PCR (qRT-PCR).

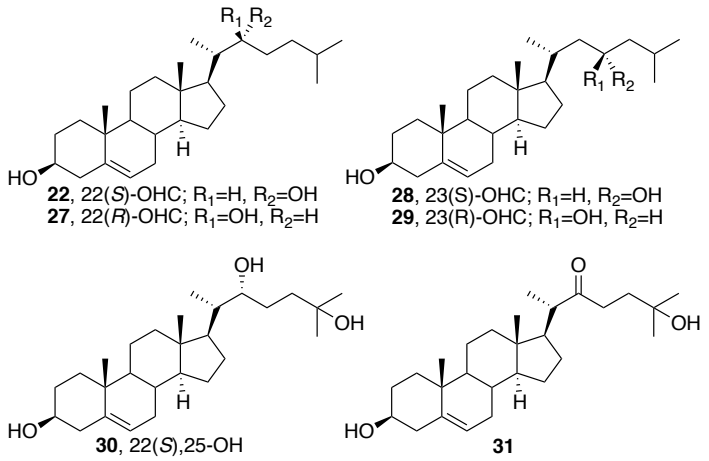

Figure 11. Representative OHCs from initial SAR studies.[107]

Table 3. *In vitro* evaluation of OHCs.[107]

OHC[a]	Gli1[b]	ABCA1[b]	Select[c]
20	92 ± 6	13 ± 2	7.1
22	53 ± 1	2.3 ± 0.1	23
23	70 ± 3	9.8 ± 1	7.1
27	4.7± 0.4	24 ± 2	--
28	87 ± 0.8	4.9 ± 0.2	18
29	32 ± 0.1	3.6 ± 1	8.9
30	9.9 ± 0.2	2.9 ± 0.1	3.3
31	6.0 ± 0.3	22 ± 2	--

[a]OHCs evaluated at 5 μM in C3H MEFs. [b]Values represent mRNA expression compared to DMSO (set to 1.0). [c]Selectivity for Gli1:ABCA1.

Similar to previous reports, significant changes in activity were observed with inversion of the hydroxyl groups, such as **28** and **29**. Comparing the activities indicated that binding to Smo may be regioselective as well. Another important observation can be seen comparing **22** and **27,** where activation of LXR, determined through mRNA expression of ABCA1, shows stereoselective preferences. It should be noted that in general, **27** is recognized as a selective endogenous LXR agonist.[108-109] The di-hydroxylated side chain of **30** was unable to synergize the agonistic activity of **22** and **23**, but resulted in essentially a loss in all activity. Interestingly, oxidation of the 22-position (**31**) yielded activity comparable to **27**, selective for LXR over Hh signaling. This suggests that LXR binding is regio- and steroselective where the carbonyl of **31** is oriented similarly to **27** and not **22** within the binding site.

Taken together, it is clear that synthetic and endogenous OHCs bind directly to the Smo-CRD to induce Hh signaling in multiple cellular models. This binding is both regio- and stereoselective in nature with significant changes in activity and selectivity observed by inversion of the hydroxylated side chains.

IV. C-20 Modified OHCs[110]

Multiple studies (discussed above) have indicated highly regio- and stereoselective binding between OHCs and the Smo-CRD; however, a few questions still remained to fully characterize this interaction. First, the importance of the C-21 methyl moiety has yet to be determined. In previous studies, the loss in activity when the C-20 stereocenter was inverted from *S* to *R* (**20** to **25**, respectively) combined with the loss in activity with the 20(*S*)-OHC enantiomer **23**, suggests that the C-21 methyl may play a role in determining activity. A second question remaining is whether binding is more regio- or stereoselective, meaning if the C-20 stereochemistry is inverted on an active OHC, such as **28**, would Hh agonistic activity remain. To evaluate these questions, a series of OHC analogues were designed in which the C-21 methyl group was removed (**26** and **27**) or inverted in the 23-OHC scaffold, **34** and **35** (**Figure 12**).

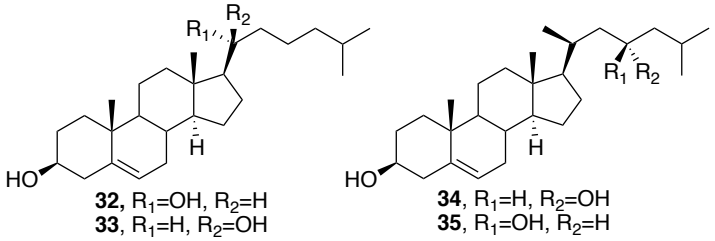

Figure 12. Target C-20 modified OHCs.

*A. Synthesis of C-20 modified OHCs **26-29***

Preparation of both analogue families began with the tetrahydropyran (THP) protection of commercially available starting materials following previous observations that the incorporation of an additional stereocenter in the THP group allowed for easier separation of isomers. For analogues with the C-21 methyl moiety removed (*des*-methyl OHCs, **32** and **33**, **Scheme 1**), 21-acetoxypregnenolone (**36**) was

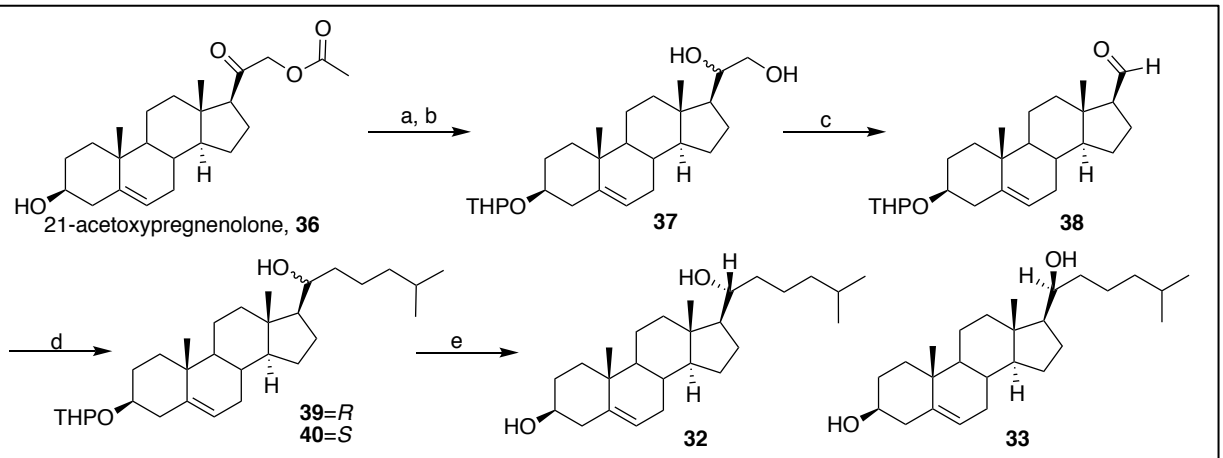

Scheme 1. Synthesis of 20-*des*-methyl OHC analogues.[109] (a)3,4-dihydropyran, p-TsOH, THF, 96%; (b) LAH, THF, 3h, 96%; (c) $NaIO_4$, THF, 1h, 92%; (d) Mg, Isopentyl bromide, THF, 55%; (e) 2N HCl, MeOH:THF, 96%.

utilized as the starting material. Following THP protection, lithium aluminum hydride-mediated reduction of the ester and ketone functionalities yielded the 1,2-diol **37**. Oxidative cleavage of **37** with sodium periodate yielded aldehyde **38,** which underwent Grignard addition with *in situ* generated isopentyl magnesium bromide to provide a mixture of THP-protected C-20 secondary alcohols, **39** and **40**. Separation of **39** and **40** by column chromatography followed by removal of the THP group by acid deprotection yielded *S*- and *R*-isomers **32** and **33**. Assignment of the C20 stereochemistry was performed by comparative ^{1}H NMR analysis and Mosher ester analysis of the THP-protected isomers **39** and **40** (See Appendix).[110]

Similarly, C-21-inverted OHC analogues **34** and **35** were synthesized from pregnenolone (**41**), **Scheme 2**. A secondary goal of this series was to shorten and improve the yield of 23(*S*)-OHC (**28**). Previously, synthesis of **28** was twelve steps from commercially available hyodeoxycholic acid with a low overall yield of 1.8%. The revised synthetic route started with THP protection of **41**. Following a previously reported procedure,[111] Grignard addition of vinyl magnesium bromide gave a mixture (1:9) of the tertiary allylic alcohols. Treatment of the mixture with pyridinium chlorchromate (PCC) resulted in oxidative rearrangement of the allylic alcohol to yield an 80:20 *E:Z* mixture of β-substituted-α,β-unsaturated aldehydes (enal), **42a** and **42b**. Following unsuccessful attempts to selectively hydrogenate the enal system, we turned to the iminium catalysts previously developed in the MacMillan laboratory. This reaction was of particular interest due its ability to convert both *E* and *Z* alkenes to a single β-stereogenic aldehyde.[112]

Utilizing the Hantzsch ester as hydride source and the (*S*)-imidazolidinone, the mixture of **42a**:**42b** was converted to aldehyde **43** [20(*R*) configuration] in good overall yield with no formation of stereoisomer **44**. Performing the same protocol on the **42a**:**42b** mixture with the (*R*)-imidazolidinone provided **44** [20(*S*) configuration] in good yield as the singular reduction product.

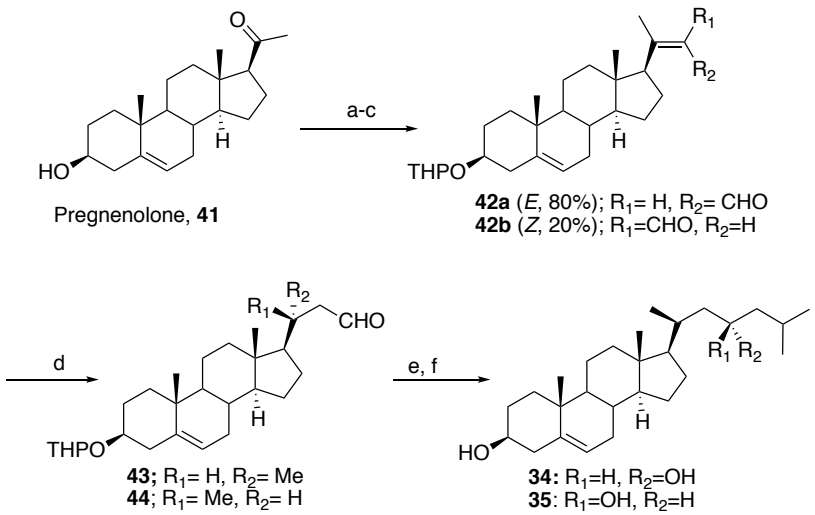

Scheme 2. Synthesis of 23-hydroxylated OHC analogues.[110] (a) 3,4-dihydro-2H-pyran, p-TsOH, THF, 96%; (b) Vinyl magnesium bromide, THF, 97%; (c) PCC, NaOAc, DCM, 64%; (d) MacMillan catalyst, Hatzsch ester, $CHCl_3$, 60 - 64%; (e) *Iso*-butyl magnesium bromide, THF, 72%; (f) 2N HCl, MeOH:THF, 96%.

Following unsuccessful asymmetric Grignard attempts to prepare 23(*S)*-OHC (**28**) from aldehyde **43**, standard Grignard addition of isobutyl magnesium bromide to either aldehyde **43** or **44** provide the corresponding 23(*S*)- and 23(*R*)-OHC analogues as a 1:1 mixture that was easily separable via standard silica gel chromatography. Finally, deprotection of the THP group afforded the 23-hydroxylated OHCs, **28-29** and **34-35.** Overall, this revised synthetic route provided 23(*S*)-OHC, **28**, in six steps with a yield of 14.2% from pregnenolone (**41**), and 28.3% overall for both isomers **28**-**29**. Previous assignments of the stereochemistry at C-23 were based on a combination of thin-layer chromatography, ^{1}H and ^{13}C NMR, and circular dichroism analysis.[108] We utilized crystal structure analysis of **4** and **13** to both unambiguously assign the stereochemistry of the C-23 hydroxyl and utilize as a base for assigning the stereochemistry of **28** and **29** (See Appendix).

B. Biological activity of C-20 modified OHCs

The C-20 modified OHC analogues were initially evaluated in the same manner as previously described in M2-10B4 cells, a multipotent murine bone stromal cell line previously utilized as a model to evaluate small molecule Hh agonists. The ability of each analogue to up-regulate known Hh (G*li1*) or LXR (*ABCA1*) target genes was measured. All OHC analogues were evaluated at 5 μM where values in **Table 4** represent fold increase in mRNA expression over DMSO levels (set to 1.0). The ability of both **28** and **29** to up-regulate *Gli1* mRNA closely mirrored that reported from OHCs prepared through our previous synthetic route.[108] Interestingly, inversion of the C-21 methyl on the 23-hydroxylated OHCs (**34** and **35**) completely abolished their ability to up-regulate *Gli1* expression. This was particularly interesting for analogue **34**, which loses all Hh agonism compared to 23(*S*)-OHC, when the C-21 methyl is inverted, suggesting that inversion of the C-21 methyl actively prevents the OHC scaffold from binding the Smo CRD. This result is supported by a previous study demonstrating that inversion of the C20-hydroxy group to 20(*R*)-OHC resulted in complete loss of Hh agonism compared to natural 20(*S*)-OHC.[107]

Table 4. Initial activity of OHC analogues in M2-10B4 cells.[110]

OHC[a]	Gli1[b]	ABCA1[b]	Selectivity[c]
DMSO	1.0	1.0	--
20	20 ± 0.7[b]	18 ± 0.2	1.1
28	18 ± 0.6	6.2 ± 0.3	2.9
29	8.7 ± 0.1	3.6 ± 0.1	2.4
32	24 ± 0.8	2.4 ± 0.1	10
33	1.3 ± 0.01	1.3 ± 0.4	--
34	1.3 ± 0.3	1.0 ± 0.3	1.3
35	0.7 ± 0.01	0.7 ± 0.2	--

[a]All OHCs tested at 5 μM. [b]Values represent fold mRNA upregulation ± SEM. [c]Selectivity for Hh signaling determined as Gli1/ABCA1. Data is average of at least three separate experiments performed in triplicate.

Interestingly, removal of the C-21 methyl moiety of 20(*S*)-OHC, as in OHC **33**, completely abolished the ability of the scaffold to up-regulate *Gli1* expression. Removal of the C-21 methyl for 20(*R*)-OHC resulted in OHC **32**, which demonstrated potent agonism of Hh signaling, an unexpected result considering that 20(*R*)-OHC is a poor activator of Hh signaling.[108] Taken together, these results strongly suggest

stereoselective interactions between the side chain of the OHC scaffold and its binding site in the Smo CRD are essential for its ability to activate Hh signaling.

Table 5. Concentration dependent pathway activation in M2-10B4 cells.[110]

OHC	Gli1	Ptch1	ABCA1
20	0.52 ± 0.04[a]	0.72 ± 0.2	4.7 ± 0.9
28	0.57 ± 0.1	0.65 ± 0.06	1.5 ± 0.2
32	1.3 ± 0.1	1.3 ± 0.01	2.8 ± 0.1

[a]Values are in mM ± SEM. Data is the average of at least three separate experiments performed in triplicate.

Based on its comparable potency and improved selectivity, we evaluated OHC **32** in a series of secondary assays to further probe its ability to activate the Hh signaling cascade. Dose-dependent evaluation of OHC **32** demonstrated that its ability to up-regulate the key Hh target genes *Gli1* and *Ptch1* was approximately two-fold less than both **20** and **28** (**Table 5**). In addition, the EC_{50} value for up-regulation of *ABCA1* by **32** was comparable to that obtained for the Hh pathway target genes, suggesting removal of the C-21 methyl also affects its ability to selectively activate Hh signaling. To confirm that GLI1 up-regulation with **32** is mediated through the Hh pathway, a competition study was performed with cyclopamine (Cyc), potent Hh-selective inhibitor known to attenuate *Gli1* expression induced by OHCs.[72-73,108] As expected, co-administration with Cyc (5 μM) abolished Gli1 up-regulation, indicating OHC **32** functions through Hh activation (**Figure 13d**).

When the Hh pathway is functionally activated in M2-10B4 cells, osteogenic differentiation is promoted, resulting in mature osteoblastic cells.[113-114] This is possible because M2-10B4 cells possess stem-like characteristics with the ability to differentiate into bone, cartilage, adipocytes, and hematopoietic supporting tissues. This differentiation process can be followed by measuring the early- (osterix, *OSX*) and late-stage (alkaline phosphatase, *ALP*) transcriptional markers of osteogenesis. Following previously utilized procedures, OHCs **20** and **32** were evaluated for osteogenic activity. Cells were treated with either OHC at 5 μM for 24, 48, or 96 hours to compare mRNA expressions of *Gli1*, *OSX*, and *ALP* (**Figure 13a-c**).

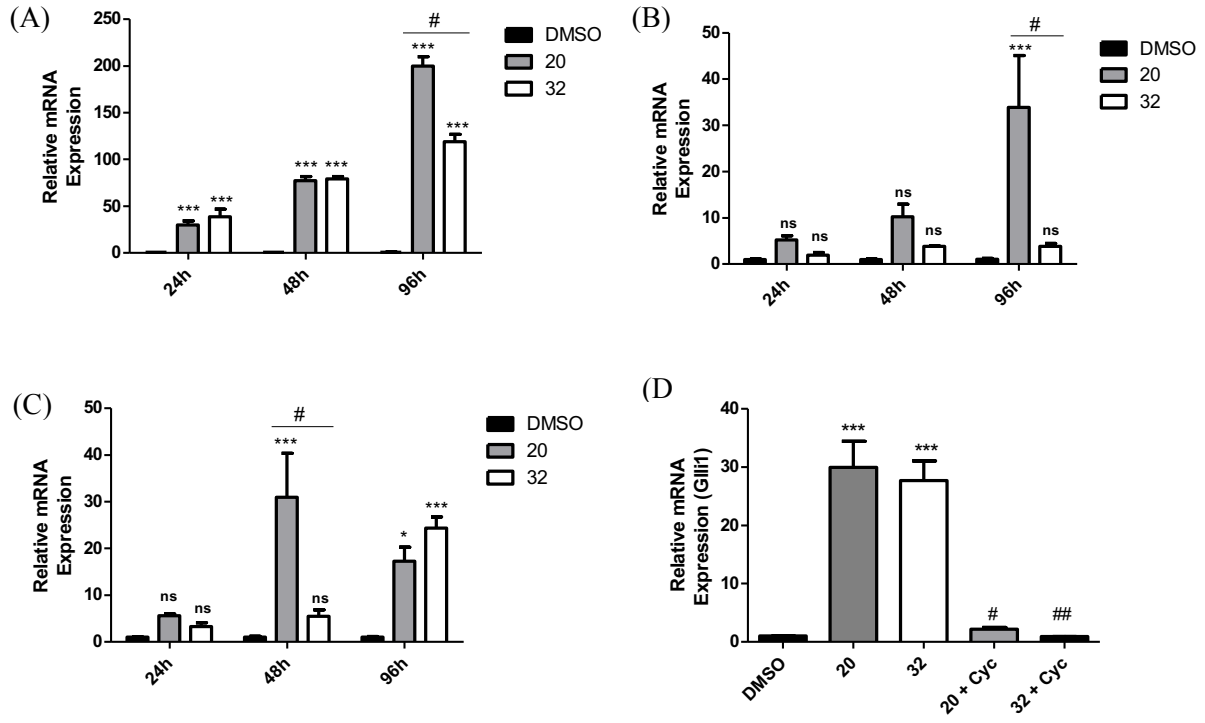

Figure 13. Induction of osteogenic differentiation by OHCs at 24, 48, or 96 hr. Up-regulation of Gli1 (A), OSX (B), and ALP (C). Statistical analysis, two-way ANOVA with Bonferroni post-test performed using GraphPad Prism5; ***p<0.001, compared with DMSO control; ns, not statistically significant compared with DMSO control; #, p<0.001, compared with OHC **32**. (D) Attenuation of **32**-mediated Gli1 up-regulation with Cyc co-administration in M2-10B4 cells. OHC and Cyc evaluated at 5 μM. Data are from a representative experiment performed in triplicate. Statistical analysis, one-way ANOVA with Tukey post-test performed using GraphPad Prism5; ***p<0.001, compared with corresponding DMSO control; ## p<0.001, #p<0.01compared with corresponding OHC alone.

Both **20** and **32** demonstrated comparable *Gli1* up-regulation after 24 and 48 hours; however, **20** continued to increase *Gli1* up to 96 hours post-treatment. After 24 hours, both compounds induced modest *OSX* and *ALP* expression. Interestingly, only **20** significantly increased *OSX* up to 96 hours. In addition, increased *ALP* expression, denoting mature osteoblasts, was observed at both 48 and 96 hours for **15**, but not until 96 hours for **32**. Taken together, this data supports the ability of both OHCs to terminally differentiate precursor cells via Hh activation, while also suggesting that **32** mediates its osteogenic differentiation through a mechanism distinct from osterix. One possible mechanism to be evaluated utilizes Runx2, runt-related transcription factor 2. Runx2 is a known as a master regulator of osteoblast differentiation[115] and has been shown to have a relationship with IHh expression.[116]

In addition, the ability of OHCs to induce osteogenesis may provide a novel method for therapeutics for diseases, such as osteoporosis; however, more mechanistic studies as to how stimulation of Hh signaling induces osteogenesis.

V. Predicting OHC Activity[117]

Following the unexpected results described above with the *des*-methyl analogues, a modeling approach was taken to explain these results and to develop a method for determining possible activities prior to testing. A homology model of the human Smo CRD (hCRD) was generated by a postdoctoral researcher in the Hadden lab, Dr R. C. Dash, using the crystal structure of the zebrafish CRD (zCRD, PDB ID: 4C79, resolution 2.3Å) as the template (**Figure 14**).[116, 117] Similar to other CRD structures found in Fz-type

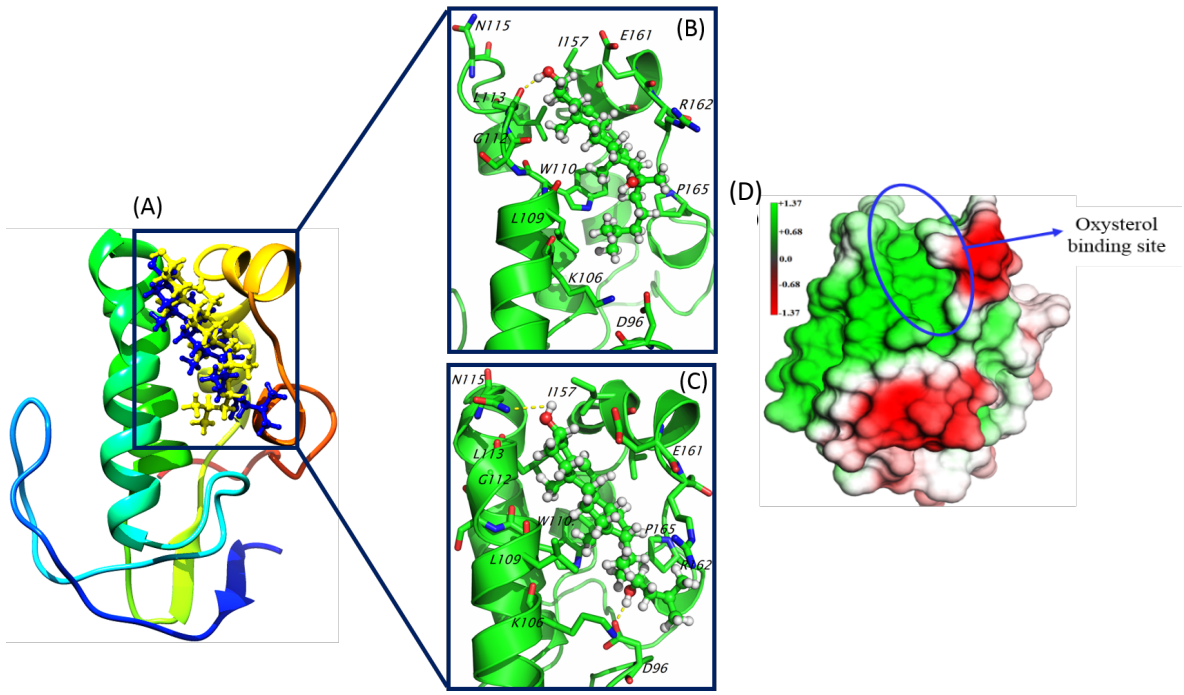

Figure 14. Average binding conformations of OHCs **20** and **35.**[117] (**A**) Comparison of average binding conformation generated from MD of compound **20** (yellow) and **35** (blue) at the oxysterol binding site of the hCRD (**B**) Average binding conformation of **20**. (**C**) Average binding conformation of **35**. Hydrogen bonds are indicated by the yellow dashed lines. Compounds are represented as ball and stick while oxysterol binding residues are represented in sticks. (**D**) The molecular surface area of the hCRD colored as per the hydrophobicity of the residues with the predicted OHC binding site encircled. Green, hydrophobic; white, neutral; red, hydrophilic.

receptors, the probable OHC binding site is located on the surface of the domain between the three core α-helices and is lined with hydrophobic residues (**Figure 14d**).

Docking studies were performed via the Schrodinger Suite package and AutoDock v4.2. The docking study demonstrates favorable steric and electrostatic interactions between **20** and the hCRD, where the tetracyclic core occupied the hydrophobic pocket formed by the α1 and α3 helices. Additionally, this conformation orientated the two methyl groups (C-18 and C-19) in a way that they became buried deeply in the hydrophobic cavity, and the 3β-hydroxyl group formed a hydrogen bond (H-bond) with the carbonyl of glycine 112 (G112) (**Figure 14b**). The remaining OHCs were docked to the hCRD model in a similar fashion (**Table 6)**.

Table 6. Comparison of OHC cellular activity and predicted binding.

OHC[a]	*Gli1* mRNA[b]	Docking Score[d]	$\Delta G_{binding}$[e]
DMSO	1.0	NA	--
20	19.9 ± 0.7	-9.04	-11.81
22	16.2 ± 2.5	-8.91	-6.69
23	1.6 ± 0.4	-9.42	-14.87
28	18.2 ± 0.6	-9.59	-7.72
29	8.7 ± 0.1	-8.80	-6.35
32	24.3 ± 0.8	-9.61	-0.72
33	1.3 ± 0.01	-10.14	-14.31
34	1.3 ± 0.3	-8.86	-12.03
35	0.7 ± 0.01	-9.26	-19.59
22-NHC	NA[c]	-9.16	-15.65

[a]All OHCs evaluated at 5 μM. [b]Value represents mRNA upregulation compared to DMSO (set to 1.0). [c]Known Hh antagonist, Ref 106. [d]Docking scores represent predicted binding energy generated by Autodock 4.0. [e]$G_{binding}$ = Total predicted binding energy in kcal/mol.

Interestingly, all compounds showed predicted binding energies that would suggest biological activity, regardless of Gli1 upregulation values, and the predicted binding energies and cell-based Hh activities were inversely correlated. Based on these results, the 23-hydroxylated OHC analogues **34** and **35** were evaluated as antagonists (**Table 7**).

Initially, OHCs **34** and **35** were evaluated in the M2-10B4 cell line and compared to the known cholesterol-based Hh pathway inhibitor, 22-NHC.[106] In this assay, multiple up-regulation methods were utilized to activate Hh signaling: (1) 23(S)-OHC (**28**), (2) recombinant SHh ligand (rSHh), and (3) SAG

Table 7. Inhibition of Hh signaling by OHCs **34-35** compared to 22-NHC.[117]

OHC	Hh activation method in M2-10B4 MEFs[a]	IC_{50} (μM)[b]	
		M2-10B4	ASZ001
34	23(*S*)-OHC (**28**)	>20	>20
	rSHh	>20	
	SAG (**17**)	>20	
35	23(*S*)-OHC (**28**)	3.7 ± 0.9	2.9 ± 0.8
	rSHh	5.2 ± 0.01	
	SAG (**17**)	4.4 ± 2	
22-NHC	23(*S*)-OHC (**28**)	5.3 ± 0.1	0.71 ± 0.3
	rSHh	4.7 ± 2	
	SAG (**17**)	6.0 ± 0.6	

[a]Agonists administered at following concentrations: **28** at 5 μM, **17** at 400 nM, and rSHh at 0.5 ng/μL. [b]IC_{50} values are Mean ± SEM of at least two separate experiments performed in triplicate.

(**17**). These three methods were chosen to fully characterize any antagonistic activity where each method targets Hh signaling differently. Specifically, rSHh activates Ptch to induce signaling whereas SAG (**17**) and **28** bind at different locations of Smo to induce signaling. These OHCs were further evaluated for antagonistic activity in ASZ001 cells, an Hh-dependent murine BCC model with a Ptch deficiency, kindly provided by Dr. Ervin Epstein at the Children's Hospital Oakland Research Institute. These cells were obtained from BCC tumors that arose in irradiated $Ptch1^{+/-}$ mice, and have lost the Ptch1 allele.[118]

Inhibitory activity of **35** and 22-NHC were comparable in M2-10B4 cells against all three activation methods; however, 22-NHC was slightly more active with sub-micromolar potency in ASZ001 cells. This difference in potency may be due to greater permeability or decreased metabolism in ASZ cells for 22-NHC.

Molecular dynamic studies were performed by Dr Radha Dash to try to explain the differences in activity between **28** and **35**, where inverting the C-21 methyl orientation results in opposite Hh activity (agonist to antagonist). The major difference was observed when snapshots of **20**, **28**, and **35** were overlaid and the C17-C20-C22-C23 dihedral angles were plotted (**Figure 15**). Inversion of the C-21 methyl group, found in **35,** appears to rigidify the *iso*-octyl side chain (**Figure 15b**), presumably due to interactions between the C-18 and C-21 methyl groups preventing complete rotation and flexibility. In turn, this leads to a synclinal orientation that orients the 23-hydroxyl group into the protein surface allowing for an

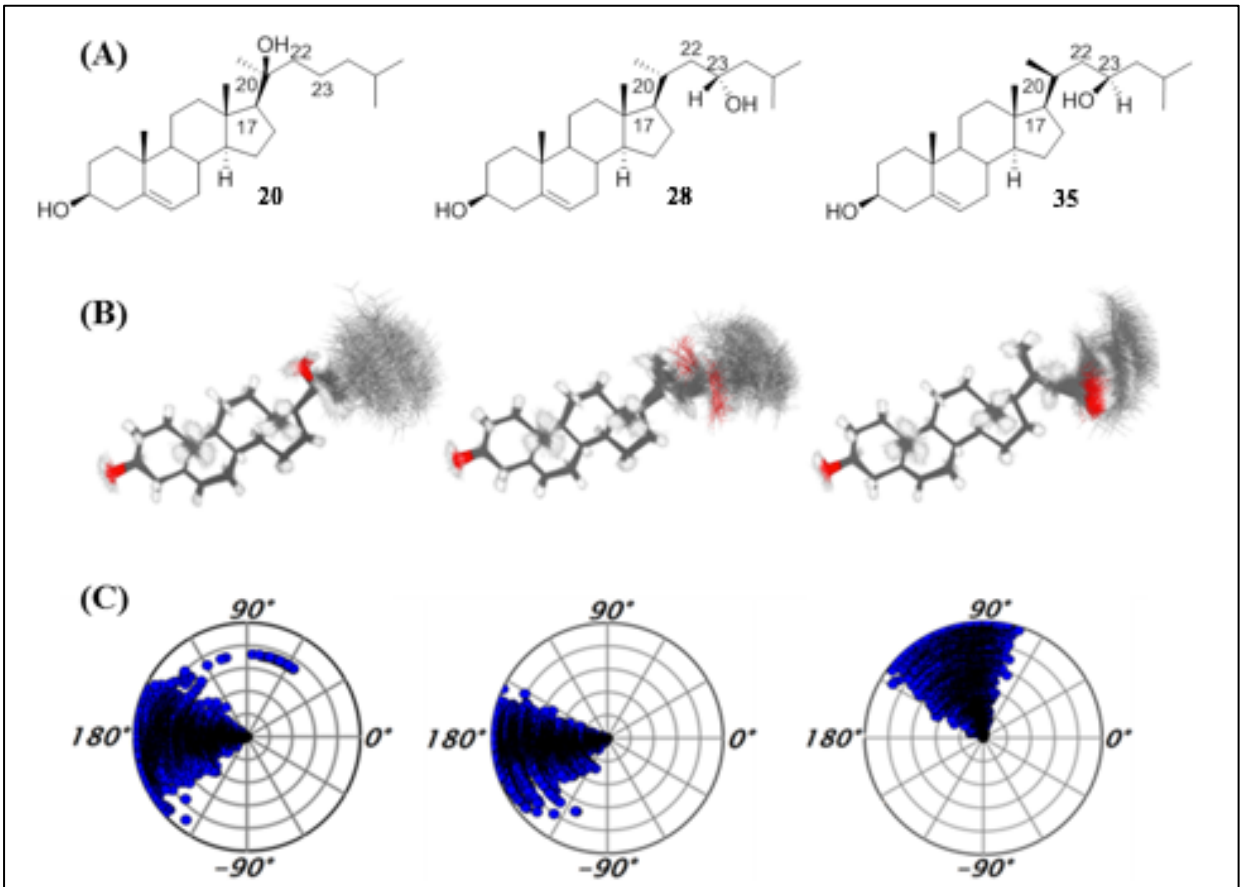

Figure 15. OHC dihedral profile.[117] (A) Two-dimensional representations of **20**, **28**, and **35**. (B) An overlay of 500 snapshot geometries for **20**, **28** and **35** from the OHC-hCRD Molecular Dynamic (MD) simulation, showing both the localized geometries of the i*so*-octyl side chain and the significant orientation of the hydroxyl group. Alignment of these snapshot geometries is based on the atoms of the tetracyclic ring of the average MD geometry. **(C)** Distribution of dihedral angles between the C-17, C-20, C-22 and C-23 atoms over a simulation time of 5 ns.

additional H-bond to form with aspartate-96 (D96) compared to **20** and **28** that show an anti-periplanar dihedral angle that orients the 23-hydroxyl group away from the protein surface and D96. This suggests that the additional binding interaction with D96 increases the binding affinity enough for **35** to become an Hh antagonist.

Conclusion

As described above, the natural endogenous ligand for Smo and the specific mechanism for Ptch regulation of Smo remain to be defined. Among the candidates for endogenous ligands are cholesterol and

oxysterols (OHCs), oxygenated metabolites of cholesterol. In recent years, the binding of OHCs and to Smo has been greatly characterized suggesting both highly regio- and stereoselective binding preferences. Adding to these studies, a series of OHC analogues (**32** – **35**) were designed and synthesized to study the importance of the C-20 stereochemistry and specifically the C-21 methyl group. Interestingly, removal of the C-21 methyl group yielded an active analogue (**32**) where the hydroxyl group was oriented in the same direction as the inactive 20(*R*)-OHC (**25**) suggesting that removal of the methyl group allows for the C20-hydroxyl group to occupy the same special arrangement and orientation as the active 20(*S*)-OHC (**20**).[109] Additionally, it was determined that changing the C20 stereochemistry (OHCs **34**-**35**) can completely change the activity of the compound from agonist to antagonist (**28** to **35**). Molecular dynamic studies revealed that inversion of the C20 stereocenter allowed for the 23-hydroxyl group to interact with the D96 residue in the CRD, increasing the binding affinity significantly to result in this activity change.[117] Taken together, these results were surprising but follow a trend observed with glucocorticoids where both agonists and antagonists have been identified with very similar overall structures.[2] It has also been reported that endogenous B-ring oxysterols inhibit Hh signaling at the level of Smo distinct from the side-chain OHC binding site.[120]

Acknowledgements

I would like to thank Radha C. Dash, PhD for performing the computational experiments including homology model generation, dock and molecular dynamics studies, and MM/GBSA calculations.

Experimental Section[109, 117]

General Information. Pregnenolone and 21-acetoxypregnenolone were purchased from Sigma-Aldrich. All other reagents were purchased from commercial sources (Fisher Scientific or Sigma-Aldrich) unless otherwise stated. Column chromatography was performed using silica gel purchased from Sorbtech (Sorbent Technologies). All ^{1}H and ^{13}C NMR data was performed on a Bruker AVANCE 500 spectrometer and analysis with MestReNova version 9.1.0. HRMS data was analyzed at the Mass Spectrometry Facility

at the University of Connecticut, performed by Dr. You-Jun Fu. FT-IR analysis was performed on a Bruker Alpha Platinum ATR instrument using OPUS software (v 7.2).

3-THP,21-acetoxypregnenolone (**36-THP**). To a solution of 21-acetoxypregnenolone (10.8 g, 31.6 mmol) in anhydrous DCM (150 mL) under argon, 3,4-dehydro-2H-furan (39.5 mmol, 3.6 mL) and a catalytic amount of *p*-toluenesulfonic acid were added. The mixture stirred for 12 hr at RT, washed with saturated sodium bicarbonate (2 X 75 mL), saturated sodium chloride (2 X 75 mL), dried over sodium sulfate, and concentrated. The mixture was purified via column chromatography (SiO_2, 10% EtOAc in Hex) to give **36-THP** as a white solid in excellent yield (13.9 g, 95%). ^{1}H (500 MHz, $CDCl_3$) δ 5.37 (m, 1H), 4.73 (m, 2H), 4.56 (d, 2H), 3.94 (m, 1H), 3.54 (m, 2H), 2.53 (m, 1H), 2.38 (m, 1H), 2.24 (m, 1H), 2.19 (s, 3H), 2.06 (m, 2H), 1.88 (m, 3H), 1.73 (m, 3H), 1.64 (m, 1H), 1.58 (m, 7H), 1.49 M, 1H), 1.42 (m, 1H), 1.31 (m, 1H), 1.21-1.07 (2H), 1.03 (s, 3H), 0.99 (m, 1H), 0.69 (s, 3H). ^{13}C NMR (126 MHz, $CDCl_3$) δ 203.7, 170.2, 141.1, 121.1, 96.9, 75.9, 69.2, 62.8, 59.3, 57.1, 49.9, 44.7, 40.2, 38.6, 37.4, 37.2, 36.8, 31.9, 31.3, 29.6, 27.9, 25.5, 24.6, 22.8, 21.0, 20.5, 20.0, 19.4, 13.1. IR (ATR FTIR): 2936, 1745, 1722, 1417, 1370, 1229, 1198, 1112, 1074, 1056, 1029, 975, 904, 837. [M+H]+, calc. 459.3111, obs. 459.3186.

1-((3*S*,10*R*,13*S*,17*S*)-10,13-dimethyl-3-((tetrahydro-2H-pyran-2-yl)oxy)-2,3,4,7,8,9,10,11,12,13,14,15,16,17-tetradecahydro-1H-cyclopenta[a]phenanthren-17-yl)ethane-1,2-diol (**37**). A solution of **THP-36** (1.0 g, 2.18 mmol) in anhydrous THF (20 mL) under argon was cooled to 0°C. Lithium aluminum hydride (1.0 M in THF, 8.8 mmol) was added drop-wise and the mixture stirred for 4 hr at 0°C. The reaction was diluted with EtOAc, quenched with cold water and filtered. The filtrate was washed, where the organic layer was collected and concentrated. Purification via flash chromatography (SiO_2, 30% EtOAc in Hex) afforded **37** as a white solid in excellent yield (1.02 g, 96%). ^{1}H NMR (500 MHz, $CDCl_3$) δ 5.36 (m, 1H), 4.74 (s, 1H), 3.94 (m, 1H), 3.67 (d, 2H), 3.51 (m, 2H), 3.38 (m, 1H), 2.38 (m, 1H), 2.22-2.11 (m, 3H), 2.00 (m, 1H), 1.87 (m, 3H), 1.74 (m, 2H), 1.66 (m, 2H), 1.55-1.47 (m, 10H),

1.27-1.11 (4H), 1.04 (s, 3H), 0.81 (s, 3H). ^{13}C NMR (126 MHz, $CDCl_3$) δ 141.2, 121.3, 96.9, 75.9, 74.6, 66.5, 62.8, 55.9, 52.4, 50.2, 42.5, 40.2, 39.7, 38.8, 37.2, 36.8, 31.9, 31.8, 31.3, 29.7, 27.9, 25.5, 24.6, 20.9, 20.1, 19.4, 12.4. IR (ATR FTIR): 3338, 2931, 1438, 1351, 1305, 1199, 1135, 1114, 1060, 1027, 972, 909, 868 $cm^{-1.}$ HRMS: $[M+H]^+$, calc. 419.3161, obs. 419.3139.

(3*S*,10*R*,13*S*,17*S*)-10,13-dimethyl-3-((tetrahydro-2H-pyran-2-yl)oxy)-2,3,4,7,8,9,10,11,12,13,14,15,16,17-tetradecahydro-1H-cyclopenta[a]phenanthrene-17-carbaldehyde (**38**). To a solution of **37** (0.75 g, 1.79 mmol) in 2:1 THF:H_2O (45 mL) was added sodium periodate (1.2 g, 5.61 mmol) and the mixture stirred at RT for 1 hr. The mixture was extracted with EtOAc (3 X 50 mL) and the organic layer was dried over sodium sulfate and concentrated. Purification via flash chromatography (10% EtOAc in Hex) afforded **38** as a white solid (0.64 g, 92%). ^{1}H NMR (500 MHz, $CDCl_3$) δ 5.37 (s, 1H), 4.74 (s, 1H), 3.94 (m, 1H), 3.54 (m, 2H), 3.38 (m, 1H), 2.35 (m, 2H), 2.04 (m, 2H), 1.88 (m, 3H), 1.76 (m, 3H), 1.29 (m, 1H), 1.15 (m, 2H), 1.04 (s, 3H), 0.79 (s, 3H). ^{13}C NMR (126 MHz, $CDCl_3$) δ 204.9, 141.1, 121.2, 96.9, 75.9, 62.84, 56.5, 50.2, 44.7, 40.2, 38.3, 37.2, 36.8, 31.8, 31.5, 29.7, 27.9, 25.5, 24.9, 21.1, 20.6, 20.1, 19.4, 13.7. IR (ATR FTIR): 2938, 2695, 1719, 1438, 1352, 1260, 1198, 1112, 1054, 1021, 973, 911, 866 cm^{-1}. HRMS: $[M-H]^+$, calc. 385.2743, obs. 385.2742; $[M+H]^+$, calc. 387.2899, obs. 387.2867

Grignard Addition to 38. To a suspension of acid activated Mg turnings (0.360 g, 14.8 mmol) in anhydrous THF (5 mL) under argon at RT was catalytic amount of Br_2Et (3 drops) and heated to 35°C. The suspension was stirred until bubbling of the Mg turnings was observed. A solution of bromo-4-methylpentane (1.6 mL, 10.9 mmol) in anhydrous THF (6 mL) was added drop-wise over 20 min to the Mg suspension and heated to 55°C. After stirring for 2 hr, the mixture was cooled to 0°C. A solution of **28** (0.700 g, 1.81 mmol) in anhydrous THF (6 mL) was added and stirred 0°C for 2 hr. The reaction was quenched with saturated ammonium chloride (15 mL) and washed with ether (2 X 25 mL). The combined organic layers were dried over sodium sulfate and concentrated. Purification via flash chromatography (10% EtOAc in Hex) afforded **39** and **40** as easily separable white solids (55% overall conversion).

(1*S*)-1-((3*S*,10*R*,13*S*,17*S*)-10,13-dimethyl-3-((tetrahydro-2H-pyran-2-yl)oxy)-2,3,4,7,8,9,10,11,12,13,14,15,16,17-tetradecahydro-1H-cyclopenta[a]phenanthren-17-yl)-5-methylhexan-1-ol (**39**). R_f 0.28 in 10:1 Hexanes:Ethyl acetate. ^{1}H NMR (500 MHz, $CDCl_3$) δ 5.40 (s, 1H), 4.76 (s, 1H), 3.97 (m, 1H), 3.58 (m, 3H), 2.41 (m, 2H), 2.13 (m, 1H), 2.02 (m, 1H), 1.91 (m, 3H), 1.76 (m, 1H), 1.68 (m, 2H), 1.57 (m, 13H), 1.40-1.20 (m, 12H), 1.06 (s, 3H), 1.00 (m, 1H), 0.92 (d, J = 7.5 Hz, 6H), 0.82 (s, 3H). ^{13}C NMR (126 MHz, $CDCl_3$) δ 141.2, 121.3, 96.8, 76.0, 74.4, 62.8, 56.7, 56.2, 50.2, 42.4, 40.3, 40.0, 39.1, 37.3, 37.2, 36.8, 31.9, 31.8, 31.3, 28.03, 25.54, 25.50, 24.6, 22.9, 22.7, 22.5, 21.0, 20.1, 19.4, 12.4. IR (ATR FTIR): 3466, 2933, 1464, 1376, 1364, 1259, 1134, 1112, 1093, 1077, 1057, 1022, 973, 910, 867 cm^{-1}. HRMS: $[M+H]^+$, calc. 473.3995, obs. 473.4140. $[M-OH]^+$, calc. 455.3889, obs. 455.3848.

(1*R*)-1-((3*S*,10*R*,13*S*,17*S*)-10,13-dimethyl-3-((tetrahydro-2H-pyran-2-yl)oxy)-2,3,4,7,8,9,10,11,12,13,14,15,16,17-tetradecahydro-1H-cyclopenta[a]phenanthren-17-yl)-5-methylhexan-1-ol (**40**). R_f 0.23 in 10:1 Hexanes:Ethyl acetate. ^{1}H NMR (500 MHz, $CDCl_3$) δ 5.39 (s, 1H), 4.76 (s, 1H), 3.96 (m, 1H), 3.58 (m, 3H), 2.38-2.24 (2H), 2.13 (m, 1H), 2.02 (m, 1H), 1.91 (m, 5H), 1.75-1.19 (30H), 1.05 (s, 3H), 0.92 (d, 6H), 0.74 (s, 3H). ^{13}C NMR (126 MHz, $CDCl_3$) δ 140.9, 121.5, 97.0, 76.0, 73.2, 62.9, 56.6, 56.3, 50.3, 41.7, 40.3, 39.1, 38.8, 37.5, 37.2, 36.9, 31.9, 31.6, 31.3, 29.7, 28.1, 25.5, 24.8, 24.2, 23.2, 22.7, 22.6, 20.8, 20.1, 19.4, 12.7. IR (ATR FTIR): 3500, 2923, 1460, 1384, 1353, 1260, 1199, 1109, 1053, 1020, 973, 911, 864 cm^{-1}. HRMS: $[M+H]^+$, calc. 473.3995, obs. 473.4028; [M-OH]+, calc. 455.3889, obs. 455.3873.

(3*S*,10*R*,13*S*,17*S*)-17-((*S*)-1-hydroxy-5-methylhexyl)-10,13-dimethyl-2,3,4,7,8,9,10,11,12,13,14,15,16,17-tetradecahydro-1H-cyclopenta[a]phenanthren-3-ol (**32**). The THP group was removed from OHC **39** by stirring in 2N HCl (10 mL) until completion (16 h). The acid was quenched with 2 M NaOH (15 mL) and extracted with EtOAc (3 x 20mL). Purification via flash chromatography (SiO_2, 20% EtOAc in Hex) afforded **32** as a white solid in excellent yield (0.063 g, 96%).

^{1}H NMR (500 MHz, $CDCl_3$) δ 5.40 (s, 1H), 3.60 (m, 2H), 2.30 (m, 2H), 2.15 (m, 1H), 2.02 (m, 1H), 1.89 (m, 2H), 1.69 (m, 2H), 1.56 (m, 8H), 1.43 (m, 2H), 1.30-1.14 (12H), 1.07 (s, 3H), 0.92 (d, 6H), 0.82 (s, 3H). ^{13}C NMR (126 MHz, $CDCl_3$) δ 140.9, 121.6, 77.3, 77.0, 76.8, 74.4, 71.8, 56.7, 56.2, 50.2, 42.4, 42.3, 40.0, 39.1, 37.3, 37.2, 36.6, 31.9, 31.8, 31.7, 28.0, 25.5, 24.6, 22.9, 22.7, 22.5, 21.0, 19.4, 12.4. IR (ATR FTIR): 3298, 2925, 1729, 1463, 1373, 1351, 1260, 1056, 1023, 954, 912 cm^{-1}. HRMS: $[M+NH_4]^+$ calc. 406.3685, obs. 406.3661; $[M-OH]^+$, calc. 371.3314, obs. 371.3302.

(3*S*,10*R*,13*S*,17*S*)-17-((*R*)-1-hydroxy-5-methylhexyl)-10,13-dimethyl-2,3,4,7,8,9,10,11,12,13,14,15,16,17-tetradecahydro-1H-cyclopenta[a]phenanthren-3-ol (**33**). The THP group was removed from OHC **33** as described above for the preparation of **32**. Purification via flash chromatography (SiO_2, 20% EtOAc in Hex) afforded **33** as a white solid in excellent yield (0.031 g, 95%). ^{1}H NMR (500 MHz, $CDCl_3$) δ 5.40 (s, 1H), 3.60 (m, 2H), 2.31 (m, 2H), 2.04 (m, 1H), 1.90 (m, 4H), 1.68 (m, 2H), 1.56 (m, 9H), 1.42 (m, 4H), 1.30-1.12 (8H), 1.06 (s, 3H), 0.92 (d, 6H), 0.75 (s, 3H). ^{13}C NMR (126 MHz, $CDCl_3$) δ 140.8, 121.6, 77.3, 77.0, 76.8, 73.2, 71.8, 56.6, 56.2, 50.2, 42.3, 41.7, 39.1, 38.8, 37.3, 37.2, 36.6, 31.9, 31.7, 31.6, 28.1, 24.8, 24.2, 23.2, 22.7, 22.6, 20.8, 19.4, 12.8. IR (ATR FTIR): 3290, 2926, 1715, 14622, 1378, 1365, 1320, 1238, 1058, 1028, 953, 936 cm^{-1}. HRMS: $[M+NH_4]^+$, calc. 406.3685, obs. 406.3658; $[M-OH]^+$, calc. 371.3314, obs. 371.3300.

1-((3*S*,10*R*,13*S*,17*S*)-10,13-dimethyl-3-((tetrahydro-2H-pyran-2-yl)oxy)-2,3,4,7,8,9,10,11,12,13,14,15,16,17-tetradecahydro-1H-cyclopenta[a]phenanthren-17-yl)ethanone, THP-pregnenolone (41-THP). To a solution of pregnenolone (10.0 g, 31.6 mmol) in anhydrous DCM (150 mL) under argon, 3,4-dehydro-2H-furan (39.5 mmol, 3.6 mL) and a catalytic amount of *p*-toluenesulfonic acid were added. The mixture stir for 12 hr at RT, washed washed with saturated sodium bicarbonate (2 X 75 mL), saturated sodium chloride (2 X 75 mL), dried over sodium sulfate, and concentrated. The mixture was purified via column chromatography (SiO_2, 10% EtOAc in Hex) to give **41-THP** as a white solid (12.2 g, 96%). Characterization matched that previously described.[119] ^{1}H NMR (500

MHz, $CDCl_3$) δ 5.37 (m, 1H), 4.75 (m, 1H), 3.93 (m, 1H), 352 (m, 2H), 2.56 (m, 1H), 2.39 (m, 1H), 2.21 (m, 1H), 2.15 (s, 3H), 2.08-2.00 (2H), 1.88 (m, 3H), 1.77-1.64 (5H), 1.59-1.47 (11H), 1.29-1.09 (3H), 1.04 (s, 3H), 0.66 (s, 3H).

(*Z*)-3-((3*S*,10*R*,13*S*,17*S*)-10,13-dimethyl-3-((tetrahydro-2H-pyran-2-yl)oxy)-2,3,4,7,8,9,10,11,12,13,14,15,16,17-tetradecahydro-1H-cyclopenta[a]phenanthren-17-yl)-2-methylbut-2-enal (**42a**) and **(*E*)-3-((3*S*,10*R*,13*S*,17*S*)-10,13-dimethyl-3-((tetrahydro-2H-pyran-2-yl)oxy)-2,3,4,7,8,9,10,11,12,13,14,15,16,17-tetradecahydro-1H-cyclopenta[a]phenanthren-17-yl)-2-methylbut-2-enal** (**42b**). A solution of **41-THP** (5.00 g, 12.5 mmol) in THF (100 mL) was cooled to -78°C under argon. Vinylmagnesium bromide (0.7 M in THF, 44.8 mL, 31.4 mmol) was added drop wise. Upon complete addition, the mixture was stirred for 1 hr at -78°C and then warmed to RT over 12 hr. The mixture was re-cooled to 0°C and quenched with saturated aqueous ammonium chloride and washed with ether (3 X 60 mL). The organic layers were combined and washed with saturated sodium chloride (1 X 100 mL), dried with sodium sulfate and concentrated. Purification with flash chromatography (SiO_2, 12% EtOAc in Hex) afforded a 1:9 mixture of alcohols as a white solid (5.2 g, 97%) that was utilized without additional separation. ^{1}H NMR (500 MHz, $CDCl_3$) δ 6.01 (dd, 1H), 5.37 (s, 1H), 5.17 (d, 1H), 4.99 (d, 1H), 4.75 (s, 1H), 3.94 (s, 1H), 3.53 (m, 2H) 2.30 (m, 2H), 2.13 (m, 1H), 1.99 (m, 1H), 1.89 (m, 3H), 1.76-1.64 (m, 5H), 1.58-1.39 (m, 14H) 1.36 (s, 3H), 1.28 (m, 1H), 1.13 (m, 2H), 1.04 (s, 3H), 0.96 (m, 1H), 0.86 (s, 3H). ^{13}C NMR (126 MHz, $CDCl_3$) δ 146.14, 140.98, 121.43, 121.27, 110.22, 96.99, 96.85, 75.92, 75.73, 63.76, 62.90, 62.81, 59.48, 56.95, 56.83, 50.13, 44.03, 42.85, 40.21, 38.89, 37.47, 37.23, 36.84, 31.89, 31.55, 31.37, 29.71, 28.78, 28.01, 25.53, 24.51, 23.84, 23.22, 22.86, 20.90, 20.09, 19.40, 13.82, 13.24. IR (ATR FTIR): 3516, 2933, 1467, 1453, 1336, 1260, 1200, 1140, 1111, 1055, 1021, 976, 911, 866 cm^{-1}. HRMS: $[M+NH_4]^+$, calc. 445.3634, obs. 446.3667.

To a suspension of pyridinium chlorochromate (5.2 g, 24.1 mmol) and sodium acetate (4.9 g, 59.7 mmol) in CH_2Cl_2 (45 mL) under argon, was added the mixture of alcohols (5.2 g, 12.13 mmol). The mixture was stirred at RT for 12 hr. The mixture was filtered through Celite, followed by copious rinsing with CH_2Cl_2

and concentrated. Purification with flash chromatography (SiO_2, 10% EtOAc in Hex) provided an 80:20 *E:Z* mixture of **42a:42b** as a white solid (3.3 g, 64%). ^{1}H NMR (500 MHz, $CDCl_3$) δ 10.10 (d, 1H), 10.00 (d, 0.2H), 6.06 (d, 0.2H), 5.95 (d, 1H), 5.39 (m, 1H), 4.92 (m, 0.2H), 4.75 (m, 1H), 4.05 (m, 0.2H), 3.95 (m, 1H) 3.53 (m, 2H), 3.25(m, 0.2H), 2.4-2.26 (m, 2H), 2.23 (s, 3H), 2.01 (m, 2H), 1.87 (m, 6H), 1.75 (m, 4H), 1.61-1.40 (m, 15H), 1.39-1.28 (m, 3H), 1.24-1.08 (m, 3H), 1.04 (s, 3H), 0.72 (s, 0.6H) 0.64 (s, 3H). ^{13}C NMR (126 MHz, $CDCl_3$) δ 191.3, 190.7, 164.3, 140.9, 131.5, 127.9, 121.2, 96.9, 75.9, 62.8, 60.2, 56.8, 56.2, 51.4, 50.2, 46.3, 45.1, 40.2, 38.7, 38.6, 37.4, 37.2, 36.8, 32.2, 31.8, 31.3, 29.6, 27.9, 25.5, 24.9, 24.4, 21.0, 20.0, 19.4, 19.3, 13.9, 13.1. IR (ATR FTIR): 2930, 1714, 1656, 1434, 1376, 1354, 1254, 1230, 1197, 1130, 1112, 1060, 1022, 972, 910, 864 cm^{-1}. HRMS: $[M+H]^+$, calc. 427.3112, obs. 427.3211.

(3*R*)-3-((3*S*,10*R*,13*R*,17*R*)-10,13-dimethyl-3-((tetrahydro-2H-pyran-2-yl)oxy)-2,3,4,7,8,9,10,11,12,13,14,15,16,17-tetradecahydro-1H-cyclopenta[a]phenanthren-17-yl)butanal (**43**). A solution of **42a**:**42b** (0.300 g, 0.706 mmol) in $CHCl_3$ (10 mL) was cooled to 0°C. The trichloroacetic acid salt of (*S*)-(+)-2-(*tert*-butyl)-3-methylimidazolin-4-one (0.038 g, 0.14 mmol) and Hantzsch ester (0.215 g, 0.85 mmol) were added and the mixture stirred at 0°C until the starting material was consumed as evidenced by continuous TLC analysis (~ 16 hr). The solution was concentrated and directly purified via flash chromatography (SiO_2, 10% EtOAc in Hex) to yield **43** as a white solid (0.195 g, 64%). Characterization matched that previously reported by the Hadden Lab.[11]

(3*S*)-3-((3*S*,10*R*,13*R*,17*R*)-10,13-dimethyl-3-((tetrahydro-2H-pyran-2-yl)oxy)-2,3,4,7,8,9,10,11,12,13,14,15,16,17-tetradecahydro-1H-cyclopenta[a]phenanthren-17-yl)butanal (**44**). A solution of **42a:42b** (0.300 g, 0.706 mmol) in $CHCl_3$ (10 mL) was cooled to 0°C. The trichloroacetic acid salt of (*R*)-2-(*tert*-butyl)-3-methylimidazolin-4-one (0.038 g, 0.14 mmol) and Hantzsch ester (0.215 g, 0.85 mmol) were added and the mixture stirred at 0°C until the starting material was consumed as evidenced by continuous TLC analysis (~ 16 hr). The solution was concentrated and directly purified via flash chromatography (SiO_2, 10% EtOAc in Hex) to yield **44** as a white solid (0.180 g, 60%). ^{1}H NMR (500

MHz, $CDCl_3$) δ 9.80 (s, 1H), 5.37 (m, 1H), 4.76 (m, 1H), 3.85 (m, 1H), 3.55 (m, 2H), 2.72 (m, 1H), 2.41-2.26 (m, 3H), 2.04 (m, 2H), 1.91 (m, 5H), 1.75 (m, 1H), 1.64 (m, 2H), 1.57 (m, 6H), 1.51 (m, 2H), 1.37 (m, 1H), 1.27- 1.12 (m, 5H), 1.05 (s, 3H), 0.97 (d, 3H), 0.76 (s, 3H). ^{13}C NMR (126 MHz, $CDCl_3$) δ 203.3, 140.9, 121.4, 96.9, 75.9, 62.9, 56.6, 55.6, 49.9, 42.4, 40.2, 39.7, 38.8, 37.4, 37.2, 36.8, 31.8, 31.3, 30.6, 29.7, 27.8, 25.5, 24.0, 21.0, 20.1, 19.9, 19.4, 12.3. IR (ATR FTIR): 2930, 1715, 1439, 1372, 1258, 1199, 1135, 1112, 1056, 1021, 974, 912, 867 cm^{-1}. HRMS: $[M+H]^+$, calc. 429.3368, obs. 429.3360.

Preparation of 23- OHCs 28 and **29.** A solution of *iso*-butylmagnesium chloride (2.0M in THF, 0.84 mL, 1.68 mmol) was cooled to 0°C in THF (5 mL) under argon. A solution of **43** (0.090 g, 0.210 mmol) in THF (5 mL) was added drop-wise and the mixture stirred at 0°C for 90 min. The reaction was quenched with saturated aqueous ammonium chloride and washed with ether (2 X 25 mL). The organic layers were dried sodium sulfate and concentrated. Purification via flash chromatography (SiO_2, 8% EtOAc in Hex) provided two separable isomers as white solids (80% overall total yield of both isomers). Characterization of fraction 1 [THP-23(*S*)-OHC, R_f 0.39 in 8:1 Hexanes:Ethyl acetate] and fraction 2 [THP-23(*R*)-OHC, R_f 0.29 in 8:1 Hexanes:Ethyl acetate] were as previously described.[107]

23(*S*)-hydroxycholesterol (**28**). Fraction 1 (0.050 g, 0.103 mmol) was dissolved in 5:1 MeOH:THF (6 mL), to which 2N HCl (2 mL) was added dropwise. The mixture was stirred at RT for 3 hr. The reaction was quenched with water (5 mL) and washed with EtOAc (2 X 20 mL). The organic layers were dried over sodium sulfate, concentrated, and purified as previously described to afford **22** as a white solid (0.040 g, 97%). Characterization matched that previously published.[107] ^1H NMR (500 MHz, $CDCl_3$) δ 5.37 (m, 1H), 3.79 (m, 1H), 3.54 (m, 1H), 2.27 (m, 2H), 2.02 (m, 2H), 1.85 (m, 4H), 1.61-1.43 (11H), 1.28 (m, 4H), 1.20-1.07 (4H), 1.03 (s, 3H), 0.98 (d, 3H), 0.94 (dd, 6H), 0.71 (s, 3H). ^{13}C NMR (126 MHz, $CDCl_3$) δ 140.8, 121.7, 71.8, 68.7, 56.9, 56.7, 50.2, 46.5, 45.2, 42.4, 42.3, 39.8, 37.3, 36.5, 33.9, 31.9, 31.6, 28.5, 24.5, 24.3, 23.9, 21.7, 21.1, 19.43, 19.42, 11.9.

23(*R*)-hydroxycholesterol (**29**). The THP group was removed from fraction 2 as described above for the preparation of **28**. Purification via flash chromatography (SiO_2, 20% EtOAc afforded) **29** as a white solid in excellent yield (0.025 g, 94%). Characterization matched that previously published.[107] ^{1}H NMR (500 MHz, $CDCl_3$) δ 5.37 (m, 1H), 3.80 (m, 1H), 3.54 (m, 1H), 2.28 (m, 2H), 2.04 (m, 1H), 2.00 (m, 1H), 1.86 (m, 3H), 1.77 (m, 1H), 1.67 (m, 1H), 1.61-1.39 (11H), 1.28 (m, 2H), 1.20 (m, 2H), 1.12-1.05 (4H), 1.03 (s, 3H), 0.99 (d, 3H), 0.93 (dd, 6H), 0.74 (s, 3H). ^{13}C NMR (126 MHz, $CDCl_3$) δ 140.77, 121.67, 71.8, 67.0, 56.84, 56.78, 50.1, 48.0, 44.5, 42.4, 42.3, 39.8, 37.3, 36.5, 32.5, 31.9, 31.7, 28.5, 24.7, 24.3, 23.3, 22.3, 21.1, 19.4, 18.7, 11.9.

Preparation of 34 and 35. Grignard addition of *iso*-butylmagnesium chloride to **44** was analogous to that described above for addition to **43**. Purification via flash chromatography (SiO_2, 8% EtOAc in Hex) provided two separable isomers as white solids (72% overall total yield of both isomers).

(2*S*,4*S*)-2-((3*S*,10*R*,13*R*,17*R*)-10,13-dimethyl-3-((tetrahydro-2H-pyran-2-yl)oxy)-2,3,4,7,8,9,10,11,12,13,14,15,16,17-tetradecahydro-1H-cyclopenta[a]phenanthren-17-yl)-6-methylheptan-4-ol (**THP-34**). R_f 0.41 in 8:1 Hexanes:Ethyl acetate. ^{1}H NMR (500 MHz, $CDCl_3$) δ 5.39 (m, 1H), 4.76 (m, 1H), 3.96 (m, 1H), 3.81 (m, 1H), 3.55 (m, 2H), 2.41 (m, 1H), 2.24 (m, 1H), 2.01 (m, 2H), 1.93-1.73 (7H), 1.66-1.45 (11H), 1.30 (m, 5H), 1.19-1.07 (5H), 1.05 (s, 3H), 0.97(dd, 6H), 0.90 (d, 3H), 0.73 (s, 3H). ^{13}C NMR (126 MHz, $CDCl_3$) δ 141.1, 121.5, 97.0, 76.0, 68.6, 62.9, 56.5, 50.2, 46.1, 44.8, 42.4, 40.3, 39.9, 38.8, 37.5, 37.2, 36.8, 32.6, 31.9, 31.3, 29.7, 28.0, 27.5, 25.5, 24.5, 24.9, 21.7, 21.0, 20.1, 19.4, 18.9, 12.3. IR (ATR FTIR): 3519, 2931, 1465, 1375, 1260, 1113, 1075, 1055, 1019, 909, 868. HRMS: [M+H]+, calc. 487.4151, obs. 487.4145; [M-OH]+, calc. 469.4046, obs. 469.4045.

(2*S*,4*R*)-2-((3*S*,10*R*,13*R*,17*R*)-10,13-dimethyl-3-((tetrahydro-2H-pyran-2-yl)oxy)-2,3,4,7,8,9,10,11,12,13,14,15,16,17-tetradecahydro-1H-cyclopenta[a]phenanthren-17-yl)-6-methylheptan-4-ol (**THP-35**). R_f 0.30 in 8:1 Hexanes:Ethyl acetate.^{1}H NMR (500 MHz, $CDCl_3$) δ 5.38

(m, 1H), 4.75 (m, 1H), 3.96 (m, 1H), 3.83 (m, 1H), 3.52 (m, 2H), 2.39-2.32 (2H), 2.01 (m, 2H), 1.88 (m, 4H), 1.76 (m, 4H), 1.63-1.35 (11H), 1.29-1.07 (9H), 1.04 (s, 3H), 0.96 (d, 6H), 0.92 (d, 3H), 0.74 (s, 3H). ^{13}C NMR (126 MHz, $CDCl_3$) δ 140.9, 121.5, 97.0, 76.01, 67.4, 62.8, 56.8, 50.2, 48.1, 44.0, 42.4, 40.1, 38.8, 37.5, 37.2, 36.8, 31.9, 31.3, 29.7, 28.1, 28.0, 25.5, 24.7, 24.2, 23.4, 22.3, 21.1, 20.1, 19.4, 18.5, 12.2. IR (ATR FTIR): 3491, 2931, 1465, 1374, 1261, 1140, 1110, 1056, 1018, 978, 864. HRMS: [M+H]+, calc. 487.4151, obs. 487.4082; [M-OH]+, calc. 469.4046, obs. 469.4035

(3*S*,10*R*,13*R*,17*R*)-17-((2*S*,4*S*)-4-hydroxy-6-methylheptan-2-yl)-10,13-dimethyl-2,3,4,7,8,9,10,11,12,13,14,15,16,17-tetradecahydro-1H-cyclopenta[a]phenanthren-3-ol (**34**). The THP group was removed from OHC **THP-34** as described above for the preparation of **28**. Purification via flash chromatography (SiO_2, 20% EtOAc afforded) **34** as a white solid in excellent yield (0.035 g, 95%). ^{1}H NMR (500 MHz, $CDCl_3$) δ 5.39 (m, 1H), 3.82 (m, 1H), 3.57 (m, 1H), 2.30 (m, 2H), 2.03 (m, 2H), 1.88 (m, 3H), 1.79 (m, 1H), 1.62 (m, 3H), 1.58-1.48 (6H), 1.34 (m, 3H), 1.30 (s, 2H), 1.24-1.09 (4H), 1.05 (s, 3H), 0.97 (dd, 6H), 0.91 (d, 3H), 0.73 (s, 3H). ^{13}C NMR (126 MHz, $CDCl_3$) δ 140.80, 121.65, 71.81, 68.61, 56.76, 56.54, 50.17, 46.09, 44.83, 42.41, 42.32, 39.89, 37.27, 36.54, 32.57, 31.91, 31.69, 29.72, 27.46, 24.50, 24.13, 23.97, 21.69, 21.06, 19.41, 18.92, 12.30. IR (ATR FTIR): 3247, 2928, 1463, 1435, 1373, 1140, 1112, 1056, 1019 cm^{-1}. HRMS: $[M+NH_4]^+$, calc. 420.3842, obs. 420.3801; $[M-OH]^+$, calc. 385.3470, obs. 385.3434

(3*S*,10*R*,13*R*,17*R*)-17-((2*S*,4*R*)-4-hydroxy-6-methylheptan-2-yl)-10,13-dimethyl-2,3,4,7,8,9,10,11,12,13,14,15,16,17-tetradecahydro-1H-cyclopenta[a]phenanthren-3-ol (**35**). The THP group was removed from OHC **THP-35** as described above for the preparation of **28**. Purification via flash chromatography (SiO_2, 20% EtOAc in Hex) afforded **35** as a white solid in excellent yield (0.034 g, 96%). ^{1}H NMR (500 MHz, $CDCl_3$) δ 5.40 (m, 1H), 3.84 (m, 1H), 3.56 (m, 1H), 2.30 (m, 2H), 2.05 (m, 2H), 1.88 (m, 3H), 1.76 (m, 3H), 1.64-1.32 (m, 11H), 1.24-1.12 (m, 7H), 1.05 (s, 3H), 0.96 (d, 6H), 0.93 (d, 3H), 0.76 (s, 3H). ^{13}C NMR (126 MHz, $CDCl_3$) δ 140.8, 121.7, 77.3, 77.0, 76.8, 71.8, 67.4, 56.9, 56.8, 50.1, 48.0,

44.0, 42.4, 42.3, 40.1, 37.3, 36.5, 31.9, 31.8, 31.7, 28.1, 24.7, 24.2, 23.4, 22.3, 21.1, 19.4, 18.5, 12.2. IR (ATR FTIR): 3332, 2936, 1460, 1433, 1382, 1305, 1055, 952 cm^{-1}. HRMS: $[M+NH_4]^+$, calc. 420.3842, obs. 420.3839; $[M-OH]^+$, calc. 385.3470, obs. 385.3434.

Biological Assay Protocols:[109]

Cell Culture and Reagents: The murine cell line, M2-10B4, was purchased from American Type Culture Collection (ATCC). M2-10B4 cells were cultured in RPMI Medium 1640 (Gibco) supplemented with 10% FBS and 1% penicillin/streptomycin. Cells were maintained using the media described above (denoted "growth" media). Media denoted as "low FBS" contained 0.5% FBS and the same percentage of other supplements as specified for growth media. Cells were grown in Corning Cell Culture, canted neck T75 or T150 flasks (Fisher Scientific) in an Autoflow IR water-jacket CO_2 incubator. Experiments were performed in BD Falcon sterile 24-well tissue culture treated plates. Dimethyl sulfoxide (DMSO) was used as solvent to prepare all drug solutions and the final DMSO concentration did not exceed 0.3%. 20(*S*)-hydroxycholesterol was purchased from Sigma-Aldrich. Cyclopamine was purchased from LC Labs.

General Procedure for analysis of Hh target gene regulation:

A) Agonist assay: M2-10B4 cells were grown to confluence in T75 flasks. Once cells reached confluence, they were plated into 24-well plates at concentration of 50,000 cells/500 µL per well in growth media. After 24 h, growth media was removed and replaced with low FBS media (500 µL/well). Cells were treated with corresponding compound- DMSO, OHC, or OHC and cyclopamine. Cells were incubated (37°C, 5% CO_2) for noted time period, at which time mRNA was isolated and evaluated as described previously.

B) Antagonist assay: M2-10B4 cells were cultured and grown under same conditions as agonist assay. After 24 h in the plates, growth media was removed and replaced by low-FBS assay media. Specific upregulation method was administered for a final concentration of: (*S*)-OHC, 5 µM; SAG, 400 nM; rSHh, 0.5 ng/µL. For ASZ001 cells, cells were plated at concentration of 10,000 cells/well in a 96 well plate and

100uL media. After 24 h, media was removed and replaced with low-FBS media and drugged 24 h later. After 48 h, mRNA was isolated and evaluated.

General Procedure for RT-PCR analysis: Following treatment and incubation, total RNA was extracted using Ambion® by Life Technologies Taqman® Fast Cells-to-CT^{TM} kit following manufacturer's instructions. Synthesis of cDNA was performed using a BioRad MyCycler. Quantitative PCR was performed on an ABI 7500 system using the following Taqman Gene Expression Primer/Probe solutions (ABI): mouse ActB (Mm00607939_s1), mouse GLI1 (Mm00494645_m1), mouse PTCH1 (Mm00436926_m1), mouse ABCA1 (Mm00442646_m1), mouse Alp1 (Mm00475834_m1), mouse sp7 (Mm04209856_m1). Relative gene expression levels were computed via the ΔΔCt method. Values represent mRNA expression relative to DMSO control (vehicle; set to 1.00). Data was analyzed using GraphPad Prism 5 and IC_{50} and EC_{50} values represent mean ± SEM for at least two separate experiments performed in triplicate.

Computational Methods[117]

Homology modeling of hCRD

The amino acid sequence of full length human Smo was extracted from the UniProt database (Accession number: Q99835). The amino acid sequence corresponding to the hCRD (63-179) was truncated from the full length human Smo receptor sequence. A homology model of hCRD was generated using the crystal structure of the zCRD (PDB ID: 4C79, resolution 2.3 Å) as the template. Sequence alignment between the hCRD and zCRD was performed in ClustalX2 using PAM350 matrix with penalties of 10 and 0.05 for gap opening and gap elongation, respectively. The hCRD homology model was prepared by submitting the sequence alignment to MODELLER v9.16, which generates the three-dimensional structures of proteins by converting the sequence alignment into a large number of spatial restraints. These spatial restraints are further optimized by the molecular Probability Density Function (molPDF), which uses conjugate gradients and molecular dynamics with a simulated annealing procedure. Through this process, one hundred distinct

models of the hCRD were generated. The molPDF, DOPE, and GA341 scoring functions were used to identify the ten most probable hCRD models. The top model was selected by utilizing the PROCHECK server to assess the stereochemical quality of the minimized protein structure. The model chosen for our subsequent docking and molecular dynamics studies demonstrated high quality stereochemical parameters with an excellent distribution of Ψ and φ angels as determined by the Ramachandran plot.

Molecular Docking

The hCRD model was prepared for docking with the protein preparation wizard module from Schrödinger (Suite 2015). All ligand structures were built using the Maestro module of the Schrödinger Suite package and energy minimized using Macromodel with the OPLS_2005 force field. AutoDock v4.2 and its graphical user interface AutoDockTools v1.5.6 were used for the docking study and visualization of docked results. The R161 residue of the hCRD was kept flexible during the molecular docking. The three-dimensional affinity and electrostatic grid boxes were generated with AutoGrid v 4.2 to provide a gridcenter that covers the entire active site (− 14.126X, 14.481Y, and − 3.31Z) [26]. The number of grid points in the X, Y, Z axis was 40 × 40 × 40 with each point separated by 0.375 Å. Lamarckian genetic algorithm (LGA) was used as a search algorithm and a maximum number of $2.5 * 10^6$ energy evaluations was set. Ten docking runs were performed and the best scoring conformations were saved for analysis. The remaining parameters were left at their default settings. The reliability of the docking results was evaluated by comparing the root-mean-square deviations (RMSDs) of the conformations and grouping similar orientations into "clusters". From our ten docking runs of OHC **20**, nine conformations were oriented in the binding site in the manner described below. Similar results were obtained from the docking runs with OHCs. As the primary orientation closely matched the docking studies described previously we utilized this orientation for our molecular dynamics studies.

Molecular Dynamics

The starting structures for molecular dynamics (MD) were obtained from the docking of OHCs in complex with hCRD. The atomic partial charges of all the OHC analogues were derived by semiempirical AM1 geometry optimization using the general AMBER force field (GAFF). To neutralize the charge of the system, sodium counter ions were placed to grids with the largest negative coulombic potentials around the protein, and the whole system was immersed in the rectangular box of TIP3P water molecules. The water box extended 8 Å away from any solute atoms. In molecular minimization and molecular dynamics simulations, particle mesh Ewald (PME) was employed to treat the long-range electrostatic interactions. Before MD simulations, the complexes were gradually relaxed using 10,000 cycles of minimization procedure (500 cycles of steepest descent and 9500 cycles of conjugate gradient minimization). After minimization, MD simulations in the NPT ensemble with a target temperature of 298 K and a target pressure of 1 atm were performed. The SHAKE procedure was employed to constrain all hydrogen atoms and the time step was set to 2.0 Fs. Before the actual MD simulations, the system was gradually heated in the NVT ensemble from 10 K to 298 K over 50 ps. Initial velocities were assigned from a Maxwellian distribution at the starting temperature. MD samplings at 5 ns were performed for all complexes.

MM/GBSA Calculations[117]

In MM/GBSA calculations, the affinity of a ligand binding to a protein can be estimated by two protocols: (1) evaluate all terms using separate trajectories of complex, protein, and ligand (separate trajectory protocol) or (2) evaluate the snapshots from a trajectory of the complex (single trajectory protocol). The single trajectory protocol was used in our studies because it is a more rapid procedure and the calculation is based upon straightforward energy equations. For specific equations please see Reference 117.

Modulation of the Hedgehog Signaling Pathway by Sterol-based Small Molecules

Chad Anthony Maschinot

Chapter 3:

Inhibition of Hedgehog Signaling by Vitamin D-Based Analogues

Introduction

As discussed in previous chapters, the Hedgehog (Hh) signaling pathway may be modulated by a number of small molecule scaffolds from sterols to larger multi-cyclic compounds like itraconazole (**4**). Development of small molecule modulators of Hh signaling has primarily focused on the design of inhibitors as anti-cancer chemotherapeutics. With the importance of cholesterol and oxysterols to Hh signaling, it is not surprising that another sterol scaffold, vitamin D (**Figure 16**) regulates Hh signaling.

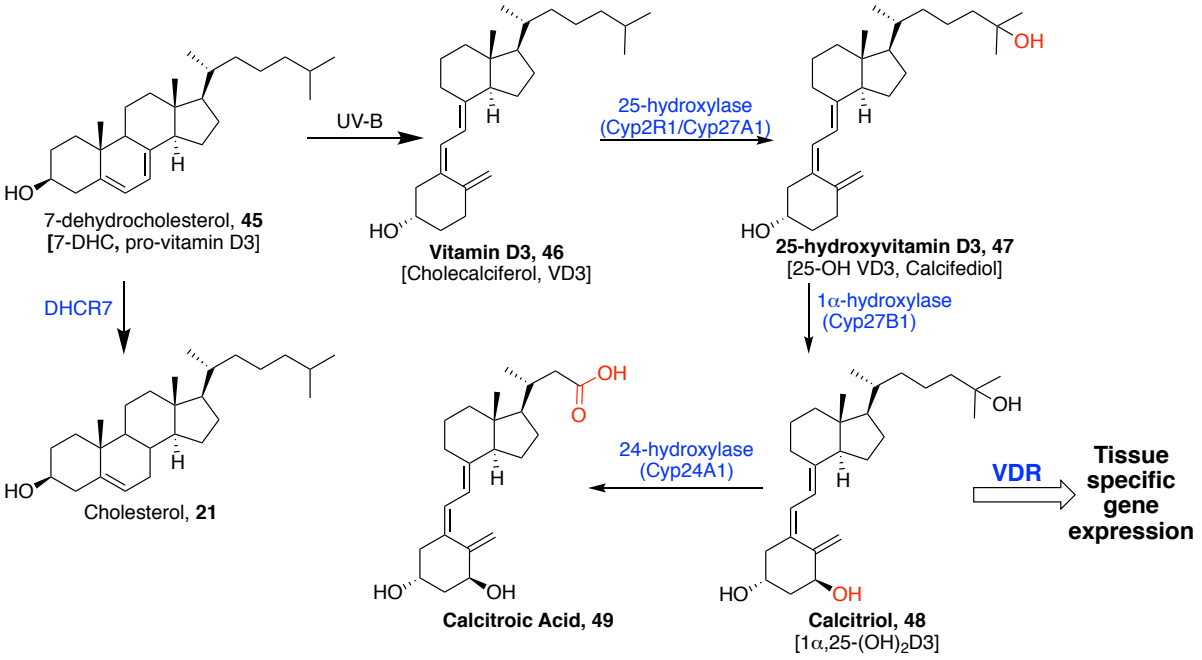

Figure 16. Vitamin D pathway and metabolism. VD3 is produced in the skin from 7-DHC under UV-B light from the sun and further hydroxylated at the C-25 position by Cyp2R1 (or Cyp27A1) in the liver to 25-OH VD3. Cyp27B1 further metabolizes 25-OH VD3 in the kidney to the biologically active metabolite calcitriol, which regulates a variety of genes through the vitamin D receptor (VDR), including Cyp24A1 which ultimate degrades calcitriol to calcitroic acid for removal. Blue=enzymatic activity, Red=Cyp hydroxylation.

I. Vitamin D Metabolism

The vitamin D metabolism pathway (**Figure 16**) is a highly regulated and complex process leading to activation of the vitamin D receptor (VDR) by its natural ligand, calcitriol (**48**). Production of calcitriol starts with the cholesterol precursor, 7-dehydrocholesterol (pro-vitamin D3, pro-VD3, **45**). In the skin, ultraviolet (UV) light, specifically UV-B, promotes the opening and isomerization of the B-ring of **45** in a two-step process to form vitamin D3 (cholecalciferol, VD3, **46**) in a temperature sensitive and non-catalytic

process.[121] Vitamin D3 can also be obtained through diet and supplementation, which is important with inconsistent production throughout the year due to varying UV-B intensity from the sun and protection from clothing and melanin in the skin.[122] A hydroxyl group is then added to the C-25 position by Cyp27A1 or Cyp2R1, where Cyp27A1 is the only mitochondrial 25-hydroxylase found throughout the body and Cyp2R1 is only found in the liver and testes.[123-124] It does appear that Cyp2R1 is the major 25-hydroxylase utilized but multiple knockout studies have suggested that other enzymes possessing 25-hydroxylase activity may be utilized with no complete reduction observed in circulating levels of 25-hydroxyvitamin D3 (25-OH VD3, calcifediol, **47**).[124] Calcitriol is further metabolized by Cyp24A1 and undergoes oxidative truncation to calcitroic acid (**48**). Importantly, Cyp24A1 is the only 24-hydroxylase shown to participate in vitamin D metabolism and is a key target gene of the vitamin D receptor (VDR), denoting a primary function of regulating cellular levels of calcitriol.[122]

II. Vitamin D and Hh signaling

With no reports of biological activities for the other metabolites, calcitriol (**48**) was long considered the biologically active metabolite, mediating its activity through VDR. In 2006, 7-DHC (**45**) was initially proposed to be an endogenous regulator of Hh signaling.[125] These studies were initially designed to identify and study the mechanism by which Ptch represses Smo activation through *Ptch1* small interfering RNA and transfection. The researchers compared the ability of media from the *Ptch1*-transfected cells and media of control-transfected cells to inhibit Hh signaling in reporter cells. The observed strong inhibitory effects on Gli activation for the *Ptch1*-transfected medium. When the media was analyzed, elevated levels of 3β-hydroxysteroids were observed in the *Ptch1*-transfected media. Furthermore, *Ptch1* siRNA decreased levels of 3β-hydroxysteroids and increased Gli reporter activity. These observations suggested that a 3β-hydroxysteroid may be an endogenous inhibitor of Hh signaling. In follow-up studies, VD3 (**46**) was identified as the hydroxysteroid scaffold responsible for inhibition of Hh signaling. This was based on

endogenous addition of VD3 being more efficient in inhibiting Gli reporter activity than the *Ptch1*-transfected medium.[125-126]

Since these studies, VD3 has been shown to inhibit Hh signaling in multiple *in vitro* and *in vivo* models. At moderate concentrations (5 and 10 μM), VD3 inhibited proliferation and reduced Gli1 expression in murine models of BCC (ASZ001, *Ptch*-deficient)[118] and MB, which both exhibit upregulated Hh signaling.[127] Accumulation of VD3, through inhibition of Cyp2R1 or exogenous addition, has been shown to antagonize Hh signaling by proposed direct interaction with the extracellular region of Smo.[128]

Based on these findings and observations that VD3 was capable of activating VDR activity, presumably through *in vitro* metabolism, multiple series of VD3 analogues were designed and synthesized by previous Hadden lab members to probe and selectively target Hh signaling (**Figure 17, Table 8**).[125,127,129-133] These studies were aimed at probing the structural requirements of the A- and *seco*-B rings, and alkyl-side chain, and provided the representative analogues **51** - **57**.

The initial studies performed by former lab members demonstrated that the northern region of VD3 (CD-rings and alkyl side chain) was required to inhibit Hh signaling, as Grundmann's alcohol (**50**) maintained anti-Hh activity comparable to VD3. Grundmann's alcohol also showed reduced activation of VDR, measured by Cyp24A1 mRNA expression.[129] To quickly study the effects that A-ring modifications

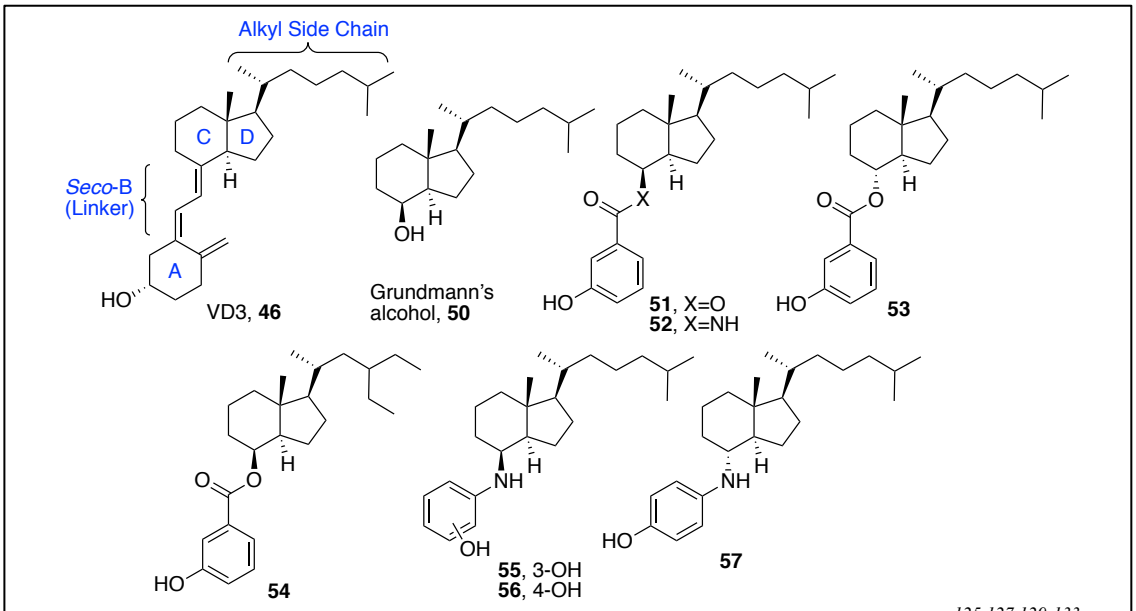

Figure 17. Representative A- and *seco*-B ring analogues previously developed.[125,127,129-133]

had on activity, a variety of A-ring mimics were coupled to **50** through an ester *seco*-B ring (synthesized by a former postdoctoral researcher, Dr Albert M. DeBerardinis).[131] These studies indicated that the incorporation of an aromatic A-ring, specifically a phenol (**51**) greatly increased anti-Hh potency from ~4 mM to ~700 nM in C3H MEFs. Unfortunately, **51** showed little consistency across cell lines with ~7-fold loss in potency between C3H and ASZ cells. Taken together with potential metabolic instability due to the ester *seco*-B, analogue **52** was synthesized with an amide *seco*-B to potentially increase stability. Analogue **52** showed similar potency in C3H cells but also showed improved consistency and potency in ASZ cells with ~2-fold loss in potency.[133]

Table 8. Inhibition of Hh signaling by lead VD3 analogues. [125,127,129-133]

	C3H MEFs			ASZ (BCC model)	
	Hh Activity[a]	**Cyp24A1[b]**	**IC_{50} (Gli1, μM)[c]**	**IC_{50} (Gli1, μM)[c]**	**Cyp24A1[b]**
VD3 (**46**)	36 ± 0.3	8,300 ± 38	4.1 ± 0.3	1.1 ± 0.01	2,200 ± 200[d]
50	46 ± 4	3.6 ± 0.5	3.1 ± 0.2	> 10	2.4 ± 0.9
51	1.9 ± 0.5	22 ± 5	0.74 ± 0.1	5.2 ± 0.2	1.9 ± 0.1
52	2.5 ± 0.1	7.0 ± 0.9	0.98 ± 0.04	1.8 ± 0.3	1.8 ± 0.2
53	31 ± 3	3.0 ± 0.5	3.9 ± 0.8	6.3 ± 1	1.6 ± 0.2
54	2.9 ± 0.3	2.8 ± 0.03	1.1 ± 0.6	1.6 ± 0.2	~10[e]
55	12 ± 0.01	17 ± 4	1.0 ± 0.1	1.7 ± 0.1	1.8 ± 0.1
56	0.7 ± 0.2	45 ± 20	0.40 ± 0.02	0.67 ± 0.02	2.7 ± 0.7
57	1.3 ± 0.6	21 ± 3	0.32 ± 0.06	0.57 ± 0.2	3.0 ± 0.8

[a]Values represent % Gli1 mRNA expression compared to OHC control (set to 100) at 5 μM. [b]Values represent relative Cyp24A1 mRNA expression compared to DMSO control (set to 1.0) at 5 μM. [c]Values represent average of at least two separate experiments performed in triplicate. [d]Compound tested at 2.5 μM, [e]Estimate based on figure (ref 132).

The stereochemistry of the CD-rings and alkyl side chain is preset for analogue development by the synthetic approach taken, as will be discussed later in this chapter; however, Dr DeBerardinis was able to invert the orientation of hydroxyl position of **50** to give ester **53**.[133] Comparison of **51** and **53** suggested that the stereochemistry of the *seco*-B region may not be important as the Gli1 IC_{50} values in ASZs were comparable. It was also determined by a former graduate student, Dr Upasana Banerjee, that the "natural" alkyl side chain is the most favorable, as **54** was the most potent analogue in the alkyl side chain studies and only showed activity comparable to **51**.[132] To further investigate the *seco*-B region, a variety of functionalities were incorporated with the phenolic A-ring.[133] Out of these compounds, the most potent

analogues were the single atom nitrogen *seco*-B (amine) analogues **55-57**. One important observation from this series was the consistency across cell lines and increased potency compared to the esters and two atom *seco*-B analogues. Additionally, the amines followed the same trend as the ester analogues where the stereochemistry of the *seco*-B region was not important for the amine analogues as **56** and **57** showed comparable activities across cell lines.

Based on these results and observations, additional analogue series were designed to continue SAR studies. With the specific mechanism of action for inhibition of Hh signaling by vitamin D unclear, these series were also aimed at probing the mechanism of action. These analogue series were broken down into three categories: (1) C-11 modified, (2) amine *seco*-B, and (3) C-25 functionalized analogues.

III. Design and Synthesis of Vitamin D Analogues

A. C-11 Modified Analogues[134]

With the primary mechanism of action for inhibition of Hh signaling by vitamin D analogues unclear, a focus was made on developing probes that could be modified by a biotin or fluorescent tag to identify the protein targets. Based on previous studies indicating that the CD-rings and alkyl side chain were required to maintain anti-Hh activity, a new series of analogues were designed with additions to the C-ring. These analogues were designed to (1) probe the binding pocket for additional interactions and spatial requirements and (2) determine if this position is suitable for label attachment.

The C-11 position was chosen for this series primarily because synthetic routes to append functional groups at this position are well-characterized and straightforward. Utilizing standard procedures, Grundmann's ketone (**58**) can be obtained in high yield from VD3 in two steps via global ozonolysis with a reductive workup and oxidation of **50** (**Scheme 3**). α,β-unsaturation of the ketone was achieved through Saegusa-Ito oxidation of the silyl enol ether intermediate to give enone **59**. A slight modification to the published route to access **59**,[135] addition of *p*-benzoquinone as a co-oxidant to regenerate Pd (II), resulted in an increased yield. The desired alkyl functionalities were added to the C-11 position via 1,4-organocuprate addition. *In situ* formation of the organocuprate from the corresponding Grignard reagent

provided a one-pot reaction to obtain the desired ketones (**60a**–**e**) in a stereoselective fashion. Standard sodium borohydride reduction followed by esterification and deprotection provided the desired esters (**61a,c**–**e**). The C-11 stereochemistry was determined by analysis of the ^{1}H NMR spectra in which the C-18 proton peak demonstrates a characteristic shift, similar to that previously reported.[135-136] Due to A1,3-strain in the C-ring, an interaction between the C-11 substituent and the C-18 methyl group would result in a downfield shift of the C-18 singlet, similar to what is observed when **52** is reduced to Grundmann's alcohol. Following the 1,4-addition to **59**, the C-18 methyl peak was observed at 0.6–0.8 ppm for **60b**–**60e**, indicating the α-orientation. For **60a**, an interaction with the C-18 methyl peak (1.1 ppm) was observed, indicating the β-orientation.

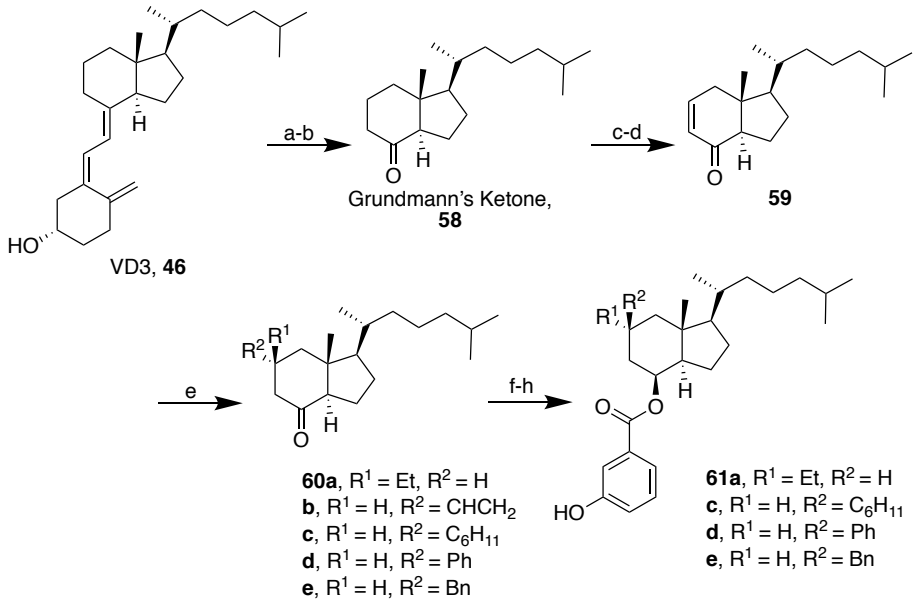

Scheme 3. Reagents and conditions: (a) i. O_3, pyridine, DCM:MeOH; ii. $NaBH_4$; 90% (b) PDC, DCM; 94% (c) i. LDA, THF; ii. TMSCl; (d) $Pd(OAc)_3$, *p*-benzoquinone, MeCN; 78% over two-steps; (e) R-MgBr, CuI, THF; 62–90% (f) $NaBH_4$, MeOH; (g) 3-OMOM-benzoic acid, DCC, DMAP, DCM; (h) (±)-CSA, MeOH; 17–32% over three-steps.

It is well-established that the reduction of **58** to Grundmann's alcohol with sodium borohydride is a highly stereoselective process that results in the β-alcohol due to the concavity and sterics of the CD-ring system favoring backside hydride addition.[137] We believe that the cuprate addition works in a similar fashion and the steric bulk of the **60b**–**e** C-11 substituents results in α-addition to minimize the A1,3-strain. The smaller ethyl substituent, in comparison to the larger ring systems, decreased the favorability for the α-orientation by reducing the potential A1,3-strain between the C-11 substituent and the C-18 methyl groups, resulting in β-substitution.

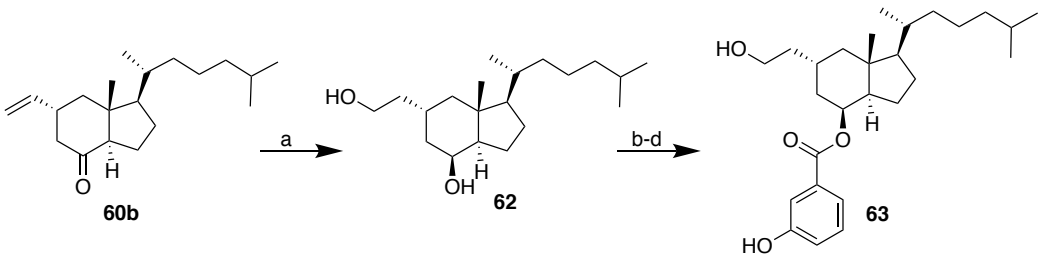

Scheme 4. Synthesis of C-11 modified analogues: (a) i. 9-BBN, THF; ii. NaOH, H_2O, H_2O_2, MeOH; 90% (b) TBSCl, imidazole, DCM; 88% (c) 3-OMOM-benzoic acid, DCC, DMAP, DCM; 55% (d) CSA, MeOH 65%.

In addition to incorporating hydrophobic functionalities, we also sought to append a hydroxyl moiety at C-11 to not only probe its effects on Hh inhibition, but also to provide a chemical handle for attaching a terminal alkyne. Analogues incorporating a terminal alkyne hold potential as probes to identify cellular proteins that bind the VD3 scaffold and mediate its anti-Hh effects. Hydroboration of the terminal olefin in **60b** with 9-borabicyclo(3.3.1)nonane (9-BBN) and reduction of the resulting aldehyde provided diol **62** (**Scheme 4**).[136] Selective protection of the primary alcohol at C-11, followed by esterification at the secondary alcohol and global deprotection provided analogue **63**.

To incorporate the terminal alkyne, selective oxidation of the secondary alcohol in **62** with 2-iodoxybenzoic acid (IBX)[138] afforded ketone **64**, allowing for esterification of the C-11 side chain hydroxyl

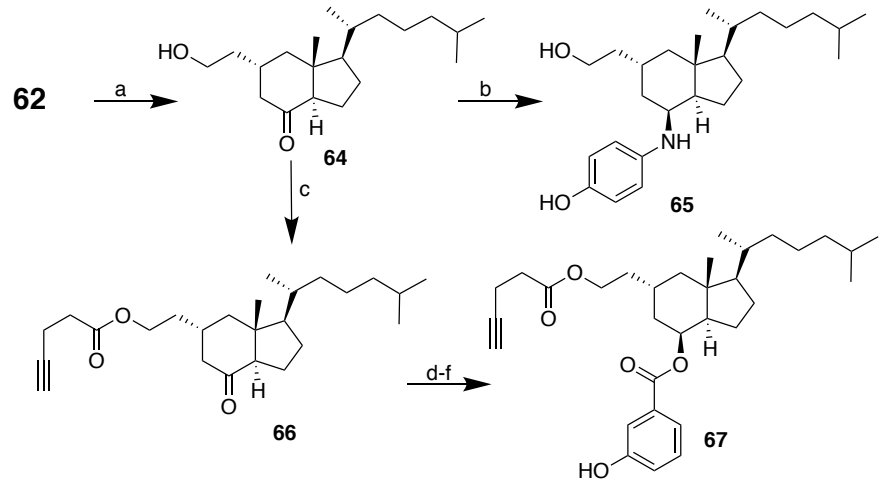

Scheme 5. Synthesis of C-11 modified analogues: (a) IBX, tetrabutylammonium bromide, DCM:H_2O; 75% (b) 4-aminophenol, $NaBH(OAc)_3$, AcOH, DCE; 12% (c) 4-pentynoic acid, DCC, DMAP, DCM; 91% (d) $NaBH_4$, MeOH; 67% (e) 3-OMOM-benzoic acid, DCC, DMAP, DCM; 60% (f) CSA, MeOH; 15%.

(**66**, **Scheme 5**). Reduction of the ketone carbonyl followed by esterification and deprotection of the phenolic 3-hydroxy A-ring yielded ester **67** in low yield. The low yield can be partially attributed to the deprotection step, which also partially cleaves the side chain ester. As noted above, our most potent VD3 analogue, **56**, incorporates a single atom amine *seco*-B between the CD-ring/side chain and the aromatic A-ring. Ketone **58** provided an opportunity to synthesize an amine linked analogue of **59** to see if the same SAR trend would be observed. Using a previously described and utilized reductive amination method with sodium triacetoxyborohydride,[139] analogue **65** was obtained from **64** as a single isomer.

B. Amine Seco-B Analogues

One of the most notable observations from previously developed analogues was a switch in the preferred A-ring hydroxyl position. When the *seco*-B region was shortened from two atoms (ester **51**) to a single atom (amines **55** - **56**), the *para*-position (**56**) was favored over the *meta* (**55**). This resulted in a ~2.5-fold difference in potency with IC_{50} values of 0.40 – 0.67 μM and 1.0-1.7 μM for **56** and **55** respectively. In the ester series, there was a 4-fold difference in potency in C3H cells favoring the 3-hydroxyl position with IC_{50} values of 0.74 and 2.8 μM for the 3-hydroxyl (**51**) and 4-hydroxyl esters respectively.[131] A second notable observation was that there was little difference between the standard α-orientation (**56**) and β-orientation of the *seco*-B region (**57**).

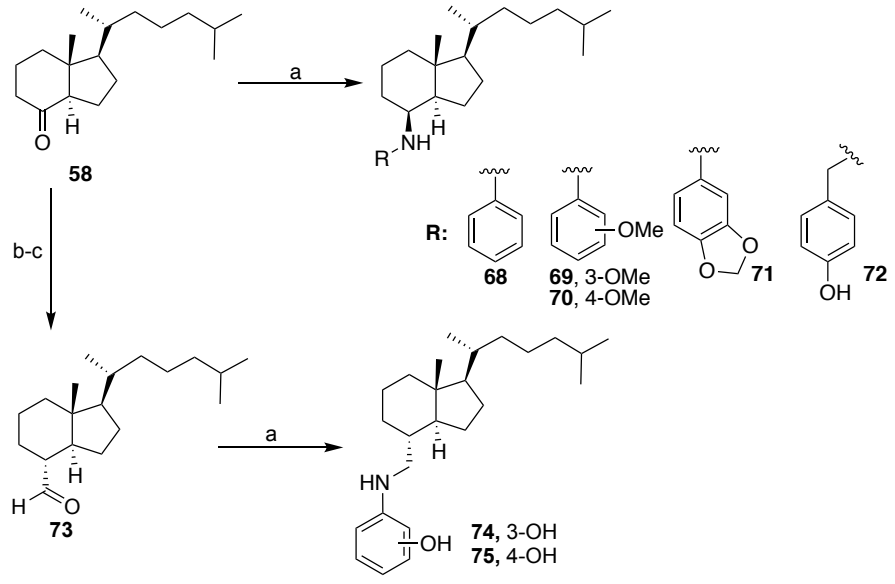

Scheme 6. Synthesis of amine *seco*-B analogues: (a) $NaBH(OAc)_3$, AcOH, R-amine, DCE; 20 – 65% (b) $PPh_3Cl(MeOMe)$, NatBuO, THF; 89% (c) 2N HCl, MeOH; 75%.

Taken with similar results for ester analogues **51** and **53**, it suggests that preference for a specific C-8 stereoisomer may not exist. With these differences observed, we designed a new series of analogues: (1) further evaluate if any other previous observations from the initial ester series[131] were altered with the shortening of the *seco*-B region, and (2) determine how lengthening of the nitrogen *seco*-B region back to two atoms by the addition of a methylene (CH_2) group would affect the inhibitory activity.

Synthesis of the nitrogen *seco*-B analogues is centered around the one pot reductive amination of the desired amine with Grundmann's ketone (**58**) or the methylene extended aldehyde (**73**). Reductive amination of **58** with sodium triacetoxy borohydride and the desired anilines yielded amines **68** – **72** (**Scheme 6**). To extend the *seco*-B region, **73** was obtained as a single isomer in high yield following hydrolysis of the enol ether obtained through a Wittig reaction with sodium *tert*-butoxide and methyoxymethyl triphenylphosonium chloride, as previously described.[133] The same reductive amination procedure was applied to give **74** – **75**.

C. C-25 Functionalized Vitamin D Analogues

After VD3 was shown to inhibit Hh signaling in 2006,[124] follow-up studies indicated that differences existed between the vitamin D metabolites.[126] It appears that as you move down the metabolic pathway from VD3 to calcitriol, the metabolites are more active against Hh signaling following the addition of hydroxyl groups to the alkyl side chain (C-25, **47**) and the 1α–position of the A-ring (**48**), **Figure 16**. With calcitriol being the biologically active metabolite and a decrease in potency previously observed with dihydroxylated analogues,[131] we designed a new series of analogues based on 25-OH VD3 (**47**) in which a C-25 hydroxyl group was incorporated. In anticipation of inducing higher VDR activation, additional analogues with a C-25 methyl ether were designed.

Using Grundmann's ketone (**58**) as a starting material, introduction of the C-25 hydroxyl moiety was performed using ruthenium (III) chloride and sodium periodate to generate ruthenium tetroxide *in-situ* (**Scheme 7**).[140] Due to steric hindrance and interactions throughout the molecule, such as those between the C-18 methyl and C-20 group, selective hydroxylation at the C-25 position was observed to give **76** in

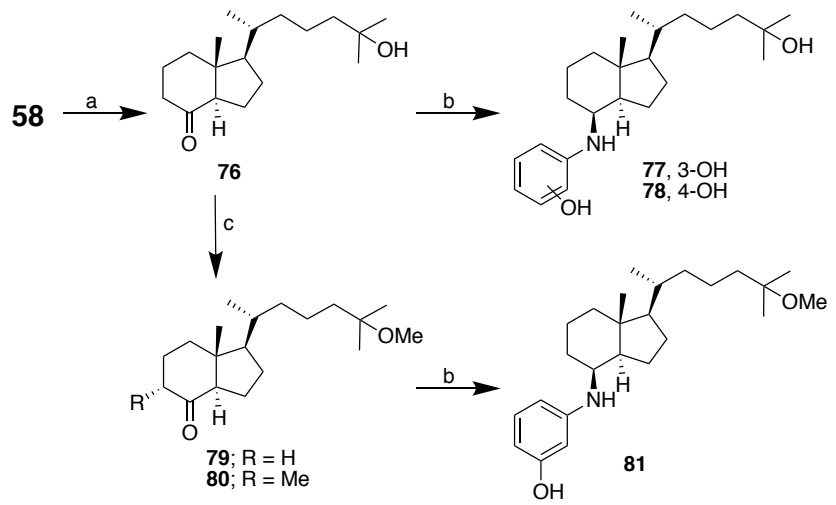

Scheme 7. Synthesis of C-25 functionalized amine analogues: (a) $RuCl_3$, $NaIO_4$, pyridine, MeCN:H_2O; 67% (b) $NaBH(OAc)_3$, AcOH, R-amine, DCE; 15 – 35 % (c) MeI, NaH, DMF; 25 %.

moderate yield (67%). Amines **77** – **78** were then obtained in one-step via the sodium triacetoxy borohydride reductive amination method previously utilized. Ether-ification at the C-25 position was performed using methyl iodide and sodium hydride to give **79** in low yield due to α-methylation at C-9. It is believed that α - methylation occurs following the desired etherification due to the presence of **79** and the "di-methylated" byproduct **80,** which showed both C-25 etherification and α-methylation. Only C-9 α-methylation was not observed. Reductive amination of **79** provided **81** in moderate yield.

To synthesize C-25 hydroxylated versions of **74** – **75**, a similar approach was taken where Wittig addition followed by enol ether hydrolysis yielded aldehyde **82** as a single isomer, **Scheme 8.** Reductive

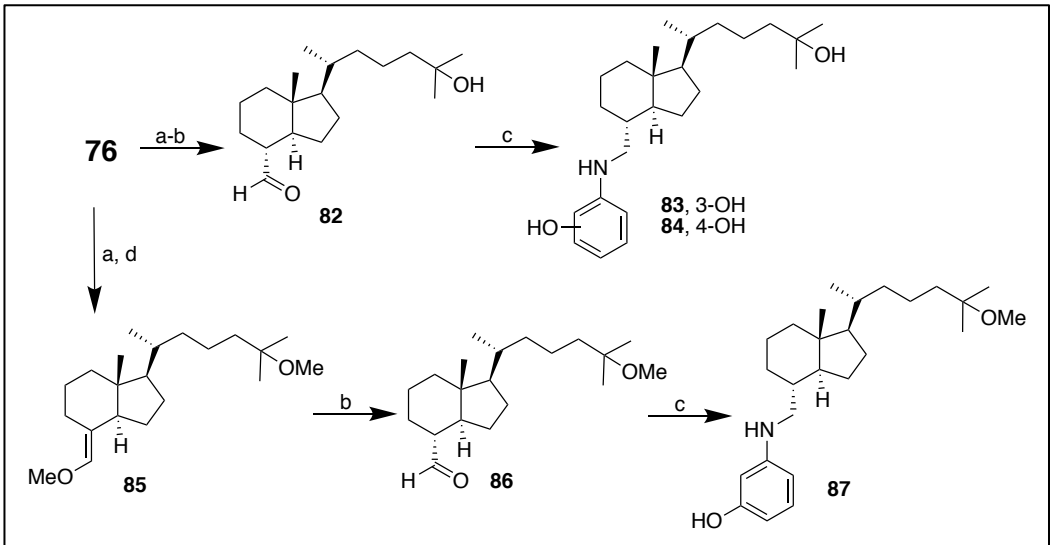

Scheme 8. Synthesis of C-25 functionalized extended amines. (a) $PPh_3Cl(MeOMe)$, NatBuO, THF; 89 % (b) 2N HCl, MeOH; 60 - 75% (c) $NaBH(OAc)_3$, AcOH, R-amine, DCE; 32 – 59 % (d) MeI, NaH, DMF; 62%.

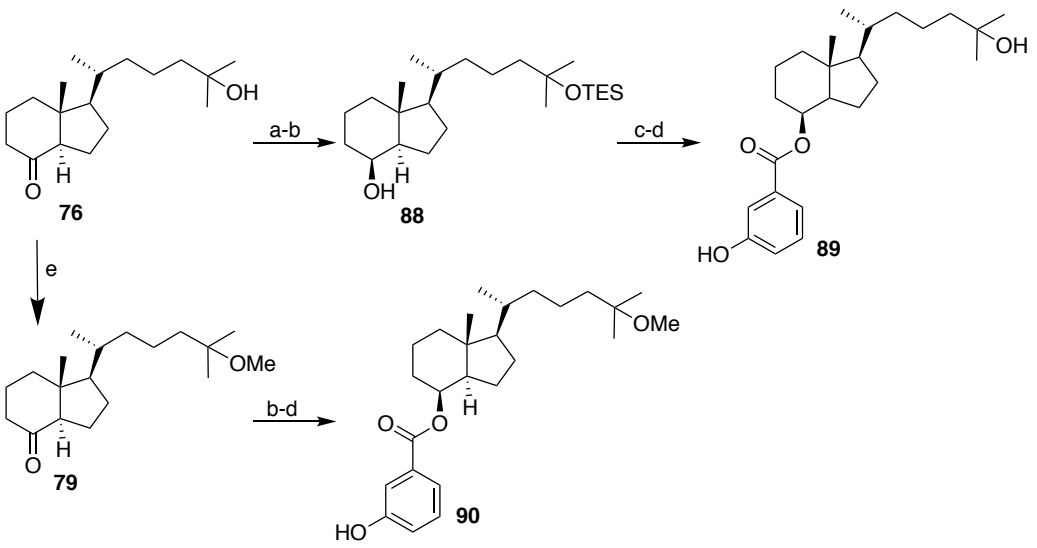

Scheme 9. Synthesis of C-25 functionalized ester analogues. (a)TES-Cl, imidazole, DMF; 94% (b) $NaBH_4$, MeOH:DCM; 88 - 92% (c) 3-OMOM-benzoic acid, DCC, DMAP, DCM; 52 - 70% (d) CAS, MeOH; 60 - 75% (e) MeI, NaH, DMF; 35%.

amination of **82** provided amines **83** – **84**. Since α-methylation was observed in the C-25 etherification of **58**, etherification of the C-25 hydroxyl group was performed on the enol ether intermediate, **85**, in moderate yield. Following hydrolysis of **85** to the corresponding aldehyde (**86**), reductive amination yielded amine **87.**

Ketone **76** provided the starting material for the synthesis of esters **89** - **90**. Protection of the C-25 hydroxyl group with triethyl silane (TES) followed by sodium borohydride reduction gave alcohol **88** (**Scheme 9**). Triethyl silane provided a useful protecting group due to the ability to remove both the C-25 TES-group and the MOM-protecting group in a single reaction with camphor sulfonic acid (CSA). Following esterification with 3-OMOM-benzoic acid, both the C-25 TES- and phenolic MOM-groups were removed in moderate yield to give ester **89**. Similarly, ester **90** was obtained in three steps from ketone **79**.

IV. Biological Evaluation of Vitamin D Analogues

Each of the synthesized analogues were evaluated in the C3H10T1/2 (C3H) mouse embryonic fibroblast (MEF) cell line to determine their ability to inhibit Hh signaling. Their ability to modulate Hh activity was measured through qPCR quantification of the Hh target gene, *Gli1*. In this cell

line, activation of Hh signaling via the addition of known Hh agonists (OHCs **20** and **22** at 5 μM each) results in reproducible *Gli1* mRNA up-regulation that is attenuated by inhibitor co-administration. For these studies, *Gli1* mRNA expression was normalized to oxysterol controls (set to 100) and all compounds were initially evaluated at 5 μM (**Tables 9 - 11**). To measure the selectivity of each compound for Hh signaling over canonical VDR signaling, the VDR target gene *Cyp24A1* was also quantified. The ability of more potent analogues to inhibit Hh signaling was further evaluated in ASZ001 cells, a murine Hh-dependent BCC cell line. Similar to evaluation of OHCs in Chapter 2, the mRNA was extracted using the commercially available Cells-to-Ct (ThermoScientific) and quantified by qPCR.

A. *Evaluation of C-11 Modified Analogues (**60** – **67**)*

Interestingly, the only hydrophobic C-11 substitution that retained the anti-Hh activity of **51** was **61a**, in which the smaller ethyl substituent is in the α-orientation (**Table 9**). By contrast all of the analogues with

Table 9. Inhibition of Hh signaling by C-11 modified VD3-analogues.[134]

	C3H MEFs[a]			ASZ Cells[a]	
	Hh Activity[b]	**Cyp24A1[c]**	**IC_{50} (Gli1, μM)**	**IC_{50} (Gli1, μM)[b]**	**Cyp24A1[c]**
OHCs	100	---	---	---	---
DMSO	---	1.0	---	---	1.0
GDC-0449	0.88 ± 0.01	1.0 ± 0.02	0.082 ± 0.007	0.040 ± 0.01	0.9 ± 0.2
VD3 (**46**)	36 ± 0.3	8,300 ± 40	4.1 ± 0.3	1.1 ± 0.01	2,200 ± 200[d]
51[d]	1.9 ± 0.5	22 ± 5	0.74 ± 0.1	5.2 ± 0.2	1.9 ± 0.1
56[d]	0.7 ± 0.2	45 ± 20	0.40 ± 0.02	0.67 ± 0.2	2.7 ± 0.7
60b	28 ± 5.0	19 ± 3	---	---	---
61a	2.0 ± 0.9	3.6 ± 3	0.92 ± 0.1	5.2 ± 0.5	1.3 ± 0.3
61c	92 ± 3	2.8 ± 1	---	---	---
61d	71 ± 10	2.3 ± 0.6	---	---	---
61e	85 ± 10	3.6 ± 1	---	---	---
62	39 ± 4	17 ± 1	4.7 ± 0.3	---	---
63	8.7 ± 2	9.0 ± 4	2.0 ± 0.2	4.1 ± 2.4	1.1 ± 0.1
65	1.1 ± 0.6	7.2 ± 2	2.7 ± 0.2	1.0 ± 0.01	2.0 ± 0.4
67	16 ± 2	4.8 ± 2	6.3 ± 3	7.5 ± 2	0.96 ± 0.2

[a]Values represent Mean ± SEM for at least two separate experiments performed in triplicate. [b]Values represent % *Gli1* mRNA expression relative to oxysterol control (set to 100). Analogues evaluated at 5 μM. [c]Values represent *Cyp24A1* mRNA expression compared to DMSO control (set to 1.0). Analogues evaluated at 5 μM. [d]Values for previously published analogues are from Reference 133.

a hydrophilic β-substituent (**62-63**, **65**, **67**) maintained activity, suggesting that larger and more rigid functional groups, such as the cyclohexyl and benzyl groups of **61c** and **61e** respectively, prevent full access of the compound to the binding pocket when they are in the β-conformation. When the lead analogues **51** and **56** were compared to their C-11 functionalized counterparts (**61a**, **63** and **65)** the functionalization increases selectivity for Hh signaling over canonical VDR. Compounds that inhibited Hh signaling at a level equal to or greater than VD3 at 5 μM were evaluated for their ability to inhibit Hh signaling in this cell line in a concentration-dependent fashion (**61a**, **62**–**63**, **65**, and **66**).

Each of these analogues demonstrated moderate concentration-dependent inhibition of Hh signaling with IC_{50} values between 0.92 and 6.3 μM. Notably, incorporation of the primary alcohol at the C-11 position (**63, 65**) resulted in an approximately 6.5-fold loss in Hh inhibitory activity. In addition, there was only a moderate loss in activity for the terminal alkyne (**67**), suggesting its potential as a chemical probe for studying VD3-mediated inhibition of Hh signaling. Next, we evaluated the ability of several of these analogues to inhibit Hh signaling in ASZ001 cells, a murine Hh-dependent BCC cell line. Similar to previous studies with VD3 analogues,[131] a modest loss in potency was observed for the ester analogues (**61a**, **63**, **67**) in the ASZ001 cells (**Table 9**). With minimal up-regulation of Cyp24A1 observed across either cell line compared to **46**, these results support the hypothesis that VD3 analogues act independent of VDR to inhibit Hh signaling. The decrease in Cyp24A1 expression compared to **51** and **56**, suggests that even small additions to the C-ring is enough to disrupt binding within the narrow ligand binding domain of VDR and reduce activation of canonical VDR signaling.

*B. Evaluation of Amine seco-B Analogues (**68** – **75**)*

Similar to previous observations with a series of ester analogues,[131] removal or masking of the aromatic hydroxyl group (**68** – **71**) resulted in complete loss of anti-Hh activity (**Table 10**). More intriguing results were observed when the *seco*-B region was extended back to two atoms. Compared to **56**, amine **72** showed a moderate loss in anti-Hh activity and a slight gain in selectivity over VDR activation in C3H cells. In

Table 10. *In vitro* evaluation of amine *seco*-B analogues.

	C3H MEFs[a]			ASZ Cells[a]	
	Hh Activity[b]	**Cyp24A1[c]**	**IC_{50} (Gli1, μM)**	**IC_{50} (Gli1, μM)**	**Cyp24A1[c]**
OHCs	100	---	---	---	---
DMSO	---	1.0	---	---	1.0
GDC-0449	0.88 ± 0.01	1.0 ± 0.02	0.082 ± 0.007	0.040 ± 0.01	0.9 ± 0.2
VD3 (**46**)	36 ± 0.3	8,300 ± 40	4.1 ± 0.3	1.1 ± 0.01	2,200 ± 200 [e]
51[d]	1.9 ± 0.5	22 ± 4	0.74 ± 0.1	5.2 ± 0.2	1.9 ± 0.1
55[d]	12 ± 0.01	17 ± 4	1.0 ± 0.1	1.7 ± 0.1	1.8 ± 0.1
56[d]	0.7 ± 0.2	45 ± 20	0.40 ± 0.02	0.67 ± 0.2	2.7 ± 0.7
68	98 ± 10	1.2 ± 0.1	>10	--	--
69	110 ± 10	1.9 ± 0.5	>10	--	--
70	73 ± 7	2.4 ± 0.9	>10	--	--
71	110 ± 1	6.1 ± 3	>10	--	--
72	4.6 ± 0.1	24 ± 0.8	3.1 ± 0.1	0.34 ± 0.02	1.1 ± 0.7 [e]
74	13 ± 8	13 ± 5	3.8 ± 0.7	1.2 ± 0.07	7.8 ± 2 [e]
75	1.9 ± 1	8.9 ± 2	0.59 ± 0.2	0.56 ± 0.08	5.8 ± 4 [e]

[a]Values represent Mean ± SEM for at least two separate experiments performed in triplicate. [b]Values represent % *Gli1* mRNA expression relative to oxysterol control (set to 100). Analogues evaluated at 5 μM. [c]Values represent *Cyp24A1* mRNA expression compared to DMSO control (set to 1.0). Analogues evaluated at 5 μM. [d]Values for previously published analogues are from Reference 133. [e]Analogue evaluated at 2.5 μM.

ASZ cells, **72** had improved activity and selectivity, and became the most potent and selective analogue. When the arrangement of the *seco*-B atoms was switched, **74** – **75**, the location of the hydroxyl group became more of a contributing factor as **75** (4-OH) showed greater potency compared to **74** (3-OH), a trend similar to the ester series as well.[131] A second noticeable result was the comparable activities for **56** and **75** in both cell lines. Comparing the activities of **56**, **72**, and **75** suggests that the aromatic A-ring may play a role in aligning the NH- group of the *seco*-B region and the northern region for binding interactions.

*C. Evaluation of C-25 Functionalized Vitamin D Analogues (77 – **90**)*

Differing results were obtained by the incorporation of the C-25 hydroxyl group or methyl ether (**Table 11**). Compared to the non-hydroxylated versions **55** – **56**, the single atom *seco*-B analogues **77** – **78** showed a slight increase in anti-Hh activity in ASZ cells along with significant upregulation of *Cyp24A1* mRNA to levels comparable to vitamin D metabolites. Masking the C-25 hydroxyl as a methyl ether (**81**) was able to

Table 31. *In vitro* evaluation of C-25 functionalized vitamin D analogues.

	C3H MEFs[a]			ASZ	
	Hh Activity[b]	**Cyp24A1[c]**	**IC_{50} (Gli1, μM)[d]**	**IC_{50} (Gli1, μM)[d]**	**Cyp24A1[c,e]**
OHCs	100	---	---	---	---
DMSO	---	1.0	---	---	1.0
GDC-0449	0.88 ± 0.01	1.0 ± 0.02	0.082 ± 0.007	0.040 ± 0.01	0.9 ± 0.2
46	36 ± 0.3	8,300 ± 40	4.1 ± 0.3	1.1 ± 0.01	2,200 ± 200
47	9.2 ± 0.4[e]	>30,000[e]	0.40 ± 0.1	0.48 ± 0.07	11,000 ± 400
48[f]	30 ± 0.1	>30,000	0.0031 ± 0.001	0.089 ± 0.04	>30,000
77	5.9 ± 0.9	>30,000	1.3 ± 0.2	0.11 ± 0.001	>30,000
78	11 ± 0.9	15,000 ± 2,000	0.89 ± 0.03	0.22 ± 0.01	>30,000
81	3.3 ± 0.7	89 ± 8	2.3 ± 0.1	0.62 ± 0.07	11, 000 ± 2,000
83	4.1 ± 0.7	34 ± 1	1.7 ± 0.1	1.3 ± 0.07	8.4 ± 2
84	5.6 ± 2	6.1 ± 0.4	0.42 ± 0.04	0.51 ± 0.09	140 ± 8
87	3.7 ± 0.7	27 ± 4	1.1 ± 0.02	0.66 ± 0.09	2,400 ± 800
89	2.9 ± 0.5	27,000 ± 800	1.1 ± 0.01	0.39 ± 0.08	>30,000
90	0.7 ± 0.1	14 ± 2	1.6 ± 0.1	1.0 ± 0.2	14 ± 2

[a]Analogue evaluated at 5 μM unless otherwise indicated. [b]Value represents % *Gli1* mRNA expression compared to OHC control (set to 100). [c]Value represents *Cyp24A1* mRNA expression compared to DMSO control (set to 1.0). [d]IC_{50} values represent average Mean ± SEM of at least two separate experiments performed in triplicate. [e]Analogue evaluated at 2.5 μM. [f]Analogue evaluated at 1 μM.

significantly reduce the Cyp24A1 upregulation compared to **77,** from >30,000 to 100 (C3H) and 11,000 (ASZ). Importantly, **81** was able to maintain a slight increase in potency compared to **55** in ASZ cells.

Surprisingly, the addition of the C-25 hydroxyl group to the extended *seco*-B analogue **74** (**83**) had little effect on anti-Hh potency and Cyp24A1 levels in either cell line. Again, little difference was seen following hydroxylation of **75** (**84**), expect for a slight increase in Cyp24A1 expression in ASZ cells (140 compared to 6-fold). Even though no major differences were observed following C-25 hydroxylation, masking of the C-25 hydroxyl of **83** (**87**) yielded interesting results. With little to no upregulation of Cyp24A1 observed and no effect on the potency following hydroxylation, it was expected to see no change following etherification of the C-25 group. Intriguingly, **87** showed an increase in anti-Hh potency from an IC_{50} of ~1.3 to 0.66 μM, as well an increase in Cyp24A1 levels from ~8 to 2,400-fold compared to **74** and **83** in ASZ cells.

D. Pharmacokinetic Studies of Vitamin D Analogues

Select analogues were then sent to Pharmaron, Inc. for pharmacokinetic (PK) studies (**Table 12**). The first take-away from this study was the overall poor solubility of the compounds, which were essentially insoluble at pH 4.0 and 7.4. This was not too surprising given the hydrophobic nature of the compounds. Overall, the most soluble compound at pH 4.0 was analogue **78** with a single-atom amine *seco*-B and C-25 hydroxylation, but showed a significant decrease in solubility at pH 7.4. Analogue **52** with the amide s*eco*-B region was the second most soluble compound at pH 4.0 and maintained solubility at pH 7.4.

Comparing the PK properties of **56**, **57**, **75** and **78**, general conclusions can be made for the amine series of analogues as all compounds contain the 4-hydroxyl phenolic A-ring moiety. Looking at compounds **56** and **57**, the only structural difference is the orientation of the *seco*-B region at C-9, where **56** maintains the α-orientation. While both compounds maintain similar solubility, the α-orientation appears to be less stable in human liver microsomes (HLMs) and has a higher clearance rate compared to the β-orientation of **57**. Similarly, the extended amine *seco*-B analogue **75** maintains β-orientation at C-9 and shows a very similar PK profile to the single atom *seco*-B analogue **57**. Addition of the C-25 hydroxylation to **56** (analogue **78**) decreased the half-life and increased the clearance rate while increasing

Table 14. Pharmacokinetic properties determined by Pharmaron, Inc.

	Pharmacokinetic Properties			
	$T_{1/2}$ (HLM, min)[a]	**Clearance (mL/min/mg protein)**	**Solubility (mg/mL)**	
			pH 4.0	**pH 7.4**
48	>120*	ND	ND	ND
51	>231	< 3	1.6×10^{-4}	6.7×10^{-4}
52	>231	< 3	2.7×10^{-4}	6.8×10^{-4}
56	57 ± 0.1	12 ± 0.2	6.2×10^{-7}	2.6×10^{-6}
57	>231	< 3	7.5×10^{-7}	2.6×10^{-7}
75	>231	< 3	1.3×10^{-7}	2.7×10^{-6}
78	31 ± 0.5	22 ± 0.4	2.4×10^{-3}	4.2×10^{-6}
81	>231	< 3	1.7×10^{-5}	1.4×10^{-5}
87	43 ± 7	16 ± 3	6.0×10^{-5}	1.2×10^{-4}
89	47 ± 1	15 ± 0.3	4.8×10^{-5}	3.1×10^{-5}
90	49 ± 7	15 ± 0.3	2.7×10^{-6}	2.3×10^{-6}

[a] Metabolic stability in human liver microsomes (HLM), time until 50% of compound disappeared. *Metabolic stability in rat liver homogenate, time until 50% of compound disappeared [Ref 141].

the solubility at pH 4.0. Although **81** has a 3-hydroxyl phenolic A-ring, masking of the C-25 hydroxyl group as the methyl-ether increased the half-life significantly and reduced clearance to values similar to the non-functionalized C-25 analogues. Furthermore, the solubility of **81** was reduced compared to **78,** but was greater than **56** – **57**.

Although not completely conclusive due to issues with obtaining results in their experiments, these studies have provided great insight into the best ways to proceed in analogue development. Taken together with the cellular data, it is becoming clearer that the orientation of the *seco*-B region is flexible and either the α- or β-orientation may be utilized for analogue development. Secondly, masking the C-25 hydroxylation may be the best way to find a balance between biological activity and stability.

Conclusion

Following reports that VD3 (**46**) inhibits Hh signaling in multiple cell lines, initial analogue development focused on increasing the selectivity for Hh signaling over canonical vitamin D receptor (VDR) signaling. Previous SAR studies indicated that the CD-rings and alkyl side chain (**50**) were required for Hh signaling,[129] and that incorporation of a phenolic A-ring and ester *seco*-B ring (**51**) increased both selective and potency over VD3.[131] Follow up studies suggested that the natural alkyl side chain was preferred,[132] and the use of an amine *seco*-B region yielded more potent analogues and greater consistency across cell lines.[133]

With the specific protein target and mechanism of action unclear, a series of analogues were developed with modifications to the C-ring to probe the binding pocket for additional interactions and determine if this position would be useful for labeling studies.[134] These additions were made to the C-11 position and ranged in size from ethyl to benzyl to propargyl groups. Overall, no significant gains in potency were achieved, but there was an immediate loss in activity as the size of the functional group changed from ethyl- (**61a**) to cyclohexyl- (**61c**). This suggests a narrow binding pocket, which would not be surprising as the theorized Hh binding partner is the transmembrane protein, Smo. As hydrophilic characteristics were introduced with **63**–**67**, inhibitory activity was restored suggesting that the binding pocket may not be as

narrow as originally thought, but flexibility and rigidity of the functional group may play a primary role for SAR at this location of the scaffold. The ethyl addition (**61a**) did increase selectivity compared to **51**, suggesting that the C-11 position may be useful to gain selectivity but not potency. The drop-off in activity calls for additional studies to determine the cause of the immediate activity loss. These studies could include computational modeling and binding studies within the potential binding pockets. Furthermore, the reduction in Cyp24A1 levels and the ability of **67** to inhibit Hh signaling suggests that the C-11 position may serve as a label attachment point for target elucidation studies that selectively identify non-VDR proteins.

The incorporation of an amine *seco*-B has provided the most potent and selective VD3 analogues to date with sub-micromolar IC_{50} values and low Cyp24A1 levels in both cell lines. Combining these results with previous SAR studies, it is clear that the free hydroxyl group of the A-ring is required to maintain anti-Hh activity. The preferred position of the hydroxyl group shifted from the 3-position of the esters and amide series (**50** - **54**) to the 4-poistion for the amine *seco*-B analogues (**56** - **57**, **72**, **75**). Additionally, extension of the initial single atom amine *seco*-B (**55** – **57**) by a methylene (CH_2) group (**74** – **75**) showed the same preference for the 4-hydroxyl over the 3-hydroxyl position. This shift may be due to the flexibility of the *seco*-B region and how it orients the hydroxyl group within the binding site. The more rigid ester and amide *seco*-B analogues are similar to the diene system of the vitamin D compounds, whereas the -CH_2NH- *seco*-B region is more flexibly and allows the same interactions to be obtained. These observations still need to be studied by computational studies, but with the mechanism of action unclear, the binding target remains in question.

As expected, addition of a C-25 hydroxyl group significantly upregulated Cyp24A1 mRNA expression across cell lines, with analogues **83** – **84** being the exception to this trend. Compared to the non-C-25 hydroxylated analogues, there were little differences in the anti-Hh activity in C3H cells; however, varying potency increases where observed in ASZ cells. Masking of the C-25 hydroxyl group via a methyl ether successful decreased Cyp24A1 expression for the single atom amine and ester *seco*-B analogues (**80** and **89**). Interestingly, the extended amine analogue **87** had greater anti-Hh potency and higher Cyp24A1

mRNA levels than the non-hydroxylated or C-25 hydroxylated versions, **74** and **83** respectively. Taken together, these results suggest that addition of the C-25 hydroxyl or methoxy increases the binding interactions to increase potency. Another potential reason for the increase in potency is an increase in cell permeability, but additional studies need to be performed to understand the increase. It was clear that as Cyp24A1 levels increased, so did anti-Hh activity. This observation suggests that VDR plays a role in controlling analogue activity and crosstalk with Hh signaling may exists. Studies to further understand these observations will be discussed in the following chapter.

Acknowledgements

I would like to thank Albert M DeBerardinis, PhD, and Upasana Banerjee, PhD, for the initial synthesis and evaluation of multiple compounds present in this text (**51**, **53-57**).

Experimental Section

General Information

VD3 used for chemical synthesis was purchased from HBC Chem, Inc. Other chemicals were purchased from Sigma–Aldrich or Fisher Scientific. ACS or HPLC grade methanol, acetone, and tetrahydrofuran (THF) were purchased from Fisher Scientific. Anhydrous DCM and THF were purchased from Sigma-Aldrich. Column chromatography was performed using silica gel purchased from Sorbtech (Sorbent Technologies). NMR data was performed on a Bruker AVANCE 500 MHz spectrometer and analysis with MestReNova version 8.0.0. HRMS data was analyzed at the Mass Spectrometry Facility at the University of Connecticut, performed by Dr. You-Jun Fu.

Synthesis Procedures

Ester 51.[127] Grundmann's alcohol **50** (0.19 mmol), dicyclohexylcarbodiimide (3 eq, 0.57 mmol), and dimethylaminopyridine (3 eq, 0.57 mmol) were dissolved in anhydrous DCM (4 mL) in an oven-dried round bottom flask. The benzyl protected 3-hydroxy benzoic acid was added and the reaction mixture

stirred overnight at RT. The crude mixtures were loaded directly on a silica column and purified with flash chromatography (4% EtOAc in Hexanes) to yield protected the ester, 60%. The protected ester (0.1 mmol) was dissolved in MeOH:THF (2:1, 6 mL). $Pd(OH)_2$ (10% on carbon, 10 mg) was then added. The flask was sealed with a rubber septum and charged with an atmosphere of hydrogen gas. The reaction was stirred overnight at RT. The reaction mixture was passed through a celite pad, rinsed with ethyl acetate (10 mL), and concentrated under reduced pressure. The crude residue was purified using flash chromatography over a packed silica column (10% EtOAc in hexanes) to yield analogue **51** in good yield (70%). ^{1}H NMR (500 MHz, $CDCl_3$) δ 7.70 (m, 1H), 7.64 (m, 1H), 7.34 (m, 1H), 7.11 (m, 1H), 6.63 (br s, 1H), 5.43 (m, 1H), 2.08 (m, 1H), 2.01 (m, 1H), 1.84 (m, 2H), 1.56 (m, 5H), 1.37 (m, 3H), 1.26 (m, 3H), 1.15 (m, 4H), 1.04 (s, 3H), 0.95 (d, J = 6.5 Hz, 3H), 0.90 (dd, J = 6.6, 1.9 Hz, 6H). ^{13}C NMR (126 MHz $CDCl_3$) δ 166.9, 156.1, 132.0, 129.7, 121.7, 120.2, 116.5, 72.2, 56.4, 51.5, 41.9, 39.8, 39.5, 35.9, 35.4, 30.5, 28.0, 27.0, 23.7, 22.8, 22.6, 22.5, 18.6, 18.0, 13.5. IR (film) vmax 3385 (bs), 3019, 2951, 2935, 2868, 1689, 1599, 1589, 1466, 1453, 1366, 1344, 1295, 1215, 1157, 1106, 1075, 1062, 982, 946, 886, 755, 680, 668. DART-HRMS: a) m/z calcd. for $C_{25}H_{37}O_3$: 385.2743 $[M-H]^+$. Found: 385.2745.

A. C-Ring Analogues 53-61[134]

Enone 59. Lithium diisopropylamine (2 eq, 1 M, 6.8 mL) was cooled to -78ºC in anhydrous THF (5 mL). Grundmann's ketone **58** (900 mg, 3.4 mmol) was dissolved in anhydrous THF (8 mL) and added dropwise over 15 min to the cooled LDA solution. The reaction stirred at -78ºC for 1 hr plus an additional 1 hr at RT. After 2 hr, the reaction mixture was cooled back to -78ºC and TMSCl (2 eq, 0.87 mL) was added. The mixture was warmed to 0ºC and stirred for 2.5 hr warming to RT. The reaction was quenched by slow addition of cold H_2O and saturated $NaHCO_3$. The organics were extracted with diethyl ether, dried over anhydrous $NaSO_4$, and concentrated. The crude silyl-enol ether was dissolved in anhydrous MeCN (30 mL). $Pd(OAc)_2$ (0.8 eq, 600 mg) was added followed by *p*-benzoquinone (0.5 eq, 185 mg) and allowed to stir overnight (16 hr) at RT. The reaction was filtered through celite and concentrated. Enone **59** was obtained via column chromatography (3% EtOAc in hexanes, 78%, 695 mg). ^{1}H NMR (500MHz, $CDCl_3$) δ 6.78 (m,

1H), 6.01 (dd, 1H), 2.64 (dd, 1H), 2.58 (t, 1H), 2.43 (d, 1H), 1.98 9m, 1H), 1.77 (m, 2H), 1.54 (m, 2H), 1.5-1.0 (10H), 0.96 (d, 3H), 0.89 (d, 6H), 0.77 (s, 3H). ^{13}C NMR (126 MHz, $CDCl_3$) δ 202.1, 147.7, 129.7, 59.4, 56.9, 47.7, 43.2, 39.6, 36.1, 35.6, 28.2, 27.6, 23.9, 22.9, 22.7, 19.6, 18.6, 12.1. Previously reported: Okamura, W. H; et al. *J. Org. Chem.* **2002**, *67*, 1637-1650.

General Procedure for C-11 additions (60a-e)

CuI (2 eq, 365 mg) was suspended in anhydrous THF (5 mL) under argon and cooled to 0ºC. Ethyl-MgBr (10 eq, 1M, 9.5 mL) was added to the suspension and stirred for 1 hr. Enone **59** (250 mg, 0.95 mmol) was dissolved in anhydrous THF (5 ml) under argon and added to the Grignard-cuprate mixture at 0ºC. The reaction was monitored by TLC and quenched with cold H_2O upon completion (~2 hr). The mixture was diluted with ethyl acetate (20 mL) and washed with 0.1N HCl (15 mL). The organics were extracted, dried over anhydrous $NaSO_4$ and concentrated. The product **60a** was purified by column chromatography (3% EtOAc in hexanes, 90 %, 250 mg). ^{1}H NMR (500 MHz, $CDCl_3$) δ 2.45 (m, 2H), 2.07 (m, 2H), 1.92 (m, 2H), 1.80 (m, 1H), 1.67 (m, 1H), 1.53 (m, 2H), 1.37 (m, 5H), 1.25 (m, 1H), 1.17 (m, 4H), 1.11 (s, 3H), 1.04 (m, 1H), 0.96 (t, 3H), 0.93 (d, 3H), 0.91 (m, 6H) .^{13}C NMR (126 MHz, $CDCl_3$) δ 215.27, 60.02, 56.52, 47.48, 45.57, 45.29, 39.48, 35.46, 34.83, 34.10, 29.72, 29.51, 28.51, 28.02, 24.22, 22.81, 22.56, 22.33, 22.04, 19.21, 11.35. HRMS: *m/z* calculated for $C_{26}H_{36}O$, $[M+H]^+$, calc. 293.2844, obs. 293.2831; $[M-OH]^+$, calc. 275.2739, obs. 275.2730.

Vinyl-substituted analogue 60b. 150 mg, 71%. ^{1}H NMR (500 MHz, $CDCl_3$) δ 5.81 (m, 1H), 5.03 (m, 2H), 2.77 (m, 1H), 2.48 (m, 1H), 2.36 (dd, 1H), 2.22(m, 1H), 2.13 (t, 1H), 1.94 (m, 1H), 1.73 (m, 1H), 1.6-1.3 (9H), 1.15 (m, 3H), 1.06 (m, 1H), 0.99 (d, 3H), 0.89 (d, 6H), 0.70 (s, 3H). ^{13}C NMR (126 MHz, $CDCl_3$) δ 210.6, 142.2, 113.5, 67.2, 56.8, 49.2, 46.9, 45.9, 40.8, 39.6, 36.1, 35.7, 28.2, 27.9, 23.9, 22.9, 19.1, 19.0, 13.3. HRMS: *m/z* calculated for $C_{20}H_{34}O$, $[M+H]^+$, calc. 291.2688, obs. 291.2715; $[M+NH_4]^+$, calc. 308.2953, obs. 308.2951.

Cyclohexyl-substituted analogue 60c. 72 mg, 62%. ^{1}H NMR (500 MHz, $CDCl_3$) δ 2.43 (q, 1H), 2.32 (dd, 1H), 2.16 (dd, 1H), 1.95 (m, 4H), 1.8-1.6 (11H), 1.52 (m, 3H), 1.3-1.1 (9H), 1.04 (m, 4H), 0.94 (m, 3H), 0.89 (m, 9H), 0.64 (s, 3H). ^{13}C NMR (126 MHz, $CDCl_3$) δ 212.3, 62.1, 56.9, 49.1, 45.0, 43.4, 43.3, 42.1, 39.6, 36.2, 35.6, 30.9, 30.2, 28.2, 27.9, 27.2, 26.8, 23.9, 22.9, 22.7, 19.1, 19.0, 13.4. HRMS: *m/z* calculated for $C_{24}H_{43}O$, $[M+H]^+$, calc. 374.3140, obs. 347.3340.

Phenyl-substituted analogue 60d. 100 mg, 78%. ^{1}H NMR (500 MHz, $CDCl_3$) δ 7.35 (m, 5H), 3.34 (m, 1H), 2.65 (m, 1H), 2.50 (m, 2H), 2.36 (m, 1H), 1.99 (m, 1H), 1.87 (m, 2H), 1.58 (m, 5H), 1.40 (m, 4H), 1.29 (s, 2H), 1.15 (m, 4H), 1.08 (m, 1H), 0.95 (d, 3H), 0.90 (m, 6H), 0.81 (s, 3H).^{13}C NMR (126 MHz, $CDCl_3$) δ 210.5, 128.9, 127.1, 126.8, 62.0, 56.9, 49.5, 49.1, 47.7, 42.9, 39.6, 35.7, 29.9, 28.2, 27.9, 23.9, 22.9, 22.7, 19.2, 19.0, 13.4. HRMS: *m/z* calculated for $C_{24}H_{36}O$ $[MH]^+$, calc. 341.2844, obs. 341.2859.

Benzyl-substituted analogue 60e. 95 mg, 88%. ^{1}H NMR (500 MHz, $CDCl_3$) δ 7.25 (m, 5H), 2.77 (dd, 1H), 2.61 (m, 1H), 2.36 (m, 1H), 2.27 (m, 1H), 2.27 (m, 2H), 1.97 (m, 2H), 1.75 (m, 1H), 1.55 (m, 2H), 1.38 (m, 8H), 1.1-1.0 (6H), 0.95 (d, 3H), 0.90 (d, 6H), 0.66 (s, 3H). ^{13}C NMR (126 MHz, $CDCl_3$) δ 137.34, 130.97, 130.58, 128.81, 127.95, 126.31, 71.96, 56.48, 53.20, 48.14, 41.64, 41.20, 39.50, 35.96, 35.24, 29.71, 28.02, 27.35, 23.84, 22.82, 22.55, 19.61, 18.28, 13.48. HRMS: *m/z* calculated for $C_{25}H_{39}O$, $[M+H]^+$, calc. 355.3001, obs. 355.3011.

General Procedure for synthesis of esters 61a-61e. $NaBH_4$ (5 eq, 40 mg) was added to a solution of ketone **60e** (75 mg, 0.21 mmol) in MeOH (8 mL) and allowed to stir for 4 hr at RT. The reaction was quenched with H_2O (10 mL), extracted with EtOAc (3 x 20 mL) and concentrated. The crude alcohol was dissolved in DCM (8 mL). DCC (2.5 eq, 108 mg), DMAP (4 eq, 103 mg) and 3-MOM-benzoic acid (4 eq, 153 mg) were added and stirred at RT overnight (12-16 hr). The reaction was concentrated *in vacu* and purified via column chromatography. The 3-OMOM-protected ester was purified (5% EtOAc in hexanes) and immediately moved forward for deprotection. To remove the MOM-protecting group, (±)-CSA (5 eq,

170 mg) was added to a solution of the protected ester in MeOH (5 mL) and stirred at RT until the reaction was complete by TLC (16 hr). The reaction mixture was concentrated and purified via column chromatography. (8% EtOAc in hexanes).

Ethyl-substituted analogue 61a. 18 mg, 32% over three steps. ^{1}H NMR (500 MHz, $CDCl_3$) δ 7.67 (d, 1H), 7.54 (s, 1H), 7.37 (t, 1H), 7.07 (m, 1H), 5.45 (m, 1H), 5.04 (bs, 1H), 2.14 (m, 1H), 2.10 (m, 1H), 1.93 (m, 1H), 1.82 (m, 1H), 1.6-1.4 (5H), 1.38 (m, 3H), 1.26 (m, 2H), 1.19 (m, 5H), 1.09 (s, 3H), 1.07 (m, 1H), 0.99 (d, 3H), 0.92 (m, 10H). ^{13}C NMR (126 MHz, $CDCl_3$) δ 155.55, 132.51, 129.69, 122.13, 119.81, 116.26, 72.34, 56.36, 52.01, 46.66, 42.66, 39.52, 37.17, 35.95, 35.44, 30.75, 29.85, 29.73, 28.04, 27.58, 23.78, 22.83, 22.58, 22.43, 18.74, 14.49, 11.56. HRMS: *m/z* calculated for $C_{27}H_{42}O_3$, $[MNH4]^+$, calc. 432.3478, obs. 432.3475.

Cyclohexyl-substituted analogue 61c. 22 mg, 20 % over three steps. ^{1}H NMR (500 MHz, $CDCl_3$) δ.66 (dd, 2H), 7.36 (t, 1H), 7.11 (m, 1H), 6.26 (s, 1H), 5.47 (s, 1H), 2.05 (m, 2H), 1.92 (m, 1H), 1.78 (m, 3H), 1.70 (m, 3H), 1.55 (m, 3H), 1.39 (m, 5H), 1.30 (m, 2H), 1.18 (m, 8H), 1.06 (s, 3H), 1.03 (m, 3H), 1.00 (m, 3H), 0.92 (m, 6H).^{13}C NMR (126 MHz, $CDCl_3$) δ 166.79, 156.05, 132.16, 129.71, 121.80, 120.14, 116.49, 72.87, 56.47, 52.00, 43.55, 42.97, 42.63, 39.53, 35.96, 35.42, 34.23, 34.19, 30.34, 30.16, 28.05, 27.59, 26.91, 26.87, 26.83, 23.77, 22.84, 22.59, 22.46, 18.80, 14.40. HRMS: *m/z* calculated for $C_{31}H_{48}O_3$, $[MNH_4]^+$, calc. 480.3478, obs. 480.3464.

Phenyl-substituted analogue 61d. 7 mg, 17% over three steps. ^{1}H NMR (500 MHz, $CDCl_3$) δ 7.71 (d, 1H), 7.58 (s, 1H), 7.39 (t, 1H), 7.35 (t, 2H), 7.28 (m, 2H), 7.24 (t, 1H), 7.12 (d, 1H), 5.57 (m, 1H), 5.03 (s, 1H), 3.23 (m, 1H), 2.26 (m, 2H), 1.96 (m, 1H), 1.85 (m, 1H), 1.75 (m, 1H), 1.75 (m, 1H), 1.65 (m, 1H), 1.6-1.3 (10H), 1.28 (m, 2H), 1.22 (s, 3H), 1.16 (m, 3H), 1.07 (m, 1H), 0.95 (s, 3H), 0.91 (dd, 6H). ^{13}C NMR (126 MHz, $CDCl_3$) δ 155.66, 146.42, 132.32, 129.76, 128.46, 127.19, 126.17, 122.10, 119.98, 116.31, 72.12, 56.50, 51.55, 48.08, 43.02, 39.50, 38.41, 35.92, 35.81, 35.45, 29.72, 28.04, 27.58, 23.76, 22.82,

22.57, 22.50, 18.76, 14.38. HRMS: *m/z* calculated for $C_{31}H_{42}O_3$, $[M-H]^+$, calc. 467.3525, obs. 467.3523.

Benzyl-substituted analogue 61e. 25 mg, 23% over three steps. ^{1}H NMR (500 MHz, $CDCl_3$) δ7.64 (d, 1H), 7.59 (s, 1H), 7.35 (t, 1H), 7.31 (m, 2H), 7.19 (m, 3H), 7.03 (m, 1H), 5.59 (s, 1h), 5.47 (s, 1H), 2.58 (d, 2H), 2.26 (m, 1H), 2.15 (m, 1H), 2.07 (m, 1H), 1.91 (m, 1H), 1.58 (m, 3H), 1.49 (s, 2H), 1.45-1.3 (7H), 1.17 (m, 4H), 1.05 (s, 3H), 1.01 (m, 1H), 0.91 (m, 9H). ^{13}C NMR (126 MHz, $CDCl_3$) δ 166.44, 155.82, 140.49, 132.19, 129.70, 129.15, 128.17, 125.82, 121.93, 120.03, 116.41, 72.21, 56.33, 51.90, 46.68, 43.70, 42.63, 39.50, 37.28, 35.91, 35.32, 31.17, 30.36, 28.03, 27.52, 23.74, 22.83, 22.58, 22.37, 18.66, 14.42. HRMS: *m/z* calculated for $C_{32}H_{44}O_3$, $[MNH_4]^+$, calc. 494.3534, obs. 494.3552.

Ethyl hydroxyl alcohol 62. Ketone **60b** (280 mg, 0.96 mmol) was dissolved in anhydrous THF (5 mL) under argon. A solution of 9-BBN (0.5 M, 4 eq, 4 mL) was added and stirred for 3.5 hr at RT. Water was slowly added until the solution became cloudy. NaOH (12 eq, 2 M, 6 mL) was added followed by MeOH (5 mL) and H_2O_2 (~30%, 2.5 eq, 1.5 mL) and stirred for 16 hr. The reaction mixture was washed with diethyl ether (2 x 15 mL), dried with anhydrous $NaSO_4$ and concentrated. Diol **62** was purified via column chromatography (25% EtOAc in hexanes, 195 mg, 65%). ^{1}H NMR (500 MHz, $CDCl_3$) δ 4.10 (s, 1H), 3.67 (m ,2H), 2.64 (s, 1H), 2.13 (m, 1H), 2.00 (d, 2H), 1.18 (m, 1H), 1.6-1.4 (4H), 1.3 (m, 6H), 1.2-1.0 (6H), 0.97 (s, 3H), 0.91 (d, 3H), 0.88 (dd, 6H).^{13}C NMR (126 MHz, $CDCl_3$) δ 69.20, 60.35, 56.72, 53.23, 48.25, 42.84, 40.20, 39.68, 39.52, 36.13, 35.45, 28.18, 27.78, 24.70, 23.95, 22.98, 22.73, 22.42, 18.82, 14.54. HRMS: *m/z* calculated for $C_{20}H_{38}O_2$, $[M+NH_4]^+$, calc. 328.3216, obs. 328.3218; $[M-OH]^+$, calc. 298.2844, obs. 298.2869.

Analogue 63. Diol **62** (95 mg, 0.31 mmol) was dissolved in anhydrous DCM (5 mL) under argon. TBSCl (1.05 eq, 51 mg) was added followed by imidazole (1.8 eq, 39 mg). After 1 hr, the reaction was quenched with H_2O (10 mL) and washed with DCM (2 x 10 mL). The organic layer was collected, dried over anhydrous $NaSO_4$ and concentrated. Mono-protected alcohol was collected via column chromatography

(3% EtOAc in hexanes, 118 mg, 90%). The TBS-protected alcohol (70 mg, 0.16 mmol) was dissolved in DCM (5 mL). DCC (3 eq, 102 mg), DMAP (4 eq, 20 mg) and 3-OMOM-benzoic acid (4 eq, 120 mg) were added and the mixture stirred for 16 hr at RT. The reaction was concentrated, and the protected ester was purified via column chromatography (2% EtOAc in hexanes). The protected ester (25 mg, 0.52 mmol) was dissolved in MeOH (5 mL) to which (±)-CSA (5 eq, 50 mg) was added and stirred at RT until the reaction was complete by TLC (18 hr). The solution was concentrated and ester **63** was purified via column chromatography (25% EtOAc in hexanes, 15 mg, 65%). ^{1}H NMR (500 MHz, $CDCl_3$) δ 7.62 (d, 1H), 7.58 (s, 1H), 7.32 (m, 1H), 7.10 (dd, 1H), 6.56 (s, 1H), 3.76 (t, 2H), 2.11 (m, 3H), 1.91 (m, 3H), 1.57 (m, 5H), 1.5-1.2 (7H), 1.17 (m, 4H), 1.06 (s, 3H), 0.97 (d, 3H), 0.91 (dd, 6H).^{13}C NMR (126 MHz, $CDCl_3$) δ 166.58, 156.07, 132.04, 129.70, 121.76, 120.15, 116.33, 72.14, 60.74, 56.33, 51.84, 46.98, 42.60, 39.91, 39.51, 37.48, 35.92, 35.41, 27.50, 25.75, 23.77, 22.83, 22.58, 22.42, 18.73, 14.37. HRMS: *m/z* calculated for $C_{27}H_{42}O_4$, $[M+H]^+$, calc. 431.3161, obs. 431.3166; $[M+NH_4]^+$, calc. 448.3427, obs. 448.3437.

Ketone 64. Tetrabutyl ammonium bromide (0.5 eq, 200 mg) was added to a slurry of IBX (3 eq, 1.1 g) in DCM:H_2O (3:1, 8 mL) and the mixture was stirred until a yellow color appeared. A solution of diol **62** (350 mg, 1.1 mmol) in DCM (2 mL) was added to the IBX mixture and stirred at RT for 4 hr. The mixture was filtered and thoroughly washed with diethyl ether. The filtrate was washed with saturated sodium thiosulfate (15 mL), water (2 x 15 mL) and brine (15 mL). The organic layer was dried with anhydrous $NaSO_4$ and concentrated. Ketone **64** was purified via column chromatography (20% EtOAc in hexanes, 260 mg, 75%). ^{1}H NMR (500 MHz, $CDCl_3$) δ 3.69 (s, 2H), 2.45 (m, 2H), 2.22 (m, 2H), 1.93 (m, 3H), 1.71 (m, 2H), 1.52 (m, 3H), 1.34 (m, 6H), 1.14 (m, 5H), 0.96 (m, 3H), 0.88 (m, 6H), 0.66 (s, 3H).^{13}C NMR (126 MHz, $CDCl_3$) δ 211.33, 61.89, 60.37, 56.55, 49.21, 47.49, 46.40, 40.11, 39.40, 35.95, 35.46, 33.30, 27.98, 27.71, 23.75, 22.77, 18.91, 13.19. HRMS: *m/z* calculated for $C_{20}H_{36}O_2$, $[M+H]^+$, calc. 309.2794, obs. 309.2776.

Amine analogue 65. Ketone **64** (100 mg, 0.32 mmol) was dissolved in dichloroethane (DCE, 6 mL). 4-aminophenol (1.5 eq, 45 mg) and $NaBH(OAc)_3$ (1.6 eq, 90 mg) were added, and the solution was stirred at

RT for 14 hr. The mixture was quenched with saturated $NaHCO_3$ (10 mL) and washed with ethyl acetate (2 x 15 mL). The organic layers were dried over anhydrous $NaSO_4$ and concentrated. Amine **65** was purified via column chromatography (25% EtOAc in hexanes, 15 mg, 12%). ^{1}H NMR (500 MHz, $CDCl_3$) δ 6.66 (d, 2H), 6.45 (d, 2H), 3.68 (m, 2H), 2.58 (m, 1H), 2.53 (m, 1H), 2.20 (m, 2H), 2.05 (m, 4H), 1.82 (m, 1H), 1.7-1.3 (10H), 1.27 (m, 1H), 1.23 (s, 3H), 1.2-1.1 (6H), 0.99 (d, 3H), 0.92 (d, 6H). ^{13}C NMR (126 MHz, $CDCl_3$) δ 148.47, 139.98, 116.68, 116.02, 74.24, 62.01, 55.64, 51.57, 47.33, 39.40, 39.20, 38.63, 36.70, 33.47, 33.16, 32.45, 28.01, 27.99, 25.68, 22.72, 22.58, 22.49, 21.30, 16.17. HRMS: *m/z* calculated for $C_{27}H_{45}NO_2$, $[MH]^+$, calc. 402.3372, obs. 402.3376.

Ketone 66. Ketone **64** (170 mg, 0.57 mmol) was dissolved in anhydrous DCM (5 mL). DCC (3 eq, 353 mg), DMAP (3 eq, 210 mg) and 4-pentynoic acid (3 eq, 155 mg) were added to the solution and it was stirred at RT for 16 hr. The reaction mixture was concentrated. Ketone **66** was purified via column chromatography (10% EtOAc in hexanes, 201 mg, 91%). ^{1}H NMR (500 MHz, $CDCl_3$) δ 4.16 (m, 3H), 2.52 (m, 5H), 2.45 (m, 1H), 2.38 (m, 1H), 2.21 (m, 2H), 1.95 (m, 4H), 1.71 (m, 5H), 1.53 (m ,3H), 1.37 (m, 9H), 1.2-1.0 (6H), 0.97 (m, 3H), 0.87 (m, 8H), 0.66 (s, 3H).^{13}C NMR (126 MHz, $CDCl_3$) δ 210.50, 171.66, 82.36, 69.13, 62.54, 61.86, 56.55, 49.06, 47.37, 46.07, 39.40, 35.95, 35.45, 33.65, 33.36, 27.98, 27.71, 23.75, 22.78, 22.53, 18.91, 18.86, 14.39, 13.17. HRMS: *m/z* calculated for $C_{25}H_{40}O_3$, $[M+H]^+$, calc. 389.3056, obs. 389.3067; $[M+NH_4]^+$, calc. 406.3321, obs. 406.3300.

Ester analogue 67. Ketone **66** (200 mg, 0.51 mmol) was dissolved in MeOH (5 mL). $NaBH_4$ (2 eq, 38 mg) was added and the mixture stirred at RT for 2 hr. The reaction was quenched with cold H_2O (10 mL) and washed with EtOAc (2 x 15 mL). The organic layers were dried over anhydrous $NaSO_4$ and concentrated. The crude alcohol was dissolved in anhydrous DCM (5 mL). DCC (3 eq, 214 mg), DMAP (3 eq, 130 mg) and 3-OMOM-benzoic acid (3 eq, 190 mg) were added and the solution was stirred at RT for 20 hr. The reaction mixture was purified via column chromatography (5% EtOAc in hexanes) to yield the MOM-protected ester in modest yield, 115 mg, 60%. (±)-CSA (5 eq, 200 mg) was added to a solution of the MOM-

protected ester (100 mg, 0.18 mmol) in MeOH (5 mL). The reaction was stirred at RT until complete consumption of the starting material by TLC (8 hr). The reaction mixture was diluted with H_2O (5 mL), saturated $NaHCO_3$ (10 mL), and extracted with ethyl acetate (2 x 15 mL). The organic layers were dried over anhydrous $NaSO_4$ and concentrated. Ester **67** was purified via column chromatography (10% EtOAc in hexanes, 27 mg, 26%). Ester **63** was also collected (25 mg) demonstrating that these deprotection conditions were capable of cleaving the propargyl ester as well. ^{1}H NMR (500 MHz, $CDCl_3$) δ 7.66 (d, 1H), 7.57 (s, 1H), 7.37 (t, 1H), 7.09 (dd, 1H), 5.46 (s, 2H), 4.22 (t, 2H), 2.54 (m, 4H), 2.10 (m, 3H), 2.00 (t, 1H), 1.91 (m, 1H), 1.6-1.3 (13H), 1.19 (m, 4H), 1.08 (s, 3H), 0.98 (d, 3H), 0.91 (dd, 6H).^{13}C NMR (126 MHz, $CDCl_3$) δ 166.24, 155.76, 132.24, 129.75, 121.99, 120.03, 116.30, 82.58, 71.97, 69.12, 63.01, 56.34, 51.79, 46.76, 42.61, 39.50, 37.41, 35.91, 35.68, 35.40, 33.45, 29.73, 28.04, 27.51, 26.45, 23.77, 22.83, 22.58, 22.41, 18.77, 14.41. HRMS: *m/z* calculated for $C_{32}H_{46}O_5$, $[M]^+$, calc. 510.3345, obs. 510.3367; $[M+NH_4]^+$, calc. 528.3689, obs. 528.3695.

*B. Amine containing seco-B Analogues **52, 55-57, 68-72***

Amide 52[133]

Ketone **58** (1.0 g, 2.5 mmol) was dissolved in 4 mL of pyridine. Hydroxylamine hydrochloride (XX mg, 9.42 mmol) was then added with stirring and was left to stir at RT for 12 h and the mixture was diluted with H_2O (10 mL) and benzene (10 mL). The mixture was washed with H_2O followed by saturated $CuSO_4$, and concentrated. Column chromatography (SiO_2, 100% Hex to 10% EtOAc in hexanes) yielded Grundmann's oxime (98%, 1.0 g). ^{1}H NMR (500 MHz, $CDCl_3$) δ 9.41 (bs, 1H) 3.27 (m, 1H), 2.09 (m, 2H), 1.93 (m, 1H), 1.78 (m, 1H), 1.67 (m, 4H), 1.54 (m, 1H), 1.35 (m, 5H), 1.28 (s, 1H), 1.16 (m, 3H), 1.05 (m, 1H), 0.96 (d, J = 6.0 Hz,3H), 0.89 (d, J = 6.1 Hz, 6H), 0.67 (s, 3H). ^{13}C NMR (126 MHz, $CDCl_3$) δ 160.5, 56.1, 54.2, 46.6, 39.6, 39.5, 36.2, 36.0, 28.1, 28.0, 24.0, 23.9, 22.9, 22.7, 21.9, 20.8, 18.9, 12.4. HRMS-ESI: *m*/*z* calcd. for $C_{18}H_{34}NO$: 280.2640 $[MH]^+$. Found: 280.2647. Oxime (380 mg, 1.36 mmol) was dissolved in anhydrous THF (10 mL) and cooled to 0 °C. $LiAlH_4$ (1.0 M; 9.50 mL, 9.52 mmol) was added drop-wise to the solution. Once all $LiAlH_4$ was added, the reaction was refluxed for 12 h. The mixture was then worked

up according to the Fieser method: the reaction was cooled to 0 °C, water (30 mL) was added, followed by 75 mL of 15% aqueous NaOH, and then 200 mL water. The mixture was warmed to RT, stirred for 0.5 h, and filtered over a celite pad. Following this protocol, the solution was washed with EtOAc (3 × 100 mL). The combined organic layers were dried over $MgSO_4$, filtered, and concentrated. The crude mixture was then dissolved in glacial acetic acid (12 mL) and zinc powder (3 mmol) was added. The mixture was refluxed until the starting material was completely consumed (5 h, by TLC). The mixture was cooled to 0 °C, quenched with saturated $NaHCO_3$, washed with EtOAc (2 × 50 mL), and concentrated. Crude Grundmann's amine was used directly in the next step. EDCI (0.689 mmol), DMAP (0.123 mmol) and 3-(benzyloxy) benzoic acid (0.679 mmol) were dissolved in 5 mL anhydrous CH_2Cl_2 and stirred for 20 min. Crude amine (120 mg, 0.45 mmoL) in 3 mL anhydrous CH_2Cl_2 was added to the reaction mixture and stirred at RT for 16 h. Column chromatography (SiO_2, 100% Hex to 5% EtOAc in hexanes) afforded the protected amide in 26 % (~6:1) yield, 55 mg . ^{1}H NMR (500 MHz, $CDCl_3$) δ 7.44 (m, 5H), 7.36 (m, 2H), 7.12 (m,1H), 6.31 (m, 1H), 5.14 (s, 2H), 4.46 (m, 1H), 2.06 (m, 1H), 1.97 (m, 1H), 1.91 (m, 1H), 1.62 (m, 6H), 1.39 (m, 4H), 1.26 (m, 4H), 1.16 (m, 4H), 1.03 (m, 1H), 0.95 (m, 6H), 0.90 (m, 6H). ^{13}C NMR (101 MHz, $CDCl_3$) δ 166.9, 159.2, 136.9, 136.8, 129.8, 128.8, 128.3, 127.8, 127.7, 118.9, 118.4, 113.4, 70.4, 56.8, 51.2, 47.9, 42.3, 39.9, 39.7, 36.1, 35.5, 31.2, 29.9, 28.2, 27.2, 23.9, 23.1, 23.0, 22.7, 18.7, 18.2, 13.9. HRMS-ESI: *m*/*z* calcd. for $C_{32}H_{46}NO_2$: 476.3528 $[MH]^+$. Found: 476.351.

To a solution of the protected amide (0.11 mmol) in MeOH:THF (3:1, 12 mL) under argon was added Pd/C (10%, 50 mg). The vessel was purged with H_2 and the mixture stirred for 12 h. The mixture was filtered through celite, rinsed with copious EtOAc (100 mL), and the filtrate was concentrated. Amide **52** was isolated by column chromatography (SiO_2, 100% Hex to 30% EtOAc in Hex) in 67% yield (~6:1), 30 mg. ^{1}H NMR (500 MHz, $CDCl_3$) δ 8.08 (s, 1H), 7.79 (s, 1H), 7.10 (m, 1H), 7.05 (m, 1H), 6.49 (m, 1H), 4.46 (s, 1H), 2.06 (m, 1H), 1.97 (m, 1H), 1.90 (m, 1H), 1.62 (m, 5H) 1.56 (m, 2H), 1.38 (m, 5H), 1.16 (m, 5H), 1.03 (m, 1H), 0.97 (s, 3H), 0.94 (d, J = 6.1 Hz, 3H), 0.90 (d, J = 6.4 Hz, 6H). ^{13}C NMR (101 MHz, $CDCl_3$) δ 167.6, 157.7, 136.0, 129.9, 119.3, 116.9, 115.6, 56.8, 51.1, 48.3, 42.3, 39.8, 39.7, 36.1, 35.5, 31.1,

28.2, 27.2, 23.9, 23.1, 23.0, 22.7, 18.7, 18.2, 13.9. IR(neat) *ν*max 3338, 2953, 1652, 1585, 1522, 1450, 1258, 1277, 1239,1146, 938, 809. HRMS-ESI: *m*/*z* calcd. for $C_{25}H_{40}NO_2$: 386.3059 $[MH]^+$. Found: 386.3037.

General Reductive Amination Procedure[133]

Ketone **58 (**160 mg, 0.6 mmol) and 4-aminophenol (130 mg, 1.2 mmol) were dissolved in 1,2-dichloroethane (8 mL). Sodium triacetoxyborohydride (380 mg, 1.8 mmoL) was added followed by acetic acid (50 μL) and titanium (IV) isopropoxide (370 μL, 1.2 mmol). The mixture was left to stir at RT or reflux for 24 - 48 h. The reaction was quenched with saturated sodium bicarbonate (20 mL) and diluted with diethyl ether (60 mL). The aqueous layer was washed with diethyl ether (3 × 60 mL) and the organic layers combined, dried over $MgSO_4$, filtered, and concentrated. Crude residue was purified by column chromatography (SiO_2, 100% Hex to 25% EtOAc in hexanes) affording recovery of the starting ketone **58** (20-60%), and the desired amine (15 - 80%).

Amine 55[133]

Reductive amination of **58** with 3-aminophenol was described previously to afford **55** as a clear oil in good yield; 80%, 170 mg. ^{1}H NMR (500 MHz, $CDCl_3$) δ 6.98 (m, 1H), 6.15 (m, 1H), 6.10 (m, 1H), 6.06 (m, 1H), 4.78 (bs, 1H), 3.68 (m, 1H), 1.98 (m, 2H), 1.85 (m, 1H), 1.63 (m, 3H), 1.50 (m, 4H), 1.32 (m, 10H), 1.15 (m, 6H), 0.99 (m, 2H), 0.94 (s, 3H), 0.89 (m, 9H). ^{13}C NMR (126 MHz, $CDCl_3$) δ 156.7, 150.0, 130.0, 105.8, 103.3, 99.1, 56.8, 51.6, 51.1, 42.1, 40.2, 39.4, 35.9, 35.3, 31.5, 30.5, 28.0, 27.0, 23.7, 23.1, 22.7, 22.6, 22.5, 18.5, 17.8, 14.1, 13.5. IR(neat) *ν*max 3388, 2986, 2866, 1614, 1506, 1464, 1371, 1333, 1272, 1179, 1155, 1077, 977, 828, 757, 686. ESI-HRMS: *m*/*z* calcd. for $C_{24}H_{40}NO$: 358.3110 $[MH]^+$. Found: 358.3115.

Amine 56[133]

Reductive amination of **58** with 4-aminophenol was described previously to afford **56** (40%, 28 mg) and **57** (14%, 10 mg) as a clear oil in low yield. ^{1}H NMR (500 MHz, DMSO) δ 8.34 (s, 1H), 6.48 (m, 4H), 4.13 (m, 1H), 3.48 (m, 1H), 1.93 (m, 1H), 1.76 (m, 3H), 1.51 (m, 4H), 1.37 (m, 7H), 1.13 (m, 7H), 1.00 (m, 2H), 0.90 (m, 6H), 0.87 (d, J = 2.3 Hz, 3H), 0.86 (d, J = 2.3 Hz, 3H). ^{13}C NMR (126 MHz, DMSO) δ 148.0, 142.1, 115.4, 113.6, 56.1, 51.8, 51.5, 41.6, 40.0, 38.9, 35.4, 34.7, 30.7, 27.3, 26.8, 23.1, 23.0, 22.6, 22.3, 18.3, 17.5, 13.2. IR(neat) *v*max 3441, 3161, 2927, 2866, 1610, 1512, 1466, 1241, 1192, 976, 795, 691. ESI-HRMS: *m*/*z* calcd. for $C_{24}H_{40}NO$: 358.3110 $[MH]^+$. Found: 358.3107.

Amine 57[133]

^{1}H NMR (500 MHz, DMSO) δ 8.30 (bs, 1H), 6.51 (m, 2H), 6.41 (m, 2H), 4.33 (m, 1H), 2.83 (m, 1H), 1.95 (m, 1H), 1.87 (m, 2H), 1.81 (m, 1H), 1.66 (m, 1H), 1.54 (m, 2H), 1.47 (m, 2H), 1.37 (m, 4H), 1.20 (m, 6H), 1.02 (m, 1H), 0.94 (d, J = 6.5 Hz, 3H), 0.89 (s, 3H), 0.88 (d, J = 2.1 Hz, 3H), 0.86 (d, J = 2.2 Hz, 3H). ^{13}C NMR (126 MHz, DMSO doped with a drop of CDCl3) δ 126.4, 118.2, 115.8, 115.5, 56.1, 55.2, 45.1, 44.9, 44.6, 38.9, 35.9, 35.8, 34.9, 34.7, 34.4, 29.0, 27.4, 27.0, 24.2, 24.0, 22.6, 22.3, 19.2, 19.1. IR(neat) *v*max 3441, 3161, 2927, 2866, 1610, 1512, 1466, 1241, 1192, 976, 795, 691. DART-HRMS: *m*/*z* calcd. for $C_{24}H_{40}NO$: 358.3110 $[MH]^+$. Found: 358.3102.

Amine 68

Reductive amination of **58** with aniline yielded amine **68**; 65%, 69 mg. ^{1}H NMR (500 MHz, $CDCl_3$) δ 7.19 (t, 2H), 6.68 (m, 1H), 6.62 (m, 2H), 3.77 (s, 1H), 2.04 (m, 2H), 1.9-1.5 (9H), 1.41 (m, 3H), 1.31 (m, 3H), 1.17 (m, 5H), 1.07 (m, 1H), 1.00 (m, 3H), 0.97 (d, J = 6.7 Hz, 3H), 0.92 (m, 6H). ^{13}C NMR (126 MHz, $CDCl_3$) δ 148.5, 129.2, 129.2, 116.4, 112.5, 56.9, 51.7, 51.1, 45.7, 42.2, 40.3, 39.5, 35.9, 35.4, 30.6, 28.0, 27.1, 23.8, 23.2, 22.8, 22.5, 18.5, 17.9, 13.6. IR(neat) *v*max 2926, 1600, 1502, 1466, 1428, 1313, 1249, 863. DART-HRMS: *m*/*z* calcd. for $C_{24}H_{39}NO$: 342.3161 $[MH]^+$. Found 342.3132.

Amine 69

Reductive amination of **58** with *m*-anisidine yielded amine **68**; 45%, 23 mg. ^{1}H NMR (500 MHz, $CDCl_3$) δ 7.09 (m, 1H), 6.24 (m, 2H), 6.16 (m, 1H), 3.81 (s, 3H), 3.75 (s, 1H), 2.03 (m, 2H), 1.9-1.5 (8H),1.40 (m, 3H), 1.31 (m, 2H), 1.17 (m, 4H), 1.06 (m, 1H), 0.99 (m, 3H),0.96 (m, 3H), 0.92 (m, 6H). ^{13}C NMR (126 MHz, $CDCl_3$) δ 160.9, 149.9, 129.9, 129.8, 105.9, 101.5, 98.4, 56.9, 55.1, 51.7, 51.1, 45.6, 42.2, 40.2, 39.5, 39.4, 36.4, 35.9, 35.4, 35.2, 30.6, 28.04, 28.01, 27.7, 27.1, 24.5, 24.4, 23.8, 23.2, 22.8, 22.5, 20.2. IR(neat) *v*max 2927, 1611, 1493, 1463, 1208, 1159, 1208, 1159, 1050, 829, 750, 686. DART-HRMS: *m*/*z* calcd. for $C_{25}H_{41}NO$: 372.3266; $[MH]^+$. Found 372.3233.

Amine 70

Reductive amination of **58** with *p*-anisidine yielded amine **70**; 42%, 32 mg. ^{1}H NMR (500 MHz, $CDCl_3$) δ 6.81 (d, *J* = 8.9 Hz, 2H), 6.59 (d, *J* = 8.8 Hz, 2H), 3.79 (s, 3H), 3.68 (s, 1H), 2.04 (m, 2H), 1.92 (m, 1H), 1.9-1.5 (7H), 1.39 (m, 3H), 1.31 (m, 2H), 1.17 (m, 5H), 1.06 (m, 1H), 1.00 (s, 3H), 0.96 (m, 3H), 0.92 (m, 6H). ^{13}C NMR (126 MHz, $CDCl_3$) δ 151.5, 143.0, 115.0, 113.8, 56.9, 55.9, 52.2, 51.9, 42.2, 40.3, 39.5, 35.9, 35.4, 30.1, 28.0, 27.1, 23.8, 23.2, 22.8, 22.6, 18.5, 17.9, 13.7. IR(neat) *v*max 2928, 2864, 1508, 1464, 1262, 1172, 1041, 814. DART-HRMS: *m*/*z* calcd. for $C_{25}H_{41}NO$: 372.3266; $[MH]^+$. Found 372.3249.

Amine 71

Reductive amination of **58** with (3,4-methylenedioxy)-aniline yielded amine **71**; 20%, 24 mg. ^{1}H NMR (500 MHz, $CDCl_3$) δ 6.68 (d, *J*= 8.3 Hz, 1H), 6.26 (s, 1H), 6.05 (m, 1H), 5.87 (m, 2H), 3.65 (s, 1H), 2.03 (m, 2H), 1.90 (m, 1H), 1.8-1.5 (8H), 1.38 (m, 4H), 1.29 (m, 2H), 1.19 (m, 5H), 1.06 (m, 1H), 0.98 (s, 3H), 0.95 (d, *J* = 6.5 Hz, 3H), 0.92 (m, 6H). ^{13}C NMR (126 MHz, $CDCl_3$) δ 148.3, 144.5, 108.6, 100.4, 95.6, 56.9, 52.2, 51.8, 42.2, 40.3, 39.5, 35.9, 35.4, 30.6, 28.0, 27.1, 23.8, 23.2, 22.8, 22.5, 18.5, 17.8, 13.6.IR(neat) *v*max 3378, 2920, 2860, 1714, 1635, 1600, 1504, 1465, 1377, 1094, 875. DART-HRMS: *m*/*z* calcd. for $C_{25}H_{39}NO_2$: 386.3059 $[MH]^+$. Found 386.3048.

Amine 72

Reductive amination of **58** with 4-hydroxybenzylamine yielded amine **72**; 32%, 10 mg. ^{1}H NMR (500 MHz, $CDCl_3$) δ 7.05 (d, *J* = Hz, 2H), 6.78 (d, *J* = Hz, 2H), 5.17 (s, 1H), 3.40 (s, 1H), 3.02 (m, 1H), 2.54 (m, 2H), 2.37 (m, 1H), 2.1-1.9 (3H), 1.75 (m, 2H), 1.67 (m, 5H), 1.55 (m, 2H), 1.48 (m, 2H), 1.35 (m, 3H), 1.15 (m, 3H), 1.06 (s, 3H), 0.90 (m, 9H). ^{13}C NMR (126 MHz, $CDCl_3$) δ 153.9, 131.6, 130.1, 115.2, 59.8, 55.0, 48.8, 39.4, 36.9, 36.7, 35.3, 34.2, 29,7, 28.3, 28.0, 26.2, 24.3, 22.8, 22.5, 22.4, 22.1, 19.1. IR(neat) *v*max 2953, 2922, 2854, 1732, 1685, 1553, 1515, 1455, 1259, 1090, 1011, 799. DART-HRMS: *m*/*z* calcd. for $C_{25}H_{42}NO$: 372.3266 $[MH]^+$. Found 372.3248.

Aldehyde 73[133]

A mixture of methoxymethyl triphenylphosphonium chloride (2.1 g, 6 mmol) in THF (30 mL) was cooled to 0 C. With vigorous stirring, sodium t-butoxide (640 mg, 5.7 mmol) was added. The heterogeneous mixture immediately changed color to yellow and on to deeper yellow and finally deep red at 0 ºC. After 30 min, a solution of **58** (400 mg, 1.5 mmol) in THF (10 mL) was added to the above mixture. TLC indicated consumption of 33 after 20 min. Water (80 mL) was added and the mixture and was washed with ethyl acetate (3 x 80 mL). The organic layers were combined, dried over $MgSO_4$, filtered, and concentrated. The crude material was purified using column chromatography (SiO_2, 100% hexanes to 2% EtOAc in hexanes) to yield the vinyl ether; 89%, 390 mg as a clear oil. ^{1}H NMR (500 MHz, $CDCl_3$) δ5.84 (m, 1H), 3.43 (s, 3H), 1.97 (m, 3H), 1.77 (m, 4H), 1.52 (m, 3H), 1.42 (m, 3H), 1.33 (m, 3H), 1.25 (m, 1H), 1.19 (m, 5H), 1.01 (m, 1H), 0.92 (d, *J* = 6.5 Hz, 3H),0.87 (d, *J* = 6.6 Hz, 3H), 0.86 (d, *J* = 6.6 Hz, 3H), 0.68 (s, 3H). ^{13}C NMR (126 MHz, $CDCl_3$) δ 138.9, 118.2, 59.3, 56.0, 52.1, 44.4, 40.4, 39.5, 36.2, 28.0, 27.9, 25.1, 23.8, 22.8, 22.5, 22.4, 21.9, 18.8, 11.6. DART-HRMS: m/z calcd. for $C_{20}H_{37}O$: 293.2844; $[MH]^+$ Found: 293.2849.

The vinyl ether refluxed in methanol (10 mL) and 3N HCl (5 mL) for 12 h. The reaction was neutralized by the addition of 2 M NaOH, and the aqueous fraction washed with ethyl acetate (3 x 50 mL). The organic

layers were combined, dried over $MgSO_4$, filtered, and concentrated. The crude material was purified using column chromatography (SiO_2, 100% hexanes to 2% EtOAc in hexanes) to yield **73** in 75%, 280 mg yield as a clear oil. ^{1}H NMR (500 MHz, $CDCl_3$) δ 9.55 (m, 1H), 2.30 (m, 1H), 1.99 (m, 1H), 1.86 (m, 1H), 1.78 (m, 1H), 1.66 (m, 2H), 1.53 (m, 2H), 1.30 (m, 8H), 1.12 (m, 5H), 1.02 (m, 1H), 0.93 (d, *J* = 46.5 Hz,3H), 0.87(d, *J* = 2.1 Hz, 3H), 0.86 (d, *J* = 2.0 Hz, 3H), 0.71 (s, 3H). ^{13}C NMR (126 MHz, $CDCl_3$) δ 205.1, 55.4, 50.6, 49.4, 42.7, 39.4, 39.4, 36.1, 35.6, 28.0, 27.8, 25.7, 24.2, 23.7, 22.8, 22.5, 20.7, 18.7, 11.6. DART-HRMS: m/z calcd. for $C_{19}H_{35}O$: 279.2688; $[MH]^+$ Found: 279.2684.

Amine 74

Reductive amination of 3-aminophenol with aldehyde **73** afforded amine **74;** 46%, 8.3 mg. ^{1}H NMR (500 MHz, $CDCl_3$) δ 7.05 (t, *J* = 8.0 Hz, 1H), 6.22 (dd, *J* = 16.9 Hz, 2H). 6.13 (s, 1H), 4.50 (bs, 1H), 3.17 (m, 1H), 2.79 (m, 1H), 2.03 (m, 1H), 1.92 (m, 2H), 1.72 (m, 2H), 1.60 (m, 3H), 1.42 (m, 3H), 1.32 (m, 1H), 1.19 (m 5H), (m, 2H), 0.99 (d, *J* = 6.5 Hz, 3H), 0.94 (dd, *J* = 6.6, 2.1 Hz, 6H), 0.74 (s, 3H). ^{13}C NMR (126 MHz, $CDCl_3$) δ 156.8, 150.2, 130.1, 105.9, 104.1, 99.6, 56.2, 53.7, 49.0, 43.2, 40.0, 39.6, 39.5, 36.5, 36.4, 36.2, 35.7, 31.2, 28.1, 28.0, 27.9, 24.6, 24.5, 23.8, 22.8, 22.6, 21.9, 18.7, 11.9. IR(neat) *ν*max 2948, 2923, 2864, 1614, 1508, 1467, 1438, 1333, 1186, 1157, 838. DART-HRMS: *m*/*z* calcd. for $C_{25}H_{42}NO$: 372.3266 $[MH]^+$. Found 372.3270.

Amine 75

Reductive amination of 4-aminophenol with aldehyde **73** afforded amine **75**; 38%, 6.2 mg. ^{1}H NMR (500 MHz, $CDCl_3$) δ 6.72 (m, 2H), 6.59 (m, 2H), 4.33 (m, 2H), 3.20 (m, 1H), 2.71 (m, 1H), 1.90(m, 4H), 1.72 (m, 2H), 1.57 (m, 3H), 1.41 (m, 5H), 1.30 (m, 2H), 1.18 (m 6H), 1.06 (m, 1H), 0.99 (m, 3H), 0.93 (m, 6H), 0.73 (s, 3H). ^{13}C NMR (126 MHz, $CDCl_3$) δ 116.2, 114.1, 56.2, 53.7, 52.1, 50.1, 45.5, 44.0, 43.1, 39.5, 36.4, 34.8, 31.2, 28.0, 27.6, 25.7, 24.4, 23.8, 22.8, 22.5, 21.9, 20.5, 19.5, 18.7, 11.8. IR(neat) *ν*max 2950, 2923,

2865, 1512, 1468, 1232, 1215, 818. DART-HRMS: *m*/*z* calcd. for $C_{25}H_{42}NO$: 372.3266 $[MH]^+$. Found 372.3268.

C. C-25 functionalized Analogues

25-OH Ketone 76

$RuCl_3$ (100 mg, 0.48 mmol) and $NaIO_4$ (1.5 g, 7.0 mmol) were suspended in H_2O (20 mL) with pyridine (40 μL, 0.49 mmol). A solution of Ketone **58** (600 mg, 2.3 mmol) in MeCN (20 mL) was added to the reaction mixture and heated at 60 ºC for 48 h. The mixture was diluted with saturated sodium thiosulfate (20 mL) and filtered through celite. The filtrate was washed with EtOAc (50 mL x 3), dried with anhydrous sodium sulfate, and concentrated *in vacu*. Ketone **76** was purified with column chromatography (22 % EtOAc in hexanes), 420 mg, 67%. ^{1}H (500MHz, $CDCl_3$) δ 2.48 (m, 1H), 2.35-2.23 (2H), 2.15 (m, 1H), 2.06 (m, 1H), 1.93 (m, 2H), 1.77 (m, 1H), 1.65-1.55 (2H), 1.51-1.35 (7H), 1.30 (m, 1H), 1.26 (s, 6H), 1.13 (m, 1H), 1.01 (d, *J* = 6.0Hz, 3H), 0.68 (s, 3H). ^{13}C NMR (126 MHz, $CDCl_3$) δ 212.0, 71.0, 62.0, 56.6, 49.9, 44.3, 41.0, 39.0, 36.2, 35.5, 29.4, 29.2, 27.5, 24.0, 20.7, 19.1, 18.7, 12.5.

Amine 77

Reductive amination of 3-aminophenol with ketone **76** afforded amine **77**; 34%, 12 mg. ^{1}H NMR (500 MHz, $CDCl_3$) δ 7.01 (t, *J* = 8.0 Hz, 1H), 6.19 (m, 2H), 6.12 (m, 1H), 3.04 (m, 1H), 2.20 (m, 1H), 1.98 (m, 2H), 1.77 (m, 2H), 1.50 (m, 10H), 1.31 (m, 1H), 1.28 (s, 6H), 1.13 (m, 2H), 1.01 (d, *J* = 6.5 Hz, 3H), 0.98 (s, 1H), 0.96 (s, 3H). ^{13}C NMR (126 MHz, $CDCl_3$) δ 156.9, 149.8, 130.1, 106.0, 103.5, 99.3, 71.4, 56.5, 53.4, 45.6, 45.3, 44.3, 36.7, 35.2, 35.2, 33.1, 29.4, 29.3, 29.2, 29.1, 27.7, 24.3, 24.2, 21.3, 20.2, 19.4. IR(neat) *ν*max 3492, 3252, 2916, 1510, 1404, 1245, 1210, 1184, 1155, 962, 816. DART-HRMS: *m*/*z* calcd. for $C_{24}H_{39}NO_2$: 374.3059 $[MH]^+$. Found 374.3068.

Amine 78

Reductive amination of 4-aminophenol with ketone **76** afforded amine **78**; 29%, 19 mg. ^{1}H NMR (500 MHz, $CDCl_3$) δ 6.71 (m, 2H), 6.53 (m, 2H), 2.96 (m, 1H), 2.17 (m, 1H), 1.97 (m, 2H), 1.80 (m, 2H), 1.68 (m, 1H), 1.58 (m, 1H), 1.47 (m, 6H), 1.27 (s, 6H), 1.11 (m, 1H), 1.00 (d, J = 6.6 Hz, 3H), 0.95 (s, 3H). ^{13}C NMR (126 MHz, $CDCl_3$) δ 147.4, 116.2, 114.8, 109.9, 71.2, 56.4, 54.9, 45.7, 45.3, 44.3, 36.7, 35.3, 35.2, 33.2, 29.7, 29.4, 29.2, 27.7, 24.5, 24.2, 21.4, 20.2, 19.4. IR(neat) *v*max 3520, 3250, 2915, 1514, 1373,1241, 1189, 1162, 1105, 910, 822. DART-HRMS: *m*/*z* calcd. for $C_{24}H_{39}NO_2$: 374.3059 $[MH]^+$. Found 374.3058.

Ketone 79 (25OMe)

Ketone **76** (100 mg, 0.38 mmol) was dissolved in 3 mL anhydrous DMF and capped with a rubber septum. MeI (250 μL, 3.9 mmol) was added followed by NaH (70 mg, 1.1 mmol). The reaction stirred at 0ºC and warmed to RT overnight. After 16 h, the reaction was quenched with H_2O and extracted with EtOAc (10 mL x 3). The organics were concentrated and purified via column chromatography (4% EtOAc in hexanes). The reaction yielded both starting material **76** (50 mg, 50 %) along with ketones **79** (27 mg, 25%) and **80** (20 mg, 17%). ^{1}H NMR (500 MHz, $CDCl_3$) δ 3.21 (s, 3H), 2.49 (m, 1H), 2.30 (m, 2H), 2.14 (m, 1H), 2.03 (m, 1H), 1.95 (m, 2H), 1.73 (m, 2H), 1.6 – 1.2 (12H), 1.18 (s, 6H), 1.12 (m, 1H), 1.00 (d, J = 6.2 Hz, 3H), 0.67 (s, 3H). ^{13}C NMR (126 MHz, $CDCl_3$) δ 212.1, 74.6, 62.0, 56.6, 49.9, 49.1, 40.9, 40.2, 39.0, 36.3, 35.5, 27.5, 25.1, 25.0, 24.0, 20.2, 19.1, 18.7, 12.5.

Ketone 80 (9-Me, 25OMe)

^{1}H NMR (500 MHz, $CDCl_3$) δ3.21 (s, 3H), 2.72 (m, 1H), 2.46 (m, 1H), 2.11 (m, 1H), 1.96 (m, 2H), 1.73 (m, 4H), 1.43 (m, 8H), 1.22 (d, J = 7.4 Hz, 3H), 1.18 (m, 6H),1.08 (m, 1H), 1.00 (d, J = 6.3 Hz, 3H), 0.68 (s, 3H). ^{13}C NMR (126 MHz, $CDCl_3$) δ 216.0, 74.6, 57.3, 56.6, 49.6, 49.1, 43.7, 40.2, 36.2, 35.5, 35.1, 30.3, 29.7, 27.6, 25.0, 20.1, 19.0, 18.7, 18.5, 13.1.

Amine 81 (4-70)

Reductive amination of 3-aminophenol with ketone **79** afforded amine **81**; 15%, 14 mg. ^{1}H NMR (500 MHz, $CDCl_3$) δ 7.02 (m, 1H), 6.16 (m, 3H), 3.73 (s, 1H), 3.23 (m, 3H), 2.02 (m, 2H), 1.9-1.3 (20H), 1.25 (m, 3H), 1.19 (s, 6H), 1.09 (m, 5H), 0.97 (m, 6H), 0.89 (m, 2H). ^{13}C NMR (126 MHz, $CDCl_3$) δ 156.8, 150.1, 130.0, 105.3, 103.3, 99.0, 74.7, 56.7, 51.6, 51.1, 49.1, 42.2, 40.3, 40.2, 36.2, 35.3, 30.6, 29.7, 27.1, 25.0, 23.2, 20.2, 18.5, 17.8, 13.6. IR(neat) *ν*max 2993, 2923, 2852, 1725, 1611, 1559, 1509, 1455, 1363, 1261, 1188, 1085, 814. DART-HRMS: *m*/*z* calcd. for $C_{25}H_{42}NO_2$: 388.3216 $[MH]^+$. Found. 388.3243.

Aldehyde 85 (25OH CHO)

Aldehyde **82** was synthesized following the same procedure as aldehyde **73** from ketone **76**; 70% over two steps, 390 mg. Although a mixture of α- and β-aldehydes were formed (2:1 mixture based on the aldehyde proton peak), a single isomer was obtained for each reductive amination procedure. ^{1}H NMR (500 MHz, $CDCl_3$) δ 9.60 (m, 0.5H), 9.53 (m, 1H), 3.47 (m, 0.5H), 3.42 (m, 1H), 1.97 (m, 2H), 1.83 (m, 4H), 1.75 (m, 2H), 1.62 (m, 6H), 1.48 (m, 12H), 1.34 (m, 2H), 1.27 (m, 10H), 1.00 (m, 6H), 0.96 (s, 3H). ^{13}C NMR (126 MHz, $CDCl_3$) δ 205.3, 71.0, 55.4, 52.1, 50.7, 49.5, 47.6, 45.7, 44.3, 43.4, 39.4, 36.6, 35.6, 35.0, 29.7, 29.3, 29.2, 27.5, 25.9, 25.7, 24.2, 23.8, 21.2, 20.7, 19.7, 19.2, 18.7, 11.6.

Amine 83

Reductive amination of 3-aminophenol with aldehyde **82** afforded amine **83**; 48%, 15 mg. ^{1}H NMR (500 MHz, $CDCl_3$) δ 7.04 (t, J = 8.0 Hz, 1H), 6.22 (m, 2H), 6.12 (s, 1H), 4.21 (bs, 1H), 3.20 (m, 1H), 2.77 (m, 1H), 2.02 (m, 1H), 1.89 (m, 2H), 1.70 (m, 2H), 1.57 (m, 3H), 1.39 (m, 3H), 1.31 (m, 1H), 1.18 (m, 8H), 0.98 (d, J = 6.5 Hz, 3H), 0.91 (m, 6H), 0.74 (s, 3H). ^{13}C NMR (126 MHz, $CDCl_3$) δ 156.7, 150.3, 130.1, 105.9, 103.9, 99.3, 56., 53.7, 48.9, 43.1, 40.0, 39.5, 36.5, 36.2, 35.7, 31.2, 28.0, 27.9, 24.6, 23.8, 22.8, 22.5, 21.9, 18.7, 11.9. IR(neat) *ν*max 2629, 1617, 1510, 1466, 1157, 755, 686. DART-HRMS: *m*/*z* calcd. for $C_{25}H_{42}NO_2$: 372.3266 $[M\text{-}O+H]^+$. Found 372.3380.

Amine 84

Reductive amination of 4-aminophenol with aldehyde **82** afforded amine **84**; 59%, 16 mg. ^{1}H NMR (500 MHz, $CDCl_3$) δ 6.73 (m, 2H), 6.60 (m, 2H), 4.12 (bs, 1H), 3.189 (m, 1H), 2.78 (m, 1H), 1.98 (m, 1H), 1.90 (m, 2H), 1.71 (m, 2H), 1.57 (m, 3H), 1.38 (m, 4H), 1.18 (m, 7H), 1.05 (m, 1H), 0.97 (d, *J* = 6.5 Hz, 3H), 0.91 (m, 6H), 0.73 (s, 3H). ^{13}C NMR (126 MHz, $CDCl_3$) δ 116.2, 114.4, 56.2, 53.7, 43.1, 40.0, 39.5, 36.4, 36.2, 35.7, 31.2, 28.0, 27.9, 24.6, 23.8, 22.8, 22.5, 21.9, 18.7, 11.8. IR(neat) *ν*max 2703, 1635, 1508, 1415, 1155, 804. DART-HRMS: *m*/*z* calcd. for $C_{25}H_{42}NO_2$: 388.3215 $[MH]^+$. Found 388.3214. $[M\text{-}O+H]^+$ calcd. 372.3266. Found 372.3249.

Enol ether 85

A mixture of methoxymethyl triphenylphosphonium chloride (1.1 g, 3 mmol) in THF (30 mL) was cooled to 0 C. With vigorous stirring, sodium t-butoxide (300 mg, 2.8 mmol) was added. The heterogeneous mixture immediately changed color to yellow and on to deeper yellow and finally deep red at 0 ºC. After 30 min, a solution of **76** (210 mg, 0.8 mmol) in THF (10 mL) was added to the above mixture. After 1 hr, TLC indicated consumption. Water (30 mL) was added and the mixture and was washed with EtOAc (3 x 30 mL). The organic layers were combined, dried over $MgSO_4$, filtered, and concentrated. The crude 25-OH enol ether was re-suspended in DMF (8 mL) and cooled to 0 ºC. MeI (0.5 mL, 8.0 mmol) was added followed by NaH (100 mg, 1.6 mmol). The reaction stirred for 4 h warming to RT. The reaction was quenched by slow addition of water (20 mL), and washed with EtOAc (3 x 20 mL). The organics were combined, dried and concentrated. Enol ether **85** was purified via column chromatography 3% EtOAc in hexanes; 145 mg, 62%. ^{1}H NMR (500 MHz, $CDCl_3$) δ 5.58 (s, 1H), 3.59 (s, 3H), 3.22 (s, 3H), 2.78 (m, 1H), 2.02 (m, 1H), 1.89 (m, 3H), 1.43 (m, 13H), 1.30 (m, 9H), 1.18 (s, 6H), 1.10 (m, 2H), 0.98 (m, 3H), 0.93 (m, 2H), 0.61 (s, 3H). ^{13}C NMR (126 MHz, $CDCl_3$) δ 139.0, 118.3, 74.7, 59.4, 55.9, 52.1, 49.1, 44.4, 40.4, 40.3, 36.5, 36.2, 29.7, 27.9, 25.1, 25.0, 22.5, 22.0, 20.3, 18.8, 11.7.

Aldehyde 86

Enol ether **85** (100 mg, 0.3 mmol) was dissolved in MeOH (10 mL) and HCl (2N, 5 mL). The reaction stirred at RT for 6 h till TLC indicated consumption. After which, the reaction as quenched by slow addition of 2M NaOH, and washed with EtOAc (3 x 15 mL). The organics were combined, dried and concentrated. Aldehyde **86** was purified via column chromatography, 4% EtOAc in hexanes; 75%, 72 mg. ^{1}H NMR (500 MHz, $CDCl_3$) δ 9.60 (s, 1H), 3.42 (m, 2H), 3.22 (s, 3H), 2.35 (m, 1H), 2.1 – 1.8 (4H), 1.71 (m, 3H), 1.61 (m, 3H), 1.43 (m, 8H), 1.18 (s, 6H), 1.09 (m, 6H), 0.99 (m, 4H), 0.93 (m, 4H), 0.89 (m, 4H), 0.76 (s, 3H). ^{13}C NMR (126 MHz, $CDCl_3$) δ 205.1, 108.8, 74.6, 55.4, 50.7, 49.5, 49.1, 40.3, 39.4, 36.5, 35.7, 31.9, 29.7, 29.3, 27.9, 25.7, 25.0, 24.2, 22.7, 20.7, 20.2, 18.7, 14.1, 11.6. DART-HRMS: *m*/*z* calcd. for $C_{25}H_{36}O_2$: 291.2688 $[MH]^+$. Found 291.2696.

Amine 87

Reductive amination of 3-aminophenol with aldehyde **86** afforded amine **87**; 32%, 18 mg. ^{1}H NMR (500 MHz, $CDCl_3$) δ 7.04 (m, 1H), 6.21 (m, 2H), 6.15 (m, 1H), 3.23 (s, 3H), 3.17 (m, 1H), 2.79 (m, 1H), 2.02 (m, 1H), 1.89 (m, 2H), 1.71 (m, 2H), 1.58 (m, 3H), 1.42 (m, 7H), 1.24 (m, 2H), 1.19 (s, 6H), 1.1 - 1.0 (4h), 0.99 (m, 3H), 0.92 (m, 3H), 0.73 (s, 3H). ^{13}C NMR (126 MHz, $CDCl_3$) δ 156.9, 130.1, 105.9, 104.1, 99.5, 74.8, 56.1, 53.6, 49.0, 43.1, 40.3, 39.9, 36.5, 36.4, 35.7, 31.2, 29.7, 27.9, 25.0, 24.6, 21.9, 20.2, 18.7, 11.9. IR(neat) *ν*max 3490, 2947, 2875, 1780, 1620, 1572, 1512, 1495, 1453, 1365, 1205, 1170, 895. DART-HRMS: *m*/*z* calcd. for $C_{26}H_{43}NO_2$: 402.3372 $[MH]^+$. Found 402.3366.

Alcohol 88

Ketone **76** (50 mg, 0.18 mmol) was dissolved in DMF (5 mL) and cooled to 0 ºC. Triethylsilyl chloride (48 mg, 0.44 mmol) was added followed by imidazole (37 mg, 0.54 mmol). The reaction was quenched by slow addition of water (15 mL) and washed with EtOAc (3 x 10 mL). The organics were combined, dried and concentrated. The 25-OTES ketone was purified via column chromatography, 5 % EtOAc in hexanes; 94%, 66 mg. Sodium borohydride (15 mg, 0.38 mmol) was added to a solution of 25-OTES ketone (60 mg, 0.15

mmol) in DCM:MeOH (2:1, 6 mL) at 0 ºC. The reaction stirred for 4 h warming to RT. The reaction was quenched by slow addition of water (10 mL) and washed with EtOAc (3 x 15 mL). The organics were combined, dried and concentrated. Alcohol **88** was purified via column chromatography, 5% EtOAc in hexanes; 90%, 60 mg. ^{1}H NMR (500 MHz, $CDCl_3$) δ 4.12 (m, 1H), 2.04 (m, 1H), 1.84 (m, 3H), 1.7 – 1.3 (13H), 1.23 (s, 6H), 1.11 (m, 3H), 0.99 (m, 11H), 0.94 (m, 3H), 0.60 (m, 6H). ^{13}C NMR (126 MHz, $CDCl_3$) δ 73.5, 69.5, 56.7, 52.6, 45.5, 41.8, 40.4, 36.3, 35.3, 33.6, 30.0, 29.8, 27.2, 22.5, 20.8, 18.5, 17.4, 13.5, 7.1, 6.8.

Ester 89 (25OH, 3-101)

Ester **89** was synthesized following the same esterification procedure as the C-11 modified analogues (**61**a-e). Ester **89** was purified via column chromatography, 15% EtOAc in hexanes; 75% 13 mg. ^{1}H NMR (500 MHz, $CDCl_3$) δ 7.62 (m, 2H), 7.34 (t, J = 7.9 Hz,1H), 7.11 (m, 1H), 5.42 (s, 1H), 2.05 (m, 2H), 1.84 (m, 3H), 1.6 – 1.4 (10H), 1.28 (s, 6H), 1.23 (m, 2H), 1.16 (m, 1H), 1.04 (s, 3H), 0.96 (d, J = 6.5 Hz, 3H). ^{13}C NMR (126 MHz, $CDCl_3$) δ 166.7, 156.2, 132.1, 129.6, 121.6, 120.2, 116.3, 72.7, 71.6, 56.4, 51.5, 44.2, 41.9, 39.9, 36.1, 35.4, 30.5, 29.3, 29.2, 27.0, 22.6, 20.8, 18.5, 18.0, 13.6. IR(neat) *ν*max 2939, 1717, 1687, 1588, 1452, 1291, 1215, 1156, 1102, 1072, 946, 917, 883, 804, 752. DART-HRMS: m/z calcd. for $C_{25}H_{38}O_4$: 420.3114 $[MNH4]^+$. Found 420.3104.

Ester 90 (25OMe, 3-151)

Sodium borohydride (13 mg, 0.32 mmol) was added to solution of ketone **79** (25 mg, 0.08 mmol) in MeOH (5 mL). After 2 h, the reaction was quenched and washed with EtOAc (3 x 15 mL). The organics were concentrated *in vacu*. 25-OMe Grundmann's alcohol (25-OMe GA) was purified via column chromatography, 8% EtOAc in hexanes; 92%, 23 mg. ^{1}H NMR (500 MHz, $CDCl_3$) δ 4.11 (m, 1H), 3.21 (s, 3H), 2.05 (m, 1H), 1.87 (m, 3H), 1.59 (m, 1H), 1.40 (m, 12H), 1.21 (m, 1H), 1.17 (s, 6H), 1.07 (m, 2H), 0.97 (s, 3H), 0.94 (d, J = 6.5 Hz, 3H). ^{13}C NMR (126 MHz, $CDCl_3$) δ 74.7, 69.4, 56.6, 52.6, 49.0, 41.8, 40.4, 40.3, 36.3, 35.2, 33.6, 27.1, 25.04, 25.02, 22.5, 20.2, 18.5, 17.4, 13.5.

25-OMe GA (20 mg, 0.07 mmol) was dissolved in DCM (10 mL). 3-OMOM-benzoic acid (42 mg, 0.23 mmol) was added followed by DMAP (27 mg, 0.21 mmol) and DCC (37 mg, 0.18 mmol). The reaction stirred at RT overnight (16 h). The reaction was purified directly via column chromatography, 5 % EtOAc in hexanes; 68%, 21 mg. ^{1}H NMR (500 MHz, $CDCl_3$) δ 7.78 (m, 1H), 7.75 (m, 1H), 7.40 (t, *J* = 7.9 Hz, 1H), 7.26 (m, 1H), 5.44 (m, 1H), 5.25 (s, 2H), 3.53 (s, 3H), 3.22 (s, 3H), 2.10 (m 1H), 2.02 (m, 1H), 1.87 (m, 2H), 1.57 (m, 5H), 1.42 (m, 6H), 1.30 (m, 4H), 1.18 (s, 6H), 1.09 (s, 3H), 0.99 (d, *J* = 6.5 Hz, 3H). ^{13}C NMR (126 MHz, $CDCl_3$) δ 166.1, 157.2, 132.3, 129.4, 123.1, 120.8, 117.2, 94.5, 74.6, 72.4, 56.4, 56.0, 51.6, 49.1, 41.9, 40.3, 39.9, 36.3, 35.4, 30.5, 27.1, 25.0, 22.6, 20.2, 18.6, 18.0, 13.5.

(±) Camphor sulfonic acid (CSA, 30 mg, 0.13 mmol) was added to a solution of MOM-protected ester (20 mg, 0.04 mol) in MeOH (5 mL) and stirred at RT overnight (16 h). The reaction was concentrated and purified via column chromatography, 8% EtOAc in hexanes; 65%, 14 mg. ^{1}H NMR (500 MHz, $CDCl_3$) δ 7.66 (m, 1H), 7.61 (s, 1H), 7.35 (t, *J* = 7.9 Hz, 1H), 7.10 (m, 1H), 6.48 (s, 1H), 5.42 (s, 1H), 3.25 (s, 3H), 2.08 (m, 2H), 1.84 (m, 2H), 1.56 (m, 5H), 1.42 (m, 5H), 1.30 (m, 3H), 1.21 (s, 6H), 1.05 (s, 3H), 0.97 (d, *J* = 6.5 Hz, 3H). ^{13}C NMR (126 MHz, $CDCl_3$) δ 166.6, 156.1, 132.2, 129.6, 121.7, 120.1, 116.2, 75.1, 72.7, 56.4, 51.5, 49.0, 41.9, 40.4, 39.9, 36.2, 35.4, 30.5, 27.0, 25.0, 24.8, 22.7, 20.3, 18.6, 18.0, 13.6. IR(neat) *ν*max 2982, 2940, 1715, 1686, 1588, 1450, 1290, 1216, 1157, 1098, 1066, 946, 918, 881, 805, 753. DART-HRMS: m/z calcd. for $C_{26}H_{40}O_4$: 434.3270 $[MNH_4]^+$. Found 434.3276.

Biological Assay Protocols

General Information

Protocols for general cell culture, qPCR (Hh pathway and VDR), and VDR binding assays are as previously described.[127, 131] 20α-Hydroxycholesterol and 22(S)-hydroxycholesterol (OHCs) were purchased from Sigma-Aldrich. VD3 for biological studies was purchased from Sigma-Aldrich and calcitriol was purchased from Caymen Chemical. Data was analyzed using GraphPad Prism 5, and reported values represent mean ± SEM for at least two separate experiments performed in triplicate.

Modulation of the Hedgehog Signaling Pathway by Sterol-based Small Molecules

Chad Anthony Maschinot

Chapter 4:

Mechanism of Action Studies Towards Inhibition of Hedgehog

Signaling by Vitamin D-based Small Molecules

Introduction

When vitamin D3 and its metabolites were identified as inhibitors of Hh signaling, initial reports suggested that inhibition was a result of direct binding to the Smoothened (Smo) receptor.[124] Additional studies have suggested a mechanism of action where the vitamin D receptor interacts with the Hh pathway to inhibit signaling.[142] The activity of the most recent analogues developed within the Hadden lab, discussed in Chapter 3, suggests that at least some of the Hh inhibitory activity is due to activation of vitamin D signaling. This hypothesis is based on similar activity to calcitriol observed for C-25 functionalized analogues. An additional trend was observed between Cyp24A1 mRNA expression and anti-Hh activity, where both appeared to increase together. This may be coincidental and a result of increased interactions with a component of the Hh pathway, but additional mechanism of action studies need to be performed to further evaluate this observation. With contradictory mechanisms of action reported, follow-up studies were designed to provide insight into the mechanism of action of vitamin D analogues.

I. Vitamin D Receptor

The vitamin D receptor (VDR) is a member of the steroid hormone nuclear receptor family and a ligand-dependent transcription factor most commonly associated with calcium and phosphorous homeostasis in the bone.[142] It is comprised of three domains: (1) N-terminal DNA binding domain (DBD) with two zinc fingers, (2) C-terminal ligand binding domain (LBD), and (3) hinge region connecting the two binding domains.[121] Crystal structures of both the ligand and DNA binding domains have been solved separately in the last 20 years,[143-144] adding greater insight into the multiple functions of VDR.

As a nuclear receptor and transcription factor, ligand bound ("active") VDR interacts with a number of coregulatory proteins such as the coactivators, DRIP (vitamin D receptor interacting protein)[145] and RXR (retinoid X receptor).[146] Unliganded ("inactive") VDR associates with corepressors, such as NCoR (nuclear receptor corepressor) and the silencing mediator of retinoic acid and thyroid hormone receptor (SMRT), and histone deacetylases (**Figure 18**).[147-148] In addition to regulation by coregulatory proteins, VDR function is tissue specific. Using three different cell types, sChIP-seq (chromatin immunoprecipitation-

sequencing) assays identified 1,600 – 2,700 specific VDR-binding sites, with only 20% of those sites found in all three assays.[149] This suggests that VDR activity is highly cell type specific and that the 20% conserved sites represent important cellular functions for all VDR expressing tissues.

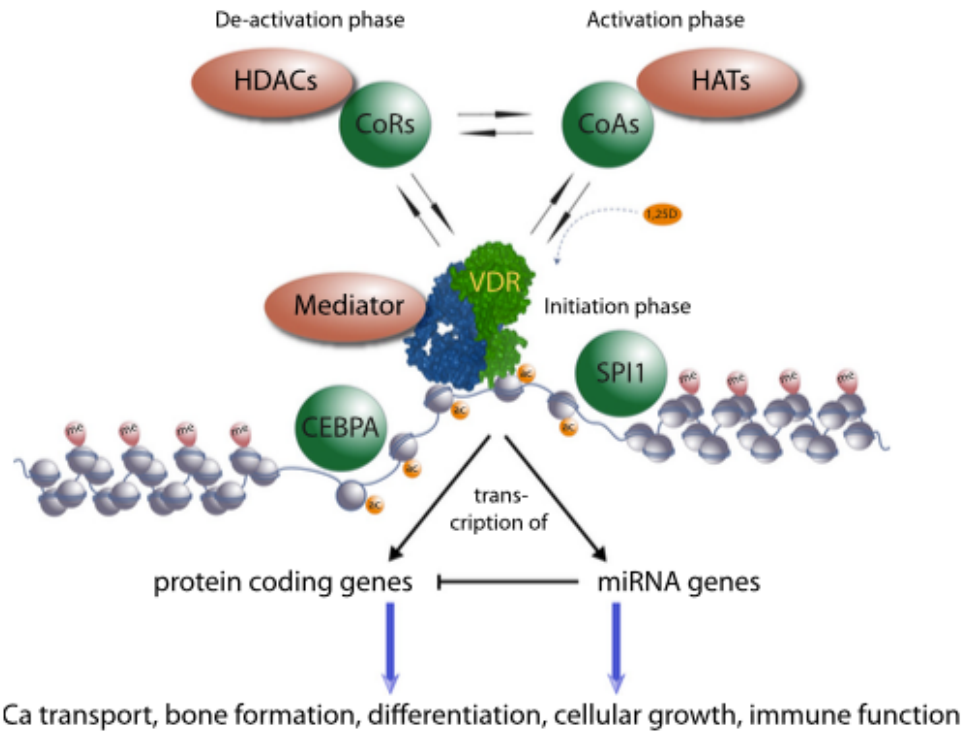

Figure 18.[147] Regulation of vitamin D receptor activity by coregulatory proteins. Unliganded (inactive) VDR associates with corepressor proteins (CoRs) by complex formation with histone deacetylases (HDACs). Ligand bound (active) VDR associates with coactivator proteins (CoAs) and histone acetyltransferases (HATs). The specific complex regulates the primary target genes for transcription, such as protein coding genes (*Cyp24A1*) or miRNAs (miR-214). Some miRNAs regulate mRNA expression of protein encoding genes, as will be discussed later in Chapter 4. CEBPA (CCAAT enhancer-binding protein alpha) and SPI1 (PU.1) represent additional transcription factors that enhance VDR activity.[147,149] Reprinted from Steroids, 78, Carlberg, C.; et al. Vitamin D receptor signaling mechanisms: Integrated actions of a well-defined transcription factor, 127-136, 2013, with permission from Elsevier.

II. Vitamin D and Cancer

As noted above, the primary functions of VDR are associated with proper bone formation where vitamin D deficiency has been linked for multiple decades to increased risk of fractures and bone disease, such as rickets.[150-151] In addition, studies in the past 15-20 years have associated vitamin D deficiency with a variety of cancers. This correlation was notably seen in the Garland and Garland report that correlated colon cancer mortality rates and UV-B exposure, as evident by the highest mortality rates observed in the

northeastern United states and decreased rates in the south and west.[152] This study suggested that increased exposure to UV-B (sunlight) lead to higher rates of vitamin D synthesis that could reduce the risk of colorectal cancer. In follow-up epidemiological studies,[153] low serum 25-OH VD3 (the accepted clinical measure for vitamin D levels) was associated with increased risk of prostate, breast, and colorectal cancer. Multiple associations have also been made between vitamin D metabolism enzymes and cancer incidences. In these studies, increased expression of Cyp24A1, or decreased expression of Cyp27B1, lead to a reduction in calcitriol production and increased cancer risk/occurance.[153] Taken together, these studies would suggest a role for calcitriol in regulating tumor growth.

Most studies of VDR and calcitriol have been performed using keratinocytes, the primary cell type of the epidermis, or outermost layer of skin cells. VDR plays a critical role in their differentiation, so these cells maintain tight control over VDR and calcitriol activity by expressing all the enzymatic machinery required for production and metabolism of calcitriol.[153] Additionally, VDR expression and activity is distinct depending on the differentiation status of the cells, with decreased VDR activity as the cells age.[142]

Skin cancers, such as BCC and squamous cell carcinoma (SCC), are some of the most common malignancies and all express VDR. Even with this relationship, there is a lack epidemiological evidence for a positive role of vitamin D and VDR in preventing skin cancer development.[154] Animal studies however suggest a protective role exists. Administration of dimethylbenzanthracene,[155] or UV-radiation,[156] to VDR null mice resulted in skin tumors formation, while no tumors were observed in control mice. In addition, Cyp27B1 null mice, which lack the ability to produce calcitriol, did not show increased susceptibility to tumor formation.[156] This study suggests that a protective role may exists for VDR itself and not calcitriol.

A few mechanisms have been proposed for this protective role. First and as previously mentioned, vitamin D signaling plays an integral and critical role in the proliferation and differentiation of keratinocytes. Secondly, vitamin D signaling regulates DNA damage repair, where VDR null mice show slowed DNA damage repair induced by UV-radition.[157] Therefore, dysregulation of VDR signaling could result in poorly differentiated cells and accumulation of mutations leading to tumor formation.

III. VDR and Signaling Pathways

Both SHh and Wnt/β-catenin signaling are associated with increased proliferation and decreased differentiation of keratinocytes, where activation of both pathways are associated with skin tumor formation.[158] In the absence of VDR, β-catenin expression increased and induced tumors resembling BCCs.[159-160] Follow-up studies indicated that many β-catenin target genes contain vitamin D response elements (VDREs) are many of the genes induced independent of canonical TCF/Lef expression. Activation of VDR shifted β-catenin target genes away from canonical TCF/Lef target genes and to VDR controlled genes, suggesting that VDR is an independent transcriptional effector of Wnt signaling. [160-161] A follow up study indicated that inactive (unliganded) VDR interacted with Lef1 and addition of calcitriol (liganded VDR) resulted in VDR-β-catenin binding.[161] More recently, several long non-coding RNAs associated with tumor formation, such as H19, are overexpressed in VDR null keratinocytes *in vitro* and *in vivo.*[162] Overexpression of H19 has been associated with dysregulation of Wnt/β-catenin signaling,[163] but this potential interaction remains to be investigated. Interactions between Hh and VDR signaling appear to be much more complicated and remain to be investigated.

A. VDR and Hedgehog Signaling

Both Hh and VDR signaling have been suggested to play a role in tumor formation, where VDR null mice show overexpression of Hh components and tumor formation.[165] However, interactions between VDR and Hh signaling are complicated as results have been contradictory. Initial reports looked to investigate the endogenous regulation of Smo and suggested that a 3β-hydroxysteroid, VD3 or 7-DHC, was secreted by Ptch and interacted with the extracellular domain of Smo to inhibit downstream signaling.[124] Based on this model, binding of Hh ligands to Ptch prevents secretion of VD3/7-DHC (**Figure 19a**). Interestingly, follow-up studies suggested that VD3 (**46**) was more active than any of the other vitamin D metabolites – 7-DHC (**45**), 25-OH VD3 (**47**), and calcitriol (**48**).[126] Additional studies have supported a mechanism of action of direct binding to Smo and independent of VDR, where calcitriol independently inhibited Hh

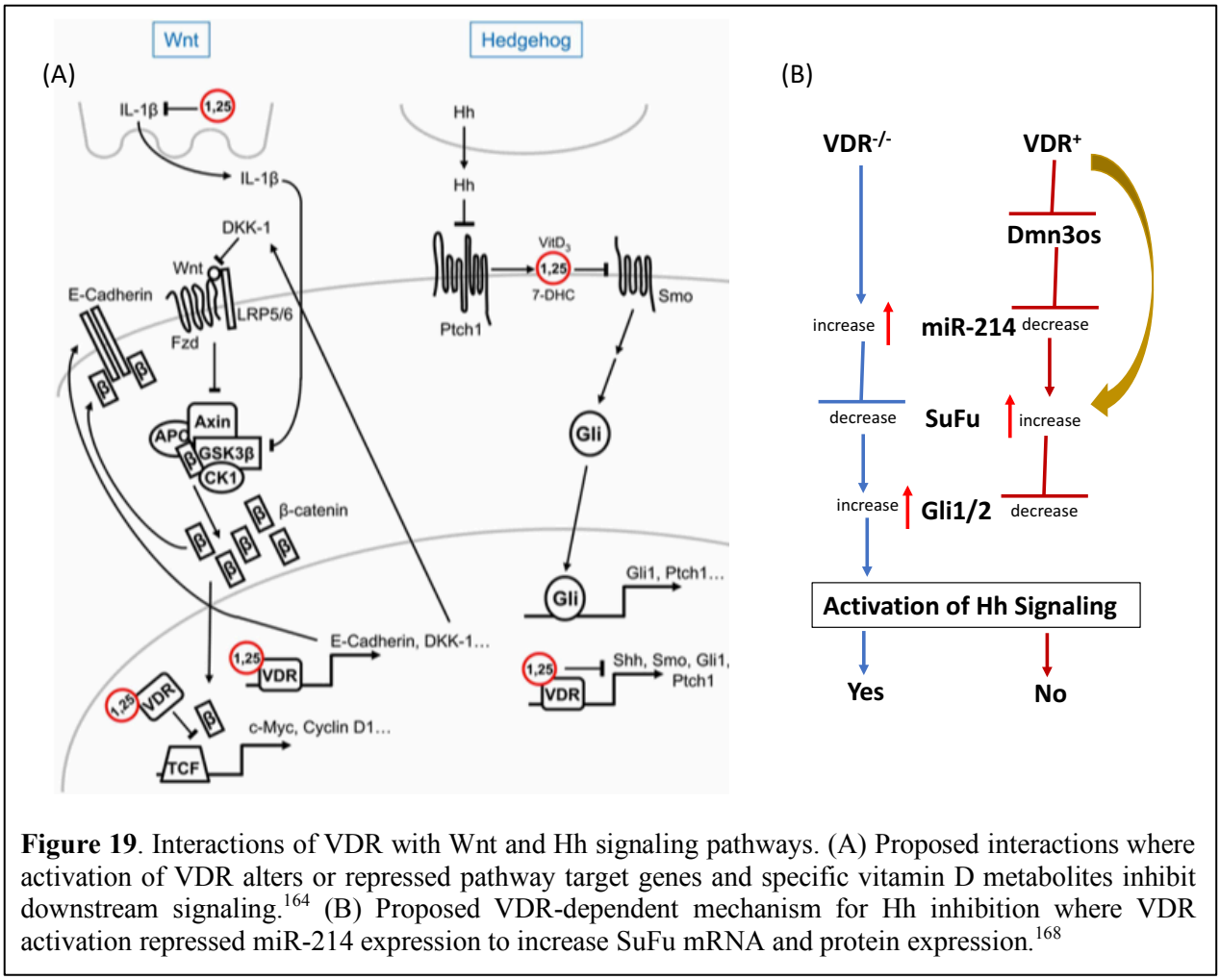

Figure 19. Interactions of VDR with Wnt and Hh signaling pathways. (A) Proposed interactions where activation of VDR alters or repressed pathway target genes and specific vitamin D metabolites inhibit downstream signaling.[164] (B) Proposed VDR-dependent mechanism for Hh inhibition where VDR activation repressed miR-214 expression to increase SuFu mRNA and protein expression.[168]

signaling and activated VDR signaling resulting in concomitant antiproliferative effects on BCC growth stronger than cyclopamine, Hh-specific inhibition.[166] It has also been suggested that the binding site is distinct from the trans-membrane (TM) region or the cysteine-rich domain (CRD).[167] In agreement with this proposal, previous studies in the Hadden lab have shown an inability of VD3 (**46**) to displace BODIPY-cyclopamine.[131]

Contradictory to these reports, evidence has also suggested VDR-dependent inhibition of Hh signaling. First, experiments performed in the Hadden lab show an increase in potency progressing down vitamin D metabolism, with calcitriol (**48**) being the most potent (Ch3, Table 11). Secondly, increases in analogue potency were observed with the incorporation of a C-25 hydroxyl group, the next metabolic step of VD3. Another recent report has proposed a crosstalk mechanism for VDR and Hh signaling (**Figure 19b**). Comparing VDR knockout ($VDR^{-/-}$) and wild-type (WT) breast cancer cells, VDR was shown to regulate a

number of micro-RNAs (miRNAs), including miR-214 which was upregulated over 40-fold in $VDR^{-/-}$ cells.[168] Further studies indicated that VDR and miR-214 were inversely correlated, and miR-214 suppressed SuFu protein expression.[168-169] This study ultimately proposed that VDR indirectly regulates SuFu mRNA and protein expression to inhibit Hh signaling through miR-214. Their results suggest that activation of VDR increased SuFu protein expression. The determined that this increase was a result of indirect repression of miR-214 expression by repressing the expression of Dnm3os, a non-coding RNA transcript of the dynamin-3 gene encoding the miR-214 cluster.[168]

IV. Mechanism of Action Studies

Based on multiple differences between published reports and experimental evidence in the Hadden lab, a series of experiments were designed to elucidate more information on the specific mechanism of action that our synthetic analogues utilize to inhibit Hh signaling. Previous studies performed by former lab members (Albert M DeBerardinis, PhD, Upasana Banerjee, PhD, and Vibhavari Sail, MS) suggested that our synthetic analogues acted independent of VDR. This interpretation was based on very low upregulation of the VDR target gene, *Cyp24A1*, and single concentration studies with $VDR^{-/-}$ cells and VDR-specific RNAi (interfering RNA), **Figure 20**.[131]

In these studies, ester **51** maintained inhibitory activity at 5 μM following the addition of VDR RNAi, while VD3 (**46**) lost all inhibitory activity under the same conditions. Calcitriol (**48**) however showed little loss in inhibitory activity, suggesting that VD3 may act through a distinct mechanism. Furthermore, VDR RNAi abolished Cyp24A1 upregulation of VD3 and calcitriol, which was not unexpected as VDR RNAi was only able to knockdown approximately half of the endogenous VDR mRNA expression.[131] Combining these results with the inability of VD3 or **51** to displace BODIPY-Cyc (**Figure 20c**), suggested that VD3 may act through VDR signaling while our analogues may act through a separate mechanism. In $VDR^{-/-}$ cells, there was no loss in anti-Hh activity for VD3 or calcitriol, which further complicated results suggesting that all compounds may act independent of VDR (**Figure 20d**).

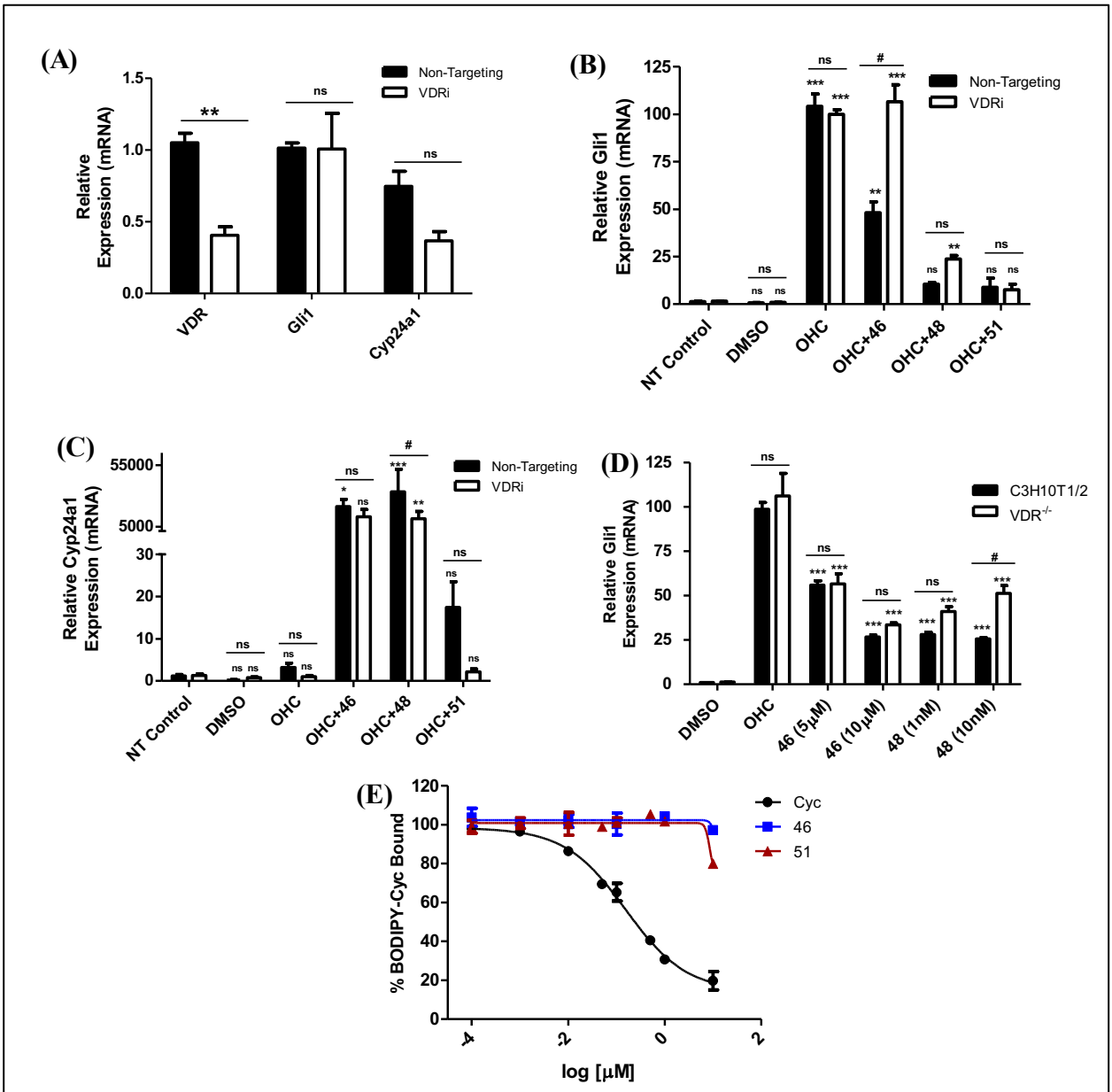

Figure 20. Initial mechanism of action studies in the Hadden lab. Relative expression of VDR, Gli1 and Cyp24A1 in response to non-targeting (filled) and VDR-specific (open) RNAi transfection. Relative expression of Gli1 (B), and Cyp24A1 (C) following RNAi and compound treatment. Statistical analysis one-way ANOVA with Tukey post-test performed with GraphPad Prism5; ***p<0.001, **p<0.01, *p<0.05, compared with corresponding RNAi treatment; # p<0.01, compared between RNAi treatments; ns, not statistically significant. (D) Comparison of Gli1 expression in $VDR^{-/-}$ (open) and C3H (closed) cells; Statistical analysis one-way ANOVA with Tukey post-test performed with GraphPad Prism5; ***p<0.001, compared with corresponding OHC treatment; #p<0.01, compared between cell lines; ns, not statistically significant. (E) BODIPY-Cyc displacement studies indicate VD3 (**46**) and ester **51** are unable to displace BODIPY-Cyc from Smo.[131]

A. Determining the Necessity of VDR

A new hypothesis was formed based on previous mechanism of action studies (**Figure 20**) and the trend that Cyp24A1 levels and anti-Hh activity increased together for vitamin D metabolites and the new analogues. This new hypothesis is that vitamin D-based compounds may be able to directly inhibit Hh signaling but also be able to further inhibit via crosstalk through VDR signaling. To evaluate this hypothesis, Cyp24A1 EC_{50} (half maximal effective concentration) values were collected in ASZ001 (ASZs) cells due to obtaining the highest Cyp24A1 values at single concentrations in ASZs, **Table 13**. A strong correlation was observed between Gli1 IC_{50} and Cyp24A1 EC_{50} values for nearly all analogues. For example, an IC_{50} value of 110 nM and an EC_{50} value of 130 nM were obtained for **78** suggesting little "true" selectivity for Hh over VDR signaling and a potential role for VDR signaling in the regulation of Hh signaling.

To further investigate potential crosstalk between the two signaling pathways, cellular-knockout models were utilized to evaluate VD3 (**46**), calcitriol (**48)**, and amines **56** and **78**. These specific analogues (**56** and **78**) were chosen because even though **78** is the C-25 hydroxylated version of **56** they had comparable IC_{50} values across cell lines, but had significantly different Cyp24A1 expressions (2 – 45-fold for **56** and >15,000-fold for **78**). With such significant Cyp24A1 differences, we hypothesized that these

Table 13. Comparison of Hh inhibitory and VDR agonistic potency in ASZ001 BCC cells.

	IC_{50} (Gli1, μM)[a]	Cyp24A1[b]	EC_{50} (Cyp24A1, μM)[a]
46	1.1 ± 0.01	2,200 ± 200	0.95 ± 0.05
47	0.48 ± 0.07	11,000 ± 400[c]	0.59 ± 0.07
48	0.089 ± 0.04	>30,000[c]	0.13 ± 0.001
77	0.11 ± 0.001	>30,000	0.13 ± 0.003
78	0.22 ± 0.01	>30,000	0.60 ± 0.08
81	0.62 ± 0.07	11, 000 ± 2,000	0.65 ± 0.05
83	1.3 ± 0.07	7.8 ± 2	> 10
84	0.51 ± 0.09	140 ± 8	1.3 ± 0.7
87	0.66 ± 0.09	2,400 ± 800	0.56 ± 0.01
89	0.39 ± 0.08	>30,000	0.44 ± 0.06
90	1.0 ± 0.2	14 ± 2	>10

[a] IC_{50} and EC_{50} values represent average Mean ± SEM of at least two separate experiments performed in triplicate. [b]Value represents Cyp24A1 mRNA expression at 2.5 μM compared to DMSO control (set to 1.0). [c]Analogue evaluated at 1 μM.

Table 14. Comparison of inhibitory activity of compounds **46**, **48**, **56**, and **78.**

	C3H[a]		ASZ001[e]			VDR$^{-/-}$ [a]	
	Cyp24A1[b]	IC_{50} (μM)[c]	Cyp24A1[b]	IC_{50} (μM)[c]	EC_{50} (μM)[d]	Cyp24A1[b]	IC_{50} (μM)[c]
VD3	8,300 ± 40	4.1 ± 0.3	2,200 ± 200	1.1 ± 0.01	0.98 ± 0.06	5.5 ± 0.1	4.5 ± 1.0
Calc[f]	>30,000	0.0031 ± 0.001	>30,000	0.089 ± 0.04	0.13 ± 0.001	530 ± 200	6.3 ± 1.0
56	45 ± 20	0.40 ± 0.02	2.7 ± 0.7	067 ± 0.02	--	8.1 ± 2	3.9 ± 0.2
78	15,000 ± 2,000	0.89 ± 0.03	>30,000	0.22 ± 0.01	0.60 ± 0.08	140 ± 30	4.9 ± 0.01
LG[f]	>30,000	0.00025 ± 0.04	13,000 ± 2,000	0.00025 ± 0.0001	0.0077 ± 0.003	250 ± 100	1.9 ± 0.2

[a]All analogues evaluated at 5 μM unless otherwise indicated. [b]Values represent Cyp24A1 mRNA expression compared to DMSO control (set to 1.0). [c] IC_{50} (Gli1, μM) and [d]EC_{50} (Cyp24A1, μM) values represent mean ± SEM for at least two separate experiments performed in triplicate. [e]Evaluated at 2.5 μM unless otherwise indicated. [f]Evaluated at 1 μM. Calc = calcitriol.

two analogues may utilize differing mechanisms to inhibit Hh signaling that may be exposed through the studies.

As a follow-up to previous studies, these four analogues were full evaluated in VDR$^{-/-}$ cells, obtained from a VDR$^{-/-}$ mouse model in the Sun lab at Rush University. These cells were upregulated by OHCs similar to C3H cells and compared to C3H and ASZ cells, **Table 14**. A non-secosteroidal VDR agonist, LG190178,[169] was kindly provided by Alexander (Leggy) Arnold, PhD, at the University of Wisconsin-Milwaukee, and used an additional method to evaluate the role VDR plays in Hh inhibition. LG190178 is selective for VDR against other nuclear receptors and no additional activities have been reported.

When the full concentration-dependent analysis was performed, all compounds except VD3 (**48**, **56** and **78**) showed both a significant loss in potency and, the expected decrease in Cyp24A1 expression. Calcitriol showed the greatest difference in activity going from an IC_{50} of 3 nM in C3H cells to 6 μM in VDR$^{-/-}$ cells with Cyp24A1 levels dropping from over 30,000 to about 500-fold. This result was unexpected for **56** as low Cyp24A1 levels were previously observed suggesting a VDR-independent mechanism.

It was originally hypothesized that the significant differences in Cyp24A1 levels for **56** and **78** was a result of opposing mechanisms where **56** acted independent of VDR and **78** acted in a VDR-dependent mechanism. The overall loss in potency suggested that all vitamin D analogues acted at least in part through

VDR. The potent activity and Gli1 expression of LG190178 across cell lines provides additional evidence for the Hh inhibitory activity of VDR.

B. Evaluation of Potential VDR-Hh Signaling Crosstalk

Based on reports by Alimirah suggesting that VDR activation induced SuFu expression to inhibit Hh signaling,[167] the same four compounds were evaluated in $SuFu^{-/-}$ MEF cells. If this proposed mechanism of Hh inhibition is correct, then a complete loss in inhibitory activity would be observed in $SuFu^{-/-}$ cells. This complete loss would be due to the inability of VDR to upregulate SuFu, as the SuFu gene is inactivated. When the four compounds were tested, a similar activity profile for Hh inhibition and VDR activation were observed, **Table 15**. Combining data from these two cell lines provides a few key insights into possible mechanism(s) of action.

First, the ability of calcitriol (**48**), **56** and **78** to maintain moderate Hh inhibitory activity in $SuFu^{-/-}$ cells suggests that these compounds in part inhibit downstream or independently of SuFu, potentially at the transcriptional level. A comparison of baseline mRNA expression (**Figure 21b**) suggests interplay between VDR and Hh may exist. When comparing the normalized mRNA values cross these cell lines, a relationship between VDR and SuFu mRNA expression appears to exist. The relative mRNA expression of VDR and

Table 15. Evaluation in Hh component knockout (KO) cells to determine the potential level of crosstalk.

	C3H[a]		$Ptch^{-/-}$ [a]		$Smo^{-/-}$ [a]		$SuFu^{-/-}$ [a]	
	Cyp24A1[b]	IC_{50} (μM)[c]	Cyp24A1[b]	IC_{50} (μM)[c]	Cyp24A1[b]	IC_{50} (μM)[c]	Cyp24A1[b]	IC_{50} (μM)[c]
46	8,300 ± 40	4.1 ± 0.3	19 ± 2	7.6 ± 2	590 ± 100	4.4 ± 0.05	2.9 ± 1.3	> 10
48[d]	>30,000	0.0031 ± 0.001	1,400 ± 500	ND*	3,600 ± 200	0.15 ± 0.07	590 ± 70	8.5 ± 3
56	45 ± 20	0.40 ± 0.02	4.7 ± 2	1.9 ± 0.06	2.1 ± 0.8	7.0 ± 4	1.2 ± 0.1	3.1 ± 0.4
78	15,000 ± 2,000	0.89 ± 0.03	3,500 ± 300	7.1 ± 0.8	2,600 ± 60	0.64 ± 0.4	51 ± 5	2.9 ± 0.3

[a]All analogues evaluated at 5 μM unless otherwise indicated. [b]Values represent Cyp24A1 mRNA expression compared to DMSO control (set to 1.0). [c]Gli1 IC_{50} values represent mean ± SEM for at least two separate experiments performed in triplicate. [d]Evaluated at 1 μM. *IC_{50} for calcitriol undetermined as concentration-dependence yielded two inflection points (See Appendix).

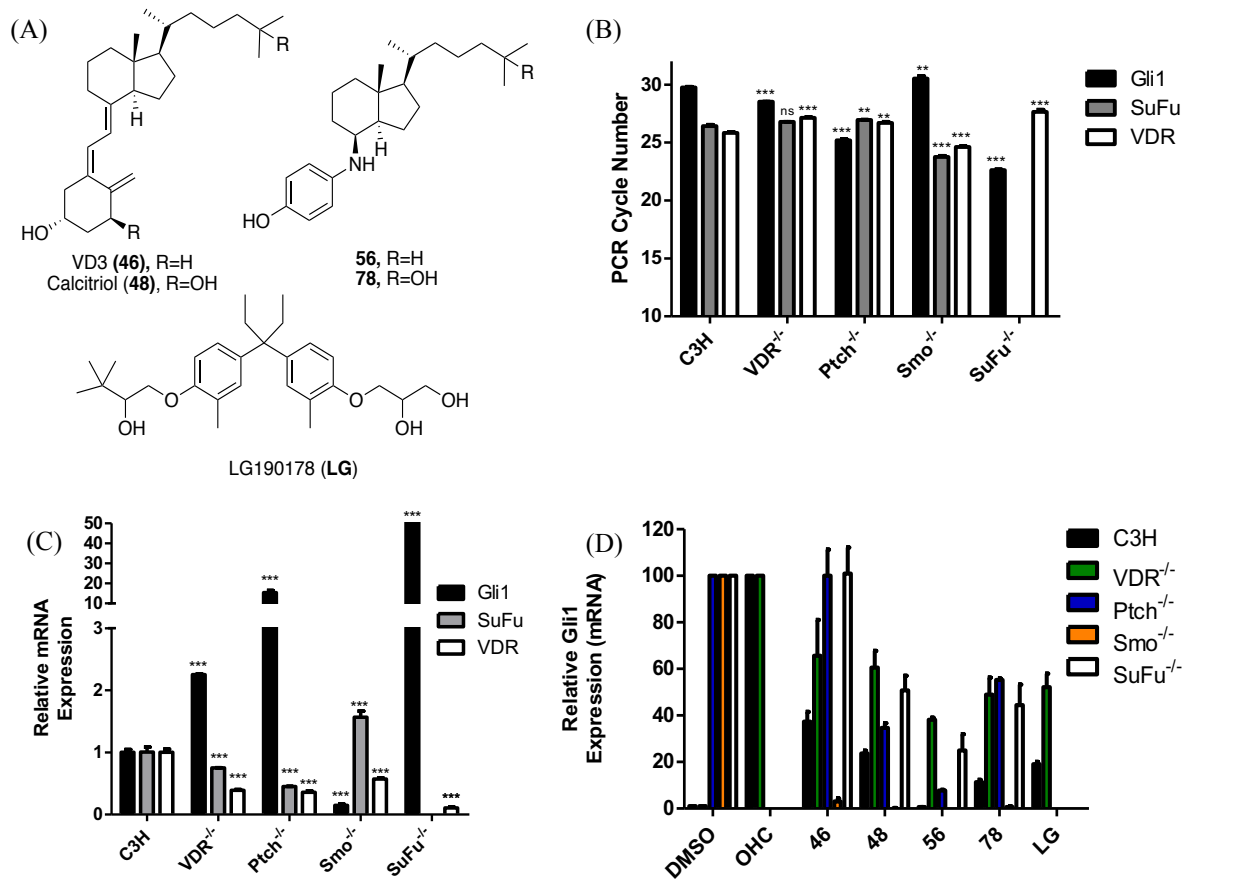

Figure 21. Evaluation of select analogues (A) in knockout cell lines. Comparison of baseline (B) cycle numbers and (C) mRNA expression of Gli1, VDR, and SuFu normalized to ActB across cell lines. Statistical analysis performed with GraphPad Prism5, one-way ANOVA with Tukey post-test; ***p<0.001, compared with C3H expression of corresponding mRNA; ns, not statistically significant compared to C3H expression. (D) Relative Gli1 mRNA expression across MEF cell lines.

SuFu appeared to change similarly and opposite Gli1 expression. Looking at the baseline mRNA expressions, we found the VDR$^{-/-}$ cells to be more of knockdown model and not a full knockout model due to residual expression levels, further complicating interpretations. Taking this into consideration, a mechanism of action completely dependent on VDR cannot be ignored. As both cell lines show a significant decrease in VDR expression and a loss in anti-Hh activity compared to both C3H and ASZ cells, it can be proposed that part of Hh inhibition is due to activation of VDR.

Since a loss of inhibition was observed in the SuFu$^{-/-}$ cells, additional studies were performed in Ptch$^{-/-}$ and Smo$^{-/-}$ cells to determine a potential level at which crosstalk between Hh and VDR may occur (**Table 15**). In the Ptch$^{-/-}$ cells, a loss in activity was observed for all compounds, suggesting that the analogues

interact before or with Ptch, and is contradictory to the previously obtained data from the SuFu$^{-/-}$ cells. Also contradictory, **48** and **78** maintained comparable activity in Smo$^{-/-}$ cells to C3H cells suggesting that they inhibit downstream of Smo. Due to very little differences observed between the control and treated cells and low the baseline expressions of the Smo$^{-/-}$ cells (**Figure 21b**), data from the Smo$^{-/-}$ cells is not taken as conclusive evidence.

An IC_{50} for **48**, calcitriol, could not be determined (ND*****) in the Ptch$^{-/-}$ cells because the concentration-dependence curve yielded two inflection points (see end of chapter, page 110). It is unknown if this is a result of experimental error due to a limit number of concentrations evaluated or indicative of two potential mechanisms, such as a VDR-independent and dependent mechanisms. Based on multiple trials resulting in the same response, the latter cannot be ruled out. If two mechanisms exist, it may suggest that direct inhibition by binding to Smo and a VDR-dependent mechanism, such as that proposed by Alimirah.[167] The loss of activity for **78** in Ptch$^{-/-}$ cells was slightly unexpected as it maintained relatively high upregulation of Cyp24A1, which may suggest that VDR crosstalk occurs at or before Ptch; however, additional studies need to be performed to evaluate this interpretation.

Taken together, the results have led us to propose a new hypothesis with regards to how vitamin D structures regulate Hh inhibition. It is hypothesized that Hh inhibition is partially obtained through a VDR-dependent mechanism where the activation of VDR prevents Hh target gene expression. The differences in Cyp24A1 expression can be explained by varying abilities of analogues to recruit specific coactivators to induce Cyp24A1 expression. Additionally, a VDR-independent mechanism likely exists due to inhibitory activity observed across all knockout cell lines, but the contradictory activities make it hard to determine a specific level and target.

V. Computational Modeling

Based on the intriguing and unexpected results following cellular evaluation of the synthetic analogues, an initial computational modeling study was performed with select analogues. Using the Schrödinger software, two models were generated. The first model generated was of the ligand binding domain (LBD)

of VDR (PDB file 1DB1). As previously mentioned, VDR is a nuclear receptor that interacts with multiple coregulatory proteins to influence its transcriptional activity. Based on the results from our cellular evaluation of the synthetic analogues, it is hypothesized that the majority of analogues do interact with VDR. We hypothesized that the differences in Cyp24A1 expression result from differing abilities to recruit coactivating proteins, such as SRC2, to induce Cyp24A1 expression. A second model generated contained the VDR-LBD and a peptide of SRC2-3, steroid receptor coactivtor 2 (PDB file 5H1E). We hoped that comparing the binding scores of both models with the cellular activity could help explain the cellular differences observed, **Table 16**.

Following the modeling studies, the compounds could be placed into four categories: (1) high VDR and high coactivator, (2) high VDR and low coactivator, (3) low VDR and low coactivator, and (4) low VDR and high coactivator docking scores. Category 1 would suggest strong binding to VDR and a stable

Table 16. Comparing cellular activity with initial computational modeling of vitamin D analogues arranged by docking score to VDR alone.

	C3H10T1/2		ASZ001		Docking Score[f]	
	IC_{50} (μM)[a]	Cyp24A1[b,c]	IC_{50} (μM)[a]	Cyp24A1[b,d]	VDR[g]	Coact.[h]
48	0.0031 ± 0.001	>25,000[e]	0.089 ± 0.04	>25,000[e]	-15.573	-13.808
47	0.40 ± 0.1	>25,000[d]	0.48 ± 0.07	11,000 ± 400[e]	-14.332	-12.681
83	1.7 ± 0.1	34 ± 0.7	1.4 ± 0.07	8.4 ± 2.0	-13.611	-11.318
90	1.6 ± 0.1	14 ± 2	1.01 ± 0.2	6.7 ± 2	-13.384	-10.865
46	4.1 ± 0.3	8,300 ± 40	1.1 ± 0.01	2,200 ± 200	-13.269	-12.176
87	1.1 ± 0.02	26 ± 4	0.66 ± 0.09	2,400 ± 800	-13.189	-11.139
89	1.1 ± 0.01	>25,000	0.39 ± 0.08	>25,000	-12.992	-12.201
77	1.3 ± 0.2	>25,000	0.11 ± 0.0004	>25,000	-12.756	-11.648
81	3.3 ± 0.7	90 ± 7	0.62 ± 0.07	11, 000 ± 2,000	-12.668	-10.691
52	0.98 ± 0.04	7.0 ± 0.9	1.8 ± 0.3	1.8 ± 0.2[c]	-12.603	-10.400
53	3.9 ± 0.8	3.0 ± 0.5	6.3 ± 1.1	1.6 ± 0.2[c]	-12.459	-11.412
84	0.42 ± 0.04	6.1 ± 0.4	0.51 ± 0.09	140 ± 8	-12.423	-10.953
56	0.40 ± 0.02	45 ± 20	0.67 ± 0.02	2.7 ± 0.7[c]	-11.846	-10.337
51	0.74 ± 0.1	22 ± 5	5.2 ± 0.2	1.9 ± 0.1[c]	-11.843	-10.648
61a	0.92 ± 0.09	3.6 ± 2	5.2 ± 0.5	1.3 ± 0.3[c]	-11.531	-11.714
55	1.0 ± 0.1	17 ± 4	1.7 ± 0.1	1.8 ± 0.1[c]	-11.208	-10.928
78	0.89 ± 0.03	15,000 ± 2,000	0.22 ± 0.01	>25,000	-11.094	-10.674
63	2.0 ± 0.2	9.0 ± 4	4.1 ± 2	1.1 ± 0.09[c]	-11.052	-10.558
72	3.1 ± 0.1	24 ±0.8	0.34 ± 0.02	1.1 ± 0.7	-8.468	-12.607

[a]IC_{50} values represent average Mean ± SEM of at least two separate experiments performed in triplicate. [b]Value represents Cyp24A1 mRNA expression compared to DMSO control (set to 1.0). [c]Analogue evaluated at 5 μM. [d]Analogue evaluated at 2.5 μM. [e]Analogue evaluated at 1 μM. [f]Docking scores represent predicted binding energy generated by Autodock 4.0. [g]VDR structure PDB file 1DB1. [h]VDR structure bound to SRC2-3 peptide, PDB file 5H1E.

complex with the coactivator peptide, which would theoretically lead to increased Cyp24A1 expression. Category 2 would suggest strong binding to VDR but a "non-stable" coactivator complex resulting in low Cyp24A1 expression. Category 3 would suggest low binding to VDR and therefore low Cyp24A1 expression.

Importantly, both calcitriol (**48**) and 25-hydroxy vitamin D3 (**47**) had the highest docking scores in both models suggesting strong binding to VDR itself and stable binding in the presence of the SRC2-3 coactivator peptide. Overall the docking scores correlated well with the observed cellular VDR agonism of the compounds; i.e., analogues that induce the highest levels of Cyp24A1 mRNA expression were also predicted to bind best in both models. Only three compounds did not follow this trend – analogues **78**, **83**, and **89.**

Overall, the models found the 3-hydroxyl position, which would explain the high scores for **83** and **90** and the low score for **78**. Analogues **83** and **90** did have lower docking scores with the presence of the coactivator peptide consistent with the low Cyp24A1 levels. Along similar lines, **78** had a relatively low docking score in both models, contradictory to the cellular data. Another puzzling result was the docking scores of **72**. Based on our hypothesis and as one of the most potent analogues, we expected **72** to have one of the highest docking scores for VDR alone and a low score for the coactivator model, but it had the opposite results.

The narrow range of scores in both models does further complicate interpretation of the results. The relatively narrow range for the VDR alone model is consistent with the hypothesis that all compounds possess the ability to bind to VDR. The narrow range for the coactivator model suggests that all compounds would have the ability to induce Cyp24A1 expression, whereas the analogues show a wide range of Cyp24A1 levels.

Conclusion

The complexity of Hh signaling has left multiple questions open, specifically the endogenous regulation of Smo, and provided multiple targets for therapeutic purposes. Multiple reports have proposed sterols as endogenous regulating small molecules, both agonists[70,73,75] and antagonists.[124] To date, the proposed antagonistic regulators of Smo are of the vitamin D scaffold, **45** – **48**. Contradictory reports exist for the specific mechanism of action utilized by vitamin D-based compounds to inhibit Hh signaling. Multiple reports propose direct inhibition of Hh signaling by binding to Smo in a VDR-independent manner.[124, 136, 165-166] In these reports, all metabolites of vitamin D signaling demonstrated the ability to inhibit Hh signaling to varying degrees.[125] More recently, a VDR-dependent mechanism was suggested. The proposed mechanism involves indirect regulation of a specific micro-RNA, miR-214, that controls the regulation of SuFu, an endogenous inhibitory protein of Hh signaling. [167,168] In this mechanism, activation of VDR downregulates the production of miR-214 resulting in upregulation of SuFu protein and mRNA, resulting in Hh inhibition.

Initial mechanistic studies performed in the Hadden lab were inconclusive, and the biological activity data for the lead analogues (**51** – **57**) suggested a VDR-independent mechanism due to strong inhibition of Hh signaling and VDR activation.[131, 133] It was also determined that VD3 (**46**) and **51,** our lead ester analogue, were unable to displace BODIPY-Cyclopamine, ruling out one known binding site on Smo.[131] Newly developed analogues (Chapter 3) have suggested more of a VDR-dependent mechanism based on significant upregulation of Cyp24A1 mRNA and increased inhibitory activity following the addition of a C-25 hydroxyl group. To further evaluate these analogues, EC_{50}'s were obtained in ASZ cells, which showed the most robust Cyp24A1 upregulation, **Table 13**. A strong correlation was observed between the Gli1 IC_{50} and Cyp24A1 EC_{50} values further suggesting potential crosstalk between VDR and Hh signaling, and a VDR-dependent mechanism of action.

A series of experiments were performed utilizing knockout cell lines to probe the specific mechanism(s) of action. These knockout (KO) lines included VDR, Ptch, Smo, and $Sufu^{-/-}$ cell lines to fully evaluate the necessity of VDR and determine which level of signaling crosstalk occurs. Unfortunately, baseline analysis of these cell lines (**Figure 21b**) indicated a few issues with this method. It was determined

that our VDR$^{-/-}$was not a complete knockout cell line. One possibility is that the method used to "knockout" the VDR gene resulted in the formation of non-functional VDR and not complete removal. If the binding region of Taqman primer used was not altered, this would explain the baseline VDR readings. Because *Cyp24A1* levels are still upregulated similar to the SuFu$^{-/-}$ cell line, it is hypothesized that a small amount of functional VDR remained after "knockout." Another issue was that Gli1 levels were very low in our Smo$^{-/-}$ line making it hard to make any conclusions based on very little difference between control and treated cycle numbers.

Overall, comparing C3H and ASZ cell data with the KO cell studies suggests that a VDR-dependent mechanism(s) exists for Hh inhibition. Even though our VDR$^{-/-}$ cells were more of a knockdown cell line, a positive correlation can be seen between VDR levels and Hh inhibitory activity. Overall, the anti-Hh activity decreased with decreases in VDR expression and activation. These studies also provided a few key insights into potential mechanism(s) of action and lay a foundation for those studies and provided a new hypothesis to be evaluated. The decrease, but not complete loss, in inhibitory activity across KO cell lines suggests that multiple mechanisms, both VDR-independent and –dependent exists. Additionally, the decrease in activity for **56** in VDR$^{-/-}$ cells was unexpected based on little upregulation of Cyp24A1 observed in C3H and ASZ cells, which had suggested a VDR-independent mechanism of action. The decrease in activity is the foundation for a new proposed mechanism of action for Hh inhibition.

Based on these studies, it is believed that both VDR - dependent and – independent mechanisms exist and work synergistically to inhibit Hh signaling. With multiple reports suggesting contradictory mechanisms, it is hard to ignore the potential for different inhibitory mechanisms to exist that are cell type specific. In this proposed mechanism, it is hypothesized that vitamin D-based compounds interact directly with the Hh pathway but also activate VDR to reduce Hh target gene expression. Furthermore, as a nuclear receptor, VDR is known to interact with multiple coregulatory proteins to regulate target gene expression. This is important because the loss in activity for **56** suggests that compounds that have low Cyp24A1 values may still inhibit through VDR without upregulating Cyp24A1. Taken together, it is suggested that vitamin

D based compounds utilize both VDR-dependent and independent mechanisms, and may not interact strongly enough with VDR to upregulate Cyp24A1 via specific coactivator recruitment.

Initial computational studies to further probe potential mechanism(s) of action through VDR suggest that all analogues have the ability to bind to VDR with differing abilities in the presence of a coactivator peptide. The results of these studies however were not as conclusive as we had hoped with a relatively narrow range of scores in both models. This narrow range suggests that all compounds have the ability to bind in both model systems and do not explain the major differences observed with the Cyp24A1 expression levels. The simple docking and non-flexible models may explain these observations, and suggests the need for more thorough and in-depth modeling studies.

Experimental Procedures

General Information. Protocols for general cell culture, qPCR (Hh pathway and VDR), and VDR binding assays are as previously described.[127, 131] 20α-Hydroxycholesterol and 22(S)-hydroxycholesterol (OHCs) were purchased from Sigma-Aldrich. VD3 for biological studies was purchased from Sigma-Aldrich and calcitriol was purchased from Caymen Chemical. Data was analyzed using GraphPad Prism 5, and reported values represent mean ± SEM for at least two separate experiments performed in triplicate.

Fluorescence Binding Assays.[131] For flow cytometry experiments, HEK293T cells were seeded in 10 cm cell culture dishes (2.5×10^6 cells) and incubated overnight (37 °C, 5% CO_2). Cells were transfected with Smo-Myc_3 expression plasmid (24 μg) using Lipofectamine 2000 reagent (60 μL) was added and the cells returned to the incubator overnight. The next day, cells were split into a single 6-well plate and incubated overnight. The next day (2 days post- transfection) cells were incubated in DMEM containing 10% FBS, BODIPY-Cyc (5 nM), and various concentrations of Cyc, VD3, or 5 at 37 °C for 4 h. Cells were trypsinized, centrifuged, and resuspended in 500 μL of phosphate buffered saline (PBS) for flow cytometry analysis. To determine transfection efficiency, cells were fixed with 2% PFA (15 min), permeabilized with 90% ethanol (30 min, 4 °C), and blocked for nonspecific binding with 10% FBS in PBS (15 min, RT). Cells

were incubated with anti-Myc antibody (1:800, Cell Signaling Technology) for 1 h at RT, followed by Alexa Flour-647 donkey anti-rabbit antibody (1:1000, Invitrogen) for 30 min at RT. Finally, cells were analyzed for green fluorescence using flow cytometry.

VDRi Assay. C3H10T1/2 cells were seeded into 24-well tissue culture treated plates 24 h prior to transfection. Lipofectamine 2000 (2.1 μL, Invitrogen) was mixed with mouse VDR-specific siRNA (2.5 μL of a 20 μM stock solution, Dharmacon) in OptimMEM reduced serum media (95.4 μL, Life Technologies). Transfection solution (100 μL/well) was added dropwise to cells supplemented with BME (400 μL/well) containing 0.5% fetal bovine serum (Atlanta Biologicals) and 1% penicillin/streptomycin/L-glutamine (Cellgro) and plates returned to the incubator (37 °C, 5% CO_2). Following a 6 h incubation period, transfection media was replaced with complete growth media and cells incubated overnight. Cells were treated with VD3 (**46,** 5 μM), calcitriol (**48**, 0.5 μM), **51** (5 μM), or control 24 h post-transfection. RNA isolation and cDNA synthesis was performed 24 h post-treatment (48 h post- transfection) using the Cells-to-Ct kit (Ambion) following the manufacturer's protocol and qPCR analysis of target genes followed standard procedures.

Calcitriol concentration-dependent graph assay in Ptch$^{-/-}$ cells appears to have two inflection points.

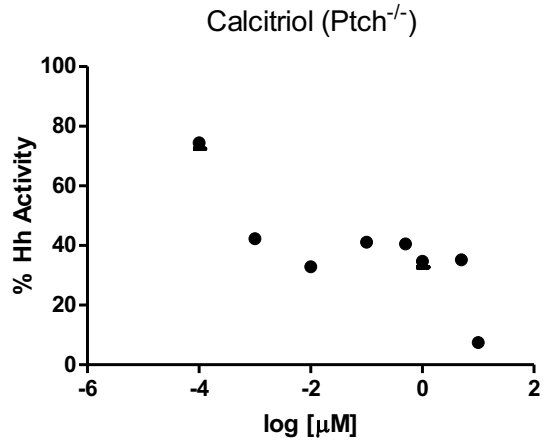

Modulation of the Hedgehog Signaling Pathway by Sterol-based Small Molecules

Chad Anthony Maschinot

Chapter 5:

Future Directions

Introduction

As discussed in Chapter 1, the Hedgehog (Hh) pathway is an embryonic signaling pathway primarily inactive in adult cells. Since its initial discovery as a key pathway responsible for embryonic patterning and development, our understanding of Hh signaling and the key components of the pathway has grown. In adult tissues, the pathway is responsible for maintaining homeostasis of stem cell populations, primarily in the skin and central nervous system.[1] Abnormal regulation of the pathway, specifically constitutive activation through mutations or irregular expression, has been linked to a variety of cancers, most notably BCC and MB. Hh signaling has since emerged as a therapeutic target with multiple components of the pathway serving as targets of interests (**Figure 22**). Among the Hh pathway components under investigation, the trans-membrane protein Smoothened (Smo) has been the most studied and targeted.

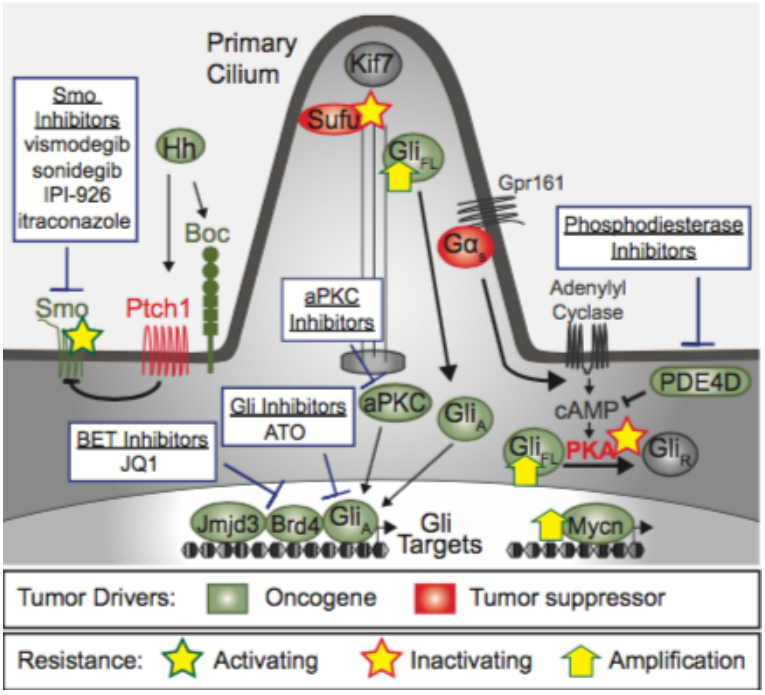

Figure 22.[16] **Representative targets and inhibitors of Hh signaling under investigating**. Tumor suppressors (red) and oncogenes (green) that have been reported in preclinical and some clinical settings to cause or maintain basal cell carcinoma (BCC) and medulloblastoma (MB) are shown. Stars (activating or inactivating mutations) and arrows (genomic amplifications) indicate pathway components implicated in resistance to Smo inhibitors. Additional inhibitors do exist that are not indicated in this image such as Ptch inhibitors and PKA agonists. Reprinted from Developmental Cell, 38, Pak, E.; et al. Hedgehog signal transduction: Key players, oncogenic drivers and cancer therapy, 333-344, 2016, with permission from Elsevier.

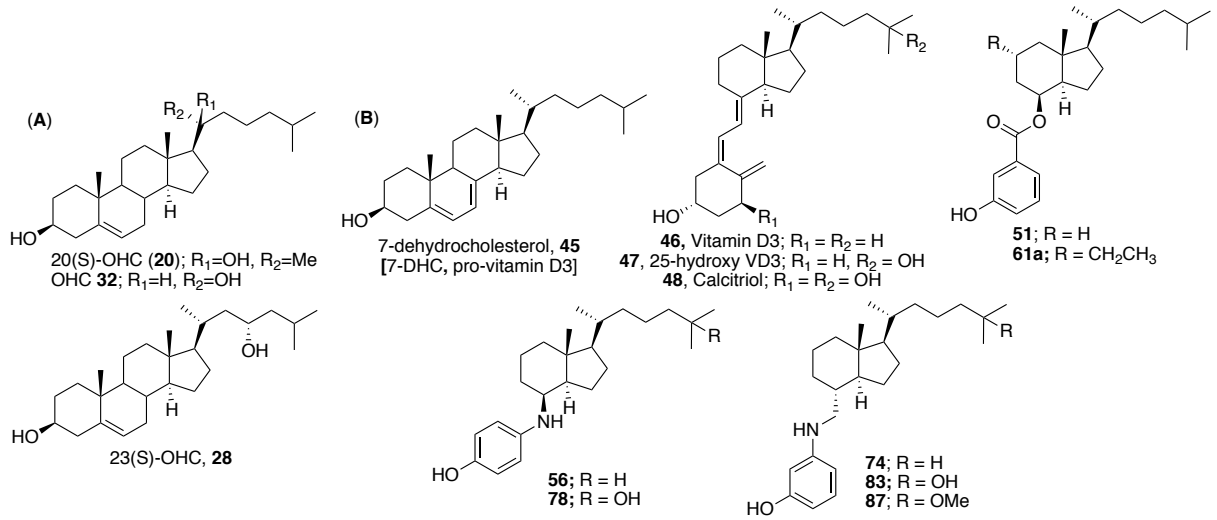

Figure 23. (A) Representative oxysterol agonists of Hh Signaling; (B) Vitamin D family and representative analogues.

Small molecule modulators of Smo have been investigated as both agonists and antagonists of Hh signaling. Among the scaffolds under investigation, two sterol scaffolds have shown therapeutic potential as anti-cancer chemotherapeutics (vitamin D) and treatment options for osteo- and neurodegenerative disorders (oxysterols) (**Figure 23**). Oxysterols (OHCs) have been well characterized as agonists of Hh signaling by direct binding to Smo, specifically the extracellular cysteine-rich domain (CRD).[2, 71-74] The specific mechanism(s) of action by which vitamin D inhibits Hh signaling is unclear. However, questions remain about their ability to treat degenerative disorders in humans.

In 2006, a 3β-hydroxysteroid, ultimately proposed to be pro-vitaminD3 or vitamin D3, was identified as an inhibitor of Hh signaling.[125] The specific mechanism of action was later proposed to be through direct binding to Smo.[118] Follow up studies have since confirmed inhibition of Hh signaling by the vitamin D family – pro-vitamin D3 (**45**), vitamin D3 (**46**), 25-hydroxyvitamin D3 (**47**) and calcitriol (**48**) – and analogues of vitamin D3.[126-134] However, contradictory mechanisms of action by which these compounds inhibit Hh signaling have been proposed. Similar to initial reports, multiple studies have proposed a mechanism independent of the vitamin D receptor (VDR).[124, 165-166] Other studies have proposed a VDR-dependent mechanism,[167] including the studies discussed here.

The initial mechanism of action studies discussed in the previous chapter (Chapter 4) suggested that crosstalk between Hh signaling and VDR exists. First, correlation between the Gli1 IC_{50} and Cyp24A1 EC_{50} values in ASZ001 cells (Ch4, Table 13) suggested that VDR may play a role in regulating Hh signaling. Secondly, knockdown of baseline VDR levels in multiple cell lines (Ch4, Figure 21) resulted in decreases in anti-Hh activity for the four compounds tested – **46**, **48**, **56**, and **78**.

Simple docking studies, described in the previous chapter, suggested that all analogues have the ability to bind to VDR. These studies looked to compare the ability of analogues to bind to VDR alone and in the presence of a coactivator peptide, SRC2-3. These studies were not conclusive due to a narrow range of docking scores and limitations with the studies. These limitations include not allowing complete flexibility of the VDR ligand binding domain (LBD) and the coactivator peptide. By not allowing flexibility in these regions, a true ranking list of the analogues could not be determined. The docking studies appeared to favor the 3-hydroxyl phenolic A-ring moiety contradictory to cellular studies where the 4-hydroxyl position yielded greater Cyp24A1 mRNA expression (Ch4, Table16).

Combining the results obtained in the Hadden lab, a hypothesis has been proposed to describe the mechanism of action by which vitamin D - based compounds inhibit Hh signaling. Based on our studies, we believe that these compounds inhibit Hh signaling at least in part through a VDR-dependent mechanism. To explain the significant differences in observed Cyp24A1 mRNA levels, we hypothesize that these differences result from different abilities to recruit coactivators of VDR to induce Cyp24A1 expression. Describe herein are proposed studies to further elucidate the mechanism by which vitamin D compounds inhibit Hh signaling and study this proposed mechanism of action.

I. Induction of Osteogenesis by Oxysterols

Studies in the Hadden lab to date have focused on the ability of OHCs to induce osteogenic differentiation in bone-marrow derived stromal cells, M2-10B4 cells. In these studies, OHCs **20** and **28** showed comparable abilities to induce osteogenic differentiation through a similar mechanism.[108] OHC **32** however appeared to induce differentiation through a different mechanism. The ability of these analogues

to induce differentiation was determined through qPCR analysis of osteogenic genes, *osterix* and *alkaline phosphatase.* To further evaluate the ability of these compounds to induce differentiation, bone-marrow derived human mesenchymal stem cells can be used to determine the ability of OHCs to induce osteogenesis in human cells (ATCC PCS-500-012). A commercially available osteocyte differentiation kit (ATCC PCS-500-052) can be used to compare the ability of OHCs to induce osteogenesis. Additionally, staining protocols may be utilized to visualize complete differentiation to osteoblasts.

Two different staining techniques can be used to compare differentiation abilities. The first staining techniques is Alizarin Red S. Alizarin Red stains extracellular calcium deposits. In contrast to undifferentiated cells, differentiated osteoblasts accumulate extracellular calcium deposits. Osteoblasts – mediated accumulation is indicative of the formation of bone mass. The second staining procedure visualizes alkaline phosphatase activity to indicate differentiation into osteoblasts. This protocol uses 5-bromo-4-chloro-3-indolyl phosphate/nitro blue tetrazolium (BCIP/NBT) as a substrate to stain cells blue-violet when alkaline phosphatase is present.

II. Vitamin D Receptor Binding Assays

Although the docking studies showed the potential for all the developed vitamin D-based analogues to bind VDR, the limitations of the studies make the results inconclusive. To follow up with these studies, biochemical assays may be utilized to determine the ability of analogues to bind to VDR. These studies would allow for flexibility in both the small molecule and protein that could not be accounted for in the docking studies. Two commercially available kits could be utilized to compare the binding affinities similar to the two docking models.

The first kit is the fluorescence polarization (FP) based PolarScreen^{TM} Vitamin D Receptor Competitor Assay Kit from ThermoFisher Scientific. This kit utilizes full-length human VDR and a proprietary fluorescent VDR ligand. The kit is also optimized for a 384-well format allowing for multiple compounds and concentrations to be evaluated in a single assay. If the analogue binds to VDR in the LBD, the analogue would displace the fluorescent ligand to ultimately give an IC_{50} value.

By utilizing full-length VDR, this assay also allows for potential allosteric sites to be explored. If one of the analogues binds to an allosteric site, it may also displace the fluorescent ligand to indicate binding. Unfortunately, the analogues may not be able to displace the fluorescent ligand whether they bind in the LBD or an allosteric site. To address this possibility, a modification of the assay could be performed. Under the standard assay format, VDR and the fluorescent ligand incubate prior to administration of the compound of interest. If the compound of interest incubates with VDR or the incubation step is removed and adding all three components simultaneously, the potential issue of "weaker" binding can be reduced by removing the need to displace the fluorescent ligand.

As the first kit can be utilized to determine and measure the ability of compounds to bind to VDR, the second kit can be used to determine if the compounds are capable of recruiting a coregulatory protein. This second kit is the LanthaScreen™ TR-FRET VDR Coactivator Assay Kit from ThermoFisher Scientific. Unlike the first kit, this kit only uses the VDR-LBD tagged with glutathione-*S*-transferase (GST) and a fluorescein-labeled TRAP220/DRIP-2 coactivator peptide. The tagged VDR-LBD is added to the compound of interest followed by addition of the coactivator peptide and a terbium (TB)-labeled anti-GST antibody. If the compound binds to the VDR-LBD, a conformational change allows for the coactivator peptide to be recruited and bind to VDR (**Figure 24**). When the Tb-labeled antibody binds to the GST tag and is excited at 340 nm, an energy transfer to the fluorescein - coactivator peptide can be detected at 520 nm. If the compound of interest does not bind to the VDR-LBD, this energy transfer does not occur and the antibody emission can be detected at 495 nm. A TR-FRET ratio of 520:495 can then be calculated to provide an EC_{50} dose-response curve.

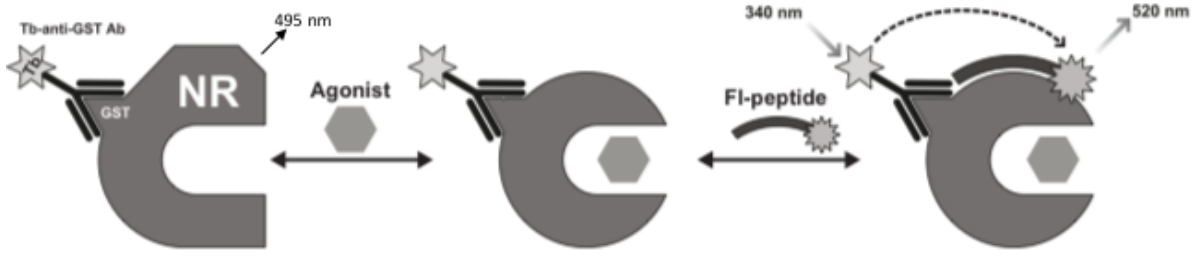

Figure 24. Principle of the TR-FRET coactivator assay (LanthaScreen). NR = Nuclear Receptor (VDR)

Similar to comparing the two docking studies, comparing the experimental values of these two kits will give a greater understanding towards analogue binding to VDR and the validity of our proposed hypothesis. Based on the proposed hypothesis, the four analogues utilized in the knockout studies would give potent IC_{50} and EC_{50} values in both assays for calcitriol (**48**) and **78,** while VD3 (**46**) and **56** would show moderate IC_{50} values for the VDR assay and weak EC_{50} values for the coactivator assay. If all compounds show similar profiles in both assays, more in-depth studies can be proposed to determine the reason for the cellular activity differences.

III. Knockdown Studies

With inconclusive results from the knockout cell line studies discussed in Chapter 4, another method may be utilized to provide insight into the specific mechanism of action that vitamin D-based compounds use to inhibit Hh signaling. Similar to previously utilized techniques in the initial mechanism studies,[131] RNA knockdown of the protein of interest in a single cell line should provide greater insight than the use of multiple knockout cells with varying baseline expressions.

Previously, siRNA knockdown of VDR was performed in C3H10T1/2 cells. These cells are well understood and have good baseline expression of all proteins of interest – Ptch, VDR, and SuFu. Additionally, C3H cells respond robustly to Hh pathway or VDR activation by small molecules. Typical PCR cycle numbers of 28 – 30 for Gli1 and 35 or more for Cyp24A1 are seen in DMSO controls compared to 22 – 25 for Gli1 and Cyp24A1 with compounds (**Figure 25A**). This robust response would allow for even small differences between concentrations and compounds to be seen more easily. Since C3H cells were previously utilized, a procedure already exists that resulted in at least 50% knockdown of *VDR* mRNA which resulted in a proportionate reduction in Cyp24A1 expression (**Figure 25B**).

Unfortunately, knockdown of mRNA expression does not always correlate with protein expression. Combining the knockdown studies with Western blot analysis of the lysates would confirm any changes. When the baseline levels of the knockout cells were compared, a theoretical relationship between VDR and SuFu could be observed where the mRNA expression of each appeared to change in a similar manner. This

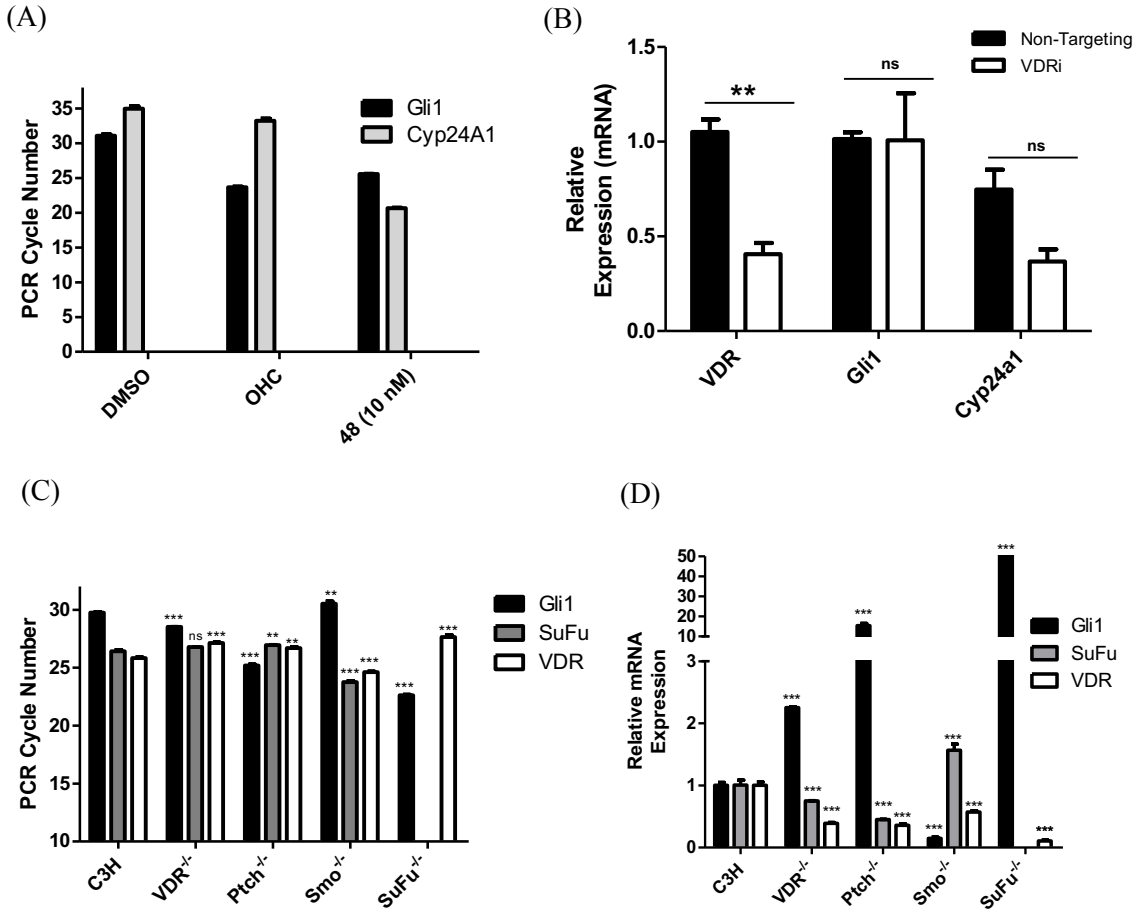

Figure 25. (A) Non-normalized cellular response of C3H cells in response to pathway activation. (B) Initial mechanism of action studies with siRNA knockdown. Statistical analysis one-way ANOVA with Tukey post-test performed with GraphPad Prism5; **p<0.01, compared with non-targeting RNAi treatment; ns, not statistically significant. Baseline comparison of knockout cell lines non-normalized (C) and normalized (D) to *ActB* of DMSO. Statistical analysis performed with GraphPad Prism5 one-way ANOVA with Tukey post-test; ***p<0.001, **p<0.01, compared with corresponding mRNA expression in C3H cells; ns, not statistically significant.

is most prominently seen in SuFu$^{-/-}$ cells which showed the lowest expression of VDR when normalized to ActB (**Figure 25D**). Similarly, Alimirah proposed that regulation of mi-RNA by VDR resulted in increases in the protein and mRNA expression of SuFu, which ultimately lead to Hh pathway inhibition. Based on the proposed mechanism of action by Alimirah,[167] it is possible that protein expression may change without changes to mRNA expression. A comparison at the protein level would allow for a more in-depth look at changes following compound administration.

The increase in activity for 25-OH VD3 (**47**) and calcitriol (**48**) compared to VD3 (**46**) suggest a role for VDR in the anti-Hh activity of these compounds. This observation also suggests that VD3 may only be activity due to *in vitro* metabolism. To study this hypothesis, mRNA knockdown of Cyp2R1 and Cyp27B1 could be performed. By knocking down these enzymes, metabolism of VD3 or 25-OH VD3 is halted leading to accumulate in cells. The activity of all three compounds could then be compared to non-transfected cells allowing for any role of vitamin D metabolism to be determined.

IV. Labeling Studies

The series of experiments described above look to determine the level at which vitamin D-based compounds inhibit Hh signaling and gain an understanding of the cellular responses to compound administration. These studies do not confirm or specifically look to identify the cellular protein target, or targets. With multiple targets proposed in previous publications, the use of labeling studies would provide more concrete evidence to the protein target(s) and allow for those target(s) to be identified. The VDR binding assays allow for the potential of the analogues to bind to VDR to be quantified but are only biochemical assays. A labeled analogue would allow for any VDR binding to be determined in cells. The more important aspect of the labeling studies would be to determine if the analogues interact with Smo.

If vitamin D-based compounds do interact directly with Smo, multiple binding sites have been proposed including the CRD and the trans-membrane region. Preliminary studies in the Hadden lab showed that neither VDR (**46**) or **51** were able to displace BODIPY-Cyc in intact cells or isolate membranes (Ch4 Figure

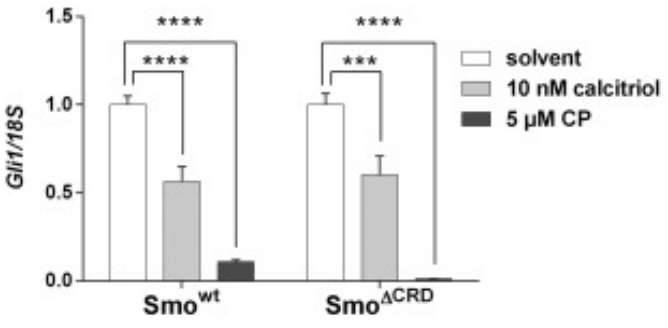

Figure 26.[167] Calcitriol mediated inhibition of Smo constructs. CP=cyclopamine

20E).[131] In 2015, calcitriol was proposed to bind to the CRD region, which would explain the inability to displace BODIPY-Cyc; however, no direct binding studies were performed.[128]

Similarly, Linder et al. showed an inability of calcitriol to displace BODIPY-Cyc.[167] They also utilized wild-type Smo (Smo^{wt}) and ΔCRD Smo ($Smo^{\Delta CRD}$) constructs in a luciferase-based assay to try to identify a specific binding site on Smo (**Figure 26**). In these studies, they showed that similar to Cyc there was no difference in inhibitory activity between the two Smo constructs. This led them to suggest that calcitriol binds to a unique TM-region of Smo, although they did not show any direct interactions.[167] Using a labeled version of vitamin D and similar Smo constructs, a binding site on Smo could be identified.

The specific label can be placed on vitamin D in multiple positions (**Figure 27**). As shown by the C-11 modified analogues (Ch3, **67**),[134] the attachment of a BODIPY or fluorescent label at the C-11 position should not interfere with binding. Additionally, when **51** and **61 – 67** are compared, modifications at this position appeared to increase selectivity for Hh signaling. Attaching a label to this position could therefore help identify a non-VDR target, such as Smo. A second position for label attachment is the C-22 position of the alkyl-side chain, accessible from vitamin D2 starting material. Finally, a third position that could be utilized is the C-2 position of the A-ring. Multiple synthetic papers have been published with C-2 modifications and shown that these modifications do not interfere with binding to VDR.[170-172] The C-2 position also provides a position opposite of the C-11 and C-22 positions. This may be important and useful if the incorporation of the larger labeling group abolishes anti-Hh activity.

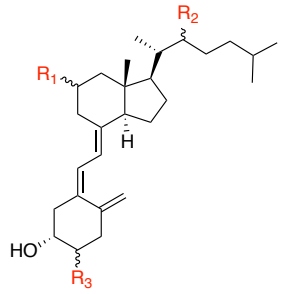

Figure 27. Label attachment positions on VD3 where R_1 = C-11; R_2 = C-22; R_3 = C-2.

V. Calcemic Effects

As discussed in Chapter 3, VDR regulates a variety of cellular process. The most notable of these processes is the regulation of calcium, which limits the clinical utility of vitamin D-based compounds. Therefore, the usefulness of vitamin D-based compounds in a clinical setting is based on their ability to avoid hypercalcemic effects.

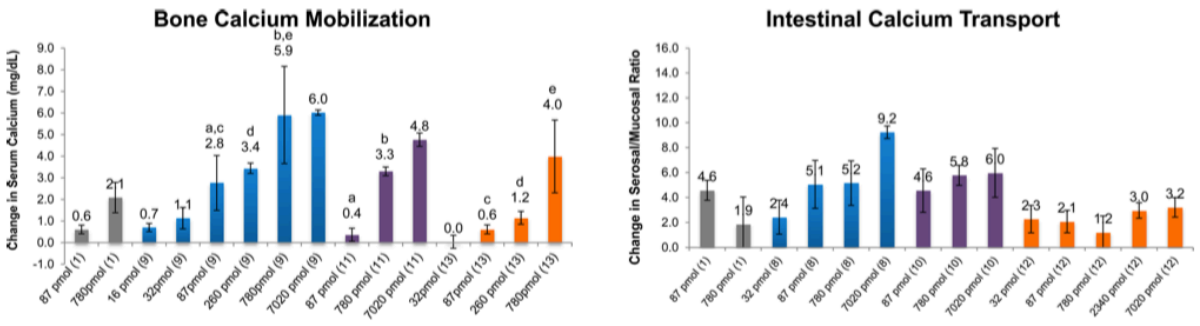

Figure 28. Example figures of calcemic activity from Reference 174. Reprinted (adapted) with permission from Sibilska, I. K.; et al. Synthesis and biological activity of 2-methylene analogues of calcitriol and related compounds. *J. Med. Chem*. **2015**, 58, 9653-9662. Copyright 2015 American Chemical Society.

Based on the cellular data and mechanism studies for the analogues described in the previous chapters, some analogues may be devoid of the hypercalcemic effects seen with calcitriol. An initial way to determine the ability of compounds to regulate calcium levels through VDR activation is to measure the expression of VDR target genes associated with calcium regulation, such as *TRPV6* (membrane calcium channel).[174] A more in-depth way to measure these effects is to use animal models. Animal models allow for calcium changes to be determined. The two changes that are typically measured are changes in serum calcium levels (bone calcium mobilization) and the serosal/mucosal calcium ratio (calcium transport), **Figure 28**.[173-176] Even if all analogues do interact with VDR to inhibit Hh signaling, if any compounds are devoid of calcemic effects they could be more clinically attractive. We know that this to be possible based on multiple reports of both secosteroidal and non-steroidal noncalcemic vitamin D mimics reported.[169, 175-176]

VI. Vitamin D Analogues

With the calcemic activity of the previous synthetic analogues unknown, incorporating functionality known to have less or minimal calcemic activity would be beneficial. Among the functionalities shown to have less calcemic activity is C-20 hydroxylation. Both 20(*R*)- and 20(*S*)-OH VD3 were first isolated in 2003 and determined to metabolites of Cyp11A1 metabolism of VD3.[178] Additional studies determined that 20(*S*)-OH VD3 was as potent, or more potent, than calcitriol in inhibiting the proliferation of normal or immortalized keratinocytes, as well as leukemia and melanoma cells.[179-182]

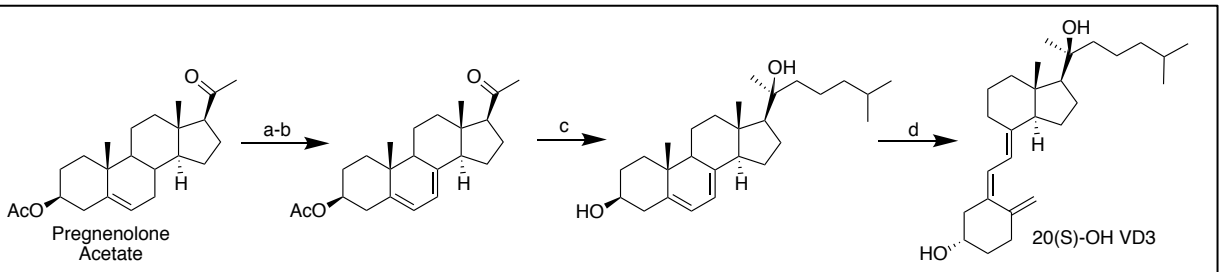

Scheme 10.[180] Reagents and conditions*:* (a) dibromantin, 2,2′-azobisisobutyronitrile, benzene/hexane (1:1), 100 °C, reflux; (b) Bu_4NBr, Bu_4NF, THF, RT; (c) Mg, 4-methylpentylbromide, THF, O°C - RT; (d) UVB irradiation, 5min followed by 3 days stirring in solution, RT.

There are currently two synthetic routes reported to synthesize these metabolites. The first synthetic route follows the endogenous metabolic pathway using commercially available pregnenolone acetate as the starting material (**Scheme 10)**.[180] Bromination at the C-7 position followed by dehydro-bromination yields 7-dehydropregnenolone acetate. Grignard addition of freshly prepared 4-methylpentylmagnesium bromide will selectively yield 20(*S*)-OH VD3. Unlike the similar Grignard addition to form OHC analogues **32 - 33**, the C-18 and C-21 methyl groups prevent front-side attack and the formation of 20(*R*)-OH VD3. Irradiation with UVB yielded a mixture of steroids that can be separated to provide 20(*S*)-OH VD3.

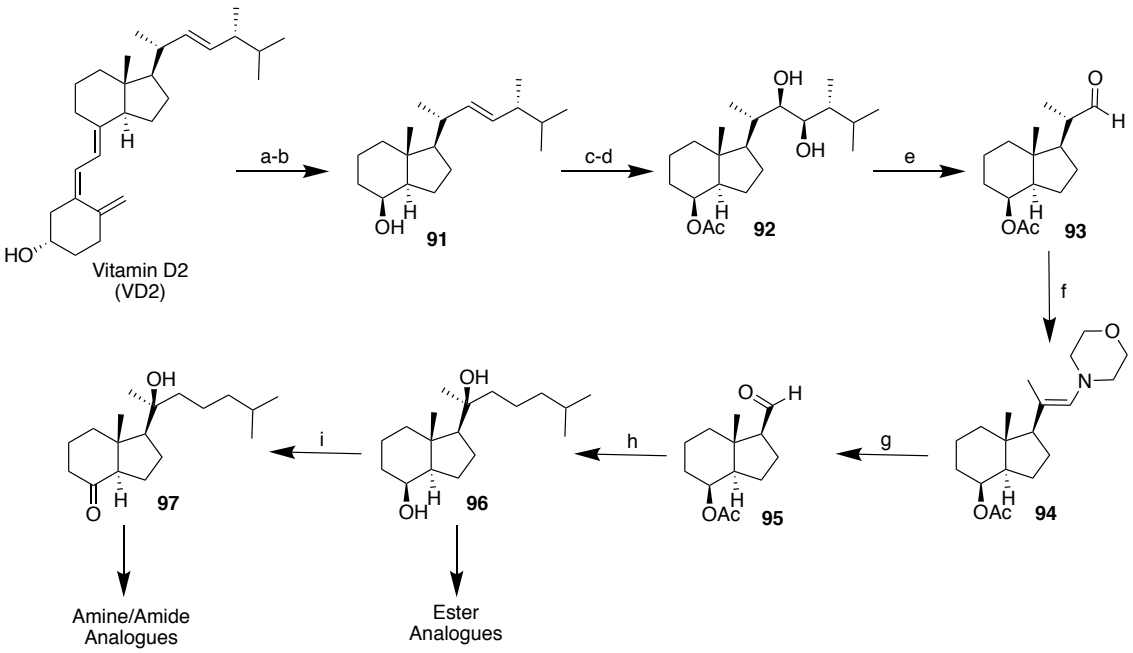

Scheme 11.[181] Reagents and conditions: (a) $KMnO_4$, EtOH–H_2O; (b) i. $Pb(OAc)_4$, Na_2CO_3, DCM; ii. Red-Al, benzene; (c) Ac_2O, Pyr, DMAP, DCM; (d) OsO_4, NMO, acetone:*t*-BuOH; (e): $NaIO_4$, H_2O:THF; (f) morpholine, *p*-TsOH, PhH, reflux; (g) $KMnO_4/Al_2O_3$, acetone; (h) Mg, 4-methylpentylbromide, THF, O°C to RT; (i) PDC, DCM.

The second synthetic route allows for analogues to be developed and uses vitamin D2 as the starting material (**Scheme 11**).[181] Regioselective dihydroxylation of the vitamin D2 triene followed by oxidative cleavage and reduction provides alcohol **91.** Protection of the hydroxyl group followed by dihydroxylation with osmium tetroxide (OsO_4) to triol **92** allows for oxidative cleavage of the side chain diol to yield aldehyde **94**. Formation of aldehyde **95** is accomplished by oxidative cleavage of enamine **94** with alumina supported potassium permanganate ($KMnO_4/Al_2O_3$). Similar to the previous route, Grignard addition of 4-methylpentylmagnesium bromide yields diol **96** stereoselectively. Alcohol **96** can then be used to synthesize new analogues or oxidized with pyridinium dichromate (PDC) to ketone **97** to provide additional analogues.

Vitamin D analogues should also be further evaluated as inhibitors of Hh signaling. The analogues can be evaluated against mutant models of Smo and in primary cancer cell lines dependent on Hh signaling, such as the MB MERP cells. These studies would be beneficial in providing additional evidence towards a mechanism of action as well as further demonstrating the ability to inhibit Hh signaling. If the compounds inhibit in a VDR-dependent manner, they should theoretically maintain potency against mutant models of Smo.

References

1. Banerjee, U.; Hadden, M. K. Recent advances in the design of Hedgehog pathway inhibitors for the treatment of malignancies. *Expert Opin. Drug Discov*. **2014**, 9, 751-771.
2. Hadden, M. K. Hedgehog pathway agonism: Therapeutic potential and small molecule development. *ChemMedChem.* **2014**, *9*, 27-37.
3. Briscoe, J.; Therond, P. P. The mechanism of Hedgehog signalling and its role in development and disease. *Nature Molec. Cell Biol.* **2013**, *14*, 416-249.
4. Humke, E. W.; Dorn, K. V.; Milenkovic, L.; Scott, M. P.; Rohatgi, R. The output of Hedgehog signaling is controlled by the dynamic association be- tween Suppressor of Fused and the Gli proteins. *Genes Dev*. **2010**, *24*, 670–682.
5. Nozawa, Y. I.; Lin, C.; Chuang, P. T. Hedgehog signaling from the primary cilium to the nucleus: an emerging picture of ciliary localization, trafficking and transduction. *Curr. Opin. Genet. Dev.* **2013**, *23*, 429–437.
6. Chen, Y.; Sasai, N.; Ma, G.; Yue, T.; Jia, J.; Briscoe, J.; Jiang, J. Sonic hedgehog dependent phosphorylation by CK1alpha and GRK2 is required for ciliary accumulation and activation of smoothened. *PloS Biol.* **2011**, *9*, e1001083.
7. Liu, Y. C.; Couzens, A. L.; Deshwar, A. R.; McBroom-Cerajewski, L. D. B.; Zhang, X.; Puviindran, V.; et al. The PPFIA1-PP2A protein complex promotes trafficking of Kif7 to the ciliary tip and Hedgehog signaling. *Sci. Signal*. **2014**, *7*, ra117.
8. He, M.; Subramanian, R.; Bangs, F.; Omelchenko, T.; Liem, K. F. Jr.; Kapoor, T. M.; Anderson, K. V. The kinesin-4 protein Kif7 regulates mammalian Hedgehog signalling by organizing the cilium tip compartment. *Nat. Cell Biol*. **2014,** *16*, 663–672.
9. Johnson, R. L.; Rothman, A. L.; Xie, J.; Goodrich, L. V.; Bare, J. W.; Bonifas, J. M.; et al. Human homolog of patched, a candidate gene for the basal cell nevus syndrome. *Science* **1996**, *272*, 1668–1671.
10. Bale, A. E.; Yu, K.-P. The hedgehog pathway and basal cell carcinomas. *Human Molec. Gen.* **2001***, 10*, 757-762.
11. Bonilla, X.; Parmentier, L.; King, B.; Bezrukov, F.; Kaya, G.; Zoete, V.; Seplyarskiy; V. B.; Sharpe, H. J.; McKee, T.; Letourneau, A. et al. Genomic analysis identifies new drivers and progression pathways in skin basal cell carcinoma. *Nat. Genet*. **2016**, *48*, 398–406.
12. Sharpe, H. J.; Wang, W.; Hannoush, R. N.; de Sauvage, F. J. Regulation of the oncoprotein Smoothened by small molecules. *Nat. Chem. Biol.* **2015**, *11*, 246-255.
13. Wechsler-Reya, R. J.; Scott, M. P. Control of neuronal pre- cursor proliferation in the cerebellum by sonic hedgehog. *Neuron* **1999**, *22*, 103–114.
14. Hatton, B. A.; Villavicencio, E. H.; Tsuchiya, K. D.; Pritchard, J. I.; Ditzler, S.; et al. The Smo/Smo model: hedgehog-induced medulloblastoma with 90% incidence and leptomeningeal spread. *Cancer Res*. **2008**, *68*, 1768–1776.
15. Kool, M.; Jones, D. T.; Jager, N.; Northcott, P. A.; Pugh, T. J.; Hovestadt, V.; Piro, R. M.; Esparza, L. A.; Markant, S. L.; Remke, M.; et al. Genome sequencing of SHH medulloblastoma predicts genotype-related response to smoothened inhibition. *Cancer Cell* **2014**, *25*, 393–405.
16. Pak, E.; Segal, R. A. Hedgehog signal transduction: Key players, oncogenic drivers and cancer therapy. *Devel. Cell* **2016**, *38*, 333-344.
17. Mao, L.; Xia, Y. P.; Zhou, Y. N.; Dai, R. L.; Yang, X.; Duan, S. J.; Qiao, X.; Mei, Y. W.; Hu, B.; Cui, H. A critical role of Sonic Hedgehog signaling in maintaining the tumorigenicity of neuroblastoma cells. *Cancer Sci.* **2009**, *100*, 1848-1855.
18. Wickström, M.; Dyberg, C.; Shimokawa, T.; Milosevic, J.; Baryawno, N.; Fuskevåg, O. M.; Larsson, R.; Kogner, P.; Zaphiropoulos, P. G.; Johnsen, J. I. Targeting the hedgehog signal transduction pathway at the level of GLI inhibits neuroblastoma cell growth *in vitro* and *in vivo*. *Int. J. Cancer* **2013**, *132*, 1516-1524.

19. Yauch, R. L.; Dijkgraaf, G. J.; Alicke, B.; Januario, T.; Ahn, C. P.; Holcomb, T.; et al. Smoothened mutation confers resistance to a hedgehog pathway inhibitor in medulloblastoma. *Science* **2009**, *326*, 572-574.
20. Dijkgraaf, G. J.; Alicke, B.; Weinmann, L.; Januario, T.; West, K.; et al. Small molecule inhibition of GDC-0449 refractory smoothened mutants and downstream mechanisms of drug resistance. *Cancer Res.* **2011,** *71*, 435-444.
21. Chen, J. K.; Taipale, J.; Young, K. E.; Maiti, T.; Beachy, P. A. Small molecule modulation of Smoothened activity. *PNAS* **2002***, 29*, 14071-14076.
22. Gupta, S.; Takebe, N.; LoRusso, P. Targeting the Hedgehog pathway in cancer. *Ther. Adv. Med. Oncol.* **2010***, 2*, 237-250.
23. Maschinot, C. A.; Pace, J. R.; Hadden, M. K. Synthetic small molecule inhibitors of Hh signaling as anti-cancer chemotherapeutics. *Curr. Med. Chem.* **2015**, *22*, 4033-4057.
24. Robarge K. D.; Brunton S. A.; Castanedo G. M.; Cui, Y.; Dina, M. S.; Goldsmith, R.; Sould, S. E.; Guichert, O.; Gunzner, J. L.; Halladay, J.; Jia, W.; et al. GDC-0449-A potent inhibitor of the hedgehog pathway. *Bioorg. Med. Chem. Lett.,* **2009**, *19*, 5576-5581.
25. Pan, S.; Wu, X.; Jiang, J.; Gao, W.; Wan, Y.; Cheng, D.; Han, D.; Liu, J.; Englund, N.; et al. Discovery of NVP-LDE225, a potent and selective smoothened antagonist. *ACS Med. Chem. Lett.* **2010***, 1*, 130-134.
26. Kim, J.; Tang, J. Y.; Gong, R.; Kim, J.; Lee, J. J.; Clemons, K. V.; Chong, C. R.; et al. Itraconazole, a commonly used antifungal that Inhibits Hedgehog pathway activity and cancer growth. *Cancer Cell* **2010***, 17*, 388-399.
27. Lauth, M.; Bergström, Å.; Shimokawa, T.; Toftgård, R. Inhibition of GLI-mediated transcription and tumor cell growth by small-molecule antagonists. *Proc. Natl. Acad. Sci. USA,* **2007**, *104*, 8455-8460.
28. Mazumdar, T.; DeVecchio, J.; Agyeman, A.; Shi, T.; Houghton, J.A. Blocking Hedgehog survival signaling at the level of GLI genes induces DNA damage and extensive cell death in human colon carcinoma cells. *Cancer Res.* **2011**, *71*, 5904-5914.
29. Huang, L.; Walter, V.; Hayes, D.N.; Onaitis, M. Hedgehog-GLI signaling inhibition suppresses tumor growth in squamous lung cancer. *Clin. Cancer Res.* **2014**, *20*, 1566-1575.
30. Ardecky, R.; Magnuson, G. K.; Zou, J.; Ganji, S. R.; Brown, B.; Ngo, T.; Lee, J.; Zeng, F-Y.; Sun, Q.; Stonich, D.; Salaniwal, S.; Sakata, T.; Rack, P. G.; et al. "Small- molecule antagonists of Gli function." Probe Reports from the NIH Molecular Libraries Program (Internet). Bethesda (MD): National Center for Biotechnology Information (US); 2010-2012 Dec 17.
31. Tang, Y.; Gholamin, S.; Schubert, S.; Willardson, M. I.; Lee, A.; Bandopadhayay, P.; Bergthold, G.; Masoud, S.; Nguyen, B.; Vue, N.; Balansay, B.; Yu, F.; Oh, S.; et al. Epigenetic targeting of Hedgehog pathway transcriptional output through BET bromodomain inhibition. *Nat. Med.* **2014**, *20*, 732-740.
32. Long, J.; Li, B.; Rodriguez-Blanco, J.; Pastori, C.; Volmar, C-H.; Wahlstedt, C.; et al. The BET bromodomain inhibitor I-BET151 acts downstream of smoothened to abrogate the growth of Hedgehog driven cancers. *J. Biol. Chem.,* **2014**, *289*, 35494-35502.
33. Li, B.; Fei, D. L.; Flaveny, C. A.; Dahmane, N.; Baubet, V.; Wang, Z.; Bai, F.; Pei, X-H.; Rodriquez-Blanco, J.; et al. Pyrvinium attenuates hedgehog signaling downstream of smoothened. *Cancer Res.,* **2014**, *74*, 4811- 4821.
34. Lum, L.; Yao, S.; Mozer, B.; Rovescalli, A.; Von Kessler, D.; Nirenberg, M.; Beachy, P. A. Identification of Hedgehog pathway components by RNAi in *Drosophila* cultured cells. *Science,* **2003**, *299*, 2039–2045.
35. Thorne, C. A.; Hanson, A. J.; Schneider, J.; Tahinci, E.; Orton, D.; et al. Small-molecule inhibition of Wnt signaling through activation of casein kinase 1. *Nat. Chem. Biol.,* **2010**, *6*, 829–836.
36. Mondal, B. C.; Mukherjee, T.; Mandal, L.; Evans, C. J.; Sinenko, S. A.; Martinez-Agosto, J. A.; Banerjee, U. Interaction between differentiating cell- and niche-derived signals in hematopoietic progenitor maintenance. *Cell,* **2011**, *147*, 1589-1600.
37. Schön, M. P.; Schön, M.; Klotz, K. N. The small antitumoral immune response modifier imiquimod interacts with adenosine receptor signaling in a TLR7- and TLR8- independent fashion. *J. Invest.*

Dermatol. **2006**, *126*, 1338–1347
38. Wolff, F.; Loipetzberger, A.; Gruber, W.; Esterbauer, H.; Aberger, F.; Frischauf, A. M. Imiquimod directly inhibits Hedgehog signaling by stimulating adenosine receptor/protein kinase A-mediated GLI phosphorylation. *Oncogene*. **2013**, *32*, 5574-5581.
39. Dellovade, T.; Romer, J. T.; Curran, T.; Rubin, L. L. The Hedgehog pathway and neurological disorders. *Annu. Rev. Neurosci.* **2006**, *29*, 539-563.
40. Varjosalo, M.; Taipale, J. Hedgehog: functions and mechanisms. *Genes Dev.* **2008**, *22*, 2454-2472.
41. Parmantier, E.; Lynn, B.; Lawson, D.; Turmaine, M.; Namini, S. S.; Chakrabarti, L.; McMAhon, A. P.; Jessen, K. R.; Mirsky, R. Schwann cell-derived desert hedgehog controls the development of peripheral nerve sheaths. *Neuron* **1999**, *23*, 713–724.
42. Yoshimura, K.; Taeda, S. Hedgehog signaling regulates myelination in the peripheral nervous system through primary cilia. *Differentiation* **2012**, *83*, S78-85.
43. Sharghi-Namini, S.; Turmaine, M.; Meier, C.; Sahni, V.; Umehara, F.; Jessen, K. R.; Mirsky, R. The structural and functional integrity of peripheral nerves depends on the glial-derived signal of desert hedgehog. *J. Neurosci.* **2006**, *26*, 6364-6376.
44. Traiffort, E.; Charytoniuk, D.; Faure, H.; Ruat, M. 1998. Regional distribution of sonic hedgehog, patched, and smoothened mRNA in the adult rat brain. *J. Neurochem.* 70:1327–30
45. Traiffort, E.; Charytoniuk, D.; Watroba, L.; Faure, H.; Sales, N.; Ruat, M. Discrete localizations of hedgehog signaling components in the developing and adult rat nervous system. *Eur. J. Neurosci.* **1999**, *11*, 3199–14.
46. Hynes, M.; Porter, J. A.; Chiang, C.; Chang, D.; Tessier-Lavigne, M.; Beachy, P. A.; Rosenthal, A. Induction of midbrain dopaminergic neurons by sonic hedgehog. *Neuron* **1995***, 15*, 35–44.
47. Tsuboi, K.; Shults, C. W. Intrastriatal injection of sonic hedgehog reduces behavioral impairment in a rat model of Parkinson's disease. *Exp. Neurol*. **2002**, *173*, 95–104.
48. Chen, M.; Qiao, H.; Su, Z.; Li, H.; Ping, Q.; Zong, L. Emerging therapeutic targets for osteoposis treatment. *Expert Opin. Ther. Targets* **2014**, *18*, 817-831.
49. Gallagher, J. C.; Sai, A. J. Molecular biology of bone remodeling: implications for new therapeutic targets for osteoporosis. *Maturitas* **2010**, *65*, 301-307.
50. Yang, J.; Andre, P.; Ye, L.; Yang, Y.-Z. The Hedgehog signaling pathway in bone formation. *Int. J. Oral Sci.* **2015**, *7*, 73-79.
51. Mak, K. K.; Bi, Y.; Wan, C.; Chuang, P. T.; Clemens, T.; Young, M.; Yang, Y. Hedgehog signaling in mature osteoblasts regulates bone formation and resorption by controlling PTHrP and RANKL expression. *Dev. Cell* **2008**, *14*, 674–688.
52. Miyaji, T.; Nakase, T.; Iwasaki, M. Kuriyama, K.; Tamai, N.; Higuchi, C.; Myoui, A.; Tomita, T.; Yosikawa, H. Expression and distribution of transcripts for sonic hedgehog in the early phase of fracture repair. *Histochem. Cell Biol*. **2003**, *119*, 233–237.
53. Fuchs, S.; Dohle, E.; Kirkpatrick, C. J. Sonic Hedgehog-mediated synergistic effects guiding angiogenesis and osteogenesis. *Vita.m Horm.* **2012**, *88*, 491–506.
54. Ohba, S.; Kawaguchi, H.; Kugimiya, F.; Ogasawara, T.; Kawamura, N.; Saito, T.; Ikeda, T.; Fuijii, K.; et al. Patched1 haploinsufficiency increases adult bone mass and modulates Gli3 repressor activity. *Dev. Cell* **2008**, *14*, 689–699.
55. Rodda, S. J.; McMahon, A. P. Distinct roles for Hedgehog and canonical Wnt signaling in specification, differentiation and maintenance of osteoblast progenitors. *Development* **2006**, *133*, 3231-3244.
56. Wu, X.; Ding, S.; Ding, Q.; Gray, N. S.; Schultz, P. G. A small molecule with osteogenesis-inducing activity in multipotent mesenchymal progenitor cells. *J. Am. Chem. Soc.* **2002**, *124*, 14520-14521.
57. Wu, X.; Walker, J.; Zhang, J.; Ding, S.; Schultz, P. G. Purmorphamine induces osteogenesis by activation of the hedgehog signaling pathway. *Chem. Biol.* **2004**, *11*, 1229-1238.
58. Sinha, S.; Chen, J. K. Purmorphamine activates the Hedgehog pathway by targeting Smoothened. *Nature Chem. Biol.* **2006**, *2*, 29-30.

59. Liu, Y.; Liu, H.; Sauvey, C.; Yao, L.; Zarnowska, E. D.; Zhang, S. C. Directed differentiation of forebrain GABA interneurons from human pluriopotent stem cells. *Nat. Protoc.* **2013**, *8*, 1670-1679.
60. Stacpoole, S. R.; Bilican, B.; Webber, D. J.; Luzhynskaya, A.; He, X. L.; Compston, A.; Karadottir, R.; Franklin, R. J.; Chandran, S. Efficient derivation of NPCs, spinal motor neurons and midbrain dopaminergic neurons from hESCs at 3% oxygen. *Nat. Protoc.* **2011**, *6*, 1229-1240.
61. Frank-Kamenetsky, M.; Zhang, X. M.; Bottega, S.; Guicherit, O.; Wichterle, H.; Dudek, H.; et al. Small-molecule modulators of Hedgehog signaling: identification and characterization of Smoothened agonists and antagonists. *J. Biol.* **2002**, *1*, 10.
62. Brunton, S. A.; Stibbard, J. H. A.; Rubin, L. L.; Guicherir, O. M.; Kruse, L. I.; Price, S.; di Lucrezia, R.; MacKinnon, C. H.; et al. Potent agonists of the Hedgehog signaling pathway. *Bioorg. Med. Chem. Lett.* **2009**, *19*, 4308-4311.
63. Pospisilik, J. A.; Schramek, D.; Schnidar, H.; Cronin, S. J.; Nehme, N. T.; Zhang, X.; Knauf, C.; Cani, P. D.; Aumayr, K.; et al. *Drosphila* genome-wide obsesity screen reveals Hedgehog as a determinant of brown versus white adipose cell fate. *Cell* **2010**, *140*, 148-160.
64. Teperino, R.; Amann, S.; Bayer, M.; McGee, S. L.; Loipetzberger, A.; Conner, T.; Jaeger, C.; Kammerer, B.; Winter, L.; Wiche, G.; et al. Hedgehog partial agonism drives Warburg-like metabolism in muscle and brown fat. *Cell* **2012**, *151*, 414-426.
65. Wichertle, H.; Lieberam, I.; Porter, J. A.; Jessell, T. M. Directed differentiation of embryonic stem cells into motor neurons. *Cell* **2002**, *110*, 385-397.
66. Wang, J.; Lu, J.; Bond, M. C.; Chen, M.; Ren, X.-R.; Lyerly, H. K.; Barak, L. S.; Chen, W. Identification of select glucocorticoids as Smoothened agonists: Potential utility for regenerative medicine. *Proc. Natl. Acad. Sci. USA* **2010**, *107,* 9323.
67. Wang, Y.; Davidow, L.; Arvanites, A. C.; Blanchard, J.; Lam, K.; Xu, K.; Oza, V.; Yoo, Y. W.; Ng, J. M. Y.; Curran, T.; Rubin, L. L.; McMahon, A. P. Glucocorticoid compounds modify Smoothened localization and Hedgehog pathway activity. *Chem. Biol.* **2012**, *19*, 972-982.
68. Lewis, P. M.; Dunn, M. P.; McMahon, J. A.; Logan, M.; Martin, J. F.; St-Jacques, B.; McMahon, A. P. Cholesterol modification of sonic hedgehog is required for long-range signaling activity and effective modulation of signaling by Ptc1. *Cell* **2001**, *105*, 599-612.
69. Bidet, M.; Joubert, O.; Lacome, B.; Ciantar, M.; Nehme, R.; Mollat, P.; Bretillon, L.; et al. The Hedgehog receptor Patched is involved in cholesterol transport. *PLoS One* **2011**, *6*, e23834.
70. Huang, P.; Nedelcu, D.; Watanabe, M.; Jao, C.; Kim, Y.; Liu, J.; Salic, A. Cellular cholesterol directly activates Smoothened in Hedgehog signaling. *Cell* **2016**, *166*, 1176-1187.
71. Corcoran, R. B.; Scott, M. P. Oxysterols stimulate Sonic hedgehog signal transduction and proliferation of medulloblastoma cells. *Proc. Natl. Acad. Sci. USA* **2006***, 103,* 8408-8413.
72. Dwyer, J. R.; Sever, N.; Carlson, M.; Nelson, S. F.; Beachy, P. A.; Parhami, F. Oxysterols are novel activators of the hedgehog signaling pathway in pluripotent mesenchymal cells. *J. Biol. Chem.* **2007**, *282*, 8959-8968.
73. Nachtergaele, S.; Mydock, L. K.; Krishnan, K.; Rammohan, J.; Schlesinger, P. H.; Covey, D. F.; Rohatgi, R. Oxysterols are allosteric activators of the oncoprotein Smoothened. *Nat. Chem. Biol.* **2012**, *8*, 211-220.
74. Kha, H. T.; Basseri, B.; Shouhed, D.; Richardson, J.; Tetradis, S.; Hagn, T. J.; Parhami, F. Oxysterols regulate differentiation of mesenchymal stem cells: pro-bone and anti-fat. *J. Bone Miner. Res.* **2004**, *19*, 830-840.
75. Bernabei, R.; Mortone, A. M.; Ortolani, E.; Landi, F.; Marzetti, E. Screening, diagnosis and treatment of osteoporosis: a brief review. *Clin. Cases Miner. Bone Metab.* **2014**, *11*, 201-207.
76. Luchetti, G.; Sircar, R.; Kong, J. H.; Nachtergaele, S.; Sagner, A.; Byrne, E. F. X.; Covey, D. F.; Siebold, C.; Rohatgi, R. Cholesterol activates the G-protein coupled receptor Smoothened to promote Hedgehog signaling. *eLIfe* **2016**, *5*, e20304.
77. Gimpl, G. Interaction of G protein coupled receptors and cholesterol. *Chem. Phys. Lipids* **2016**, *199*, 61-73.
78. Brown, A. J; Jessup, W. Oxysterols: Sources, cellular storage and metabolism, and new insights into

their roles in cholesterol homeostasis. *Molec. Aspects Med.* **2009**, *30*, 111-122.
79. Gill, S.; Chow, R.; Brown, A. J. Sterol regulators of cholesterol homeostasis and beyond: The oxysterol hypothesis revisited and revised. *Prog. Lipid Res.* **2008**, *47*, 391-404.
80. Kandutsch, A. A.; Chen, H. W. Inhibition of sterol synthesis in cultured mouse cells by 7α-hydroxycholesterol, 7β-hydroxycholesterol, and 7-ketocholesterol. *J. Biol. Chem*. **1973**, *248*, 8408–8417.
81. Kandutsch, A. A.; Chen, H. W.; Heiniger, H. J. Biological activity of some oxygenated sterols. *Science* **1978**, *201*, 498–501.
82. Briggs, M. R.; Yokoyama, C.; Wang, X.; Brown, M. S.; Goldstein, J. L. Nuclear protein that binds sterol regulatory element of low density lipoprotein receptor promoter I. Identification of the protein and delineation of its target nucleotide sequence. *J. Biol. Chem.* **1993,** *268*, 14490–6.
83. Radhakrishnan, A.; Sun, L. P.; Kwon, H. J.; Brown, MS.; Goldstein, J. L. Direct binding of cholesterol to the purified membrane region of SCAP: mechanism for a sterol- sensing domain. *Mol. Cell* **2004**, *15*, 259–268.
84. Radhakrishnan, A.; Ikeda, Y.; Kwon, H. J.; Brown, M. S.; Goldstein, J. L. Sterol-regulated transport of SREBPs from endoplasmic reticulum to golgi: oxysterols block transport by binding to Insig. *Proc. Natl. Acad. Sci. USA* **2007**, *104*, 6511–8518.
85. Gelissen, I. C.; Harris, M.; Rye, K.-A.; Quinn, C.; Brown, A. J.; Kockx, M.; et al. ABCA1 and ABCG1 synergize to mediate cholesterol export to ApoA-I. *Arterioscler. Thromb. Vasc. Biol.* **2006**, *26*, 534–540.
86. Svensson, S.; Ostberg, T.; Jacobsson, M.; Norstrom, C.; Stefansson, K.; Hallen, D.; et al. Crystal structure of the heterodimeric complex of LXRalpha and RXRbeta ligand-binding domains in a fully agonistic conformation. *Embo. J.* **2003**, *22*, 4625–4633.
87. Chen, W.; Chen, G.; Head, D. L.; Mangelsdorf, D. J.; Russell, D. W. Enzymatic reduction of oxysterols impairs LXR signaling in cultured cells and the livers of mice. *Cell Metab.* **2007**, *5*, 73–79.
88. Spann, N. J.; Glass, C. K. Sterols and oxysterols in immune cell function. *Nat. Immunol.* **2013**, *14*, 893-900.
89. Ogawa, S.; Lozach, J.; Benner, C.; Pascual, G.; Tangirala, R. K.; Westin, S. *et al.* Molecular determinants of crosstalk between nuclear receptors and toll-like receptors. *Cell* **2005,** *122*, 707–721.
90. Joseph, S.B.; Castrillo, A.; Laffitte, B.A.; Mangelsdorf, D. J.; Tontonoz, P. Reciprocal regulation of inflammation and lipid metabolism by liver X receptors. *Nat. Med.* **2003**, *9*, 213–219.
91. Tontonoz, P.; Mangelsdorf, D. J. Liver X receptor signaling pathways in cardiovascular disease. *Mol. Endocrinol.* **2003***, 17*, 985–993.
92. Im, S. S.; Yousef, L.; Blaschitz, C.; Jiu, J. Z.; Edwards, R. A.; Young, S. G.; Raffatellu, M.; Osborne, T. F. Linking lipid metabolism to the innate immune response in macrophages through sterol regulatory element binding protein-1a. *Cell Metab.* **2011**, *13*, 540–549.
93. Liu, S. Y.; Aliyari, R.; Chikere, K.; Li, G.; Marseden, M. D.; Smith, J. K.; et al. Interferon-inducible cholesterol-25-hydroxylase broadly inhibits viral entry by production of 25-hydroxycholesterol. *Immunity* **2013**, *38*, 92–105.
94. Bauman, D. R.; Bitmansour, A. D.; McDonald, J. G.; Thompson, B. M.; Liang, G.; Russell, D. W. 25-hydroxycholesterol secreted by macrophages in response to Toll-like receptor activation suppresses immunoglobulin A production. *Proc. Natl. Acad. Sci. USA* **2009**, *106*, 16764-16769.
95. Pereira, J. P.; Kelly, L. M.; Xu, Y.; Cyster, J. G. EBI2 mediates B cell segregation between the outer and centre follicle. *Nature* **2009**, *460*, 1122–1126.
96. Liu, C.; Yang, X. V.; Wu, J.; Kuei, C.; Mani, N. S.; Zhang, L.; Yu, J.; et al. Oxysterols direct B-cell migration through EBI2. *Nature* **2011,** *475*, 519–523.
97. Arensdorf, A. M.; Marada, S.; Ogden, S. K. Smoothened regulation: A tale of two signals. *Trends in Pharm. Sci.* **2016**, *37*, 62-72.
98. Chen, Y.; Struhl, G. In vivo evidence that Patched and Smoothened constitute distinct binding and transducing components of a Hedgehog receptor complex. *Development* **1998**, *125*, 4943–4948.

99. Taipale, J.; Cooper, M. K.; Maiti, T.; Beachy, P. A. Patched acts catalytically to suppress the activity of Smoothened. *Nature* **2002**, *418*, 892–897.
100. Mukhopadhyay, S.; Rohatgi, R. G-protein-coupled receptors, Hedgehog signaling and primary cilia. *Semin. Cell Dev. Biol.* **2014**, *33*, 63–72.
101. Rohatgi, R.; Scott, M.P. Patching the gaps in Hedgehog signalling. *Nat. Cell Biol*. **2007**, *9*, 1005–1009.
102. Cooper, M. K.; Wassif, C. A.; Krakowlak, P. A.; taipale, J.; Gong, R.; Kelly, R. I.; Porter, F. D.; Beachy, P. A. A defective response to Hedgehog signaling in disorders of cholesterol biosynthesis. *Nat. Genet.* **2003**, *33*, 508-513.
103. Gimpl, G.; Burger, K.; Fahrenholz, F. Cholesterol as modulator of receptor function. *Biochemistry* **1997**, *36*, 10959–10974.
104. Saxena, R.; Chattopadhyay, A. Membrane cholesterol stabilizes the human serotonin(1A) receptor. *Biochim. Biophys. Acta* **2012**, *1818*, 2936–2942.
105. Mondal, S.; Johnston, J.M.; Wang, H.; Khelashvili, G.; Filizola, M.; Weinstein, H. Membrane driven spatial organization of GPCRs. *Sci. Rep.* **2013,** *3*, 2909.
106. Song, Y.; Kenworthy, A. K.; Sanders, C. R. Cholesterol as a co-solvent and a ligand for membrane proteins. *Protein Sci*. **2014**, *23*, 1–22.
107. Nedelcu, D.; Liu, J.; Xu, Y.; Jao, C.; Salic, A. Oxysterol binding to the extracellular domain of Smoothened in Hedgehog signaling. *Nat. Chem. Biol.* **2013**, *9*, 557-564.
108. Corman, A. C.; DeBerardinis, A. M.; Hadden, M. K. Structure-activity relationships for side chain oxysterol agonists of the Hedgehog signaling pathway. *ACS Med. Chem. Lett.* **2012**, *3*, 828-833.
109. Janowski, B. A.; Willy, P. J.; Devi, T. R.; Falck, J. R.; Mangelsdorf, D. J. An oxysterol signaling pathway mediated by the nuclear receptor LXRα. *Nature* **1996**, *383*, 728-731.
110. Maschinot, C. A.; Corman, A. C.; DeBerardinis, A. M.; Hadden, M. K. Synthesis and evaluation of osteogenic oxysterols as Hedgehog pathway activators. *ChemMedChem.* **2016**, *11*, 679-686.
111. Drew, J.; Letellier, M.; Morand, P.; Szabo, A. G. Synthesis from pregnenolone of fluorescent cholesterol analogue probes with conjugated unsaturation in the side chain. *J. Org. Chem.* **1987**, *52*, 4047-4052.
112. Ouellet, S. G.; Tuttle, J. B.; MacMillan, D. W. C. Enantioselective organocatalytic hydride reduction. *J. Am. Chem. Soc.* **2005**, *127*, 32-33.
113. Giannoudis, P. V.; Dinopoulos, H.; Tsirisdis, E. Bone substitutes: An update. *Injury,* **2005**, *36*, S20-S27.
114. Olkkonen, V. A.; Beaslas, O.; Nissila, E. Oxysterols and their cellular effectors. *Biomolecules* **2012**, *2*, 76-103.
115. Bruderer, M.; Richards, R. G.; Alini, M.; Stoddart, M. J. Role and regulation of RUNX2 in osteogenesis. *Eur. Cell Mater.* **2014**, *28*, 269-286.
116. Yoshida, C. A.; Yamamoto, H.; Fujita, T.; Furuichi, T.; Ito, K.; Inoue, K.; Yamana, K.; Zanma, A.; Tekada, K.; Ito, Y.; Komori, T. Runx2 and Runx3 are essential for chondrocyte maturation, and Runx2 regulates limb growth through induction of Indian hedgehog. *Genes Dev.* **2004**, *18*, 952-963.
117. Dash, R. C.; Maschinot, C. A.; Hadden, M. K. A molecular dynamics approach to identify an oxysterol-based hedgehog pathway inhibitor. *Biochim. Biophys. Acta* **2017**, *1861*, 168-177.
118. Tang, J. Y.; Xiao, T. Z.; Oda, Y.; Chang, K. S.; Shpall, E.; Wu, A.; et al. Vitamin D3 inhibits hedgehog signaling and proliferation in murine basal cell carcinomas. *Cancer Prevention Research* **2011**, *4*, 744-751.
119. Nachtergaele, S.; Whalen, D. M.; Mydock, L. K.; Zhao, Z.; Malinauskas, T.; Krishnan, K.; Ingham, P. W.; Covey, D. F.; Siebold, C.; Rohatgi, R. Structure and function of the Smoothened extracellular domain in vertebrate Hedgehog signaling. *eLife* **2013,** *2*, e01340.
120. Sever, N.; Mann, R. K.; Xu, L.; Snell, W. J.; Hernandez-Lara, C. I.; Porter, N. A.; Beachy, P. A. Endogenous B-ring oxysterols inhibit the Hedgehog component Smoothened in a manner distinct from cyclopamine or side-chain oxysterols. *Proc. Natl. Acad. Sci. USA* **2016,** *113,* 5904-5909.

121. Bikle, D. D. Vitamin D metabolism, mechanism of action, and clinical applications. *Chem. Biol.* **2014**, *21*, 319-329.
122. Webb, A. R.; DeCosta, B. R.; Holick, M. F. Sunlight regulates the cutaneous production of vitamin D3 by causing its photodegradation. *J. Clin. Endocrinol. Metab*. **1989**, *68*, 882–887.
123. Cheng, J. B.; Motola, D. L.; Mangelsdorf, D. J.; Russell, D. W. De-orphanization of cytochrome P450 2R1: a microsomal vitamin D 25-hydroxilase. *J. Biol. Chem.* **2003** *Sep 26; 278,* 38084-38093.
124. Zhu, J. G.; Ochalek, J. T.; Kaufmann, M.; Jones, G.; Deluca, H. F. CYP2R1 is a major, but not exclusive, contributor to 25-hydroxyvitamin D production in vivo. *Proc. Natl. Acad. Sci. USA*. **2013**, *110*, 15650–15655.
125. Bijlsma, M. F.; Spek, C. A.; Zivkovic, D.; van de Water, S.; Rezaee, F.; Peppelenbosch, M. P. Repression of smoothened by patched-dependent (pro)-vitamin D3 secretion. *PLoS Biol.* **2006**, *4*, e232.
126. Banerjee, U.; Ghosh, M.; Hadden, M. K. Evaluation of vitamin D3 A-ring analogues as hedgehog pathway inhibitors. *Bioorg. Med. Chem. Lett.* **2012**, *22*, 1330-1334.
127. DeBerardinis, A. M.; Banerjee, U.; Hadden, M. K. Identification of vitamin D3-based hedgehog pathway inhibitors that incorporate an aromatic A-ring isostere. *ACS Med. Chem. Lett.* **2013**, *4*, 590-595.
128. Cortes, M.; Liu, S. Y.; Kwan, W.; Alexa, K.; Goessling, W.; North, T. E. Accumulation of the vitamin D precursor cholecalciferol antagonizes hedgehog signaling to impair hemogenic endothelium formation. *Stem Cell Reports* **2015**, *5*, 471-479.
129. DeBerardinis, A. M.; Banerjee, U.; Miller, M.; Lemieux, S. M.; Hadden, M. K. Probing the structural requirements for vitamin D3 inhibition of hedgehog signaling. *Bioorg. Med. Chem. Lett.* **2012**, *22*, 4859-4863.
130. DeBerardinis, A. M.; Lemieux, S. M.; Hadden, M. K. Analogues of the Inhoffen-Lythgoe diol with anti-proliferative activity. *Bioorg. Med. Chem. Lett.* **2013**, *23*, 5367-5370.
131. DeBerardinis, A. M.; Madden, D. J.; Banerjee, U.; Sail, V.; Raccuia, D. S.; et al. Structure-activity relationships for vitamin D3-based aromatic A-ring analogues as hedgehog pathway inhibitors. *J. Med. Chem.* **2014**, *57*, 3724-3736.
132. Banerjee, U.; DeBerardinis, A. M.; Hadden, M. K. Design, synthesis, and evaluation of hybrid vitamin D3 side chain analogues as hedgehog pathway inhibitors. *Bioorg. Med. Chem.* **2015**, *23*, 548-555.
133. DeBerardinis, A. M.; Raccuia, D. S.; Maschinot, C. A.; Thompson, E.; Hadden, M. K. Vitamin D3 analogues that contain modified A- and seco-B rings as hedgehog pathway inhibitors. *Euro. J. Med. Chem.* **2015**, *93*, 156-171.
134. Maschinot, C. A.; Hadden, M. K. Synthesis and evaluation of vitamin D3 analogues with C-11 modification as inhibitors of hedgehog signaling. *Bioorg. Med. Chem. Lett.* **2017**, *27*, 4011-4014.
135. Sestelo, J. P.; Mourino, A.; Sarandeses, L. A. Synthesis of vitamin D3 and calcitriol dimers as potential chemical inducers of vitamin D receptor dimerization. *J Org Chem*. **2000,** *65*, 8290-8296.
136. D'Halleweyn, C.; Van Haver, D.; Van der Eycken, J.; De Clercq, P.; Vandewalle, M. Synthesis of (C-11)-substituted analogues of 1α,25-dihydroxyvitamin D3. *Bioorg. Med. Chem. Lett.* **1992**, *2*, 477-480.
137. Peterson, P. E.; Leffew, R. L. B.; Jensen, B. L. Syudies of the ketone obtained from the ozonolysis of vitamin D. Molecular mechanics calculations for it and related hydrindanones. *J. Org. Chem.***1986,** *51*, 1948-1954.
138. Kuhakarn, C.; Kittigowittana, K.; Pohmakotr, M.; Reutrakul, V. IBX/n-Bu4NBr/CH2Cl2–H2O: a new mild system for selective oxidation of secondary alcohols, In *Tetrahedron* **2005**, *61*, 8995-9000.
139. Abel-Magrid, A. F.; Carson, K. G.; Harris, B. D.; Maryanoff, C. A.; Shah, R. D. Reductive amination of aldehydes and ketones with sodium triacetoxyborohydride. Studies on direct and indirect reductive amination procedures. *J. Org. Chem.* **1996**, *61*, 3849-3862.
140. McNeill, E.; Du Bois, J. Ruthenium-catalyzed hydroxylation of unactivated tertiary C-H bonds. *J. Am. Chem. Soc.* **2010**, *132*, 10202-10204.
141. Werz, O.; Wiesinger, H.; Steinmeyer, A.; Steinhilber, D. New vitamin D receptor agonists with decreased metabolic stability. *Biochem. Pharma.* **2000**, *59*, 1597-1601.

142. Hadden, M. K. Hedgehog and vitamin D signaling pathways in development and disease. *Vitamins and Hormones* **2016**, *100*, 231-253.
143. Rochel, N.; Wurtz, J. M.; Mitschler, A.; Klaholz, B.; Moras, D. The crystal structure of the nuclear receptor for vitamin D bound to its natural ligand. *Mol. Cell* **2000***, 5*, 173–179.
144. Shaffer, P. L.; Gewirth, D. T. Structural analysis of RXR-VDR interactions on DR3 DNA. *J. Steroid. Biochem. Mol. Biol.* **2004**, *89-90*, 215-219.
145. Rachez, C.; Lemon, B. D.; Suldan, Z.; Bromleigh, V.; Gamble, M.; Naar, A. M.; et al. Ligand-dependent transcription activation by nuclear receptors requires the DRIP complex. *Nature* **1999**, *398*, 824-828.
146. Carlberg, C.; Bendik, I.; Wyss, A.; Meier, E.; Sturzenbecker, L. J.; Grippo, J. F.; et al. Two nuclear signalling pathways for vitamin D. *Nature* **1993**, *361*, 657–60.
147. Carlberg, C.; Campbell, M. J. Vitamin D receptor signaling mechanisms: Integrated actions of a well-defined transcription factor. *Steroids* **2013**, *78*, 127-136.
148. Dhawan, P.; Wieder, R.; Christakos, S. CCAAT enhancer-binding protein alpha is a molecular target of 1,25-dihydroxyvitamin D3 in MCF-7 breast cancer cells. *J. Biol. Chem.* **2009**, *284*, 3086-3095.
149. McCollum, E.; Simmonds, N.; Becker, J.; Shipley, P. Studies on experimental rickets, XXI: an experimental demonstration of the existence of a vitamin which pro- motes calcium deposition. *J Biol Chem.* **1922**, *53*, 293–312.
150. Utiger, R. The need for more vitamin D. *N Engl J Med.* **1998**, *338*, 828–829.
151. Garland, C. F.; Garland, F. C. Do sunlight and vitamin D reduce the likelihood of colon cancer? *Int. J. Epidemiol.* **1980**, *9*, 227–231.
152. Deeb, K. K.; Trump, D. L.; Johnson, C. S. Vitamin D signaling pathways in cancer: potential for anticancer therapeutics. *Nat. Cancer* **2007**, *7*, 684-700.
153. Bikle, D. D. Vitamin D regulated keratinocyte differentiation. *J. Cell. Biochem.* **2004**, *92*, 436–444.
154. Bikle, D. D.; Elalieh, H.; Welsh, J.; Oh, D.; Cleaver, J.; Techert, A. Protective role of vitamin D signaling in skin cancer formation. *J. Steroid Biochem. Mol. Biol.* **2013**, *136*, 271-279.
155. Zinser, G. M.; Sundberg, J. P.; Welsh, J. Vitamin D(3) receptor ablation sensitizes skin to chemically induced tumorigenesis. *Carcinogenesis* **2002**, *23*, 2103–2109.
156. Ellison, T. I.; Smith, M. K.; Gilliam, A. C.; et al. Inactivation of the vitamin D receptor enhances susceptibility of murine skin to UV-induced tumorigenesis. *J. Invest. Dermatol*. **2008,** 128, 2508–2517.
157. Demetriou, S. K.; Ona-Vu, K. Teichert, A. E.; et al. Vitamin D receptor mediates DNA repair and is UV inducible in intact epidermis but not in cultured keratinocytes. *J. Invest. Dermatol*. **2012**, *132*, 2097-2100.
158. Bikle, D. D.; Oda, Y.; Tu, C-L.; Jiang, Y. Novel mechanisms for the vitamin D receptor (VDR) in the skin and in skin cancer. *J. Steroid Biochem. Mol. Biol.* **2015**, *148*, 47-51.
159. Palmer, H. G.; Anjos-Afonso, F.; Carmeliet, G.; Takeda, H.; Watt, F. M. The vitamin D receptor is a Wnt effector that controls hair follicle differentiation and specifies tumor type in adult epidermis, *PLoS One* **2008**, *3*, e1483.
160. Jiang, Y. J.; Teichert, A. E.; Fong, F.; Oda, Y.; Bikle, D. D. 1α,25(OH)2- Dihydroxyvitamin D3/VDR protects the skin from UVB-induced tumor formation by interacting with the β-catenin pathway, *J. Steroid Biochem. Mol. Biol*. **2013,** *136*, 229–232.
161. Lisse, T. S.; Saini, V.; Zhao, H.; Luderer, H. F.; Gori, F.; Demay, M. B. The vitamin D receptor is required for activation of cWnt and Hedgehog signaling in keratinocytes. *Mol. Endocrinol.* **2014**, *28*, 1698-1706.
162. Yiang, Y. J.; Bikle, D. D. LncRNA: a new player in 1α,25(OH)2 vitamin D3/VDR protection against skin cancer formation. *Exp. Dermatol.* **2014**, *23*, 147-150.
163. Honda, S.; Arai, Y.; Haruta, M.; Sasaki, F.; Ohira, M.; Yamaoka, H.; et al. Loss of imprinting of IGF2 correlates with hypermethylation of the H19 differentially methylated region in hepatoblastoma. *Br. J. Cancer* **2008**, *99*, 1891-1899.

164. Larriba, M. J.; Gonzalez-Sancho, J. M.; Bonilla, F.; Munoz, A. Interaction of vitamin D with membrane-based signaling pathways. *Front. Physiol.* **2014**, *5 (60)*, doi:10.3389/fphys.2014.00060.
165. Teichert, A. E.; Elalieh, H.; Elias, P. M.; Welsh, J.; Bikle, D. D. Overexpression of hedgehog signaling is associated with epidermal tumor formation in vitamin D receptor-null mice. *J. Investig. Dermatol*. **2011**, *131*, 2289–2297.
166. Uhmann, A.; Niemann, H.; Lammering, B.; Henkel, C.; Heb, I.; Nitzki, F.; et al. Antitumoral effects of calcitriol in basal cell carcinoma involve inhibition of hedgehog signaling and induction of vitamin D receptor signaling and differentiation. *Mol. Cancer Ther.* **2011**, *10*, 2179-2187.
167. Linder, B.; Weber, S.; Dittmann, K.; Adamski, J.; Hahn, H.; Uhmann, A. A functional and putative physiological role of calcitriol in Patched1/Smoothened interaction. *J. Biol. Chem.* **2015**, *290*, 19614-19628.
168. Alimirah, F.; Peng, X.; Gupta, A.; Yuan, L.; Welsh, J.; Cleary, M.; Mehta, R. G. Crosstalk between the vitamin D receptor (VDR) and miR-214 in regulating SuFu, a hedgehog pathway inhibitor in breast cancer. *Exp. Cell Research* **2016**, *349*, 15-22.
169. Flynt, A. S.; Li, N.; Thatcher, E. J.; Solnica-Krezel, L.; Patton, J. G. Zebrafish miR-214 modulates hedgehog signaling to specify muscle cell fate. *Nat. Genet.***2007**, *39*, 259-263.
170. Boehm, M. F.; Fitzgerald, P.; Zou, A.; Elgort, M. G.; Bischoff, E. D.; Mere, L.; et al. Novel nonsecosteroidal vitamin D mimics exert VDR-modulating activities with less calcium mobilization than 1,25-dihydroxyvitamin D3. *Chem. Biol.* **1999**, *6*, 265-275.
171. Sicinski, R. R.; Prahl, J. M.; Smith, C. M.; DeLuca, H. F. New 1α,25-dihydroxy-19-norvitamin D3 compounds of high biological activity: synthesis and biological evaluation of 2-hydroxymethyl, 2-methyl, and 2-methylene analogues. *J. Med. Chem.* **1998**, *41*, 4662-4674.
172. Vanhooke, J. L.; Benning, M. M.; Bauer, C. B.; Pike, J. W.; DeLuca, H. F. Molecular structure of the rat vitamin D receptor ligand binding domain complexed with 2-carbon-substituted vitamin D3 hormone analogues and a LXXLL-containing coactivator peptide. *Biochemistry* **2004**, *43*, 4101-4110.
173. Chen, T. C.; Persons, K. S.; Zheng, S.; Mathieu, J.; et al. Evaluation of C-2-substituted 19-nor-1α,25-dihydroxyvitamin D3 analogs as therapeutic agents for prostate cancer. *J. Steroid Biochem. Mol. Biol.* **2007**, *103*, 717-720.
174. Sibilska, I. K.; Szybinski, M.; Sicinski, R. R.; Plum, L. A.; DeLuca, H. F. Synthesis and biological activity of 2-methylene analogues of calcitriol and related compounds. *J. Med. Chem.* **2015**, *58*, 9653-9662.
175. Pike, J. W.; Zella, L. A.; Meyer, M. B.; Fretz, J. A.; Kim, S. Molecular actions of 1,25-dihydroxyvitamin D3 on genes involved in calcium homeostasis. *J. Bone Miner. Res.* **2007**, *22*, V16-V19.
176. Wang, J.; Slominski, A.; Tuckey, R. C.; Janjetovic, Z.; et al. 20-hydroxyvitamin D3 inhibits proliferation of cancer cells with high efficacy while being non-toxic. *Anticancer Res.* **2012**, *32*, 739-746.
177. Brown, A. J.; Ritter, C. R.; Finch, J. L.; Morrissey, J.; et al. The noncalcemic analogue of vitamin D, 22-oxacalcitriol, suppresses parathyroid hormone synthesis and secretion. *J. Clin. Invest.* **1989**, *84*, 728-732.
178. Guryev, O.; Carvalho, R. A.; Usanov, S.; Gilep, A.; Estabrook, R. W. A pathway for the metabolism of vitamin D3: unique hydroxylated metabolites formed during catalysis with cytochrome P450scc (CYP11A1). *Proc. Natl. Acad. Sci. USA* **2003**, *100*, 14754-14759.
179. Slominski, A. T.; Janjetovic, Z.; Fuller, B. E.; et al. Products of vitamin D3 or 7-dehydrocholesterol metabolism by cytochrome P450scc show anti-leukemia effects, having low or absent calcemic activity. *PLoS ONE* **2010**, *5*, e9907.
180. Li, W.; Chen, J.; Janjetovic, Z.; et al. Chemical synthesis of 20*S*-hydroxyvitamin D3, which shows antiproliferative activity. *Steroids* **2010**, *75*, 926-935.
181. Wang, Q.; Lin, Z.; Kim, T-K.; Slominski, A. T.; Miller, D. D.; Li, W. Total synthesis of biologically active 20*S*-hydroxyvitamin D3. *Steroids* **2015,** *104*, 153-162.

Modulation of the Hedgehog Signaling Pathway by Sterol-based Small Molecules

Chad Anthony Maschinot

Appendix

OHC Crystal Structure Data
Obtained by Dr Victor Day at the University of Kansas

OHC 28

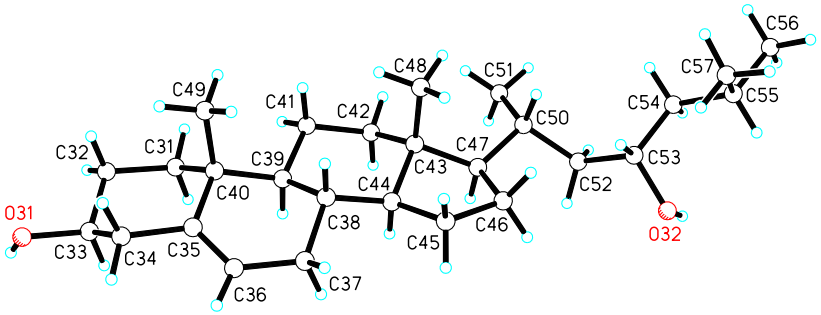

OHC 29

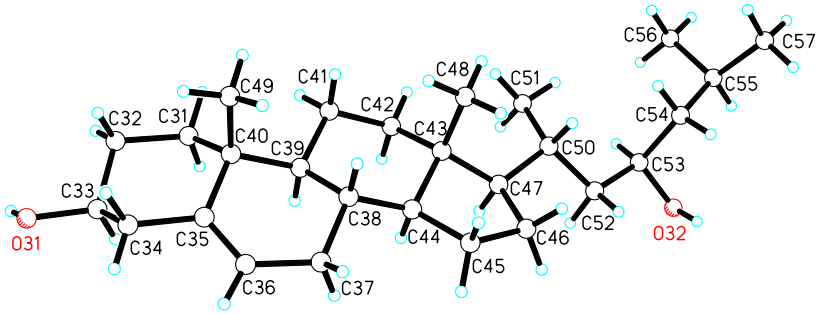

NMR Spectra

I. Oxysterols (OHC) Analogues

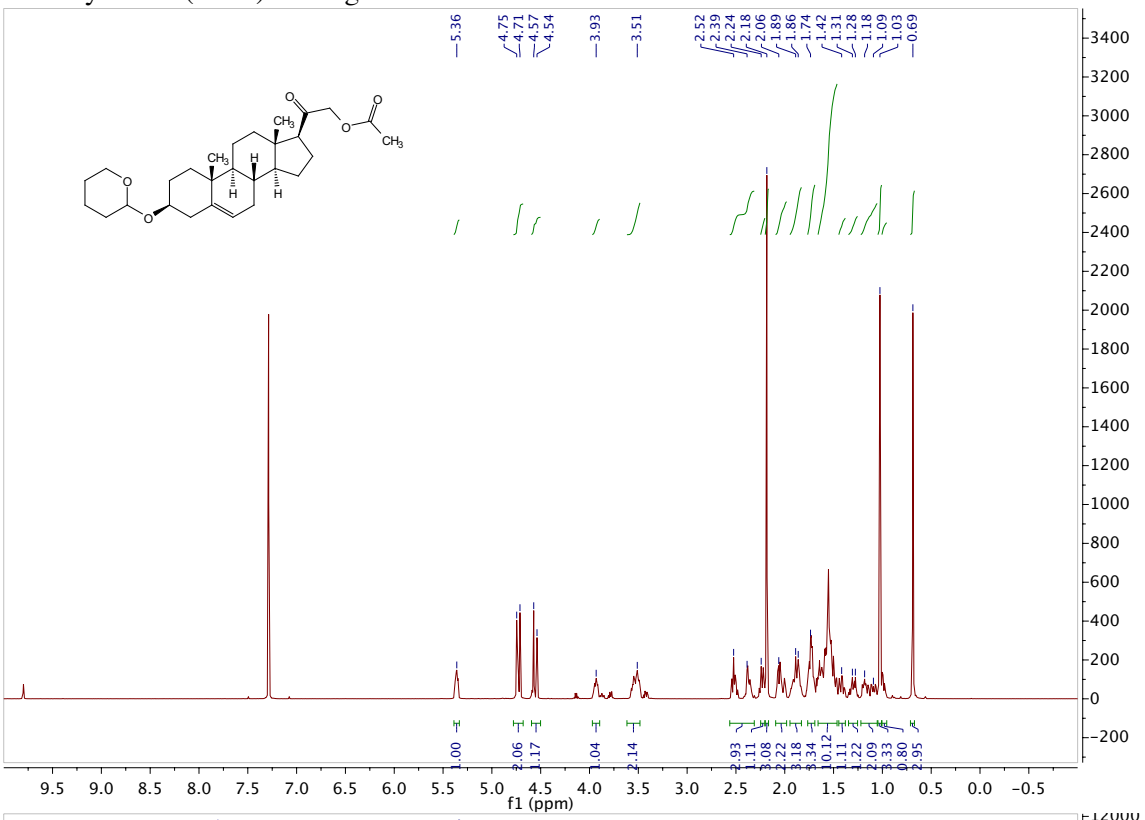

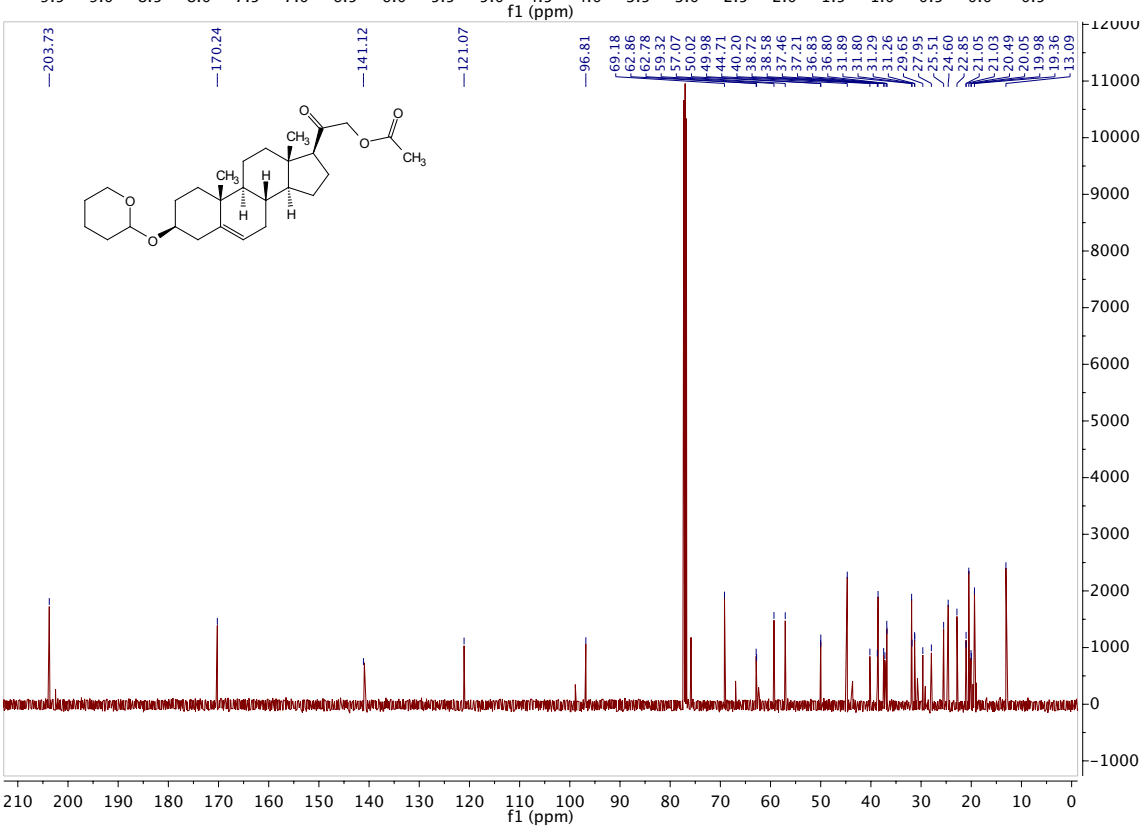

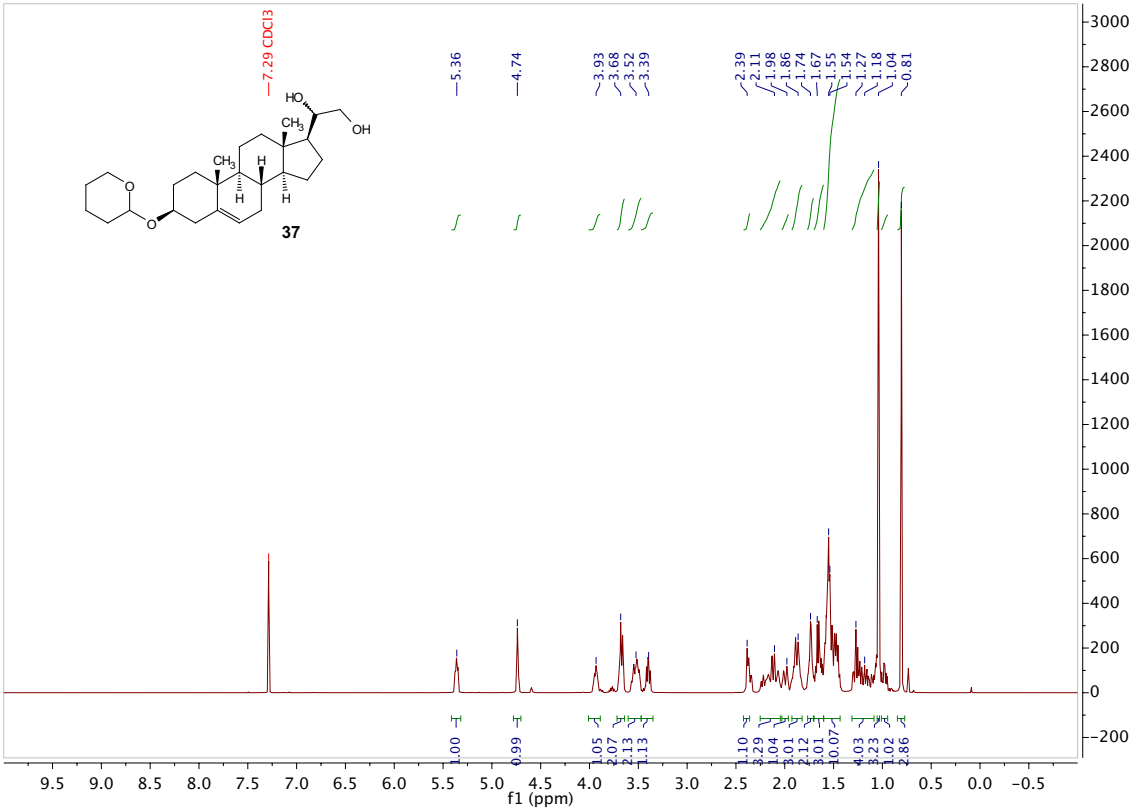
7.29 CDCl3
5.36
4.74
3.93
3.68
3.52
3.39
2.39
2.11
1.98
1.86
1.74
1.67
1.55
1.54
1.27
1.18
1.04
0.81
1.00
0.99
1.05
2.07
2.13
1.13
1.10
8.29
1.04
3.01
2.12
3.01
10.07
4.03
3.23
1.02
2.86
HO
OH
CH3
CH3
H
H
H
O
O
37
f1 (ppm)

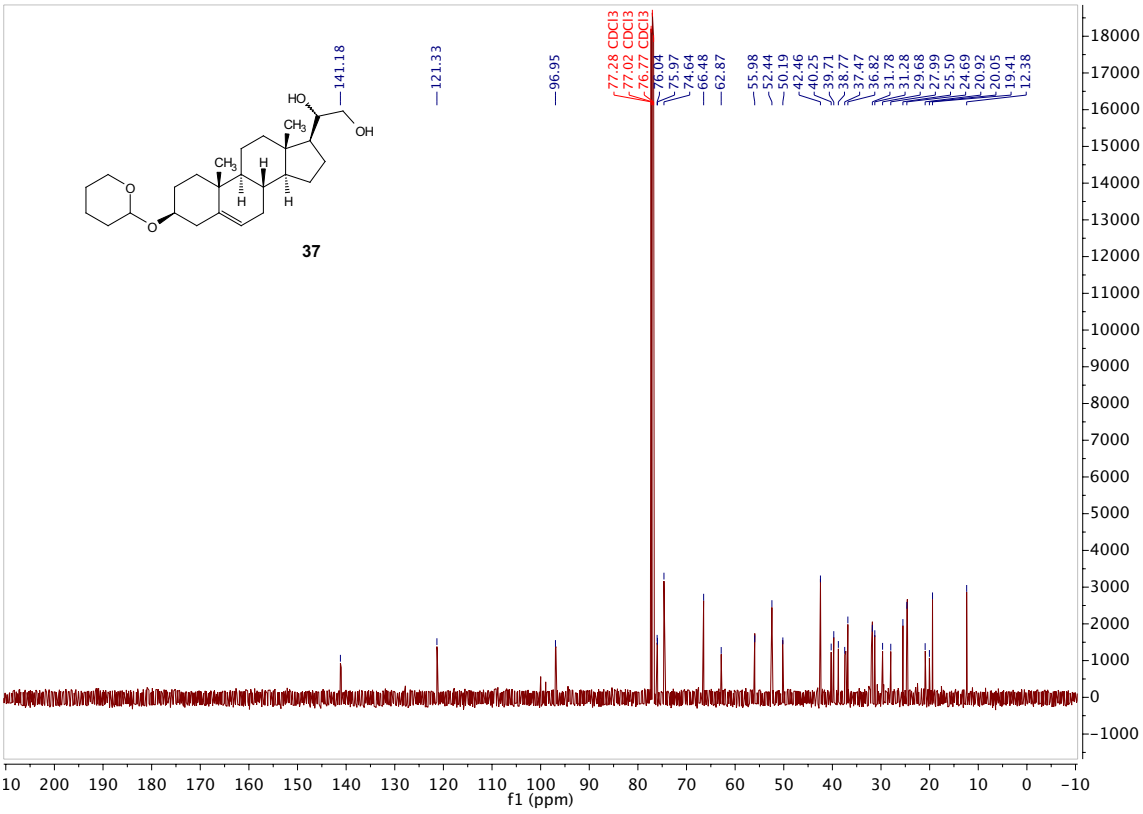
141.18
121.33
96.95
77.28 CDCl3
77.02 CDCl3
76.77 CDCl3
76.04
75.97
74.64
66.48
62.87
55.98
52.44
50.19
42.46
40.25
39.71
38.77
37.47
36.82
31.78
31.28
29.68
27.99
25.50
24.69
20.92
20.05
19.41
12.38
HO
OH
CH3
CH3
H
H
H
O
O
37
f1 (ppm)

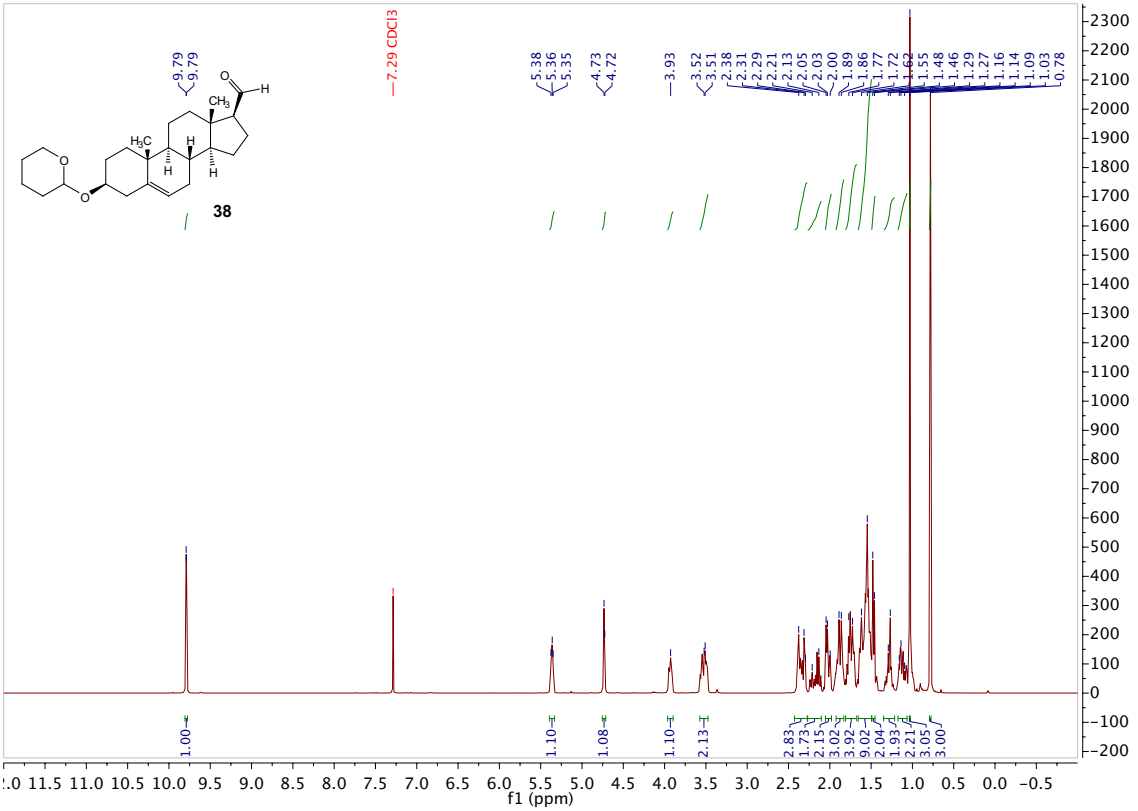
38
f1 (ppm)

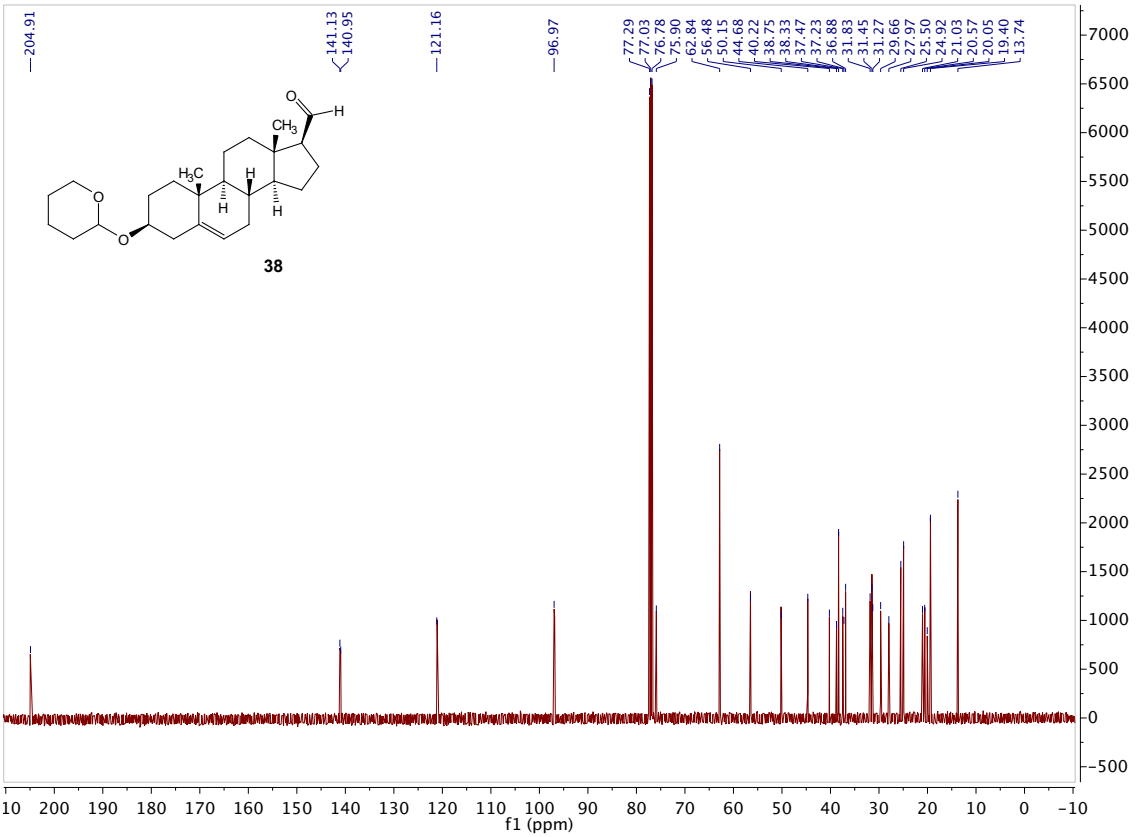
38
f1 (ppm)

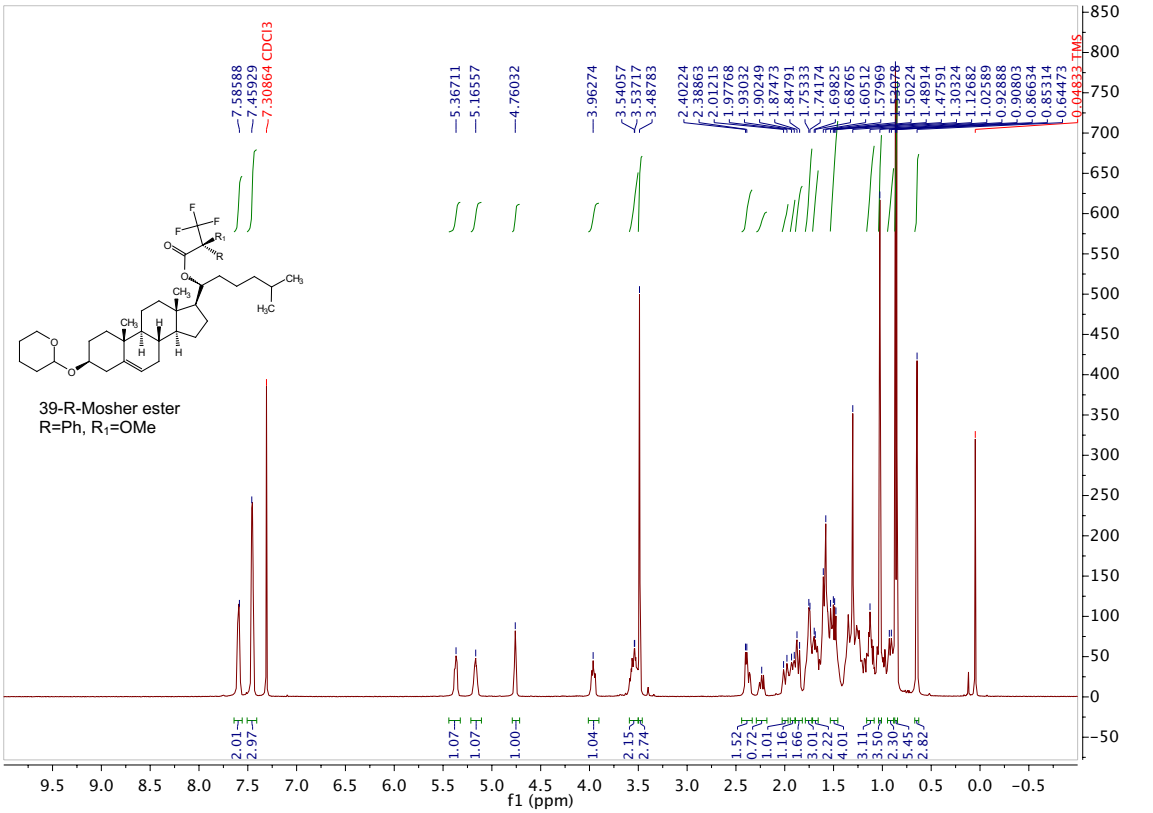
39-R-Mosher ester
R=Ph, R1=OMe
f1 (ppm)

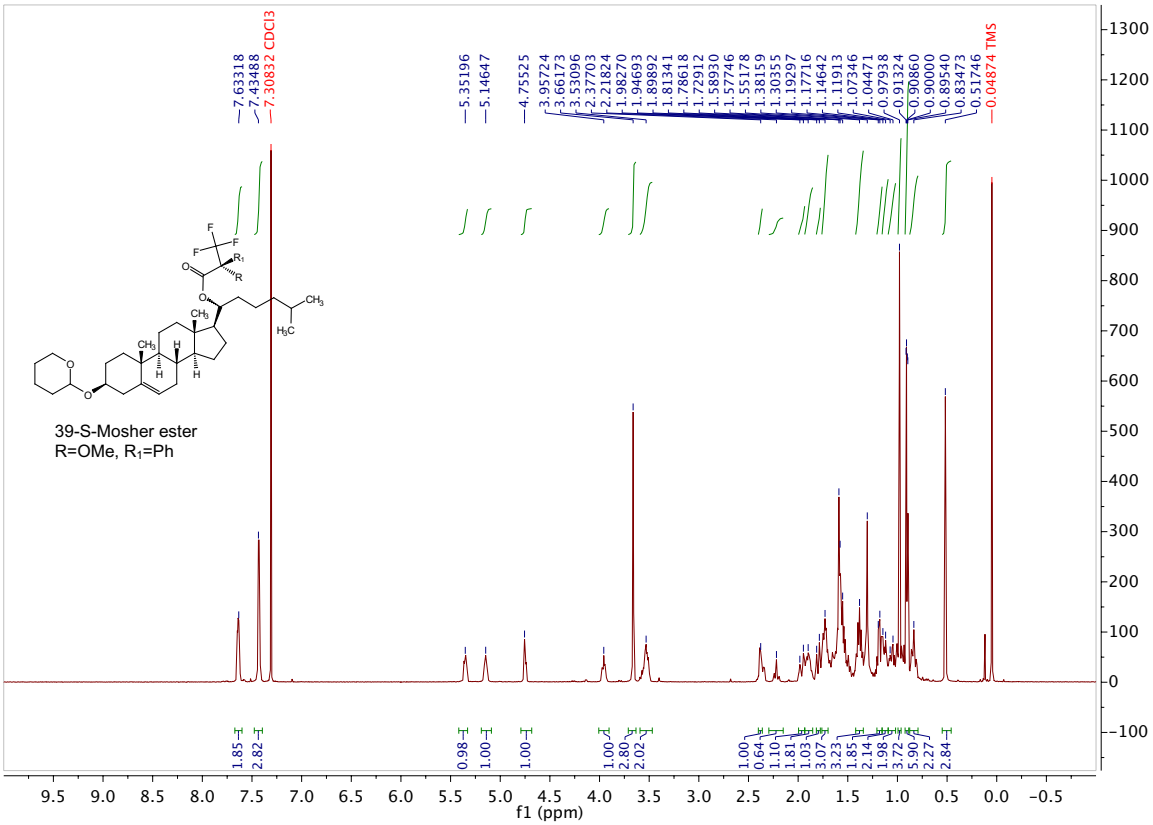
39-S-Mosher ester
R=OMe, R1=Ph
f1 (ppm)

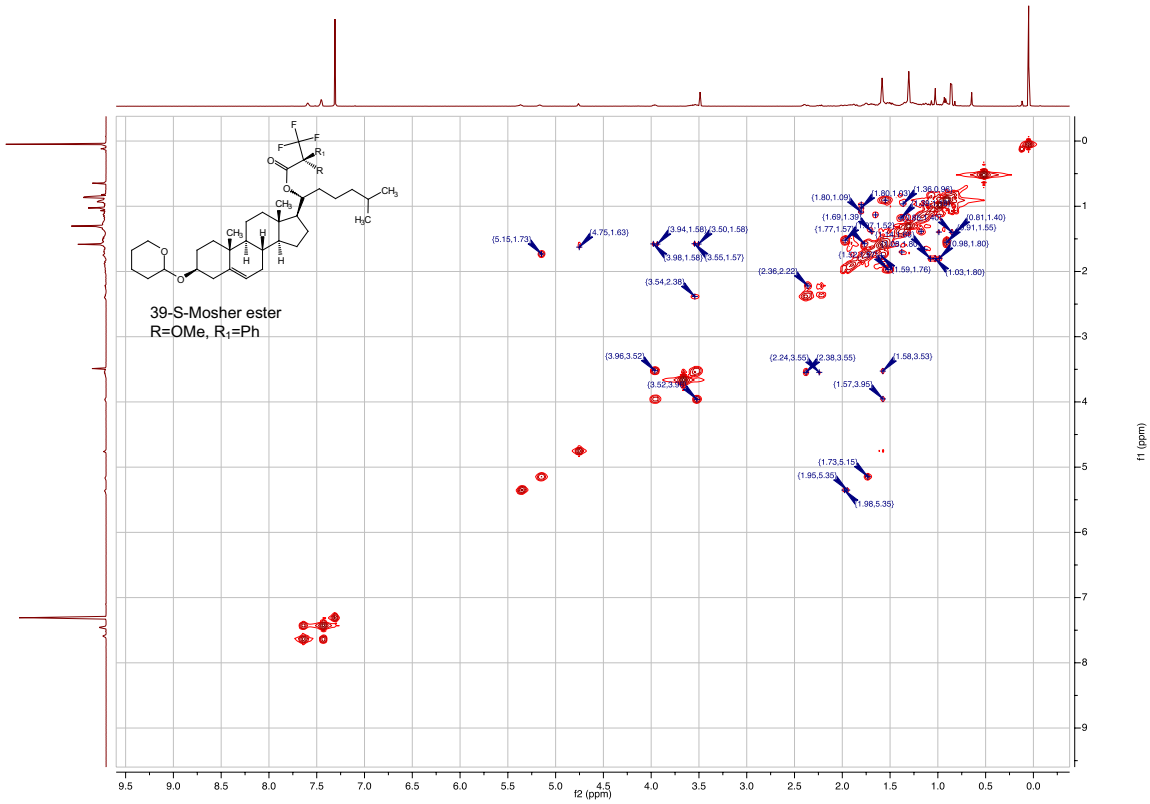

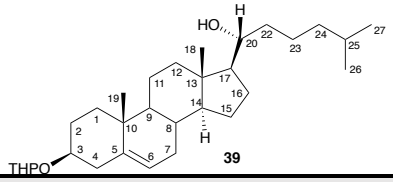

H assignment	S-MTPA-39 ester (ppm)	R-MTPA-39-ester (ppm)	$\Delta\delta^{SR}$ (ppm)
17	1.732	1.748	-0.016
18	0.517	0.645	-0.128
19	0.979	1.026	-0.047
26/27	0.902	0.859	0.043
7	1.965	1.995	-0.030
20	5.146	5.165	-0.019
12	1.759	1.772	-0.013
22	1.898	1.861	0.037
25	1.553	1.481	0.072
4	2.375	2.390	-0.015
4	2.218	2.236	-0.018

Based on reference (Hoye, T. R., et al. *Nature Protocols*, **2007,** *10*, 2451), $\Delta\delta^{SR}$ shift indicates R_1 or R_2 moiety of the compound, where positive shift corresponds to R_1 (side chain) and negative shift R_2 (tetracyclic body).

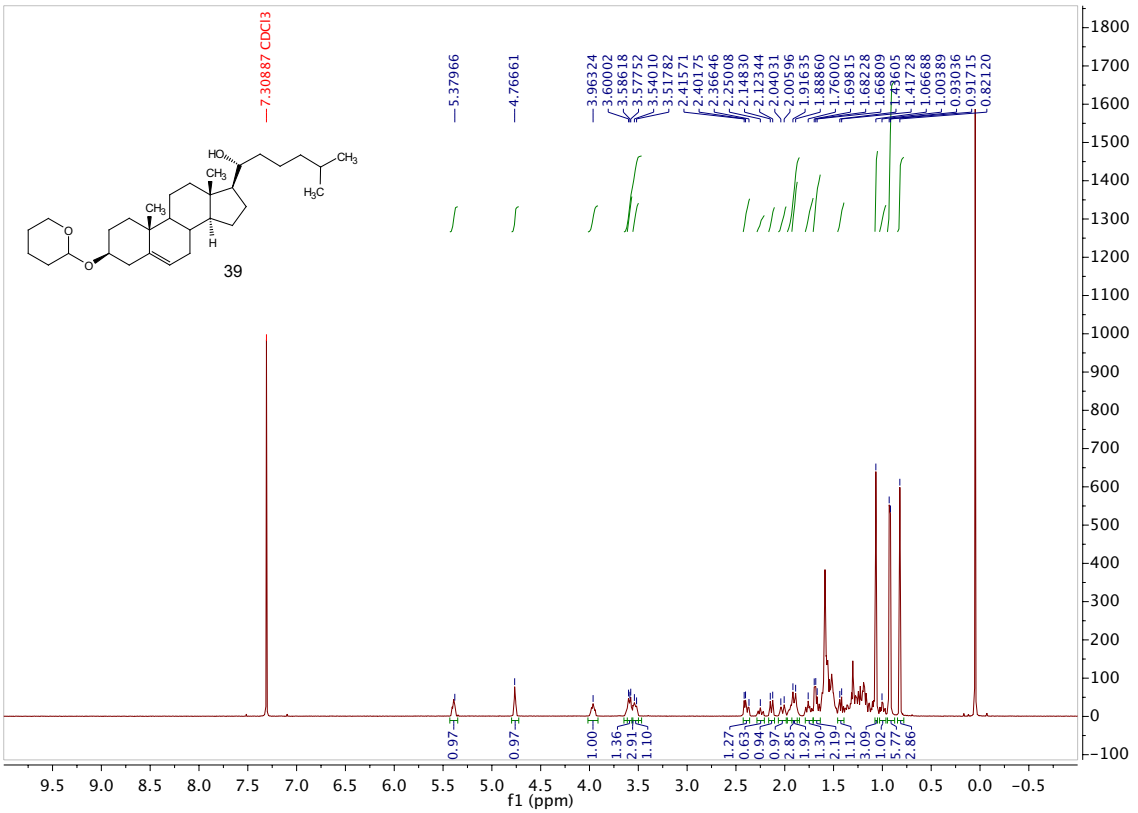
7.30887 CDCl3
5.37966
4.76661
3.96324
3.60002
3.58618
3.57752
3.54010
3.51782
2.41571
2.40175
2.36646
2.25008
2.14830
2.12344
2.04031
2.00596
1.91635
1.88860
1.76002
1.69815
1.68228
1.66809
1.43605
1.41728
1.06688
1.00389
0.93036
0.91715
0.82120
0.97
0.97
1.00
1.36
2.91
1.10
1.27
0.63
0.94
0.97
2.85
1.92
1.30
2.19
1.12
3.09
1.02
5.77
2.86
HO
CH3
CH3
H3C
CH3
H
O
O
39
f1 (ppm)

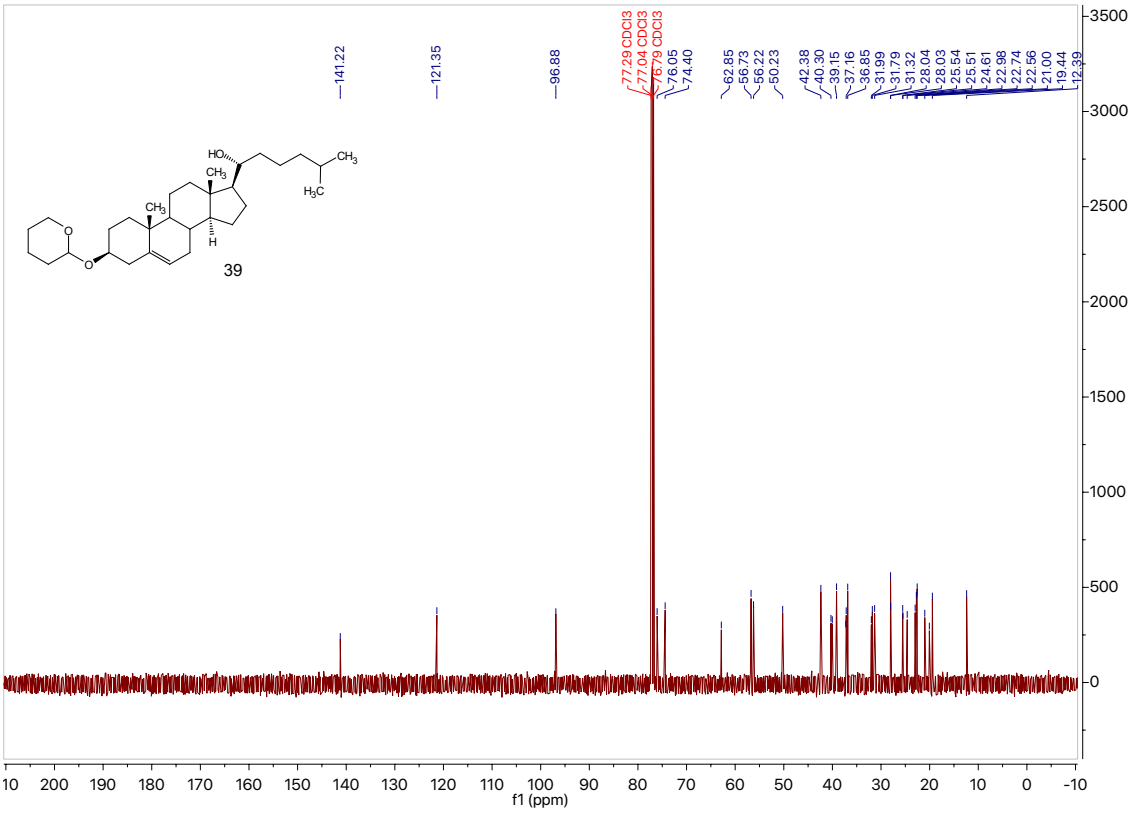
141.22
121.35
96.88
77.29 CDCl3
77.04 CDCl3
76.79 CDCl3
76.05
74.40
62.85
56.73
56.22
50.23
42.38
40.30
39.15
37.16
36.85
31.99
31.79
31.32
28.04
28.03
25.54
25.51
24.61
22.98
22.74
22.56
21.00
19.44
12.39
HO
CH3
CH3
H3C
CH3
H
O
O
39
f1 (ppm)

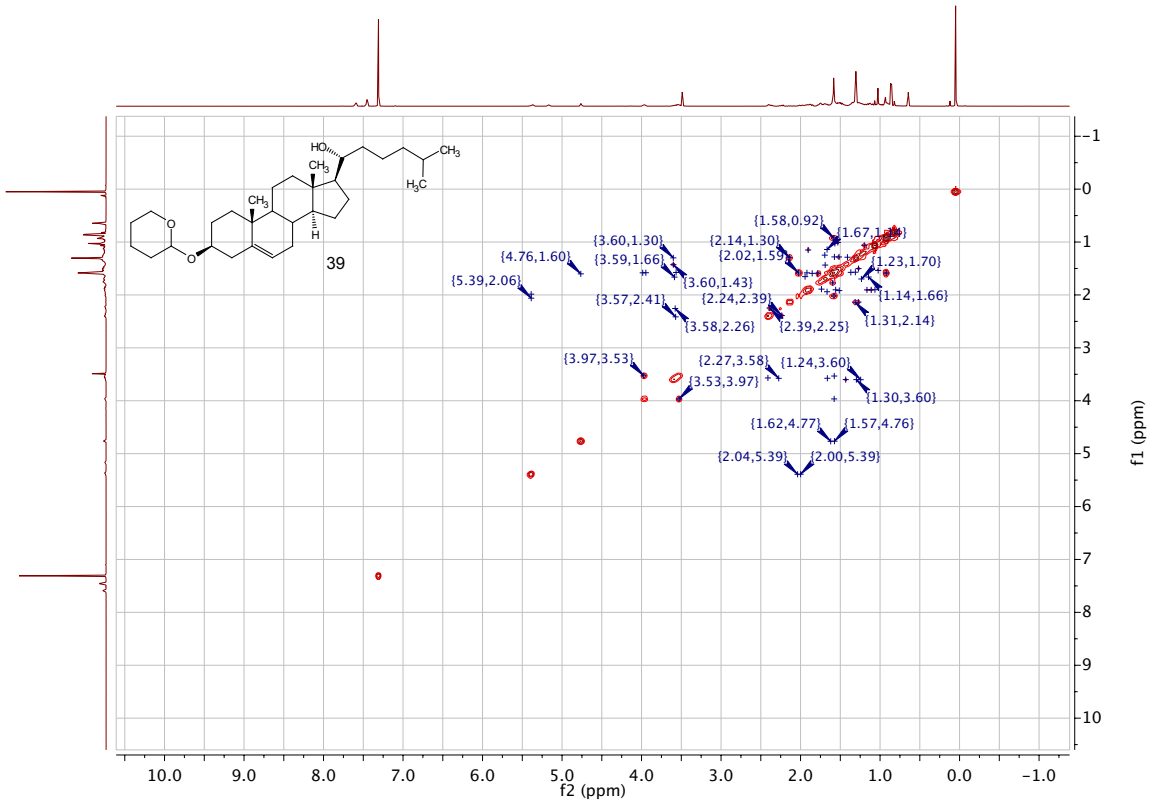
39
{1.58,0.92}
{1.67,1.34}
{3.60,1.30}
{2.14,1.30}
{4.76,1.60}
{3.59,1.66}
{2.02,1.59}
{1.23,1.70}
{5.39,2.06}
{3.60,1.43}
{1.14,1.66}
{3.57,2.41}
{2.24,2.39}
{1.31,2.14}
{3.58,2.26}
{2.39,2.25}
{3.97,3.53}
{2.27,3.58}
{1.24,3.60}
{3.53,3.97}
{1.30,3.60}
{1.62,4.77}
{1.57,4.76}
{2.04,5.39}
{2.00,5.39}
f2 (ppm)
f1 (ppm)

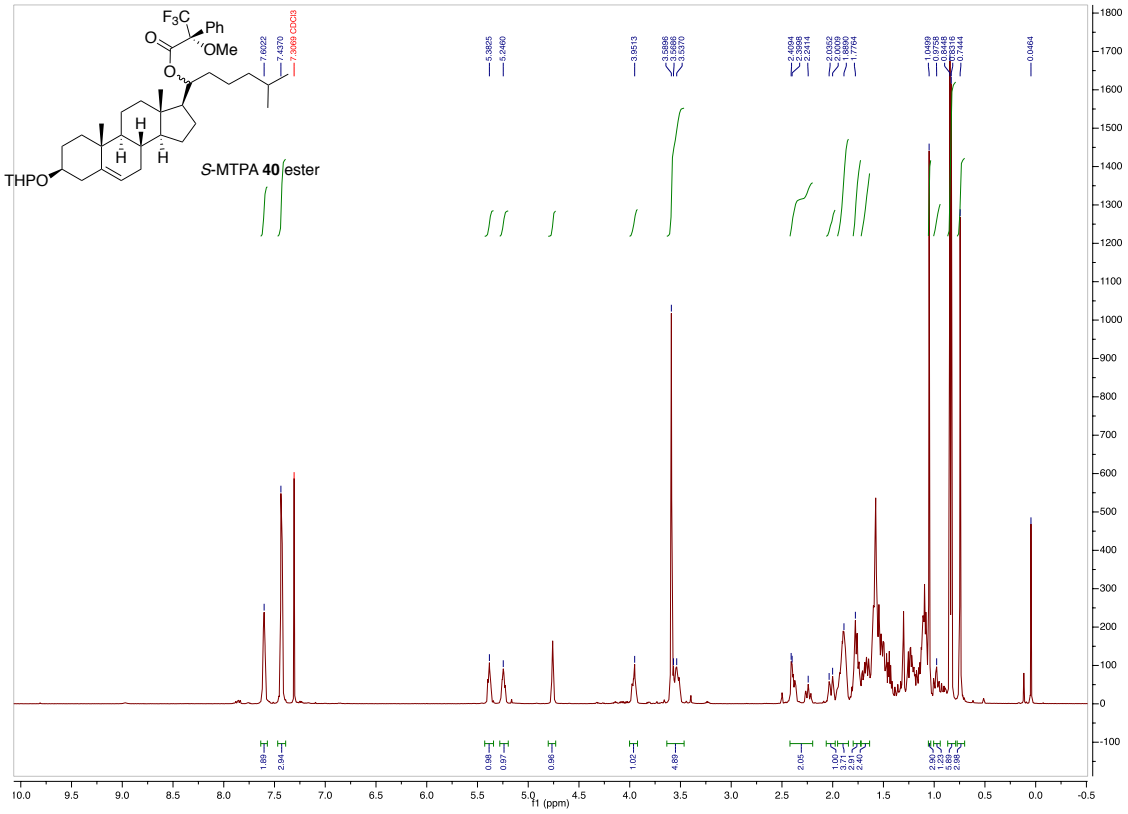
THPO
S-MTPA 40 ester
f1 (ppm)

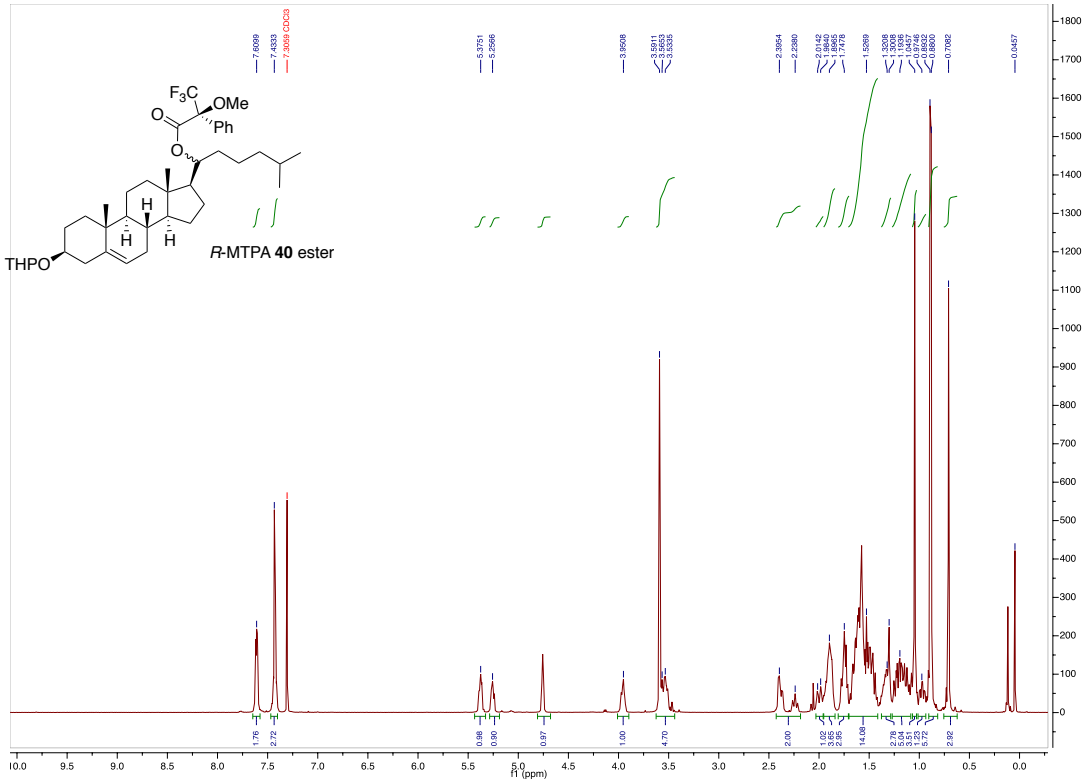

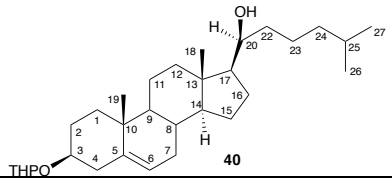

H assignment	S-MTPA-40 ester (ppm)	R-MTPA-40-ester (ppm)	$\Delta\delta^{SR}$ (ppm)
18	0.744	0.708	0.036
19	1.050	1.045	0.005
26/27	0.838	0.887	-0.049
7	2.018	1.999	0.019
20	5.246	5.257	-0.011
4	2.404	2.395	0.009
4	2.241	2.238	0.003

Based on reference (Hoye, T. R., et al. *Nature Protocols*, **2007,** *10*, 2451), $\Delta\delta^{SR}$ shift indicates R_1 or R_2 moiety of the compound, where positive shift corresponds to R_1 (side chain) and negative shift R_2 (tetracyclic body).

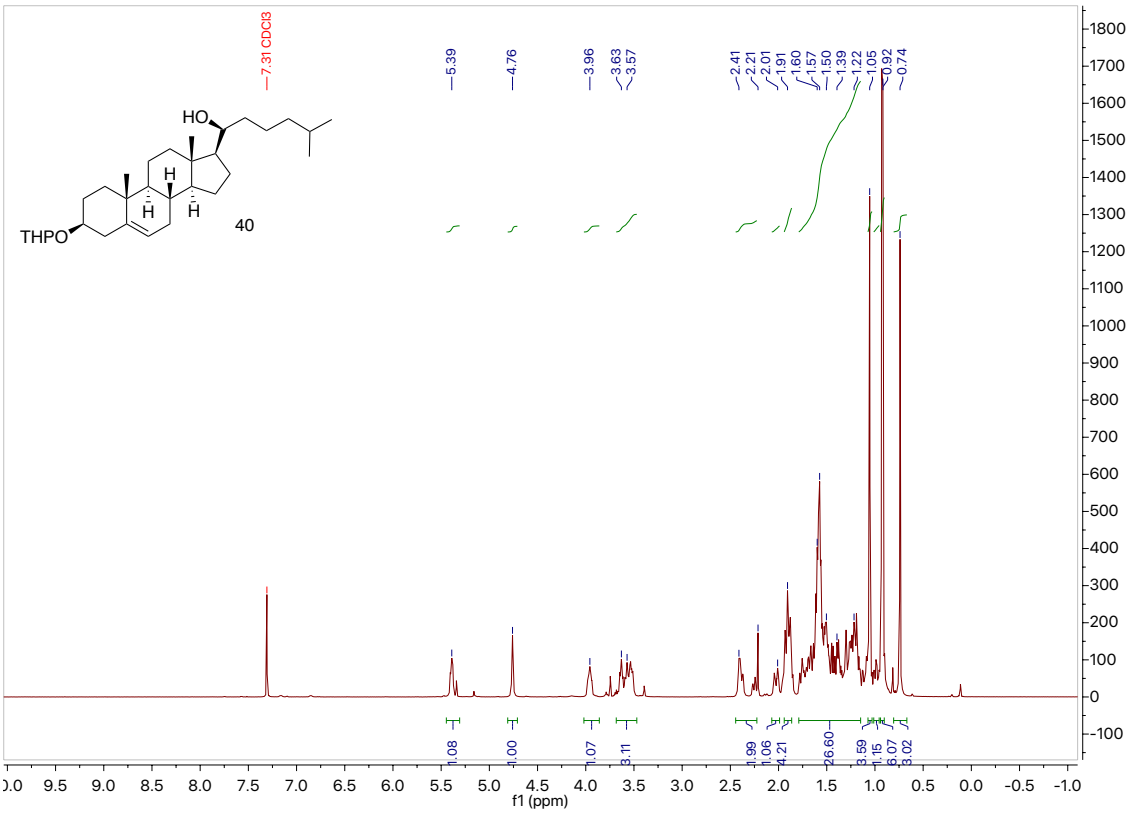
7.31 CDCl3
5.39
4.76
3.96
3.63
3.57
2.41
2.21
2.01
1.91
1.60
1.57
1.50
1.39
1.22
1.05
0.92
0.74
HO
H
H
H
THPO
40
1.08
1.00
1.07
3.11
1.99
1.06
4.21
26.60
3.59
1.15
6.07
3.02
f1 (ppm)

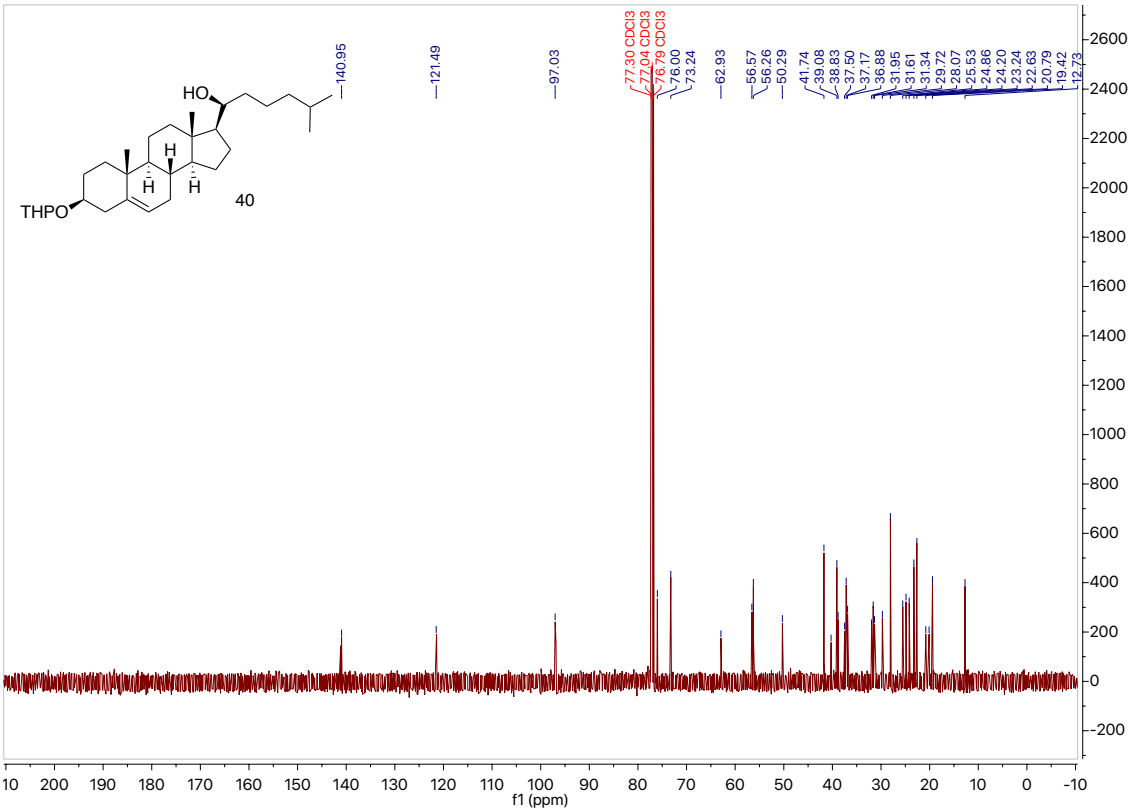
140.95
121.49
97.03
77.30 CDCl3
77.04 CDCl3
76.79 CDCl3
76.00
73.24
62.93
56.57
56.26
50.29
41.74
39.08
38.83
37.50
37.17
36.88
31.95
31.61
31.34
29.72
28.07
25.53
24.86
24.20
23.24
22.63
20.79
19.42
12.73
HO
H
H
H
THPO
40
f1 (ppm)

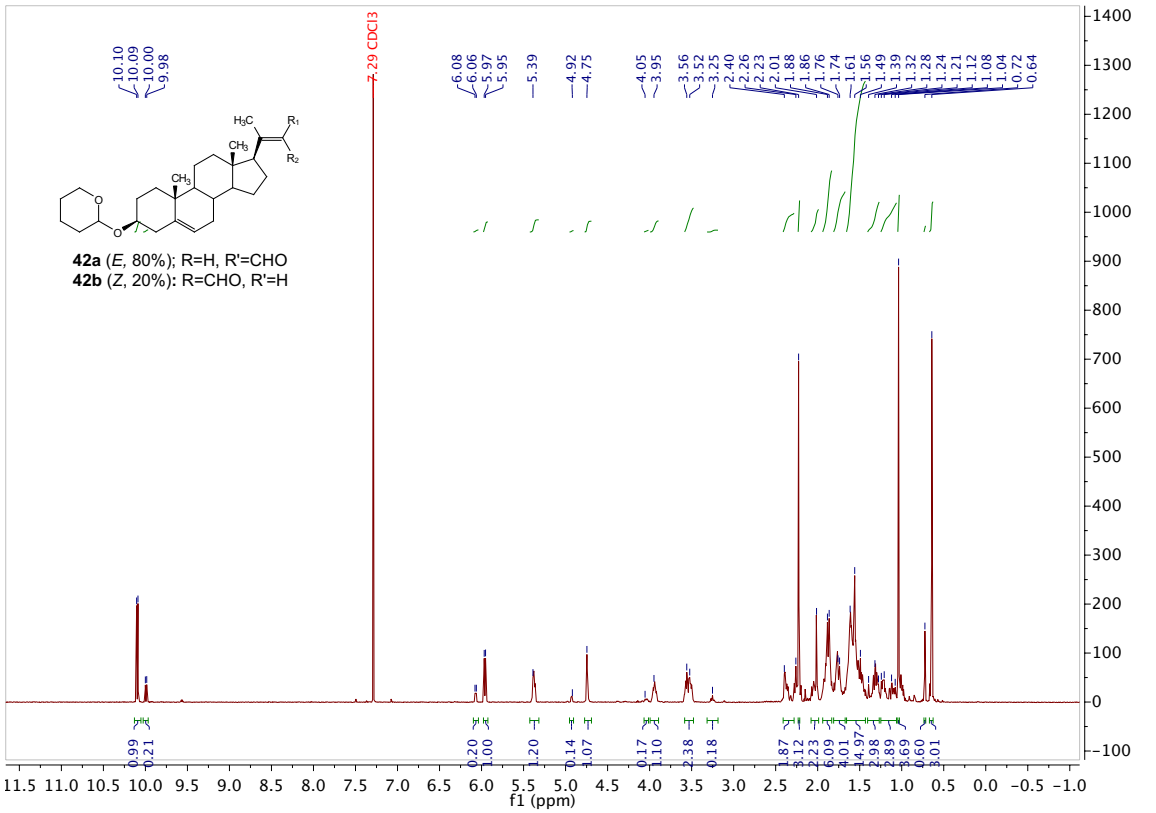
7.29 CDCl3
10.10
10.09
10.00
9.98
6.08
6.06
5.97
5.95
5.39
4.92
4.75
4.05
3.95
3.56
3.52
3.25
2.40
2.26
2.23
2.01
1.88
1.86
1.76
1.74
1.61
1.56
1.49
1.39
1.32
1.28
1.24
1.21
1.12
1.08
1.04
0.72
0.64
0.99
0.21
0.20
1.00
1.20
0.14
1.07
0.17
1.10
2.38
0.18
1.87
3.12
2.23
6.09
4.01
14.97
2.98
2.89
3.69
0.60
3.01
f1 (ppm)
42a (E, 80%); R=H, R'=CHO
42b (Z, 20%): R=CHO, R'=H

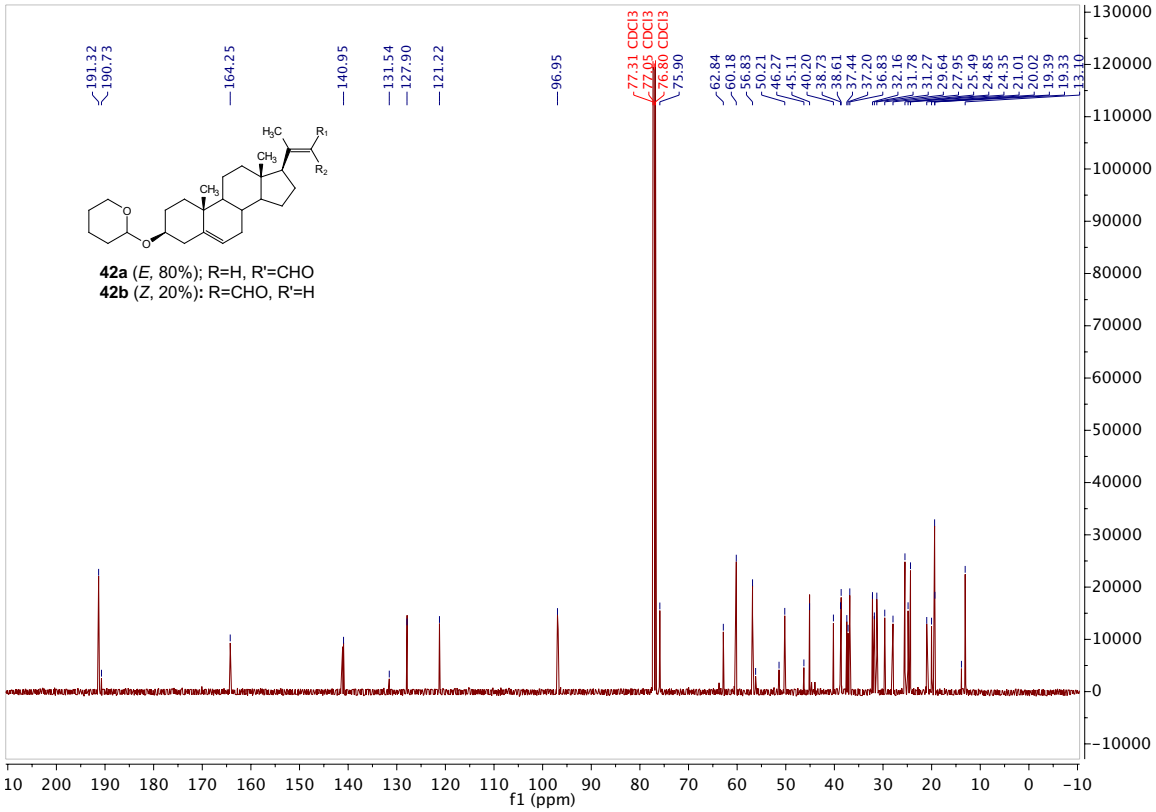
191.32
190.73
164.25
140.95
131.54
127.90
121.22
96.95
77.31 CDCl3
77.05 CDCl3
76.80 CDCl3
75.90
62.84
60.18
56.83
50.21
46.27
45.11
40.20
38.73
38.61
37.44
37.20
36.83
32.16
31.78
31.27
29.64
27.95
25.49
24.85
24.35
21.01
20.02
19.39
19.33
13.10
f1 (ppm)
42a (E, 80%); R=H, R'=CHO
42b (Z, 20%): R=CHO, R'=H

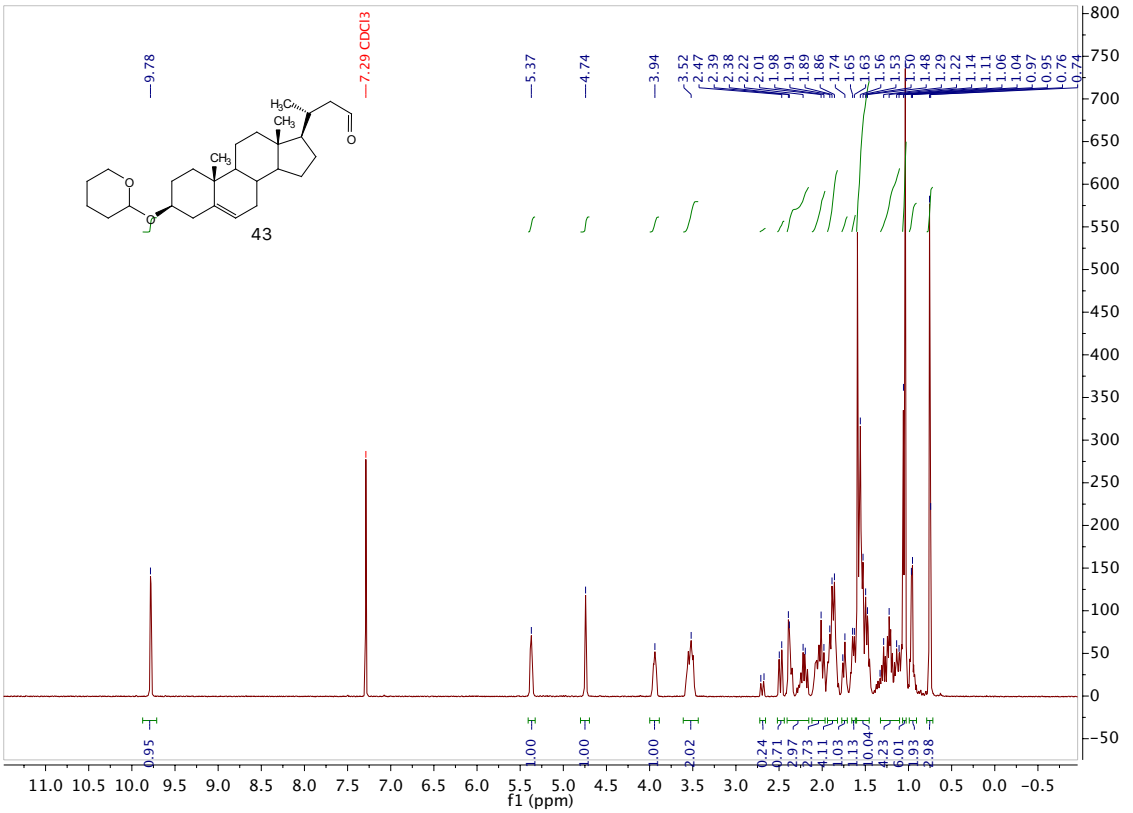
9.78
7.29 CDCl3
5.37
4.74
3.94
3.52
2.47
2.39
2.38
2.22
2.01
1.98
1.91
1.89
1.86
1.74
1.65
1.63
1.56
1.53
1.50
1.48
1.29
1.22
1.14
1.11
1.06
1.04
0.97
0.95
0.76
0.74
43
f1 (ppm)

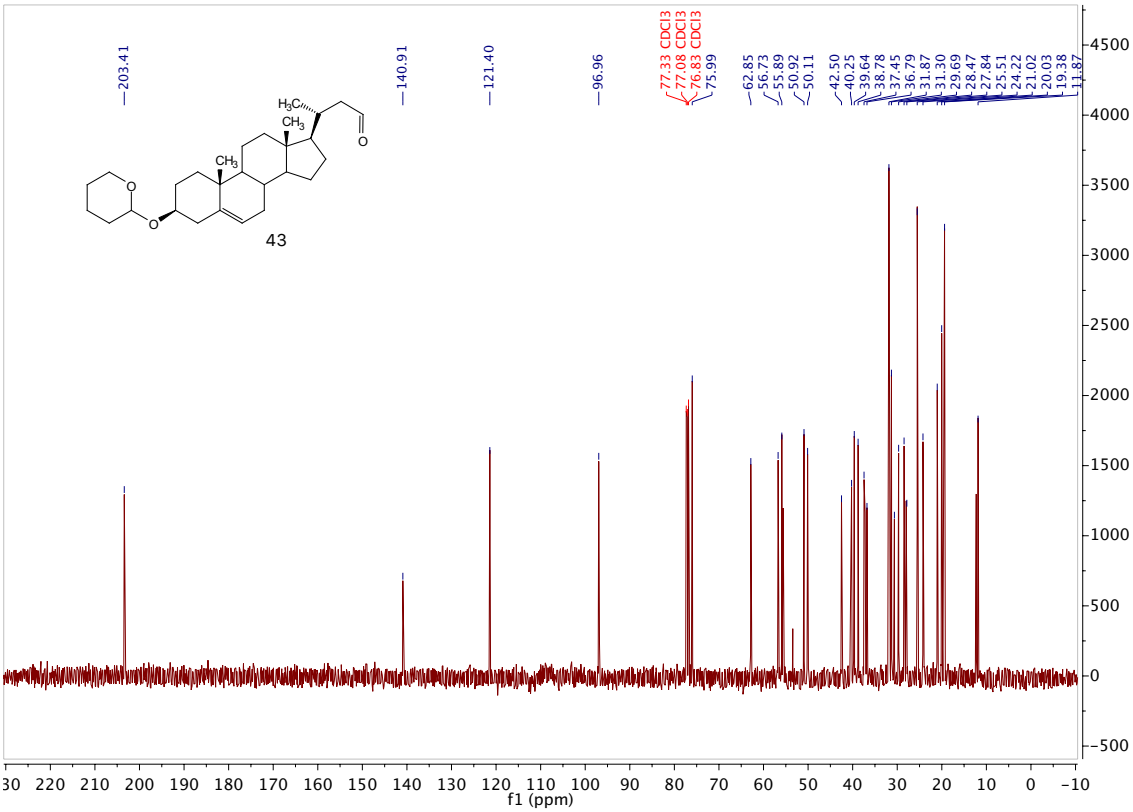
203.41
140.91
121.40
96.96
77.33 CDCl3
77.08 CDCl3
76.83 CDCl3
75.99
62.85
56.73
55.89
50.92
50.11
42.50
40.25
39.64
38.78
37.45
36.79
31.87
31.30
29.69
28.47
27.84
25.51
24.22
21.02
20.03
19.38
11.87
43
f1 (ppm)

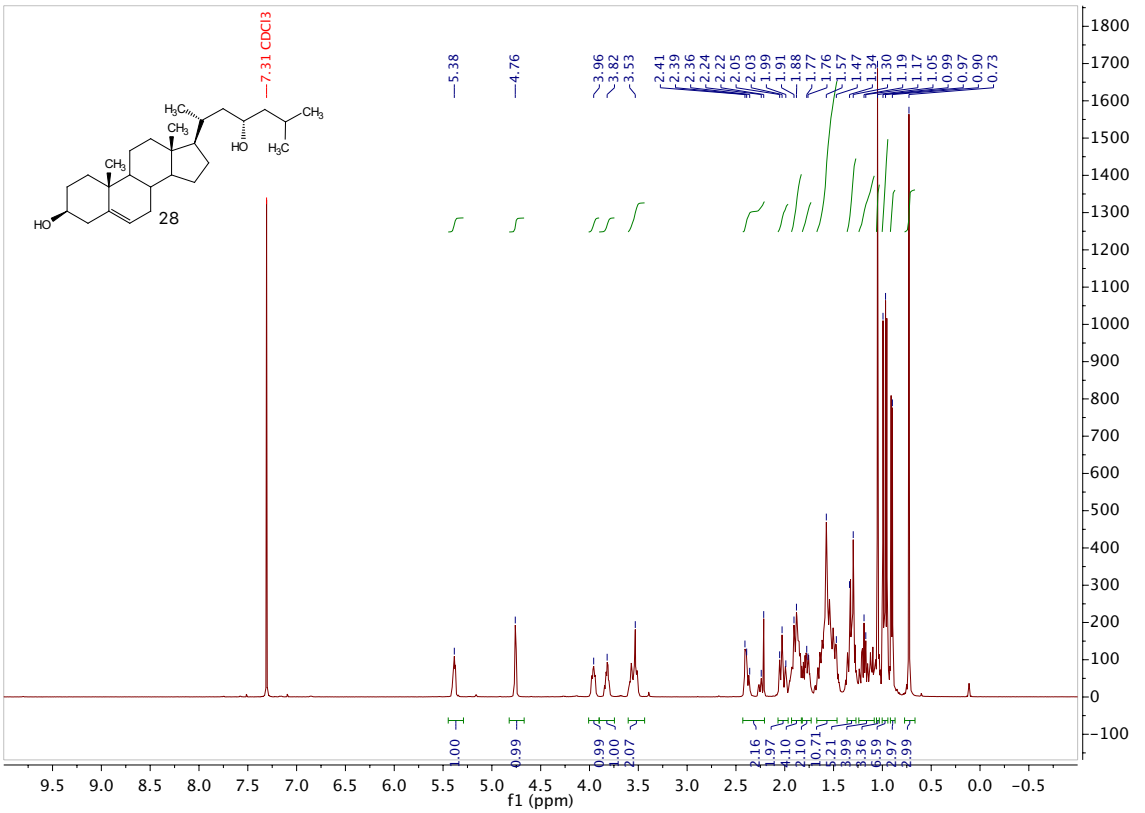
7.31 CDCl3
5.38
4.76
3.96
3.82
3.53
2.41
2.39
2.36
2.24
2.22
2.05
2.03
1.99
1.91
1.88
1.77
1.76
1.57
1.47
1.34
1.30
1.19
1.17
1.05
0.99
0.97
0.90
0.73
28
f1 (ppm)

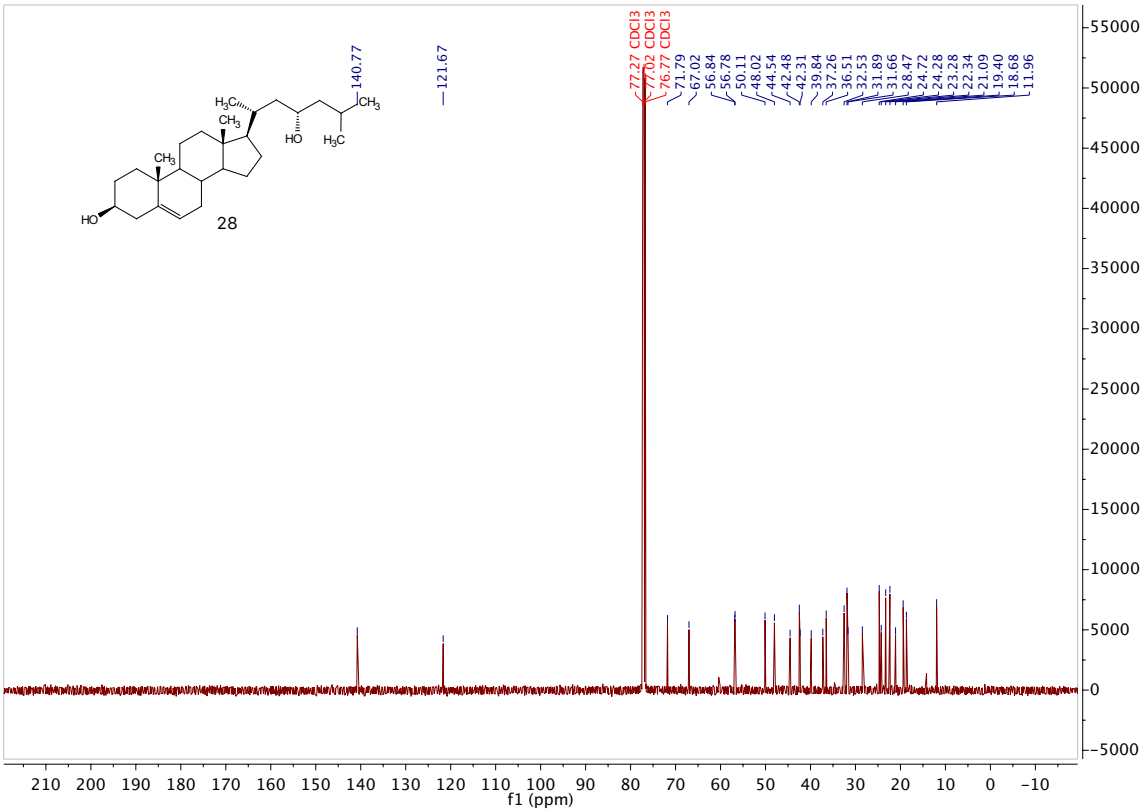
140.77
121.67
77.27 CDCl3
77.02 CDCl3
76.77 CDCl3
71.79
67.02
56.84
56.78
50.11
48.02
44.54
42.48
42.31
39.84
37.26
36.51
32.53
31.89
31.66
28.47
24.72
24.28
23.28
22.34
21.09
19.40
18.68
11.96
28
f1 (ppm)

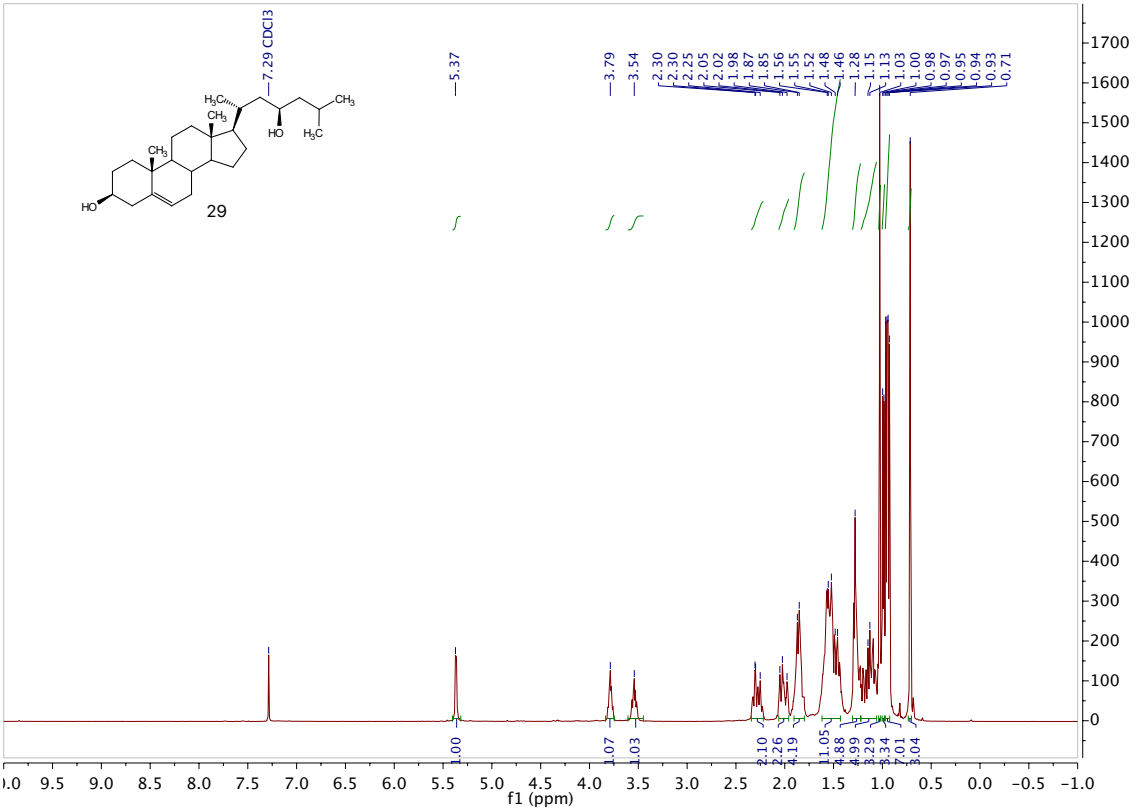
7.29 CDCl3
5.37
3.79
3.54
2.30
2.30
2.25
2.05
2.02
1.98
1.87
1.85
1.56
1.55
1.52
1.48
1.46
1.28
1.15
1.13
1.03
1.00
0.98
0.97
0.95
0.94
0.93
0.71
29
1.00
1.07
1.03
2.10
2.26
4.19
11.05
4.88
4.99
3.29
3.34
7.01
3.04
f1 (ppm)

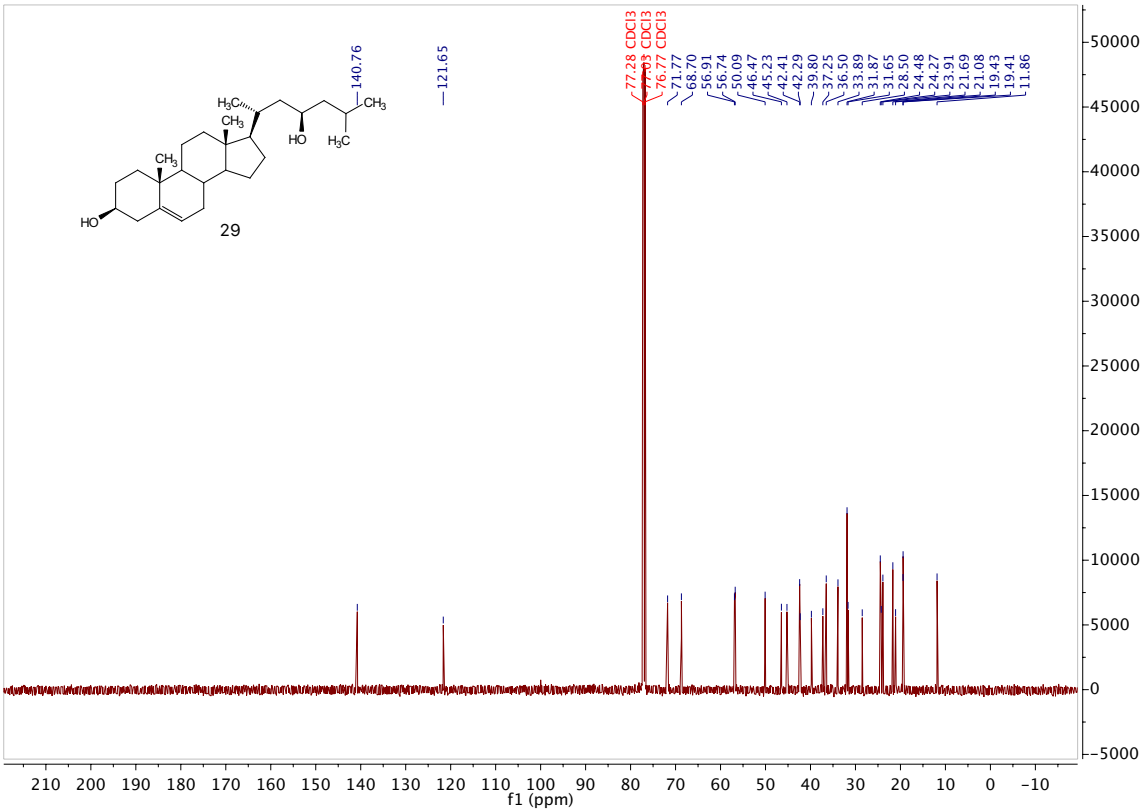
140.76
121.65
77.28 CDCl3
77.03 CDCl3
76.77 CDCl3
71.77
68.70
56.91
56.74
50.09
46.47
45.23
42.41
42.29
39.80
37.25
36.50
33.89
31.87
31.65
28.50
24.48
24.27
23.91
21.69
21.08
19.43
19.41
11.86
29
f1 (ppm)

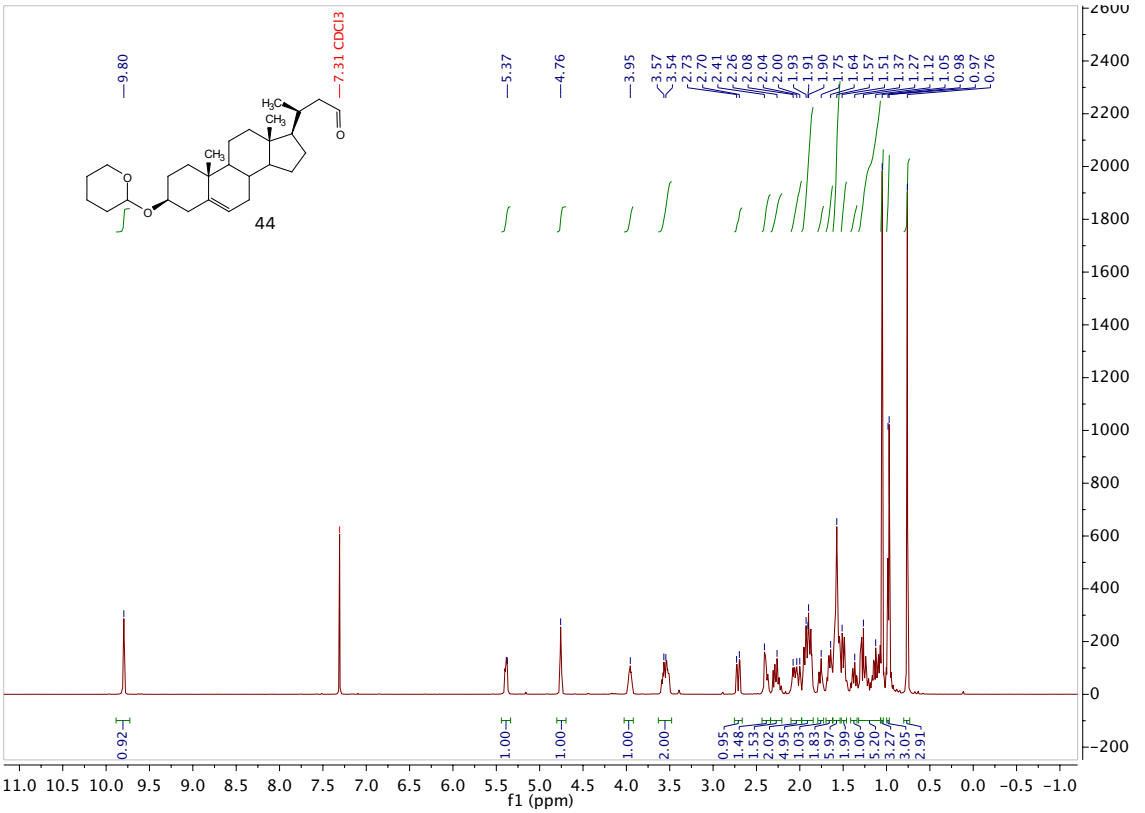
9.80
7.31 CDCl3
5.37
4.76
3.95
3.57
3.54
2.73
2.70
2.41
2.26
2.08
2.04
2.00
1.93
1.91
1.90
1.75
1.64
1.57
1.51
1.37
1.27
1.12
1.05
0.98
0.97
0.76
44
0.92
1.00
1.00
1.00
2.00
0.95
1.48
1.53
2.02
4.95
1.03
1.83
5.97
1.99
1.06
5.20
3.27
3.05
2.91
f1 (ppm)

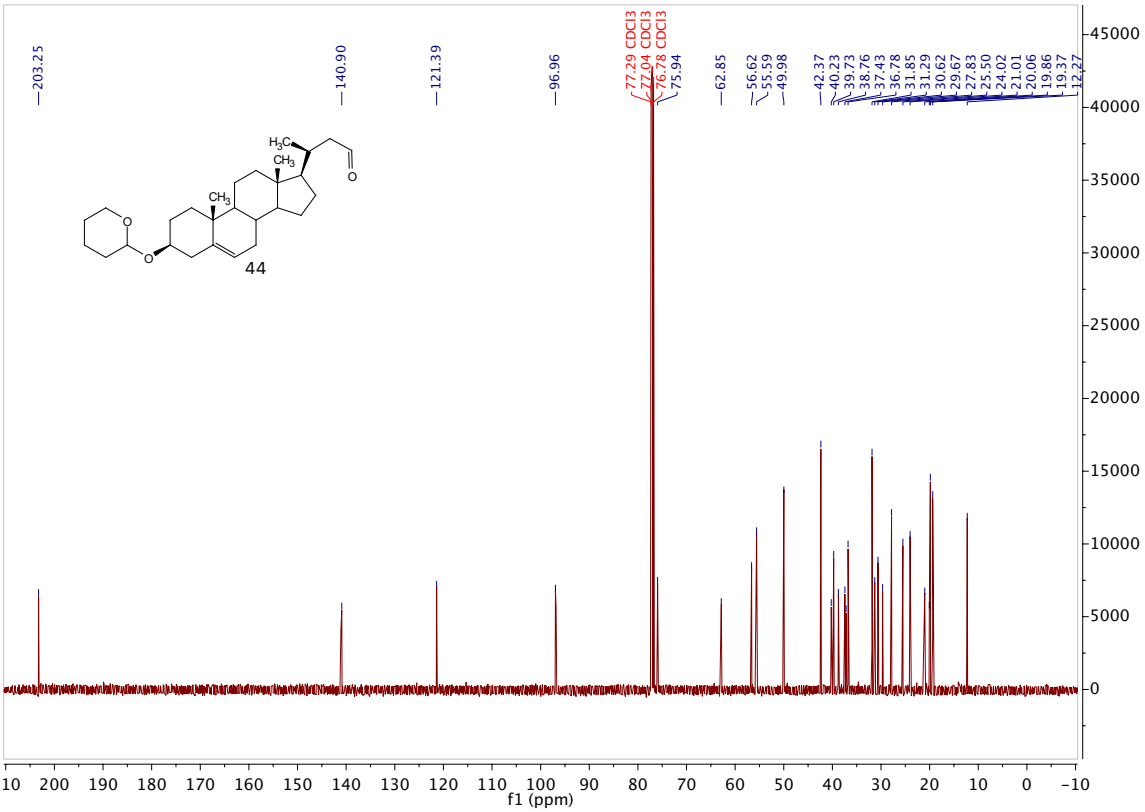
203.25
140.90
121.39
96.96
77.29 CDCl3
77.04 CDCl3
76.78 CDCl3
75.94
62.85
56.62
55.59
49.98
42.37
40.23
39.73
38.76
37.43
36.78
31.85
31.29
30.62
29.67
27.83
25.50
24.02
21.01
20.06
19.86
19.37
12.27
44
f1 (ppm)

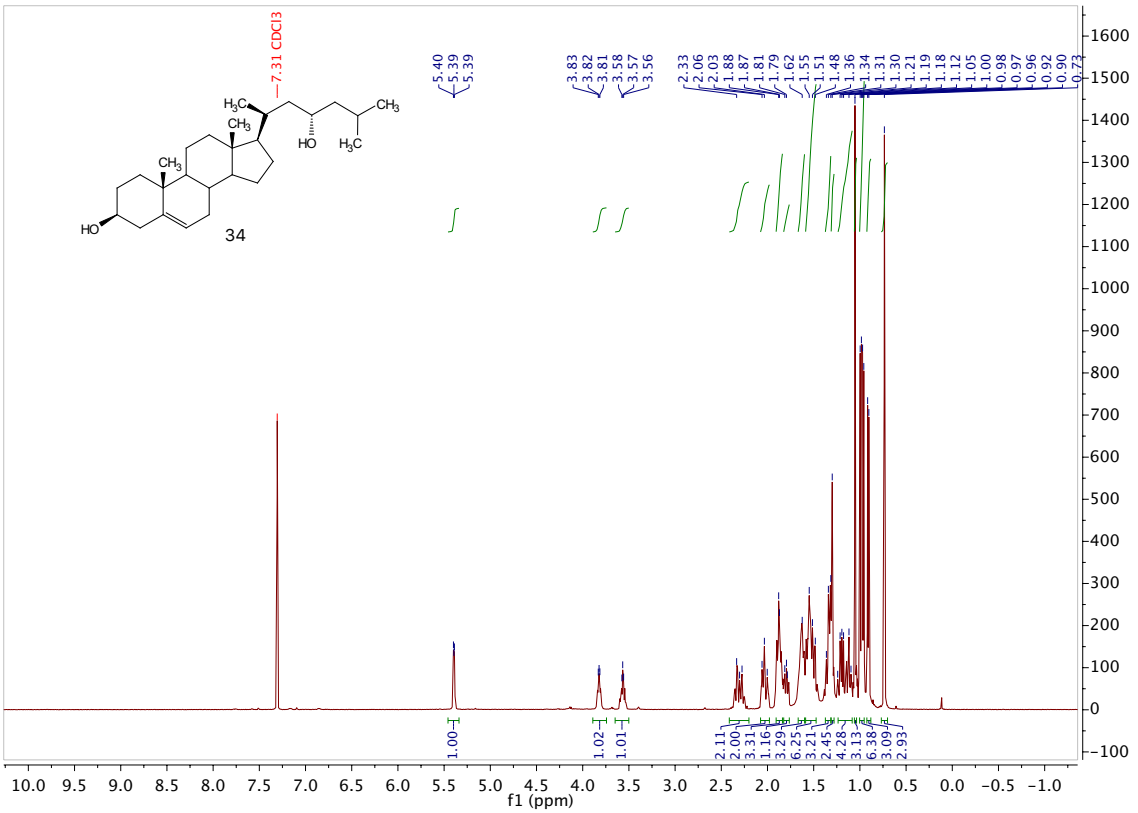
7.31 CDCl3
5.40
5.39
5.39
3.83
3.82
3.81
3.58
3.57
3.56
2.33
2.06
2.03
1.88
1.87
1.81
1.79
1.62
1.55
1.51
1.48
1.36
1.34
1.31
1.30
1.21
1.19
1.18
1.12
1.05
1.00
0.98
0.97
0.96
0.92
0.90
0.73
1.00
1.02
1.01
2.11
2.00
3.31
1.16
3.29
6.25
3.21
2.45
4.28
3.13
6.38
3.09
2.93
f1 (ppm)
34

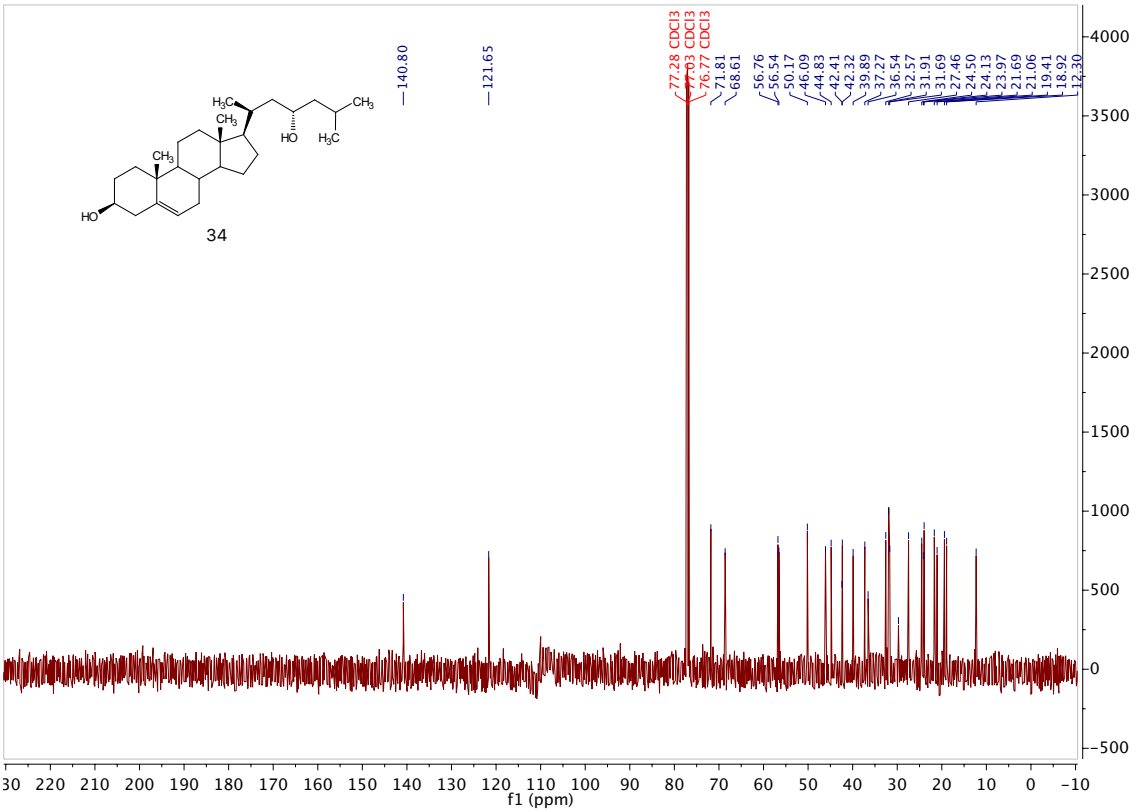
140.80
121.65
77.28 CDCl3
77.03 CDCl3
76.77 CDCl3
71.81
68.61
56.76
56.54
50.17
46.09
44.83
42.41
42.32
39.89
37.27
36.54
32.57
31.91
31.69
27.46
24.50
24.13
23.97
21.69
21.06
19.41
18.92
12.30
f1 (ppm)
34

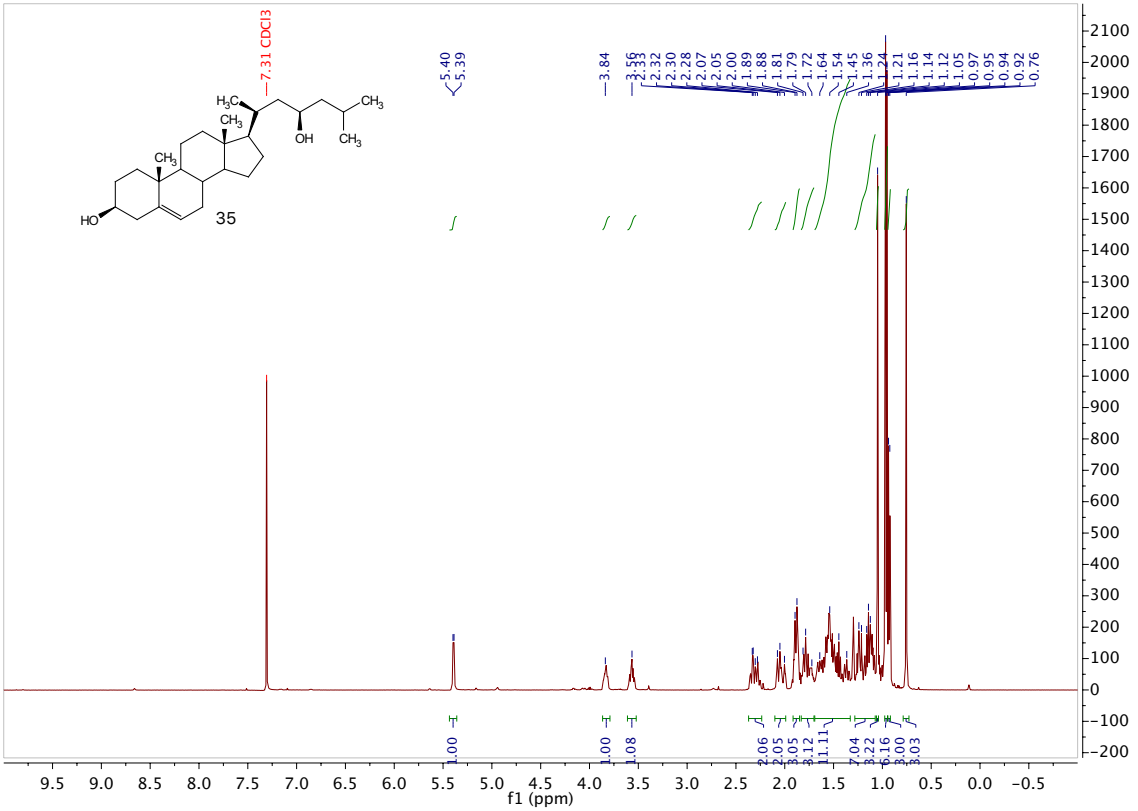
7.31 CDCl3
5.40
5.39
3.84
3.56
2.33
2.32
2.30
2.28
2.07
2.05
2.00
1.89
1.88
1.81
1.79
1.72
1.64
1.54
1.45
1.36
1.24
1.21
1.16
1.14
1.12
1.05
0.97
0.95
0.94
0.92
0.76
1.00
1.00
1.08
2.06
2.05
3.05
3.12
11.11
7.04
3.22
6.16
3.00
3.03
35
f1 (ppm)

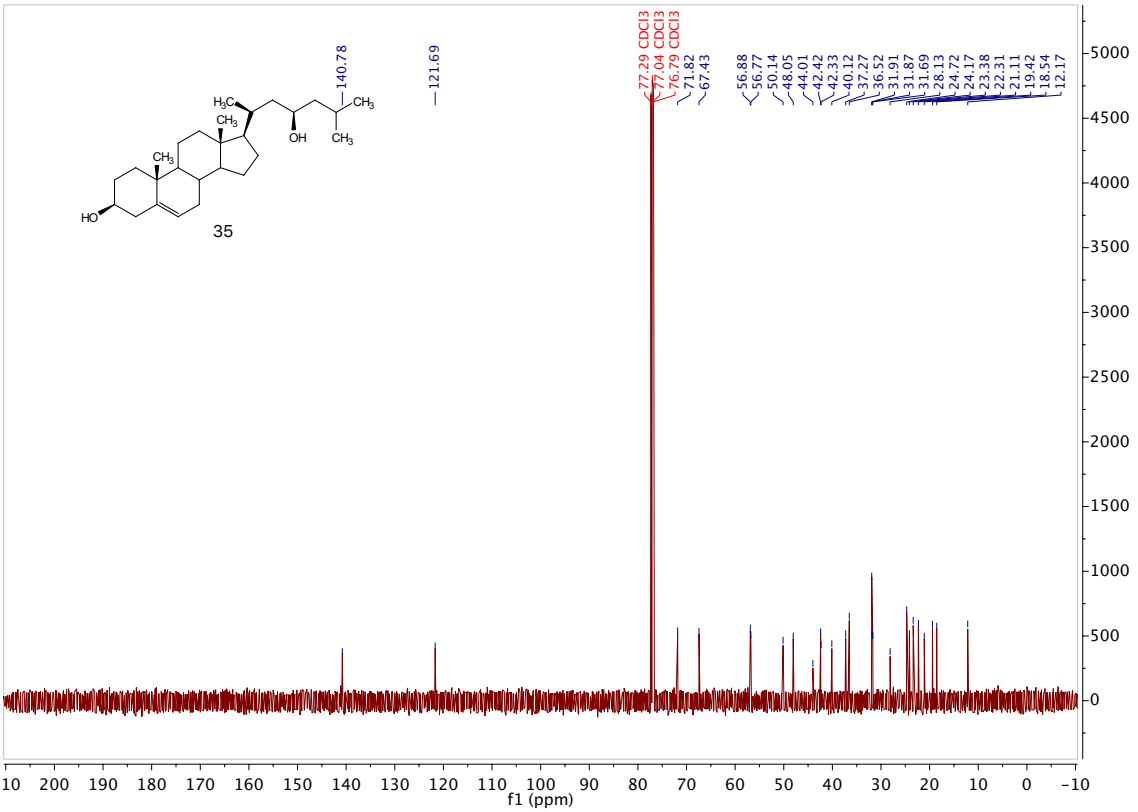
140.78
121.69
77.29 CDCl3
77.04 CDCl3
76.79 CDCl3
71.82
67.43
56.88
56.77
50.14
48.05
44.01
42.42
42.33
40.12
37.27
36.52
31.91
31.87
31.69
28.13
24.72
24.17
23.38
22.31
21.11
19.42
18.54
12.17
35
f1 (ppm)

II. Vitamin D Analogues

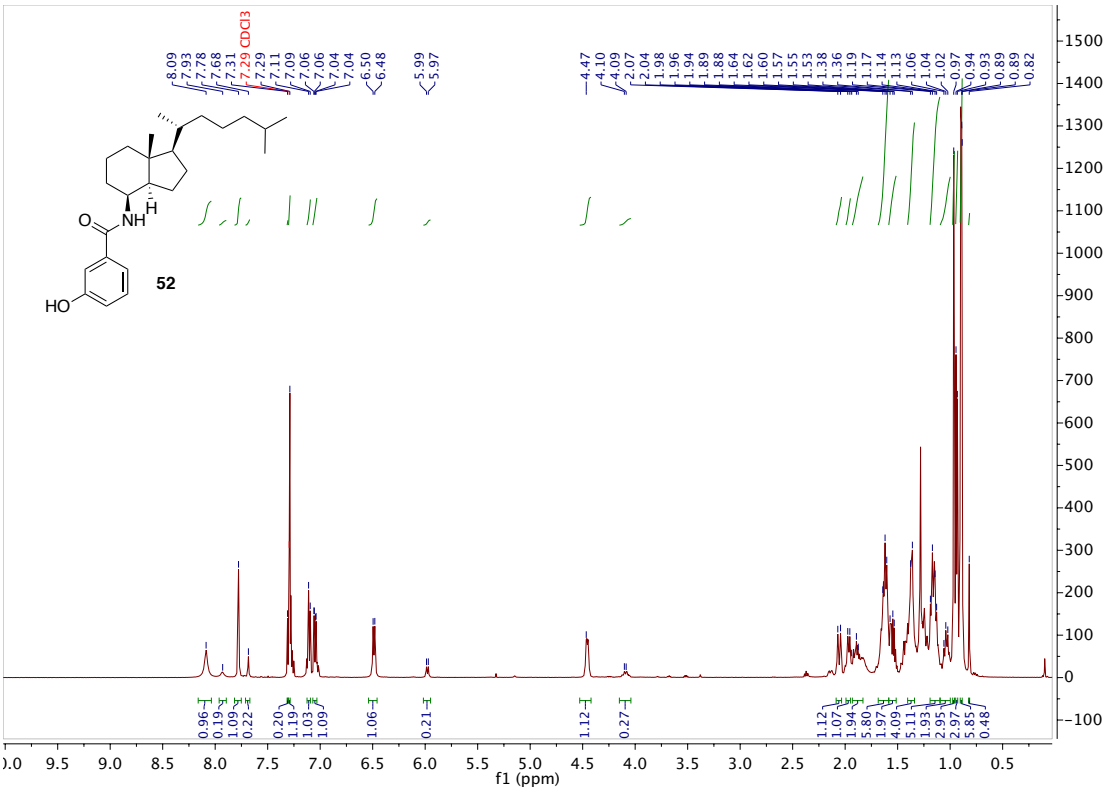

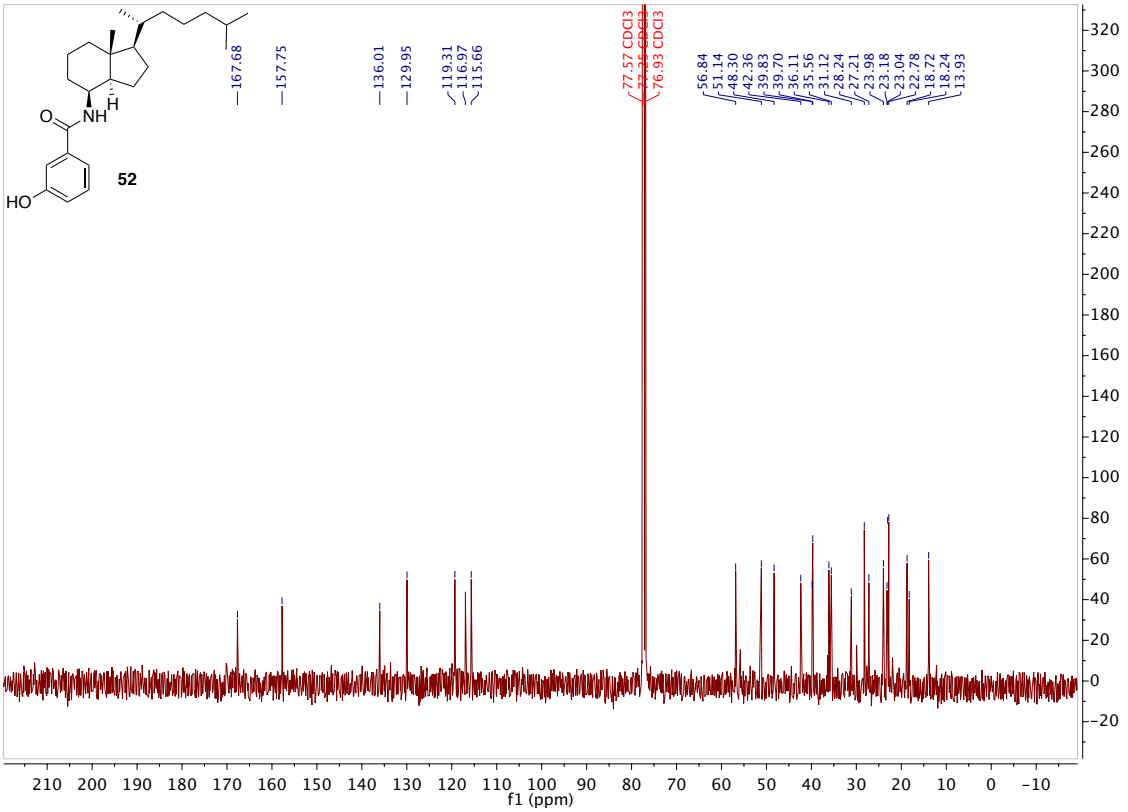

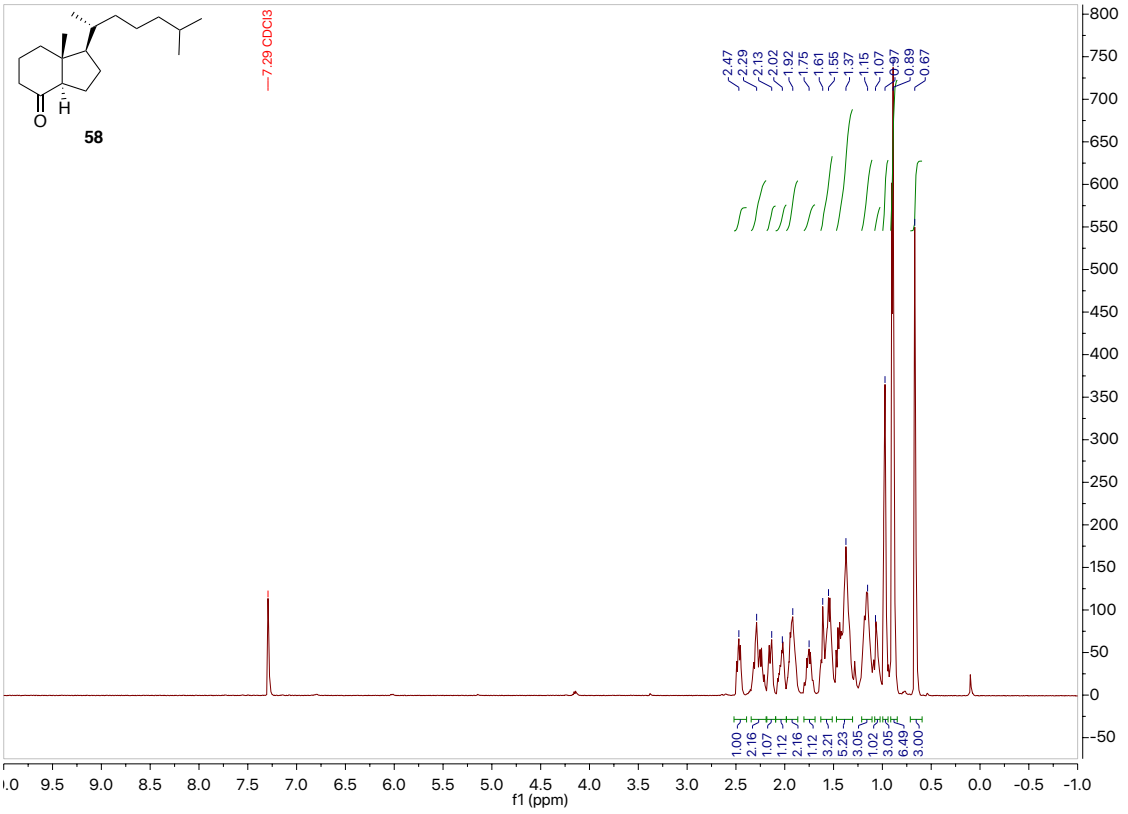
58
7.29 CDCl3
2.47
2.29
2.13
2.02
1.92
1.75
1.61
1.55
1.37
1.15
1.07
0.97
0.89
0.67
1.00
2.16
1.07
1.12
2.16
1.12
3.21
5.23
3.05
1.02
3.05
6.49
3.00
f1 (ppm)

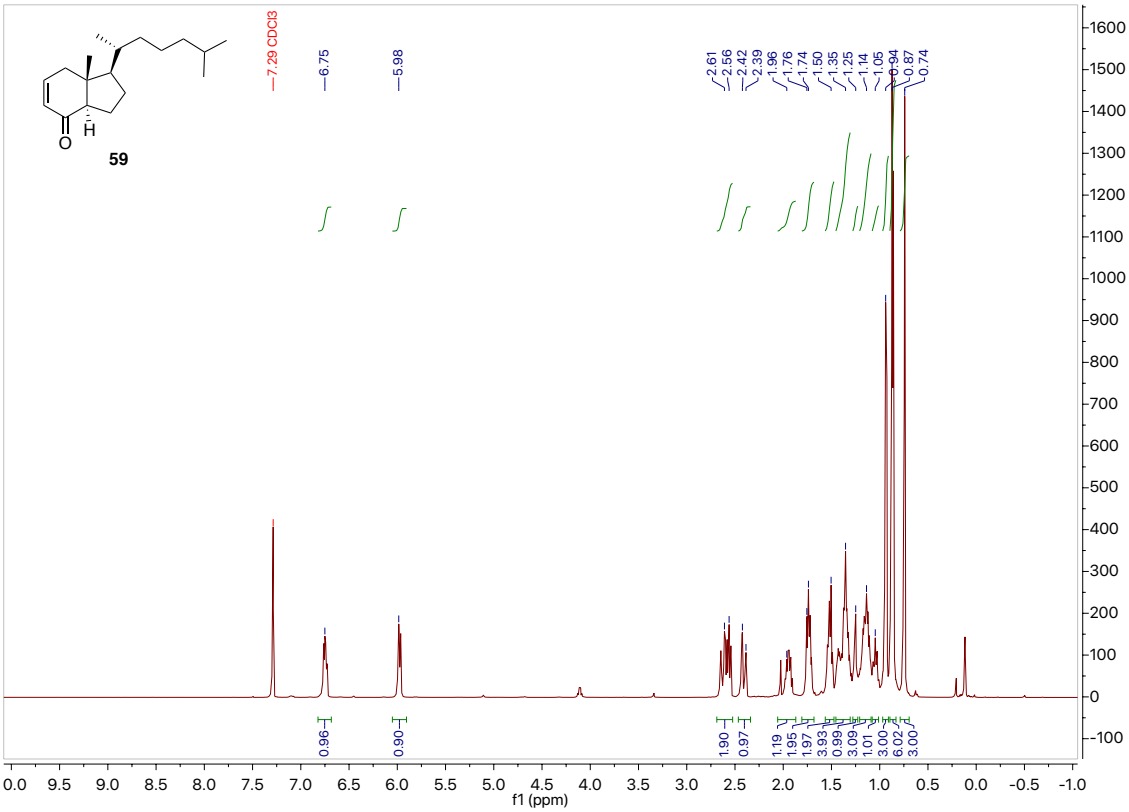
59
7.29 CDCl3
6.75
5.98
2.61
2.56
2.42
2.39
1.96
1.76
1.74
1.50
1.35
1.25
1.14
1.05
0.94
0.87
0.74
0.96
0.90
1.90
0.97
1.19
1.95
1.97
3.93
0.99
3.09
1.01
3.00
6.02
3.00
f1 (ppm)

a. C-11 Modified Analogues

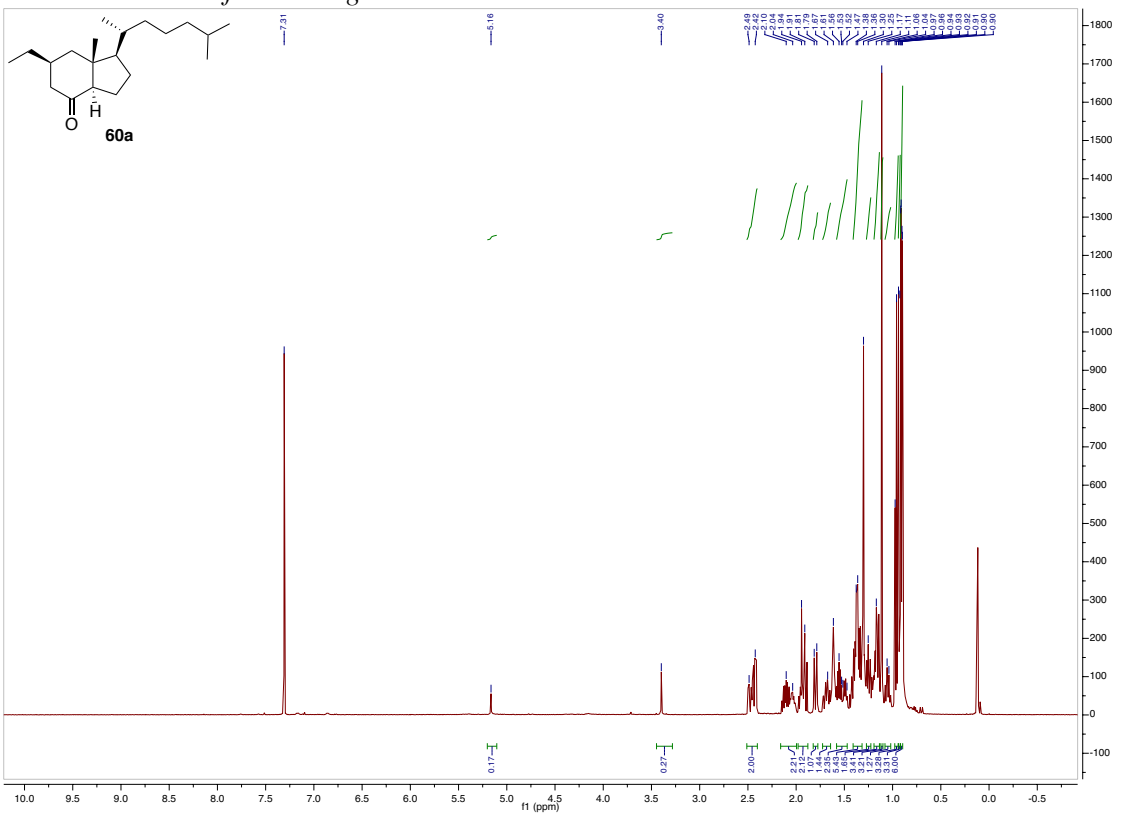

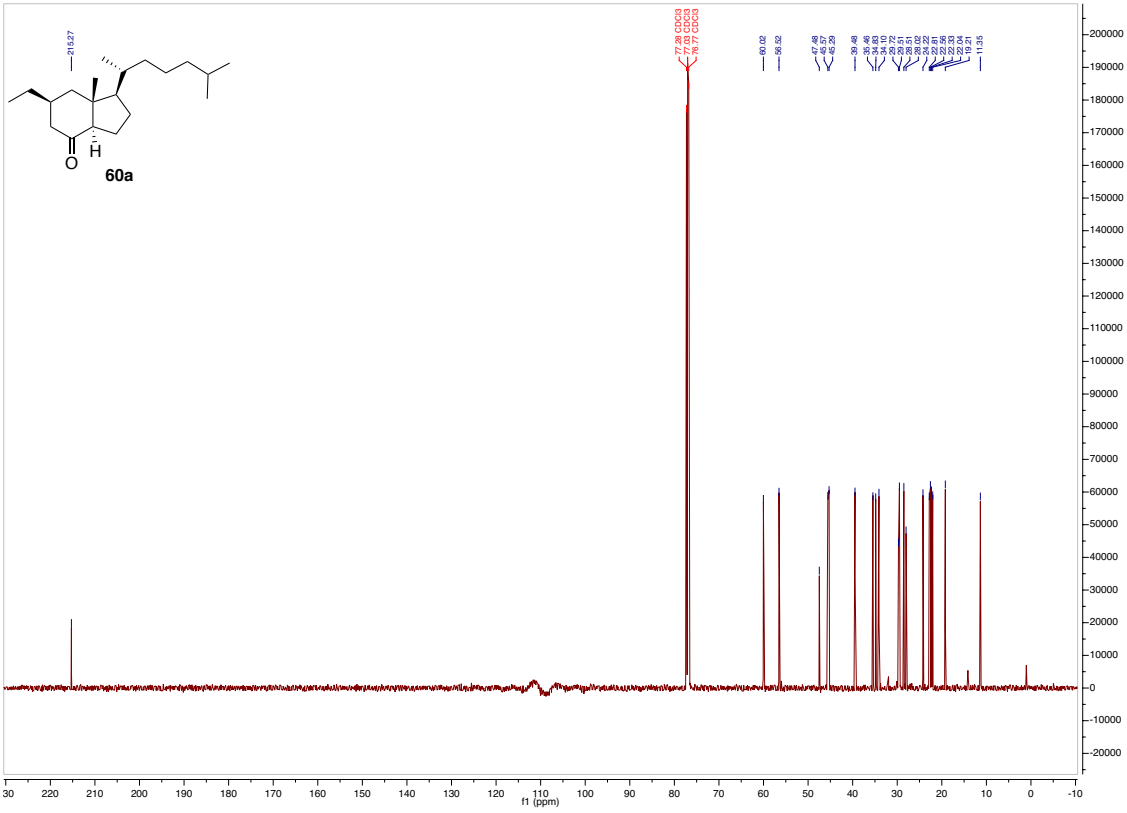

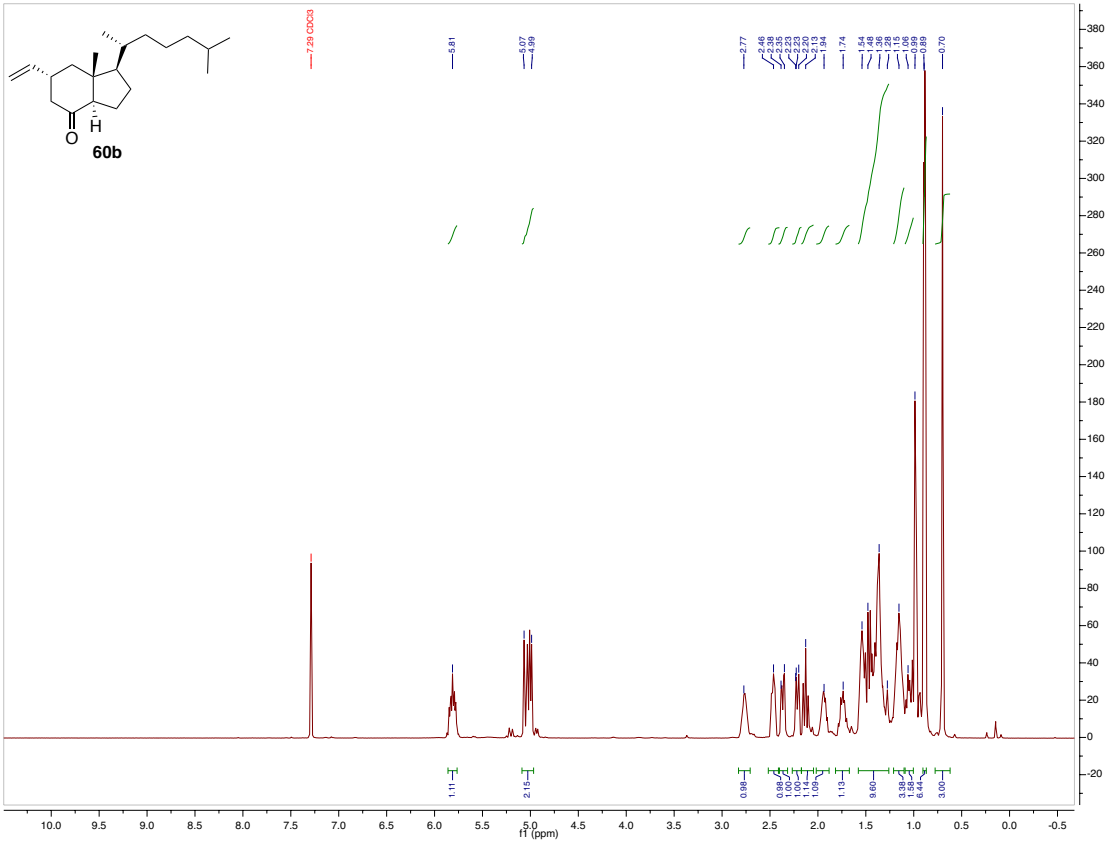
60b
7.29 CDCl3
5.81
5.07
4.99
2.77
2.46
2.38
2.35
2.33
2.23
2.20
2.13
1.94
1.74
1.54
1.48
1.36
1.28
1.15
1.06
0.89
0.70
1.11
2.15
0.98
0.98
2.00
1.00
1.14
1.08
1.13
9.60
1.98
1.58
6.44
3.00
f1 (ppm)

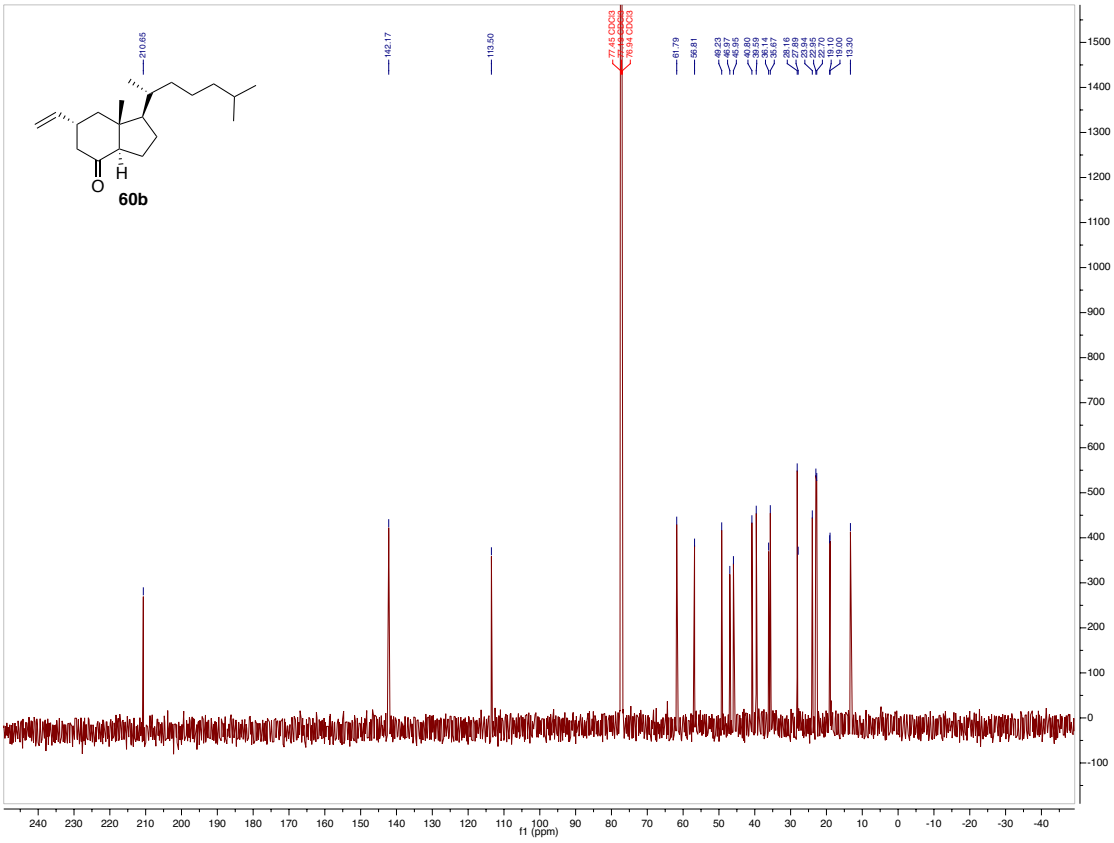
60b
210.65
142.17
113.50
77.48 CDCl3
77.16 CDCl3
76.84 CDCl3
61.79
56.81
46.23
46.97
45.95
45.59
39.50
36.14
35.67
28.16
27.89
23.94
22.80
22.70
19.10
19.00
13.30
f1 (ppm)

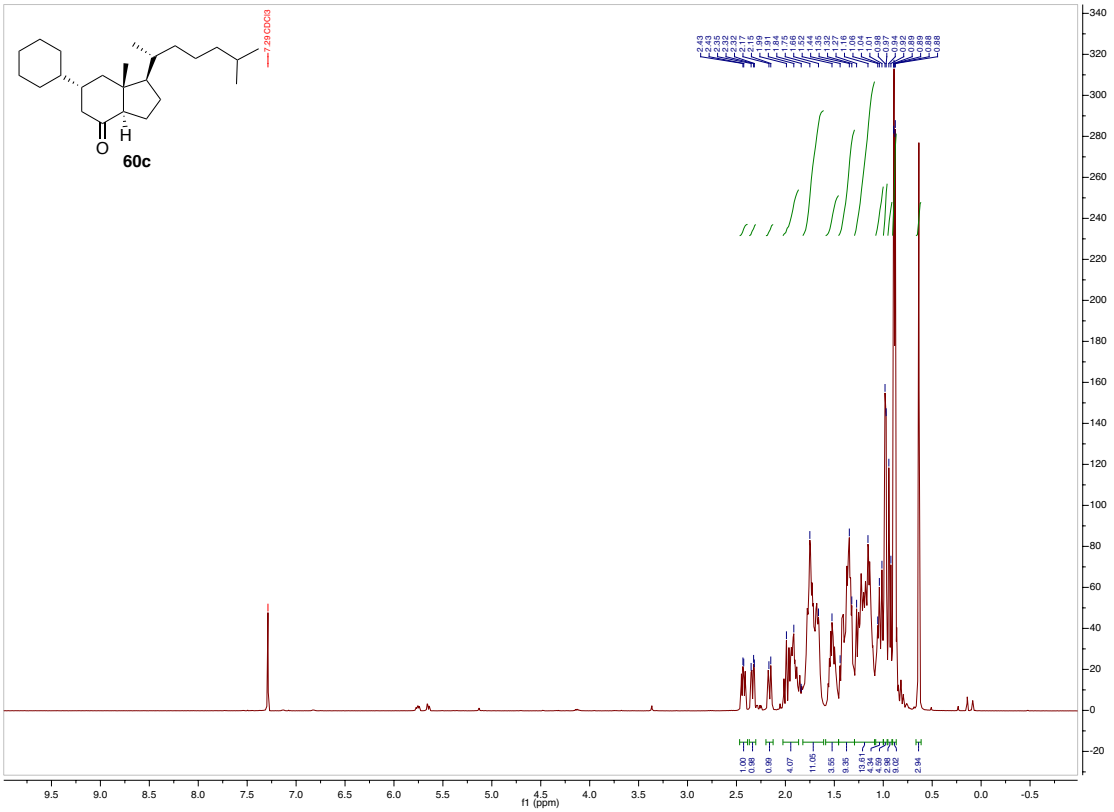
60c
f1 (ppm)

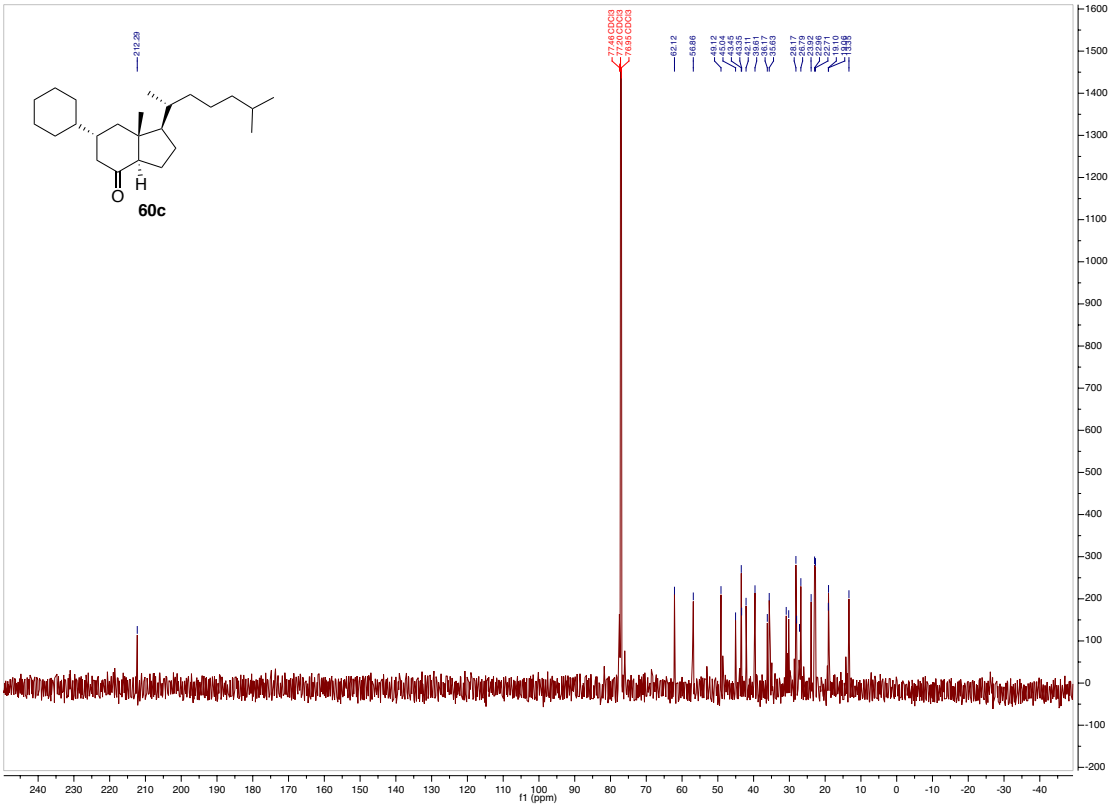
60c
f1 (ppm)

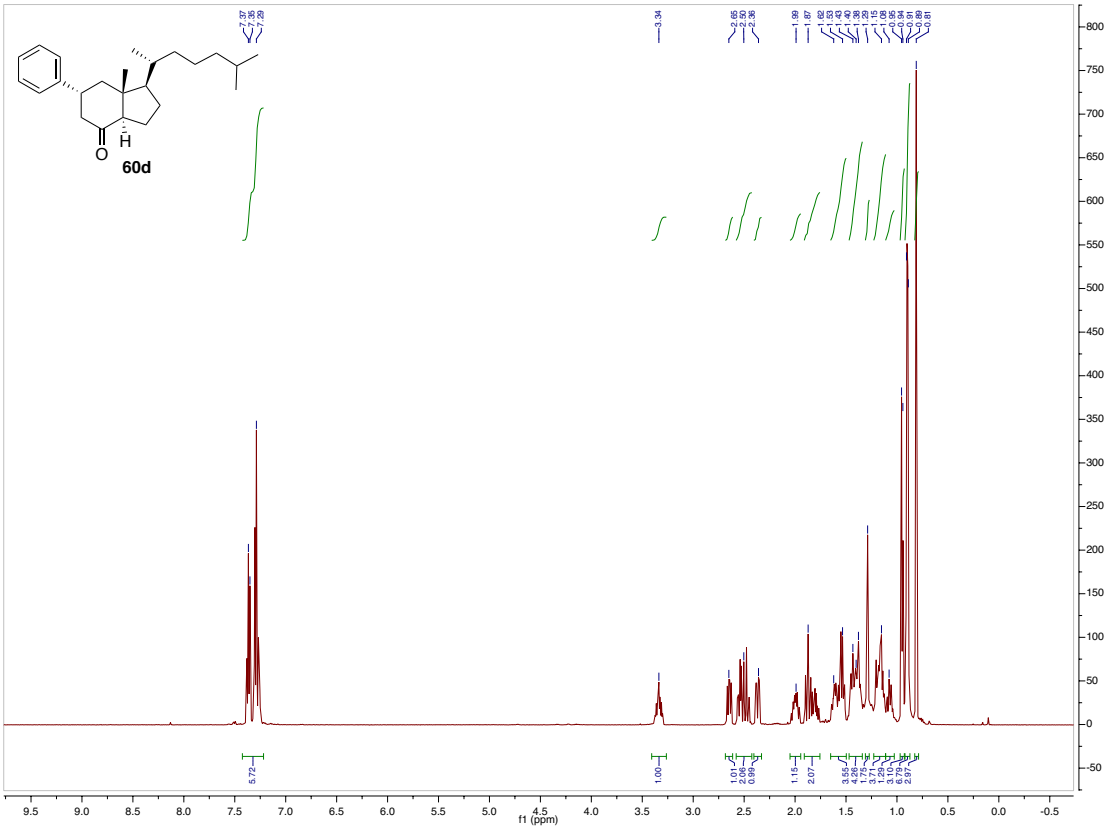
60d
f1 (ppm)

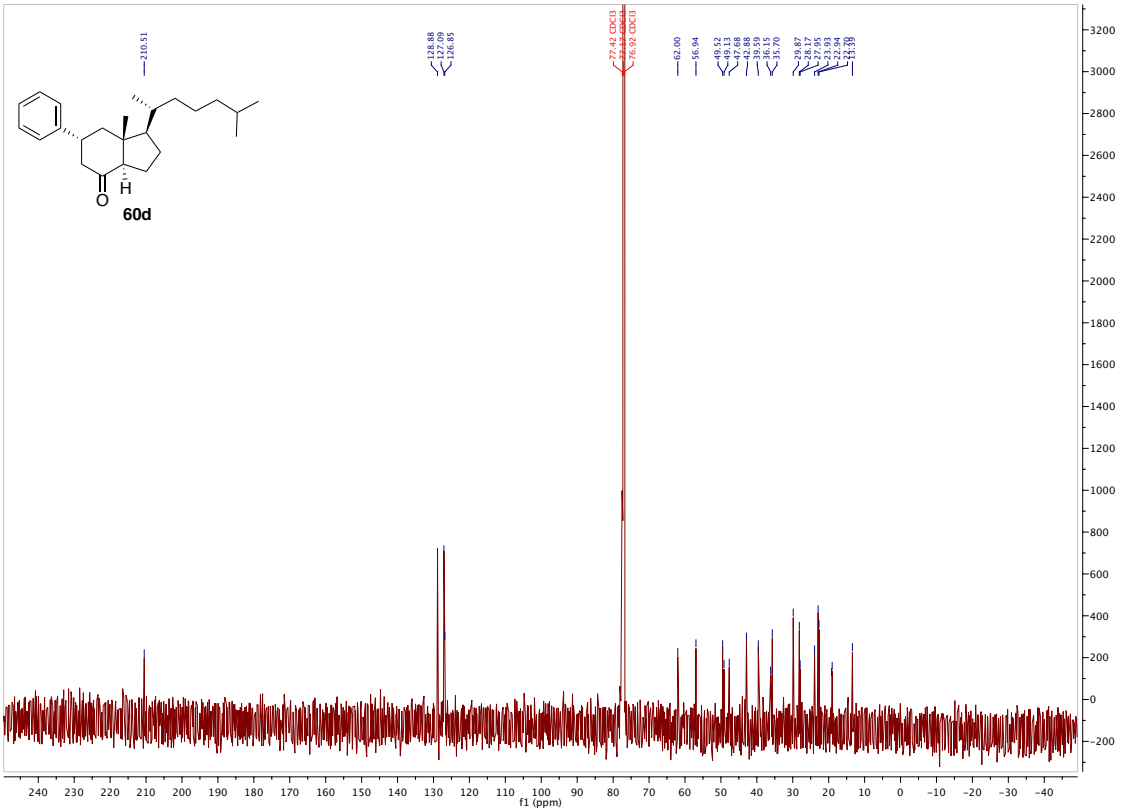
60d
f1 (ppm)

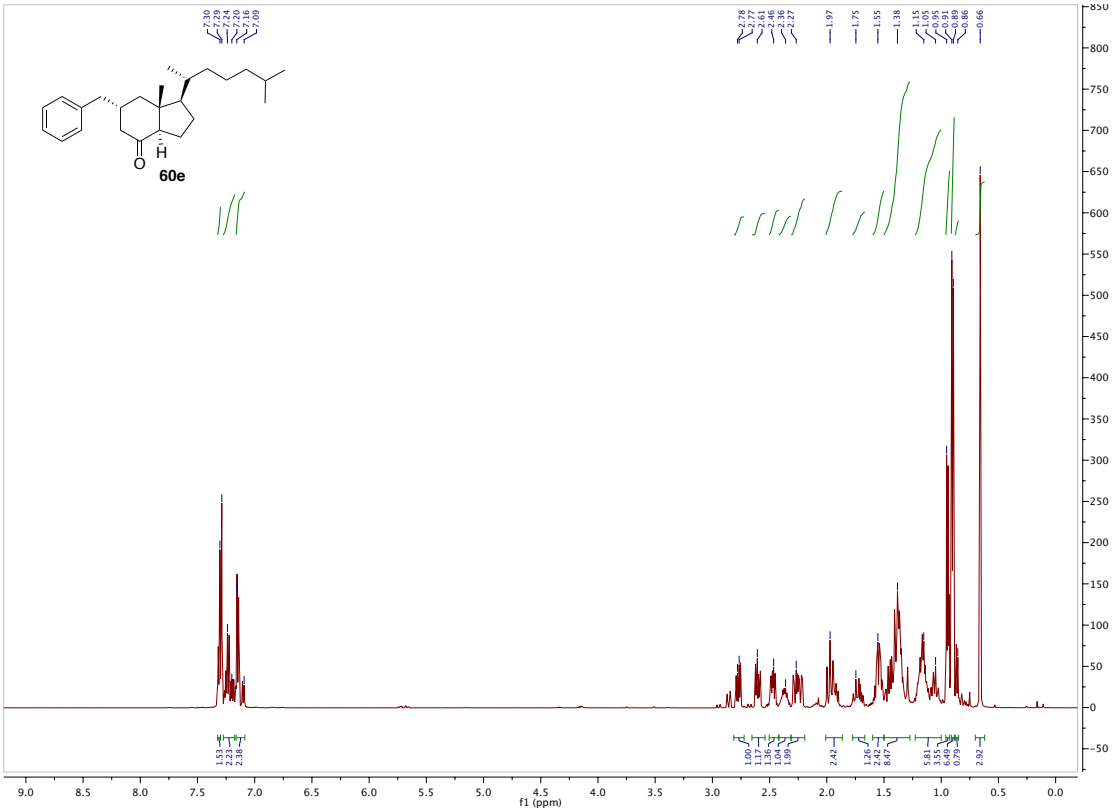
60e
f1 (ppm)

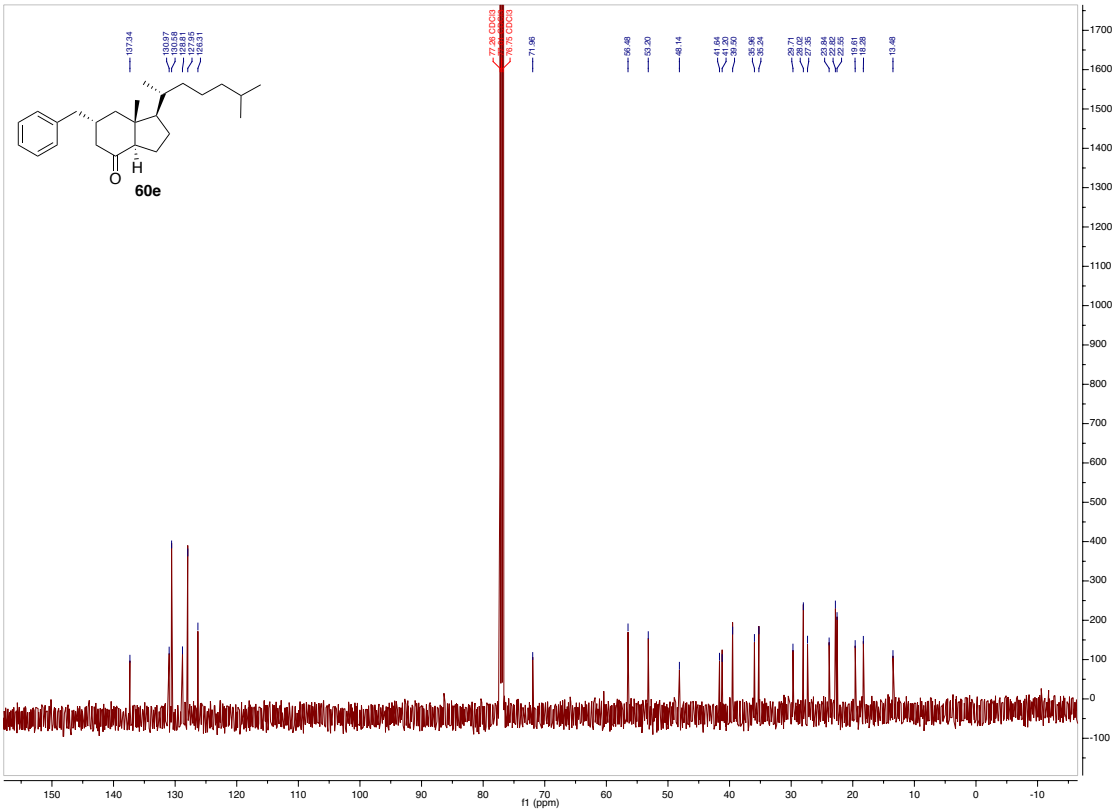
60e
f1 (ppm)

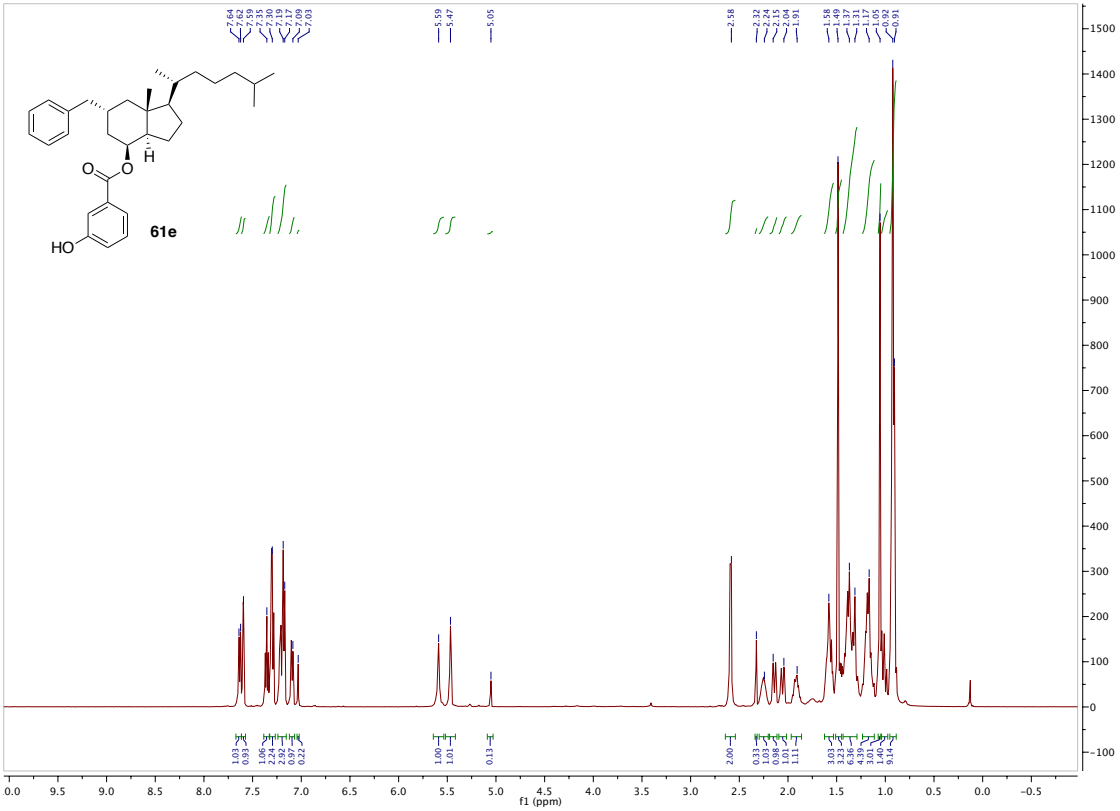
61e
HO
O
O
H
f1 (ppm)

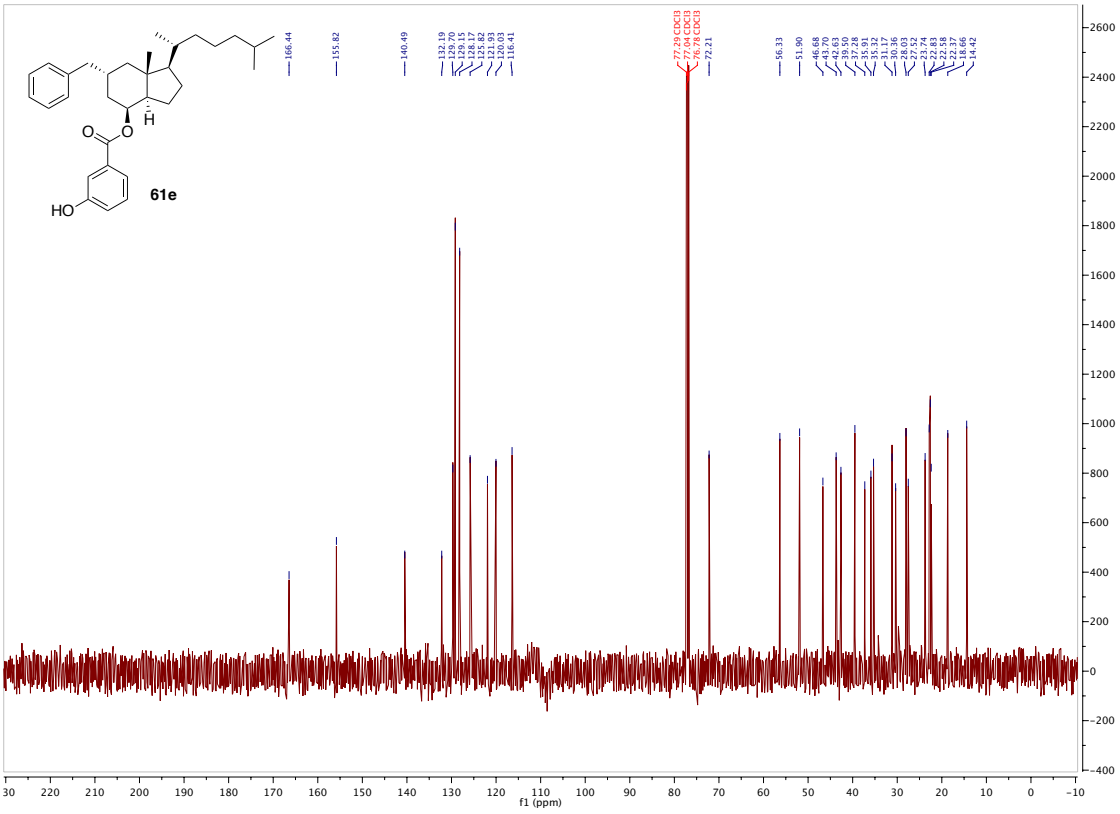
61e
HO
O
O
H
f1 (ppm)

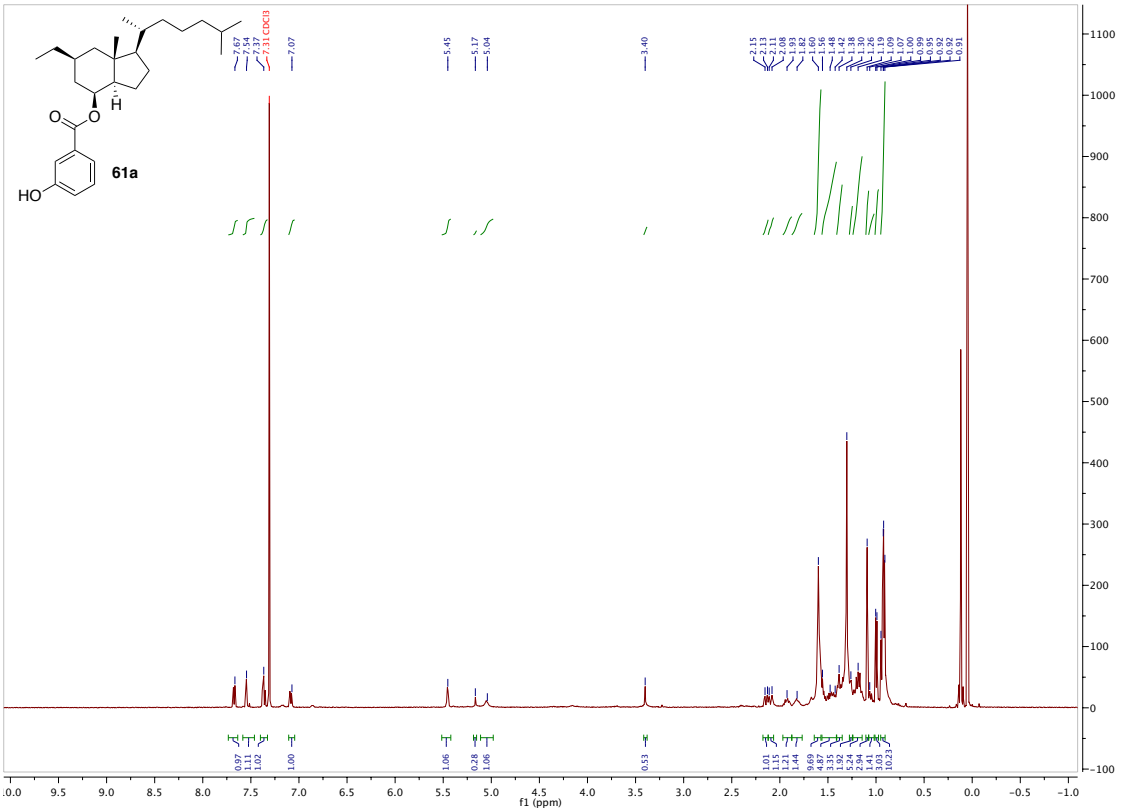
61a
HO
O
O
H
7.67
7.54
7.31 CDCl3
7.07
5.45
5.17
5.04
3.40
2.15
2.13
2.11
2.08
1.93
1.83
1.60
1.56
1.48
1.42
1.38
1.30
1.26
1.19
1.09
1.07
1.00
0.99
0.95
0.93
0.92
0.91
0.97
1.11
1.02
1.00
1.06
0.28
1.06
0.53
1.01
1.15
1.21
1.44
9.69
4.87
3.52
5.24
2.34
1.41
3.03
10.23
f1 (ppm)

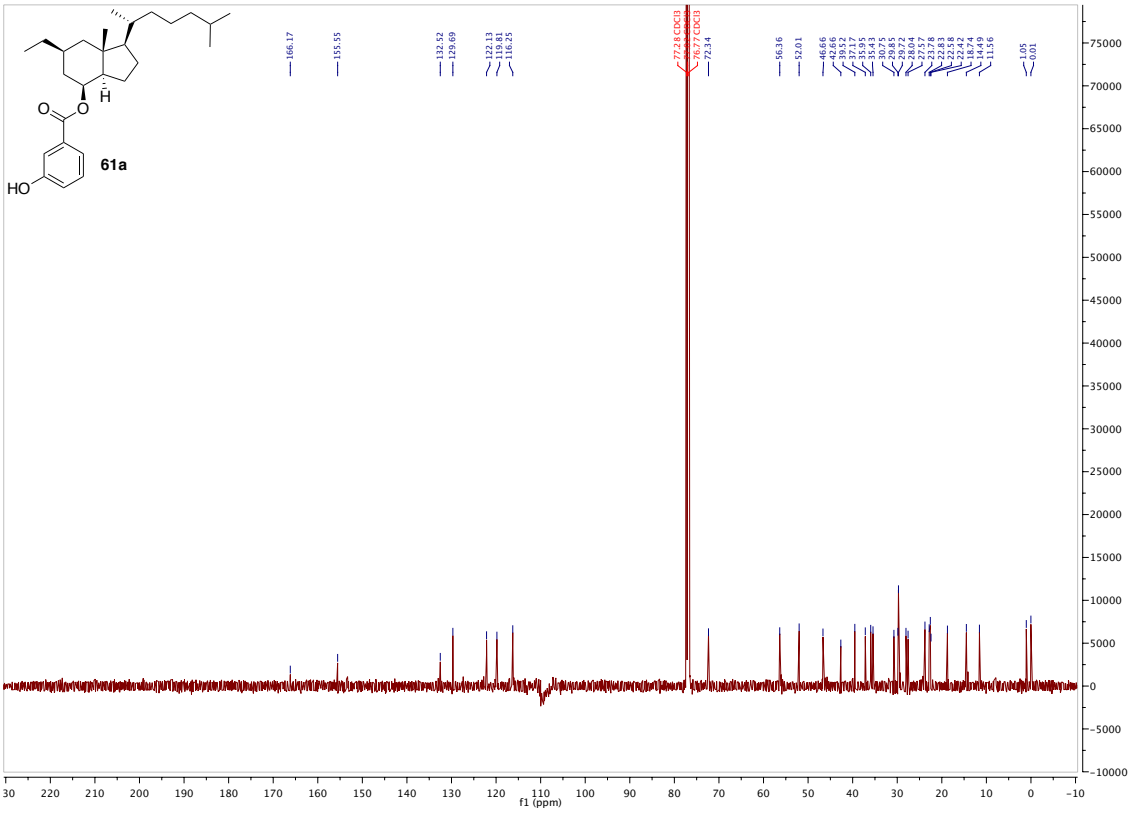
61a
HO
O
O
H
166.17
155.55
132.52
129.69
122.13
119.81
116.25
77.28 CDCl3
77.02 CDCl3
76.77 CDCl3
72.34
56.36
52.01
46.66
42.66
39.72
37.17
35.95
35.43
30.75
29.85
28.72
28.04
27.57
23.78
23.33
22.58
22.42
18.74
14.49
11.56
1.05
0.01
f1 (ppm)

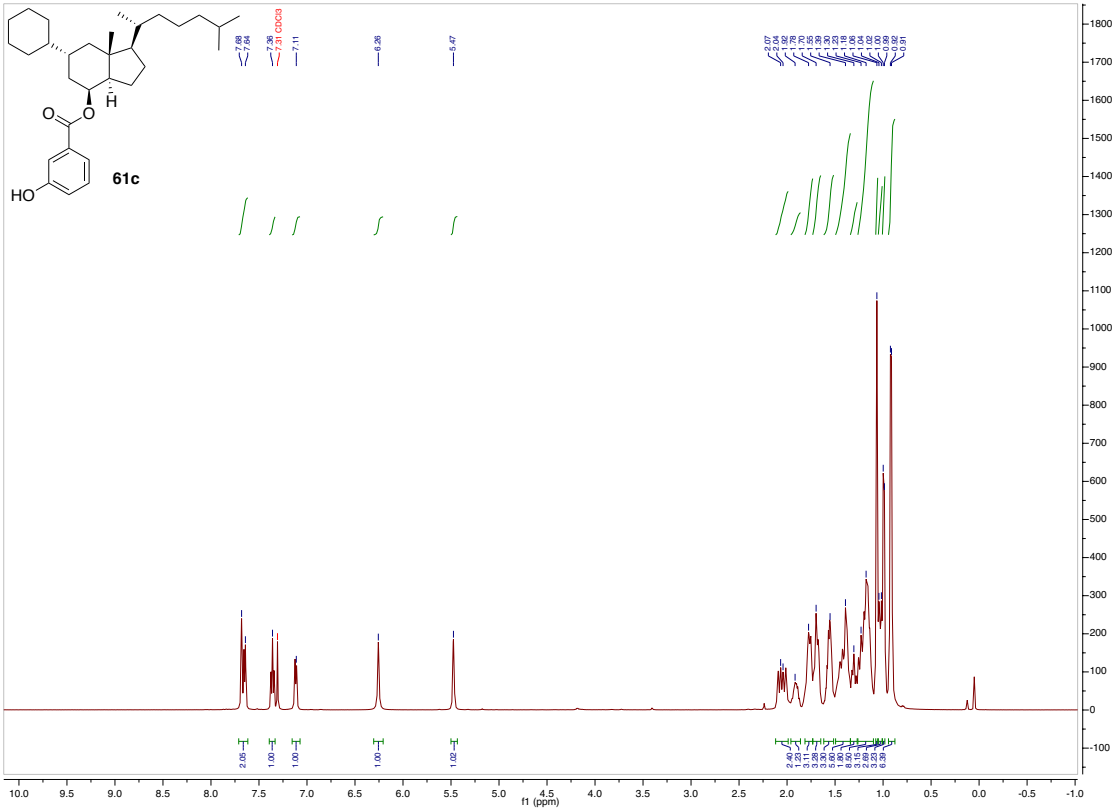
61c
HO
O
O
H
f1 (ppm)

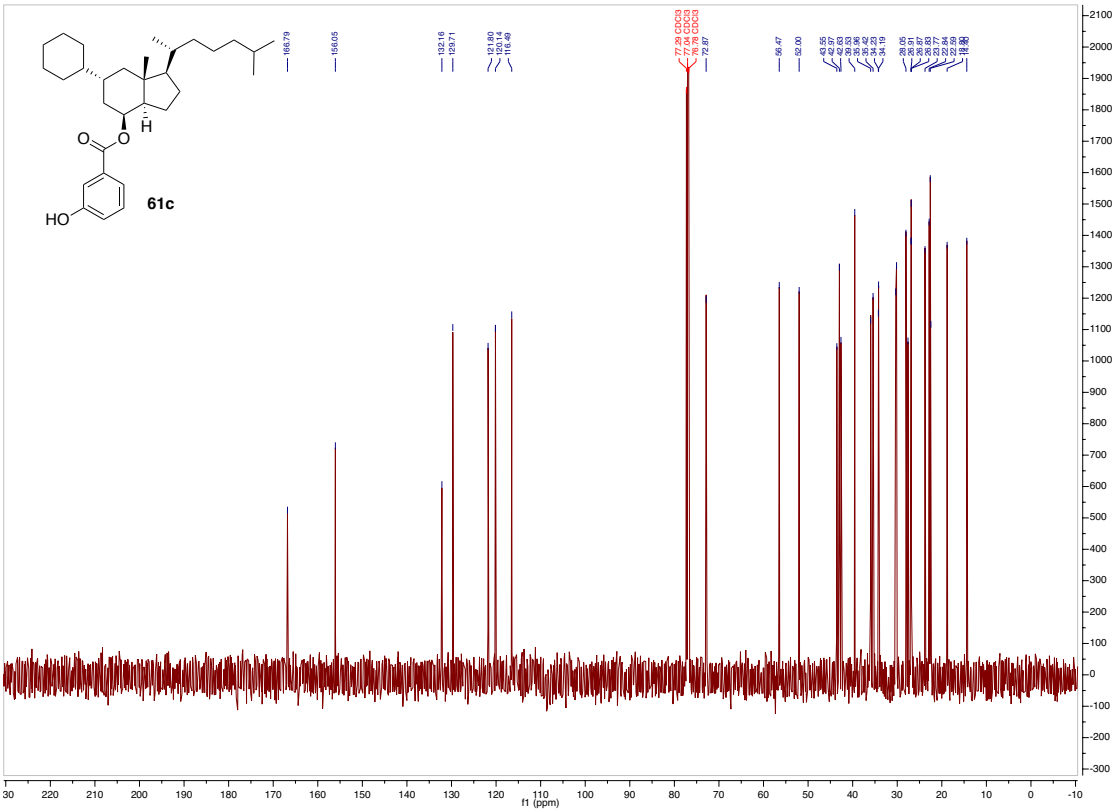
61c
HO
O
O
H
f1 (ppm)

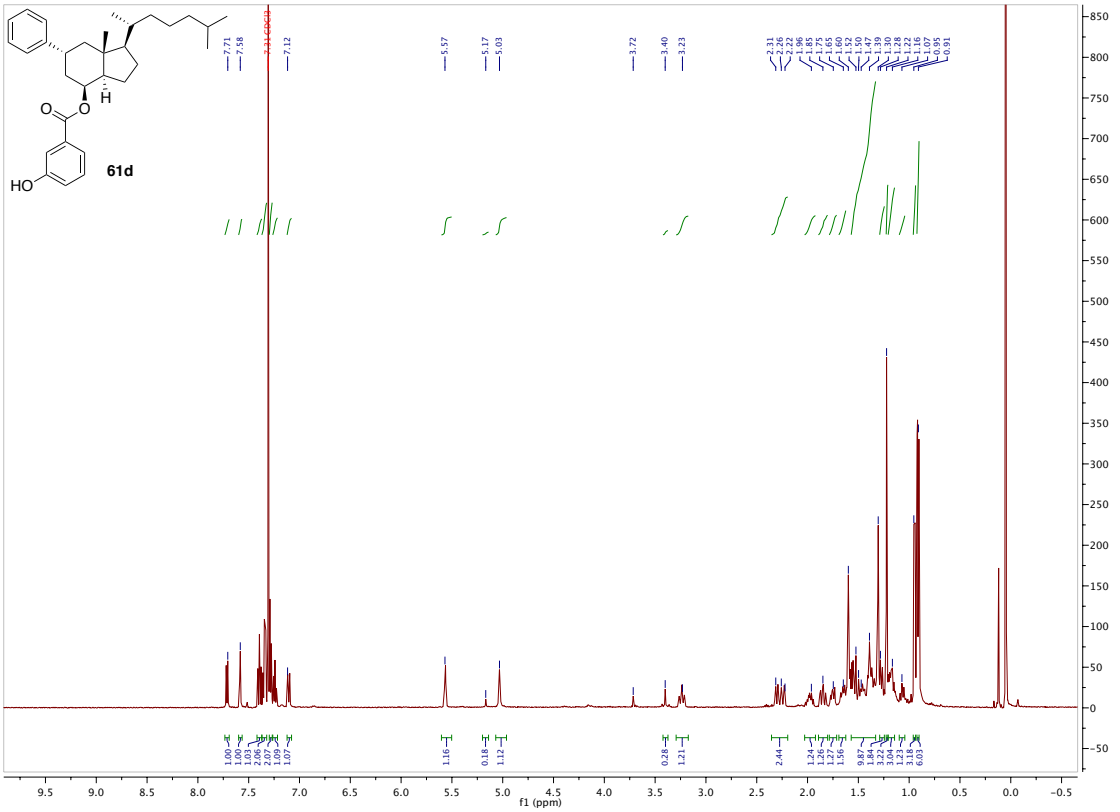
61d
HO
O
O
H
f1 (ppm)

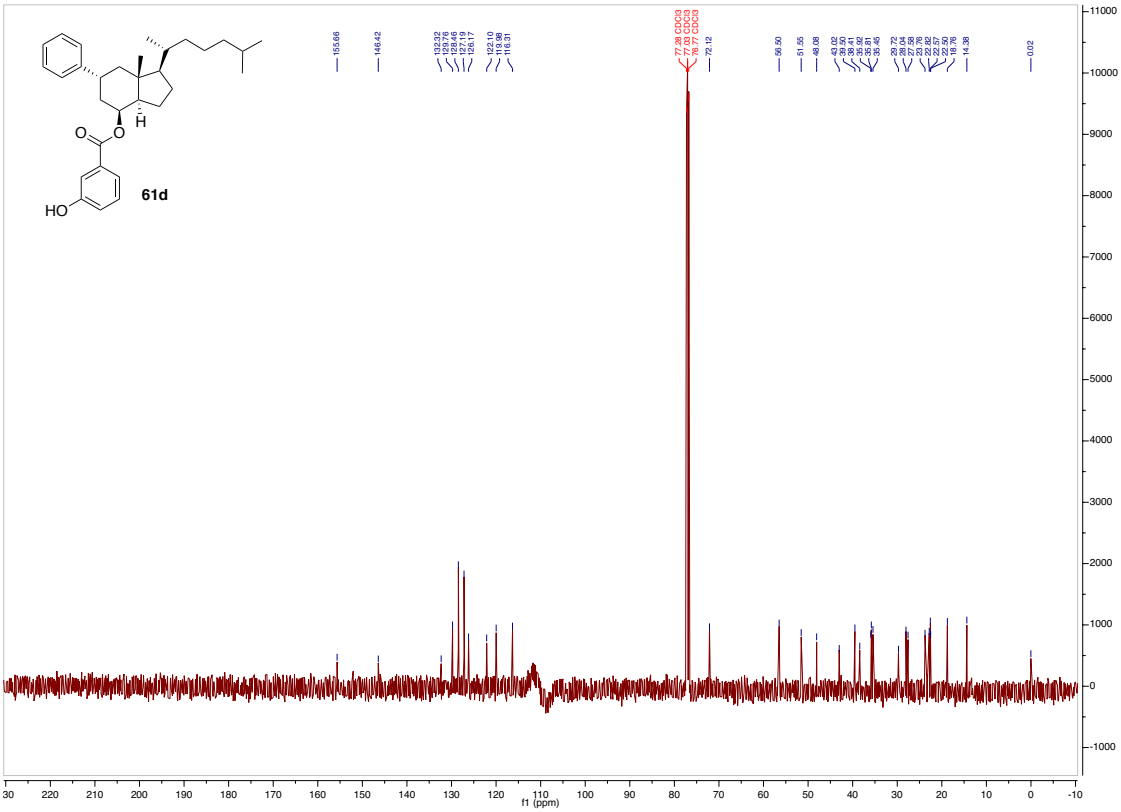
61d
HO
O
O
H
f1 (ppm)

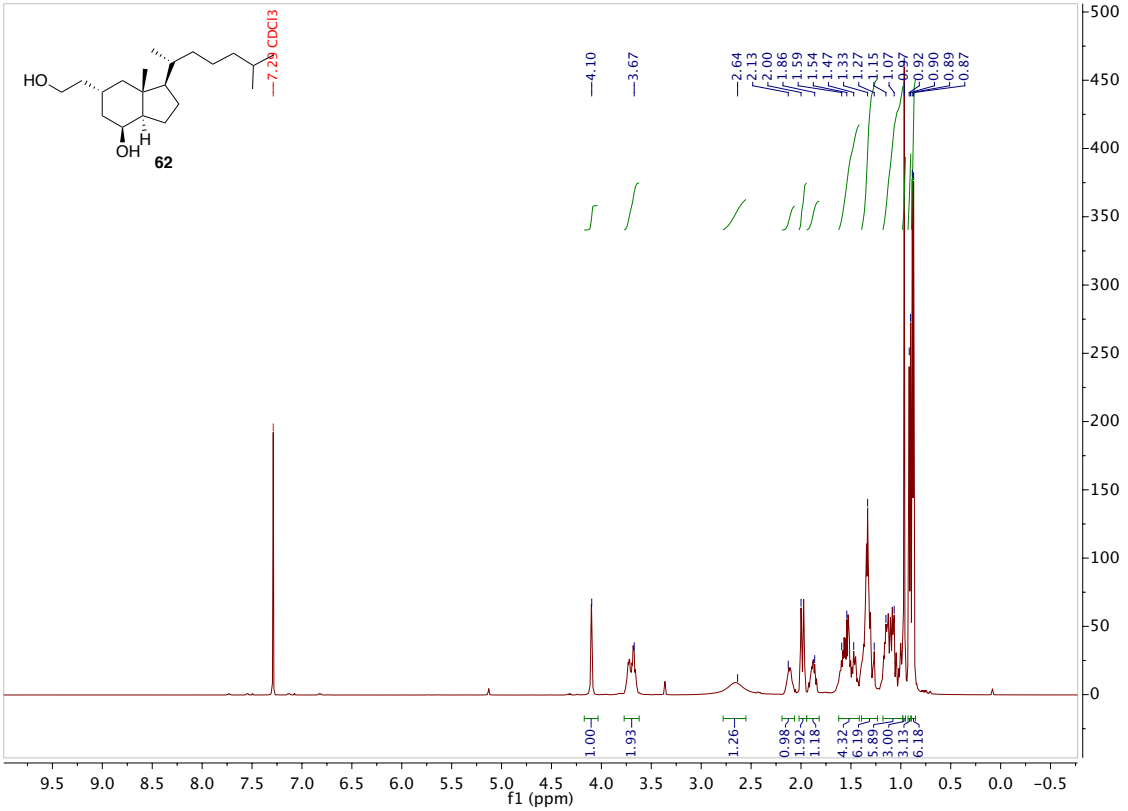
HO
OH
H
62
7.29 CDCl3
4.10
3.67
2.64
2.13
2.00
1.86
1.59
1.54
1.47
1.33
1.27
1.15
1.07
0.97
0.92
0.90
0.89
0.87
1.00
1.93
1.26
0.98
1.92
1.18
4.32
6.19
5.89
3.00
3.13
6.18
f1 (ppm)

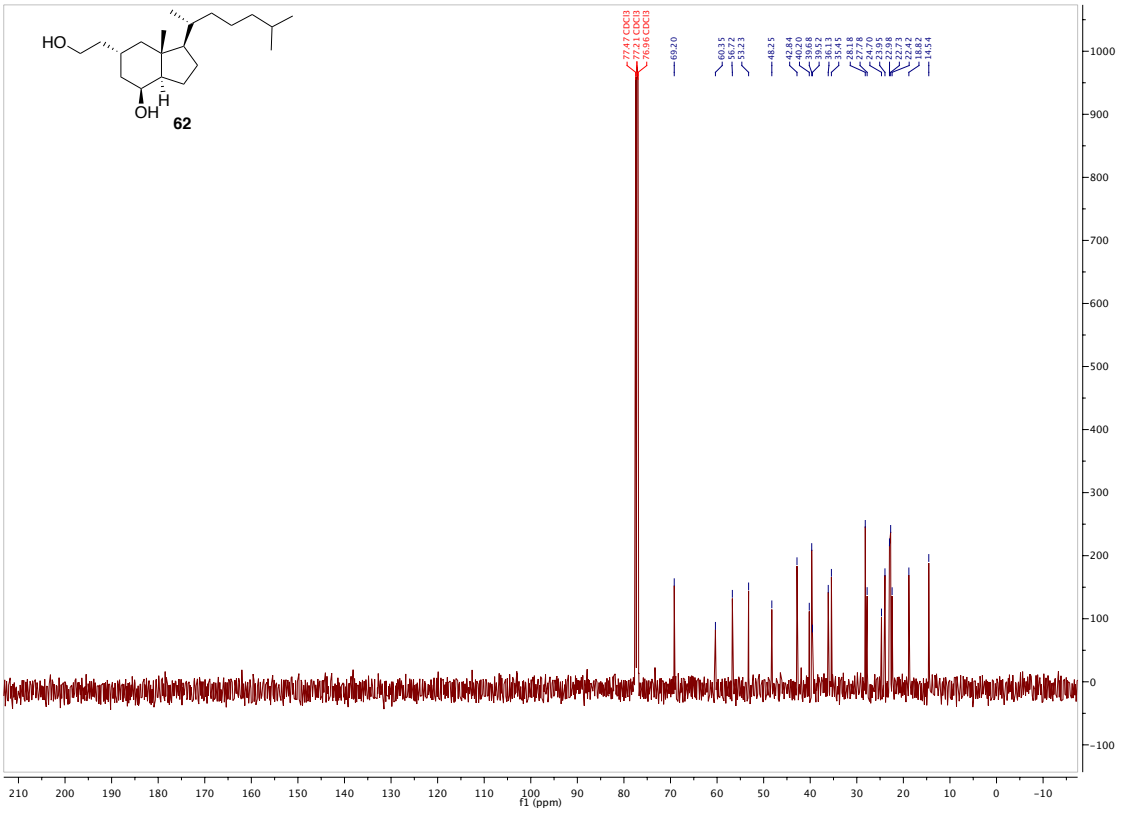
HO
OH
H
62
77.47 CDCl3
77.21 CDCl3
76.94 CDCl3
69.20
60.35
56.72
53.23
48.25
42.84
40.20
39.68
39.52
36.13
35.45
28.18
27.76
24.70
23.95
22.98
22.73
22.42
18.82
14.14
f1 (ppm)

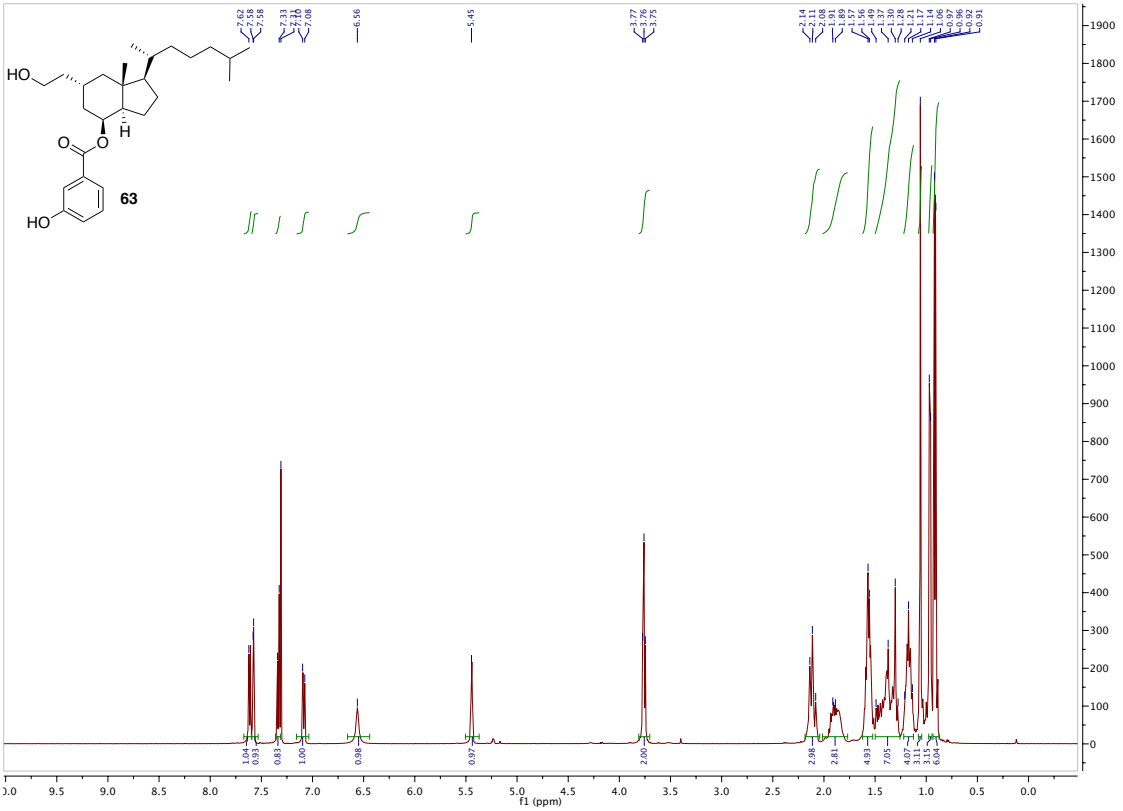
HO
O
O
H
HO
63
f1 (ppm)

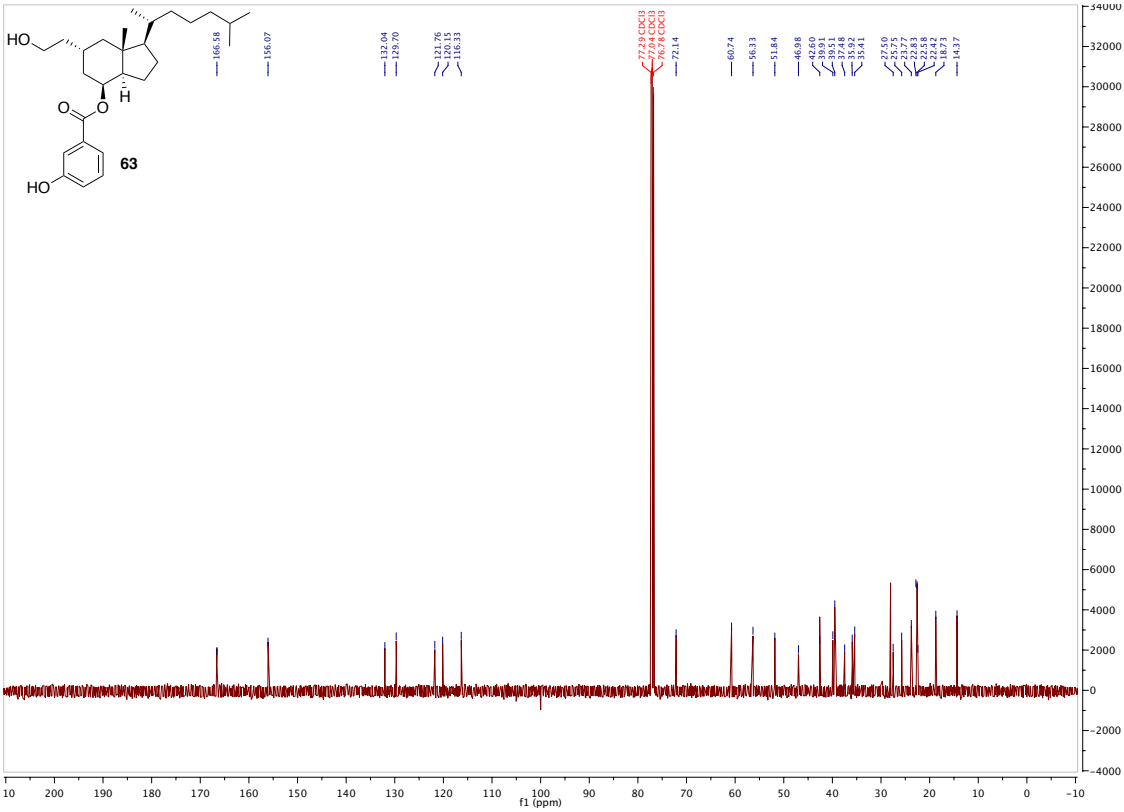
HO
O
O
H
HO
63
f1 (ppm)

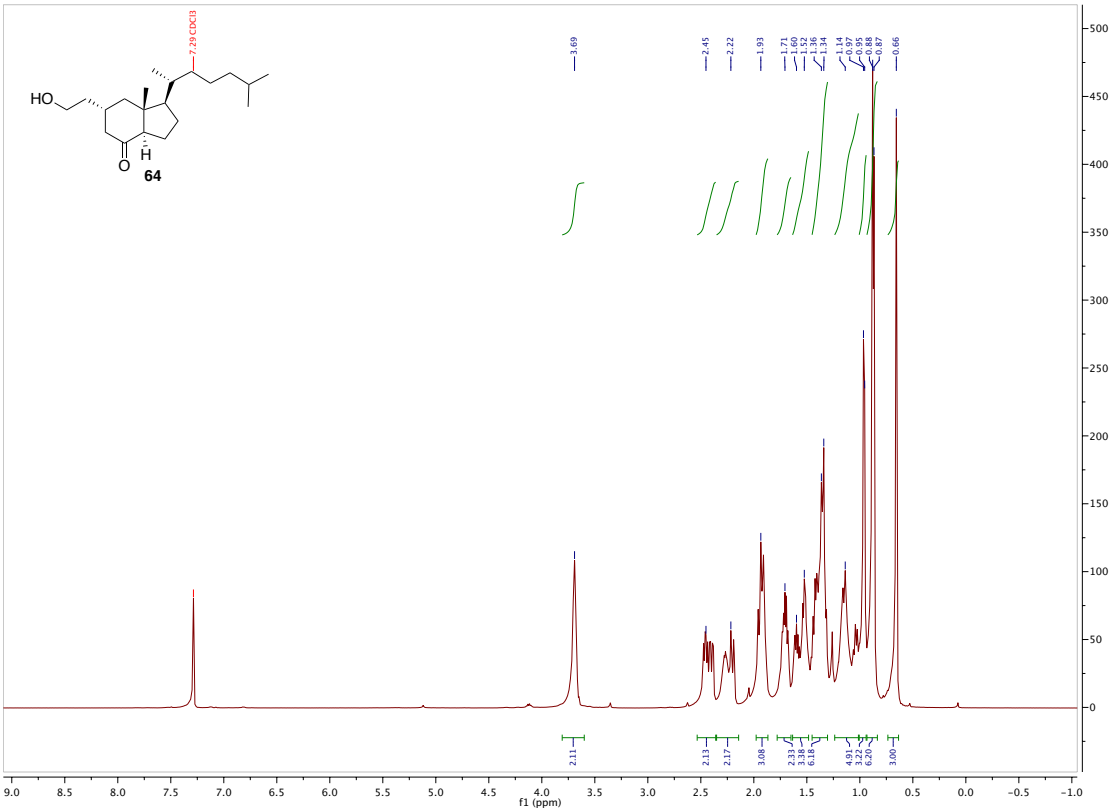
HO
O
H
64
7.29 CDCl3
3.69
2.45
2.22
1.93
1.71
1.60
1.52
1.36
1.34
1.14
0.97
0.95
0.88
0.87
0.66
2.11
2.13
2.17
3.08
2.33
3.38
6.18
4.91
3.22
6.20
3.00
f1 (ppm)

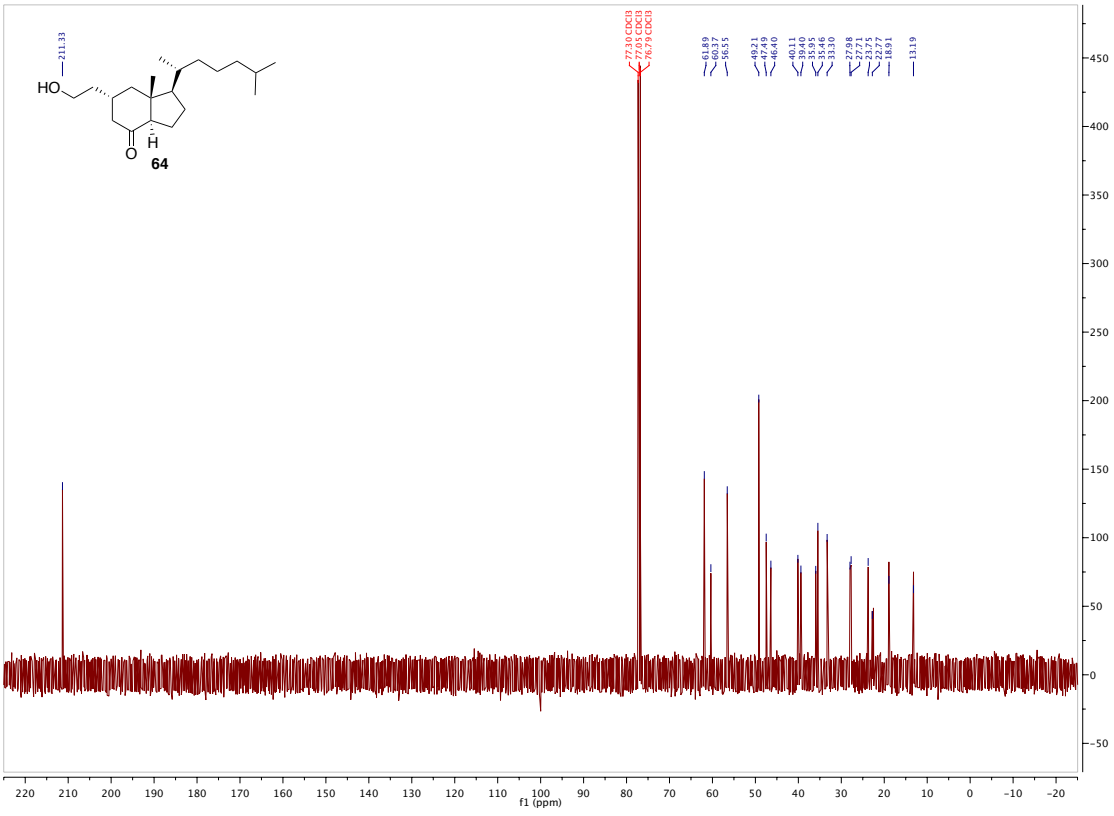
HO
O
H
64
211.33
77.30 CDCl3
77.05 CDCl3
76.79 CDCl3
61.89
60.37
56.55
49.21
47.49
46.40
40.11
39.60
35.95
35.46
33.30
27.98
27.71
23.25
22.77
18.91
13.19
f1 (ppm)

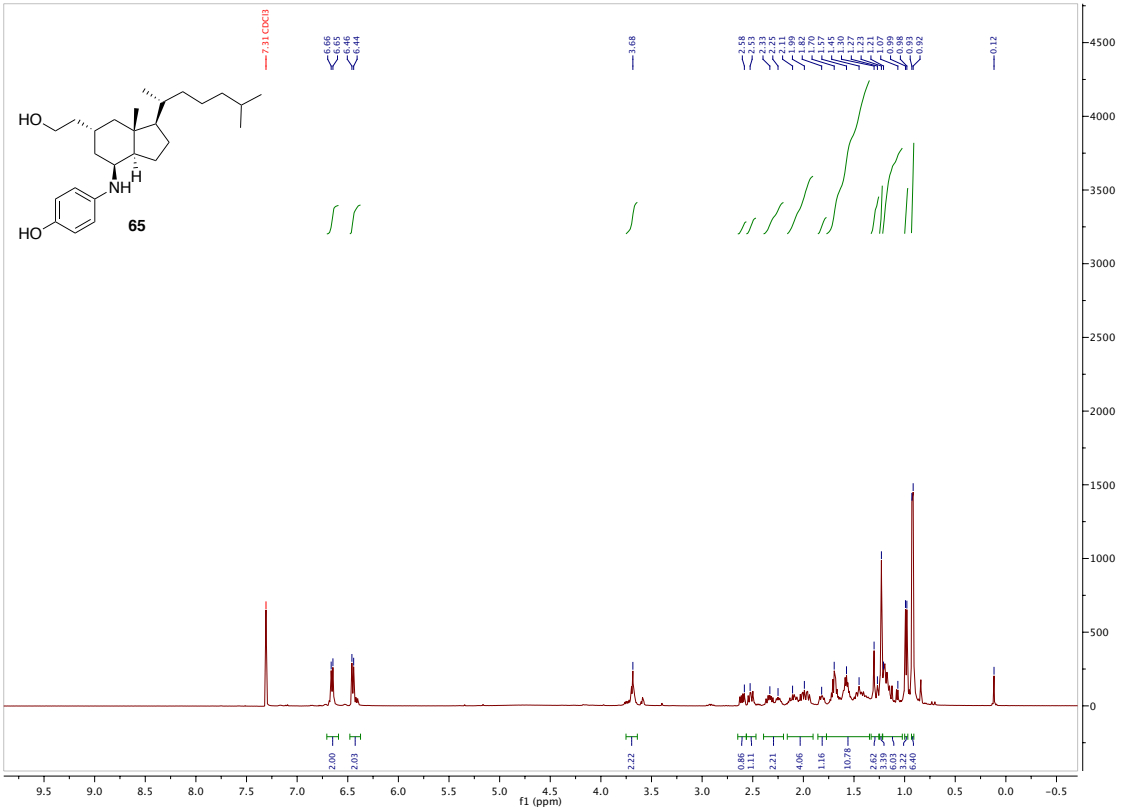
HO
NH
H
HO
65
f1 (ppm)

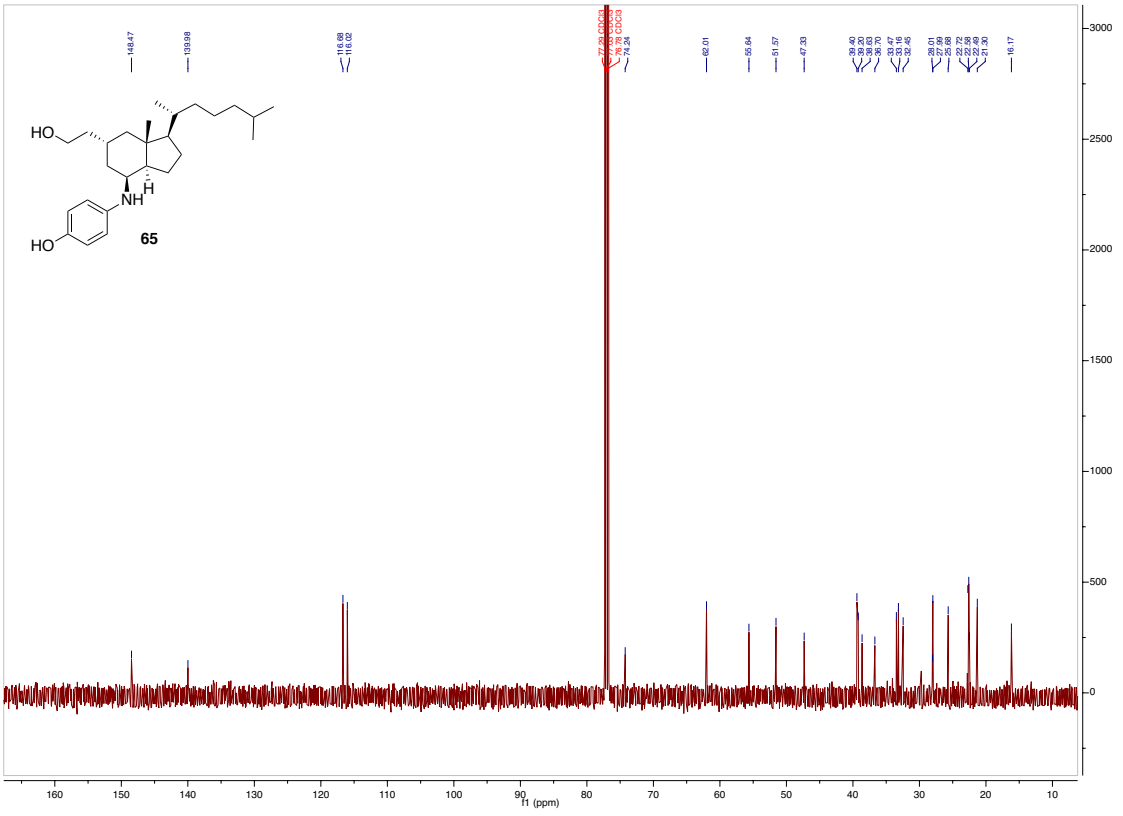
HO
NH
H
HO
65
f1 (ppm)

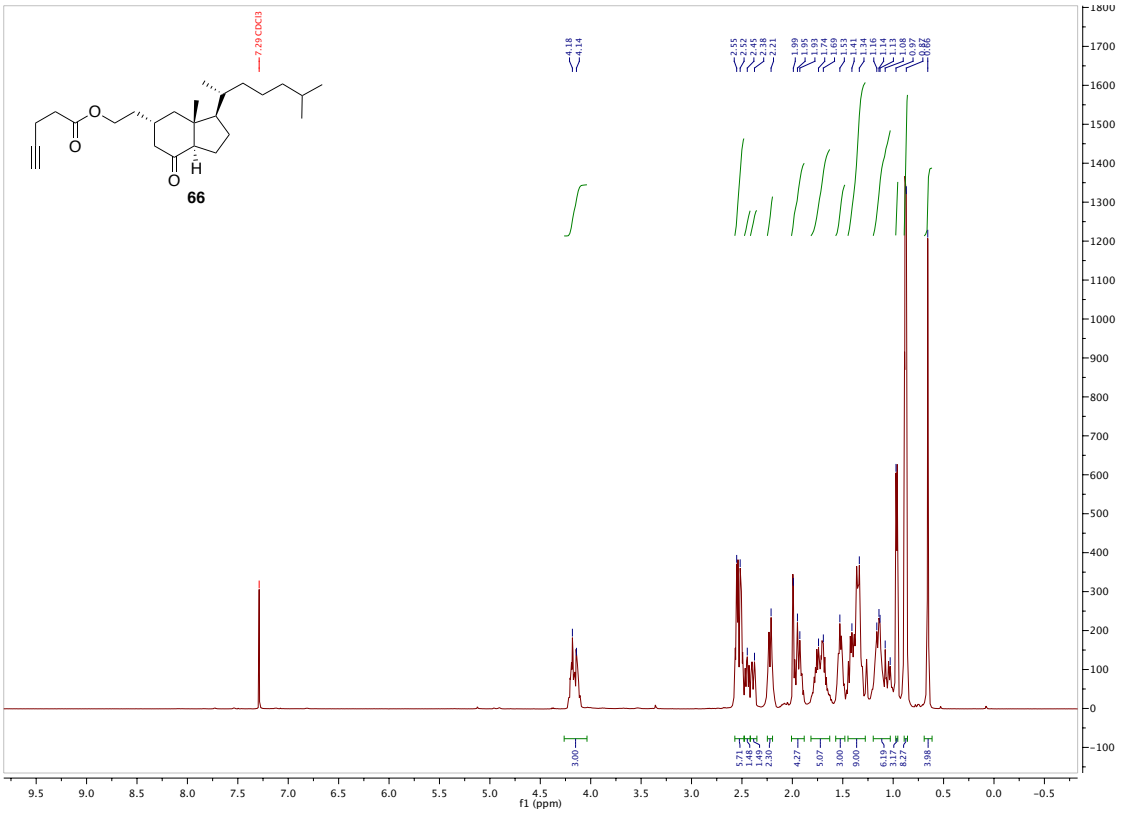
66
f1 (ppm)

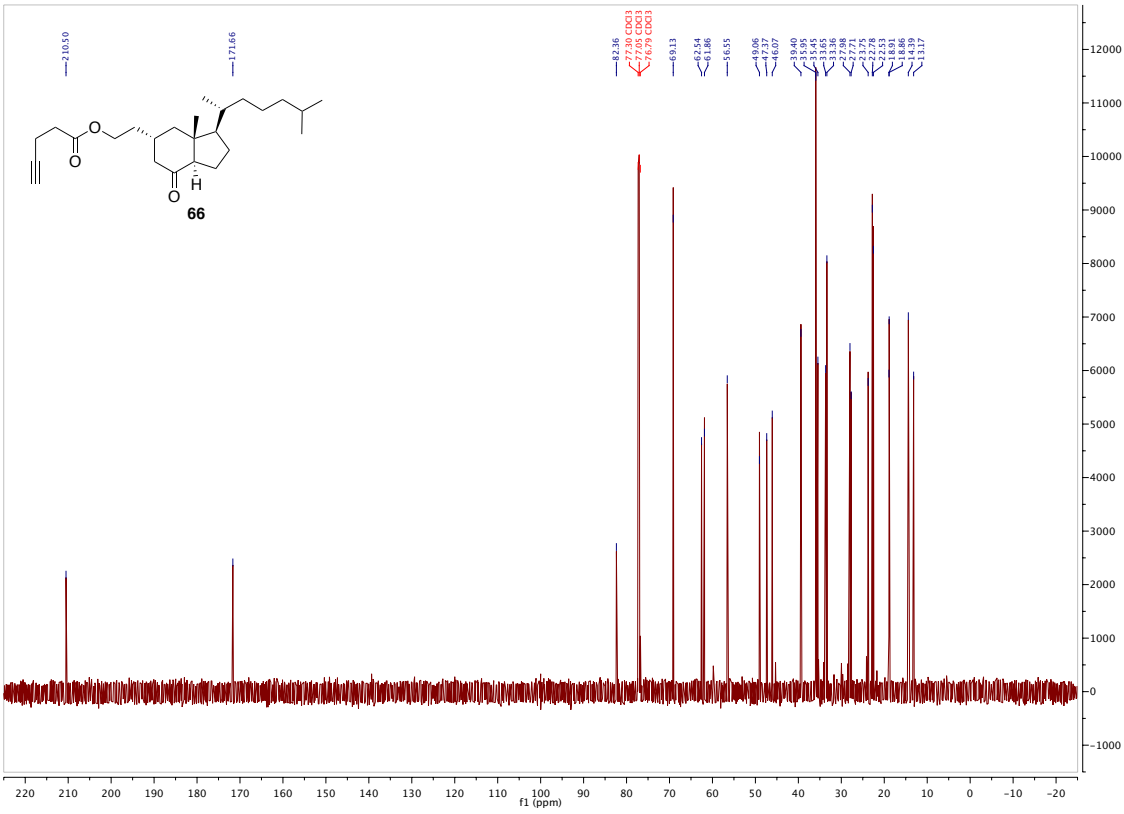
66
f1 (ppm)

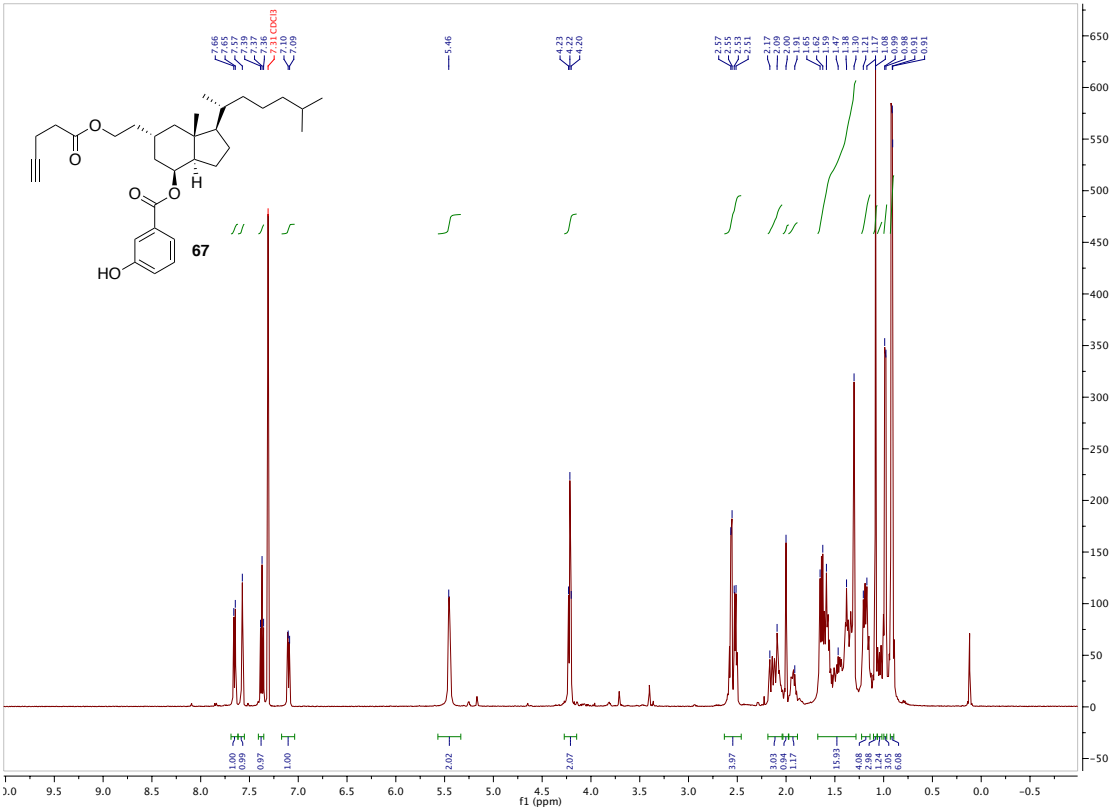
67
HO
f1 (ppm)

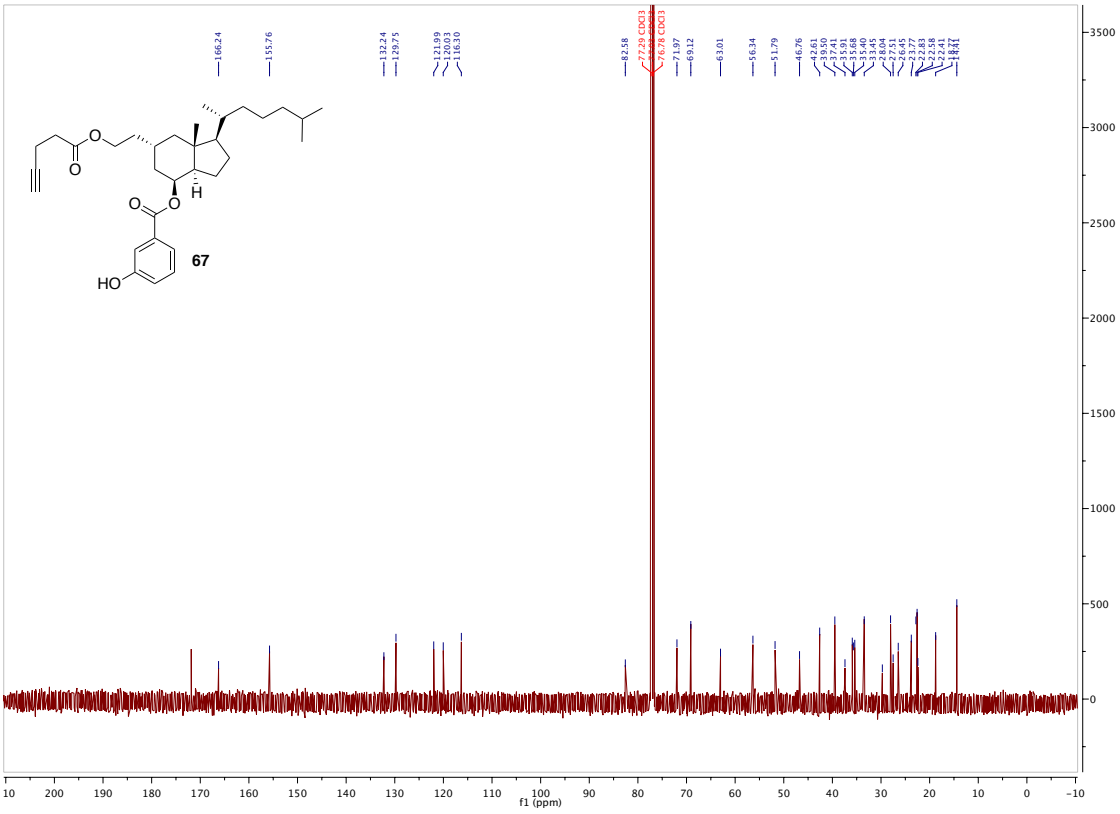
67
HO
f1 (ppm)

b. Amine seco-B Analogues

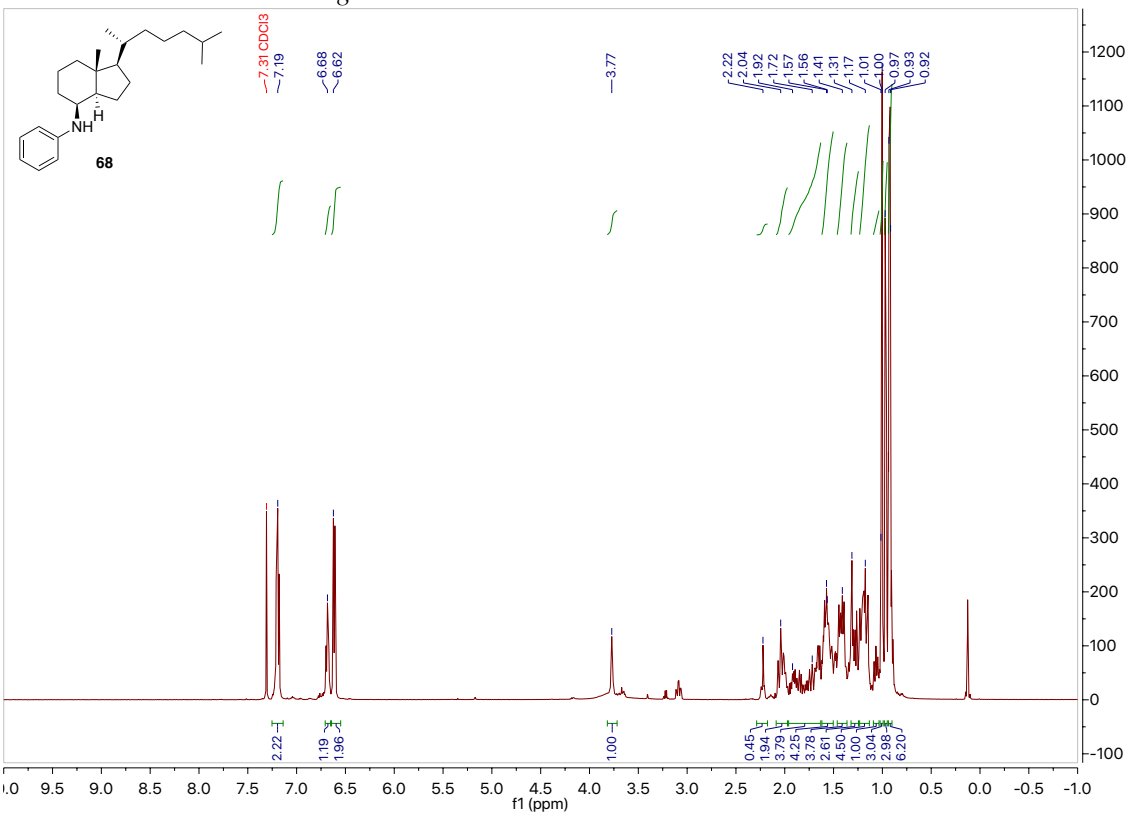

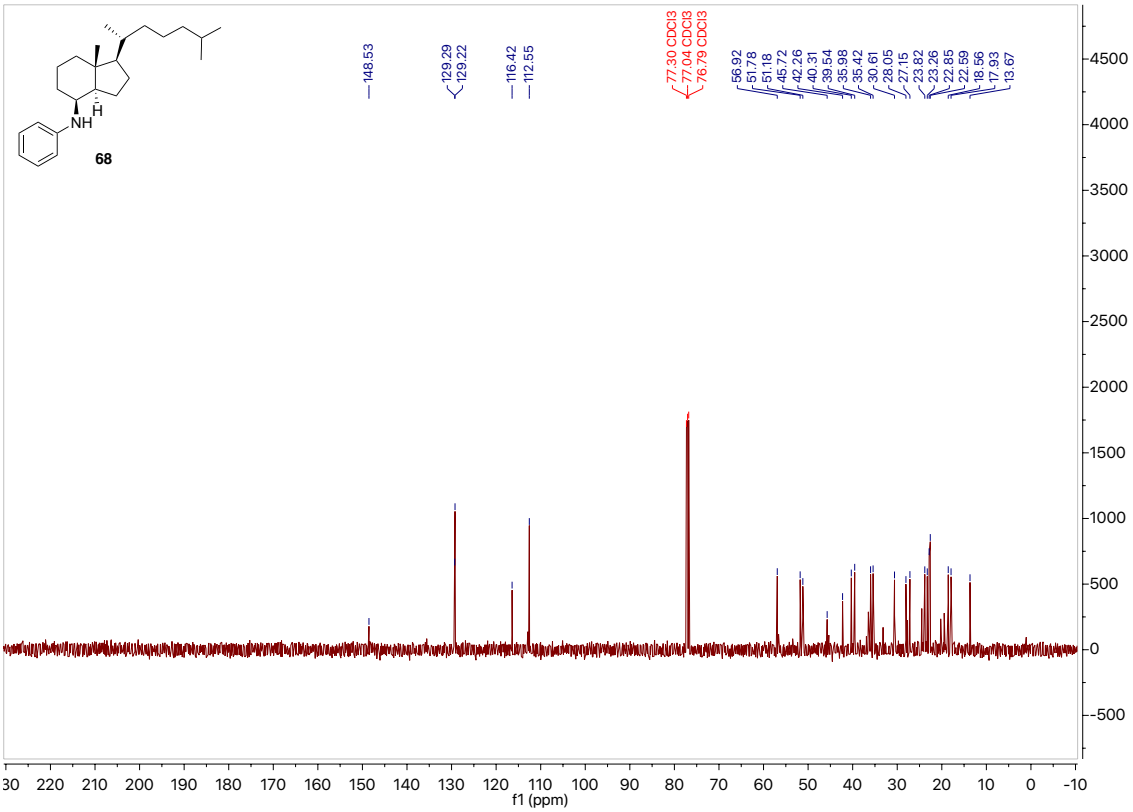

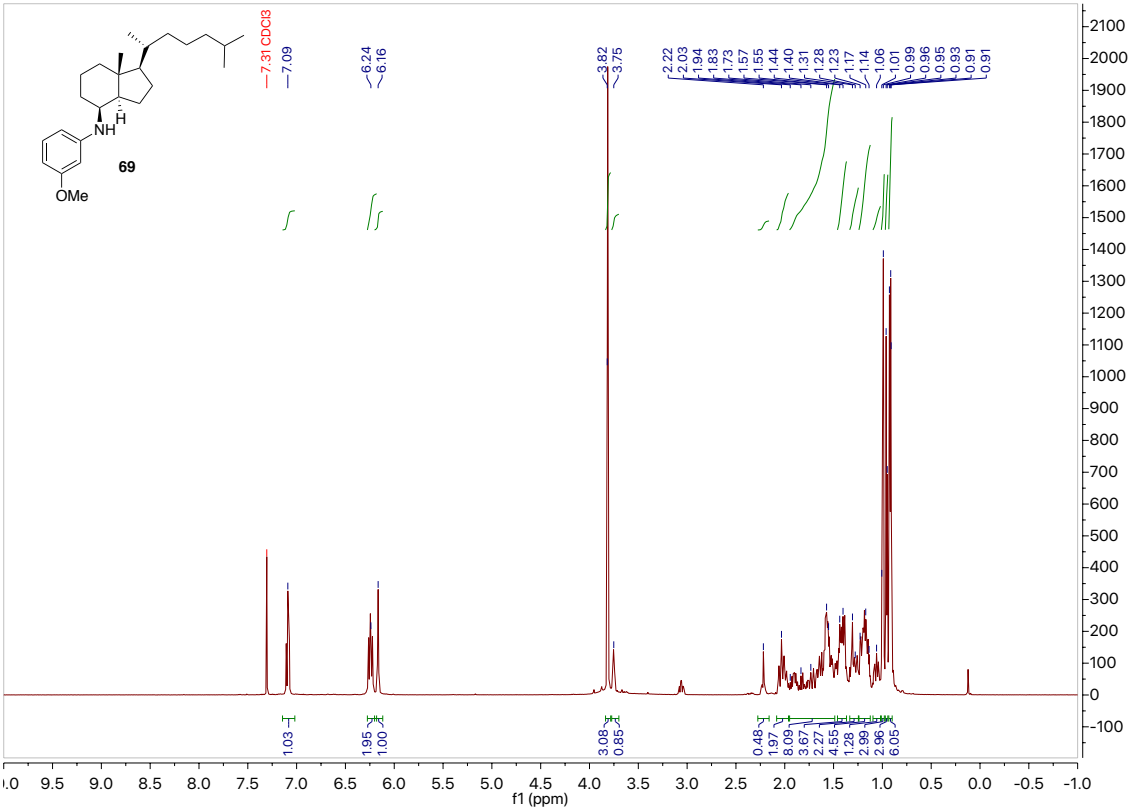
7.31 CDCl3
7.09
6.24
6.16
3.82
3.75
2.22
2.03
1.94
1.83
1.73
1.57
1.55
1.44
1.40
1.31
1.28
1.23
1.17
1.14
1.06
1.01
0.99
0.96
0.95
0.93
0.91
0.91
NH
H
69
OMe
1.03
1.95
1.00
3.08
0.85
0.48
1.97
8.09
3.67
2.27
4.55
1.28
2.99
2.96
6.05
f1 (ppm)

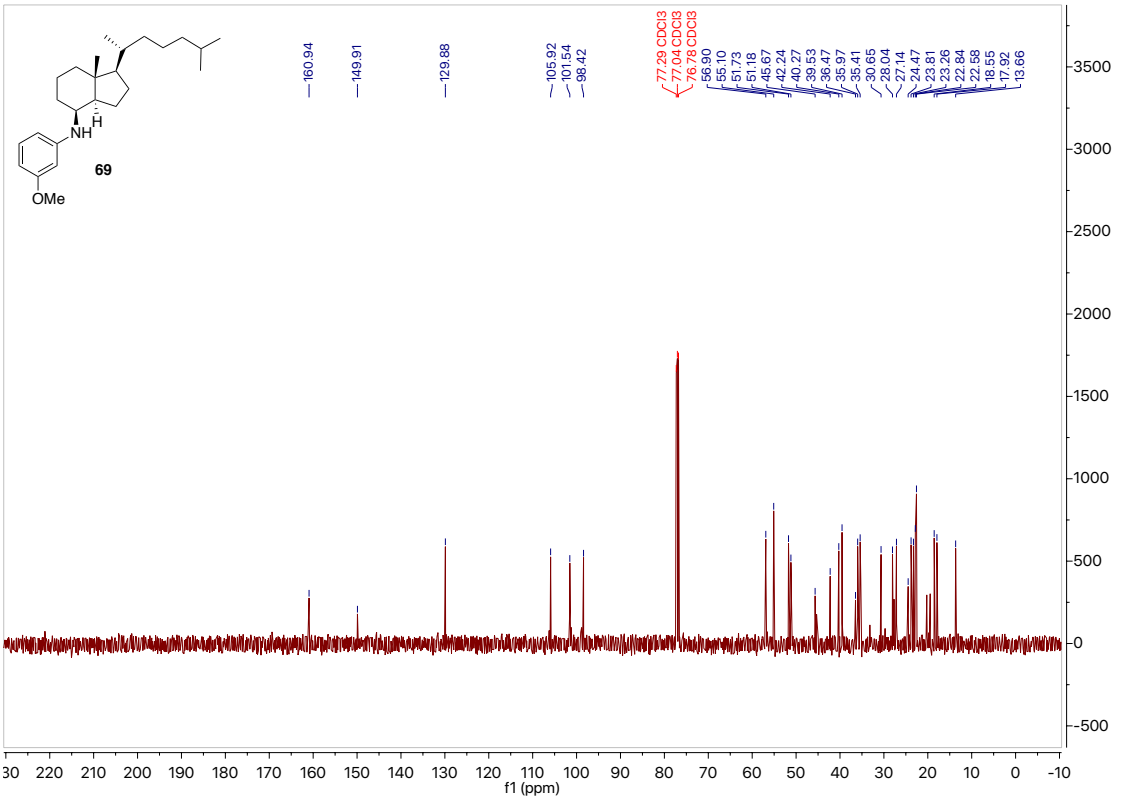
160.94
149.91
129.88
105.92
101.54
98.42
77.29 CDCl3
77.04 CDCl3
76.78 CDCl3
56.90
55.10
51.73
51.18
45.67
42.24
40.27
39.53
36.47
35.97
35.41
30.65
28.04
27.14
24.47
23.81
23.26
22.84
22.58
18.55
17.92
13.66
NH
H
69
OMe
f1 (ppm)

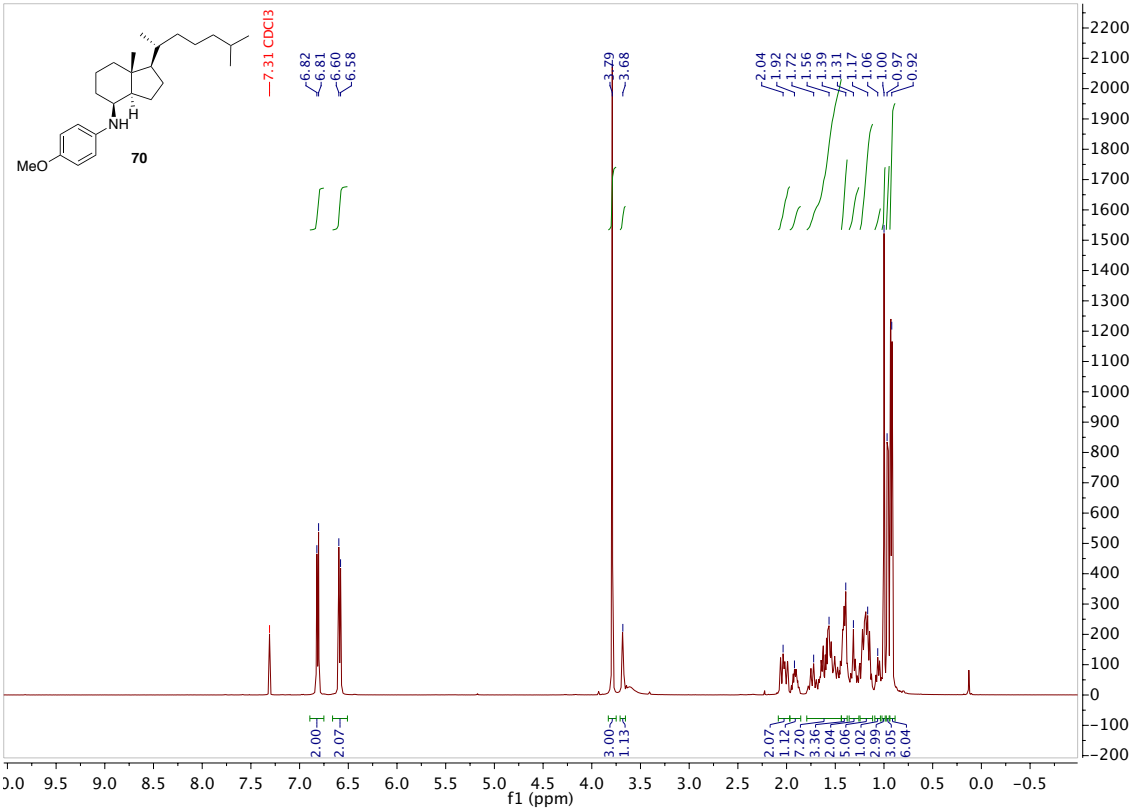
7.31 CDCl3
6.82
6.81
6.60
6.58
3.79
3.68
2.04
1.92
1.72
1.56
1.39
1.31
1.17
1.06
1.00
0.97
0.92
NH
MeO
70
2.00
2.07
3.00
1.13
2.07
1.12
7.20
3.36
2.04
5.06
1.02
2.99
3.05
6.04
f1 (ppm)

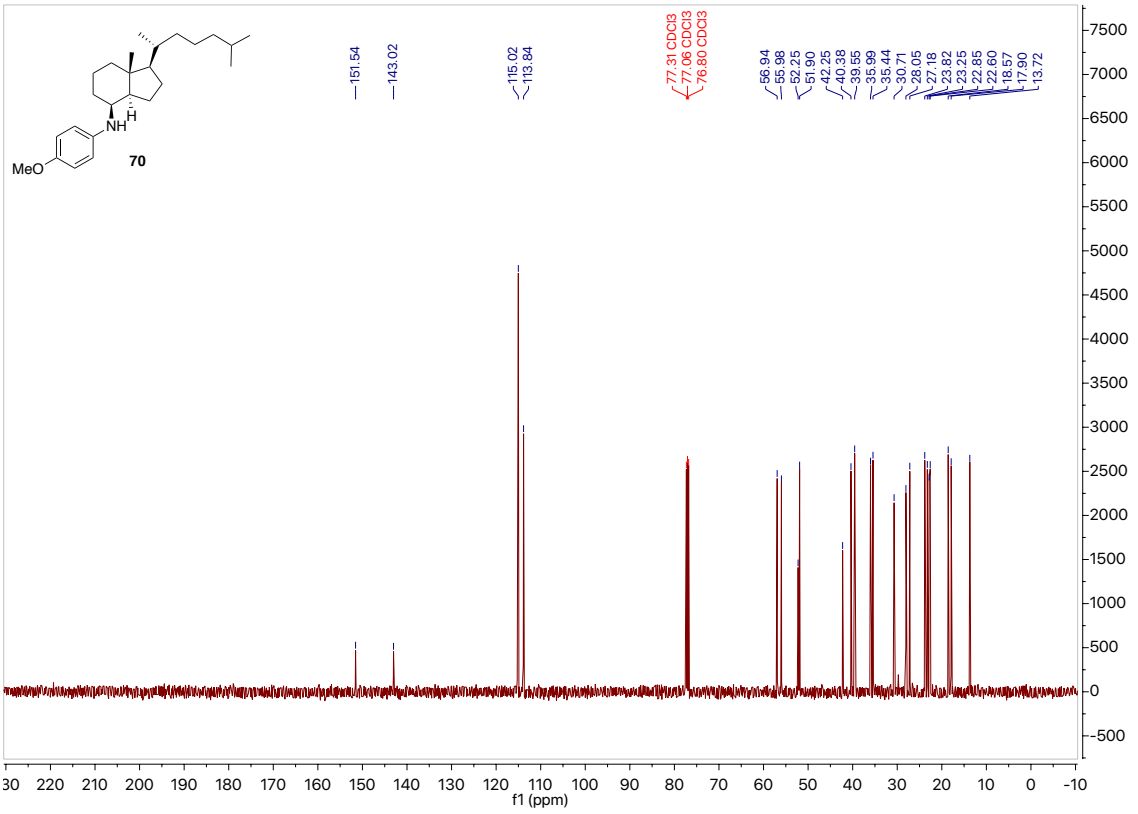
151.54
143.02
115.02
113.84
77.31 CDCl3
77.06 CDCl3
76.80 CDCl3
56.94
55.98
52.25
51.90
42.25
40.38
39.55
35.99
35.44
30.71
28.05
27.18
23.82
23.25
22.85
22.60
18.57
17.90
13.72
NH
MeO
70
f1 (ppm)

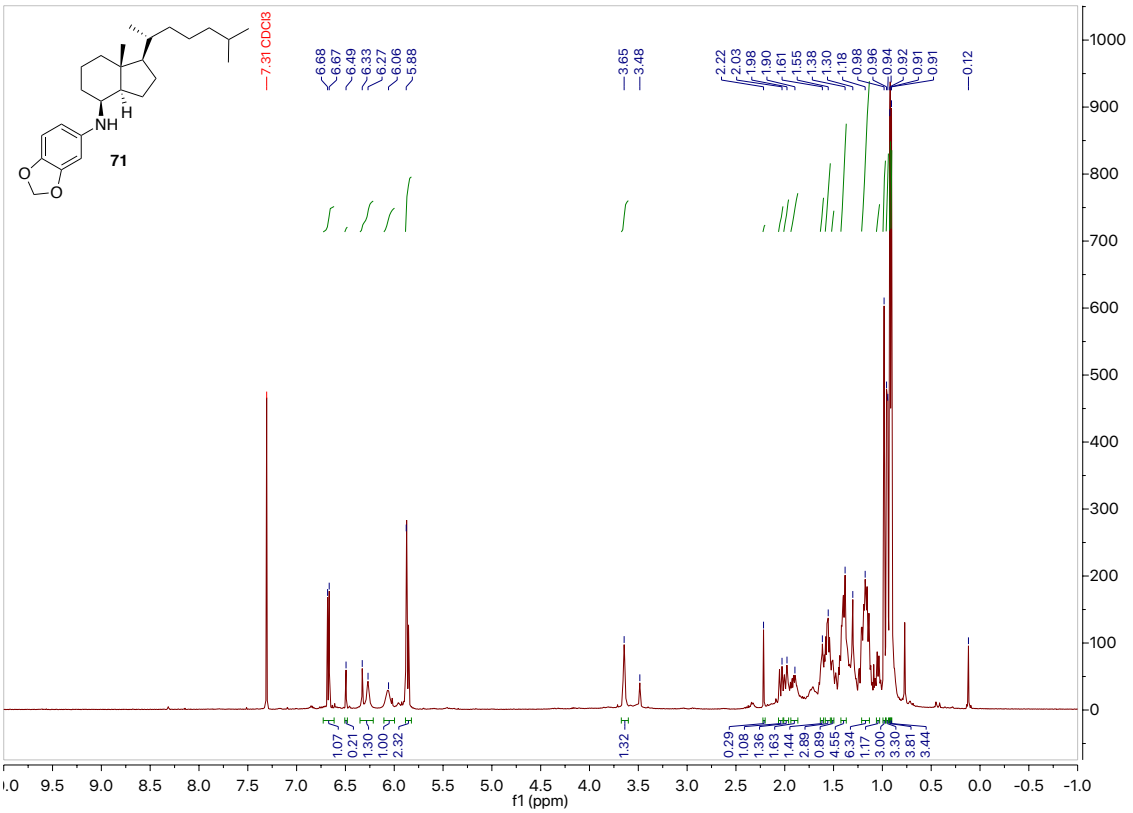
7.31 CDCl3
6.68
6.67
6.49
6.33
6.27
6.06
5.88
3.65
3.48
2.22
2.03
1.98
1.90
1.61
1.55
1.38
1.30
1.18
0.98
0.96
0.94
0.92
0.91
0.91
0.12
71
f1 (ppm)

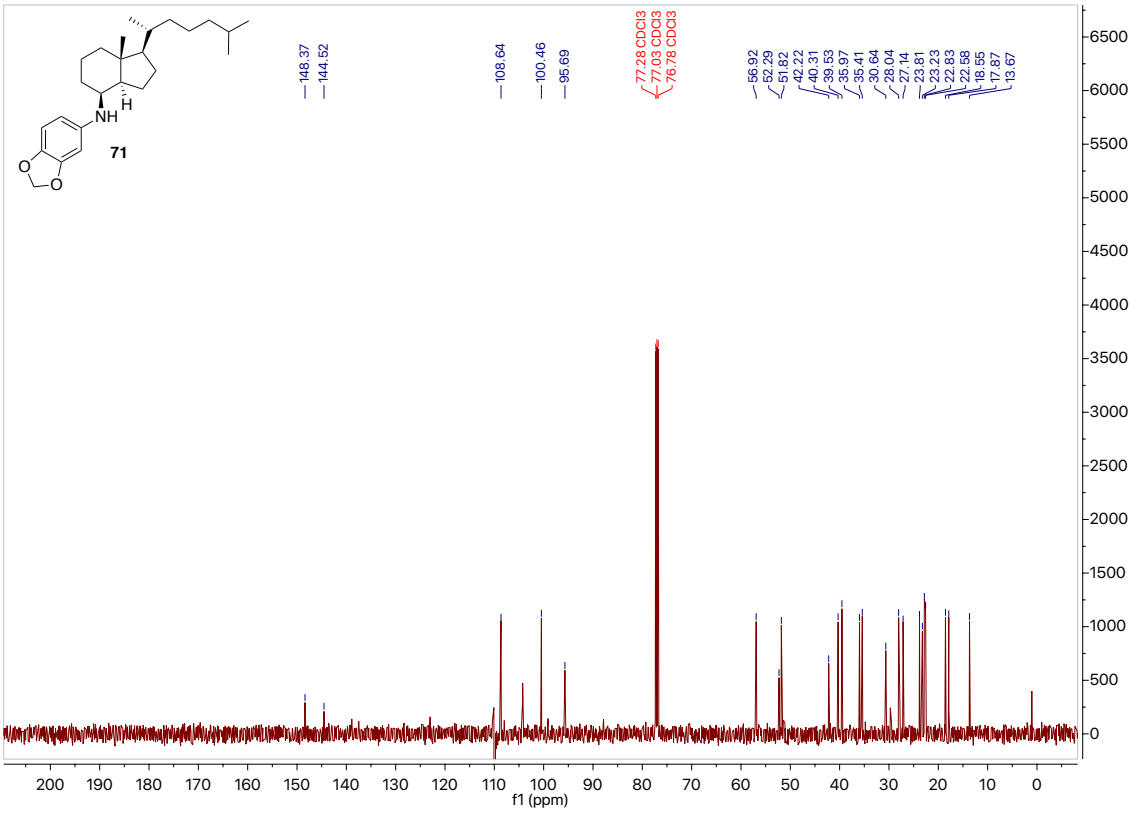
148.37
144.52
108.64
100.46
95.69
77.28 CDCl3
77.03 CDCl3
76.78 CDCl3
56.92
52.29
51.82
42.22
40.31
39.53
35.97
35.41
30.64
28.04
27.14
23.81
23.23
22.83
22.58
18.55
17.87
13.67
71
f1 (ppm)

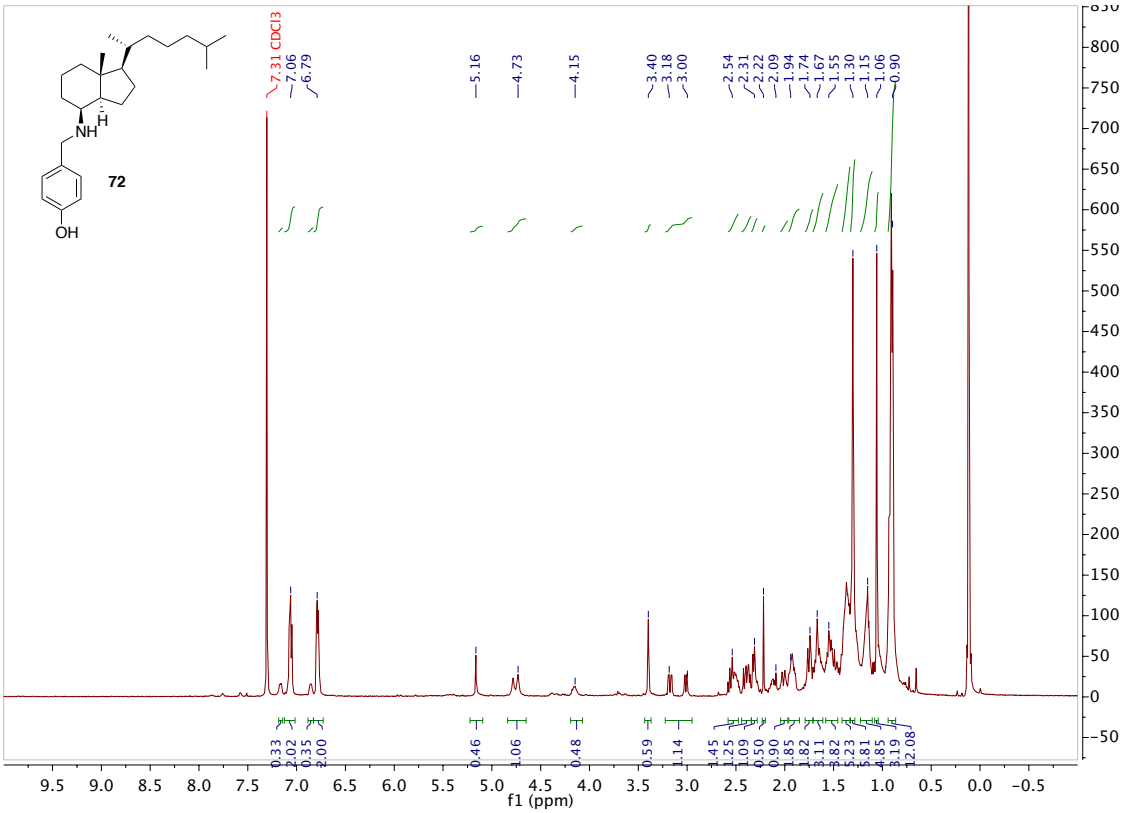
72
NH
H
OH
7.31 CDCl3
7.06
6.79
5.16
4.73
4.15
3.40
3.18
3.00
2.54
2.31
2.22
2.09
1.94
1.74
1.67
1.55
1.30
1.15
1.06
0.90
0.33
2.02
0.35
2.00
0.46
1.06
0.48
0.59
1.14
1.45
1.25
1.09
0.50
0.90
1.85
1.82
3.11
3.82
5.23
5.81
4.85
3.19
12.08
f1 (ppm)

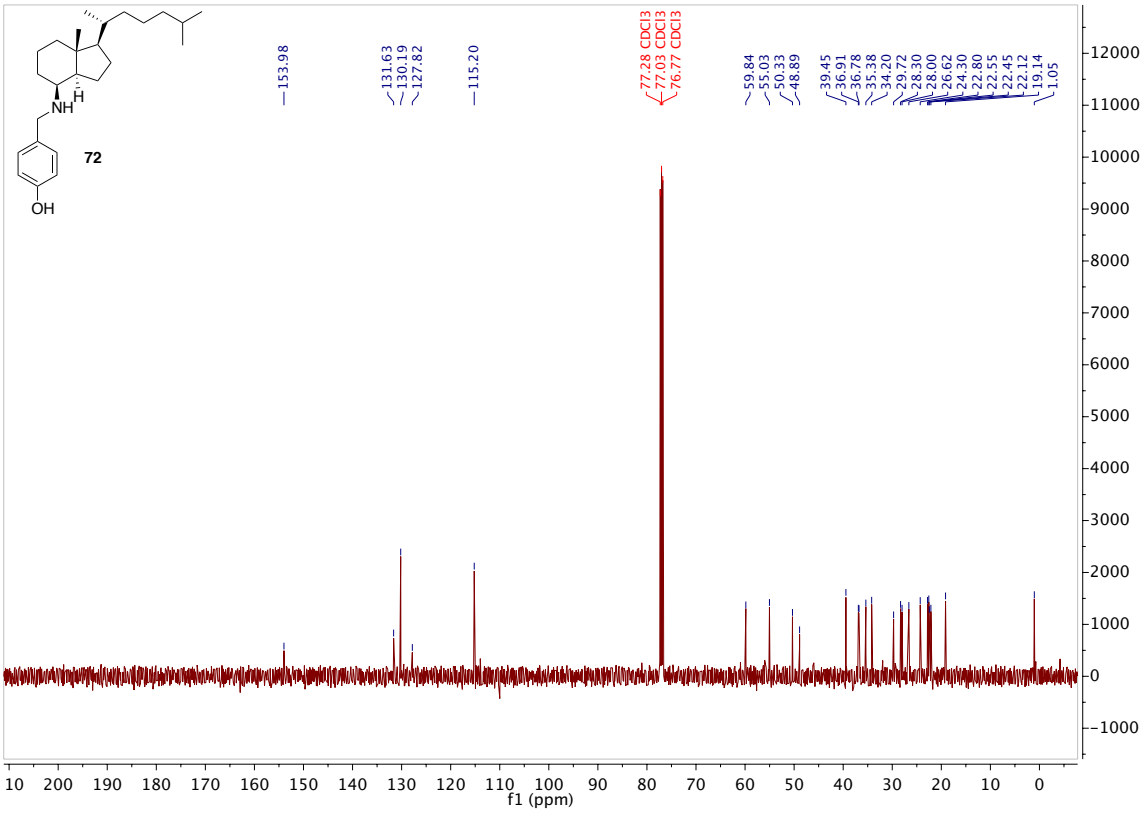
72
NH
H
OH
153.98
131.63
130.19
127.82
115.20
77.28 CDCl3
77.03 CDCl3
76.77 CDCl3
59.84
55.03
50.33
48.89
39.45
36.91
36.78
35.38
34.20
29.72
28.30
28.00
26.62
24.30
22.80
22.55
22.45
22.12
19.14
1.05
f1 (ppm)

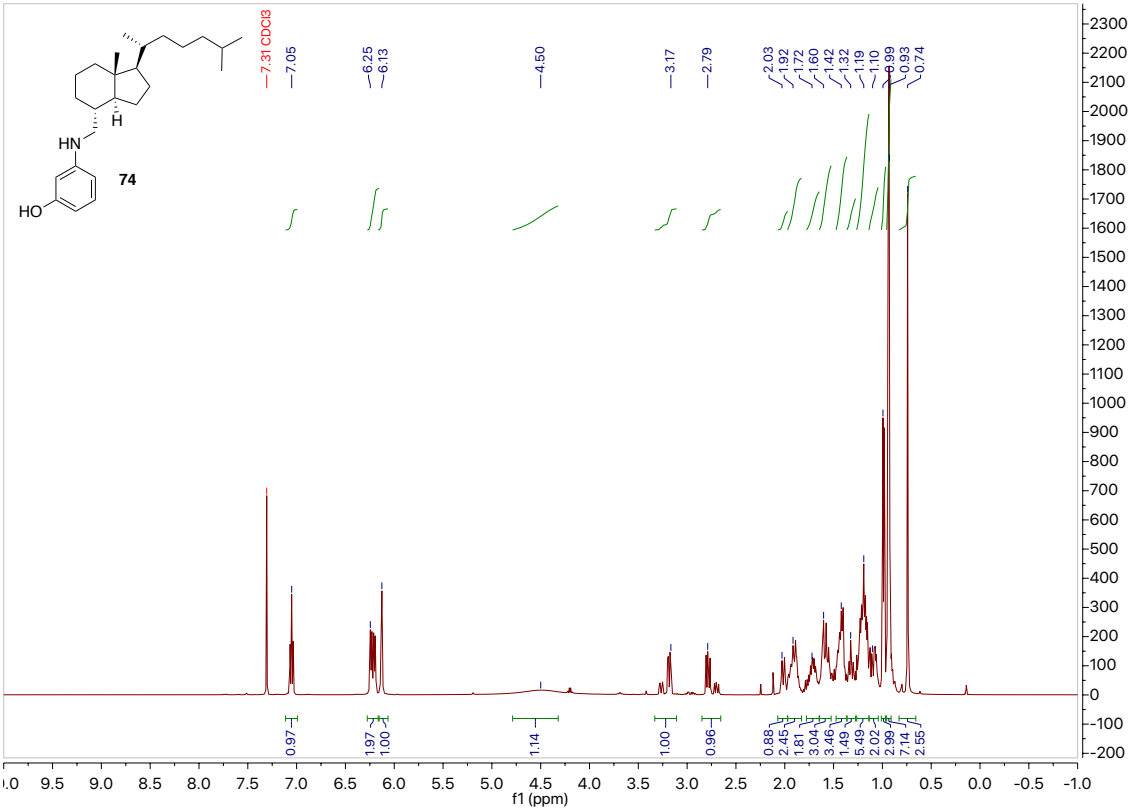
7.31 CDCl3
7.05
6.25
6.13
4.50
3.17
2.79
2.03
1.92
1.72
1.60
1.42
1.32
1.19
1.10
0.99
0.93
0.74
HN
H
HO
74
0.97
1.97
1.00
1.14
1.00
0.96
0.88
2.45
1.81
3.04
3.46
1.49
5.49
2.02
2.99
7.14
2.55
f1 (ppm)

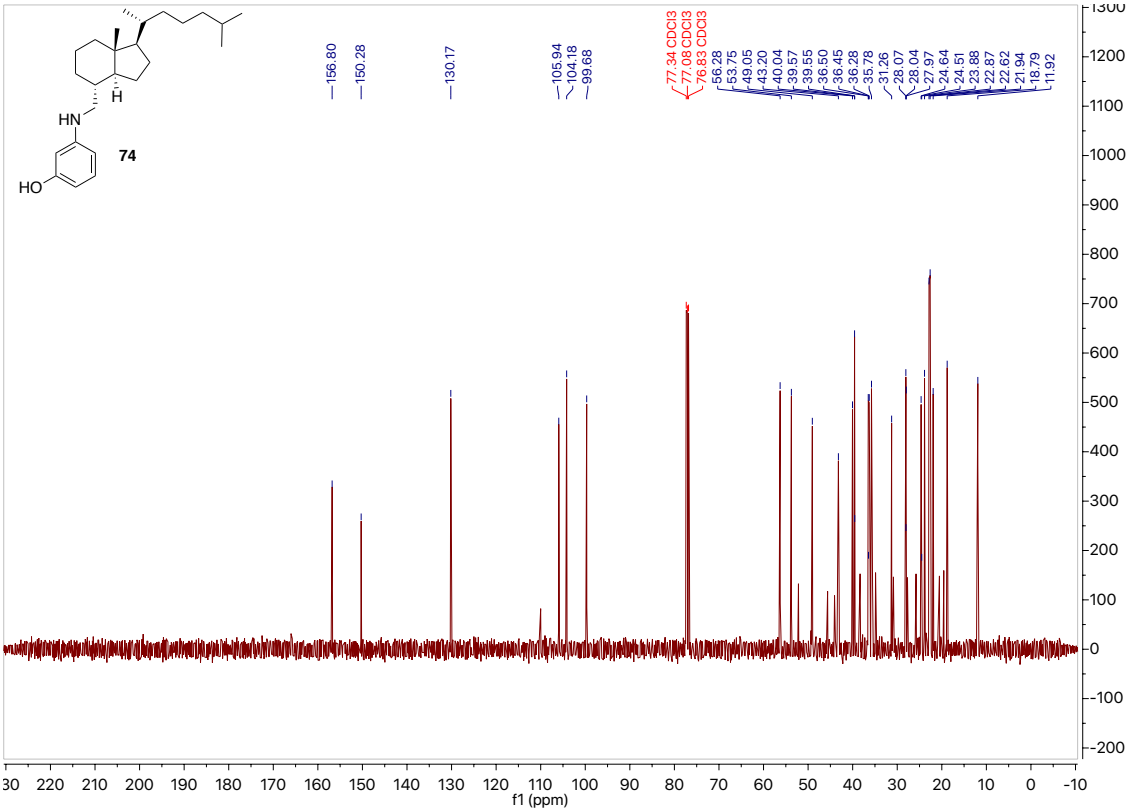
156.80
150.28
130.17
105.94
104.18
99.68
77.34 CDCl3
77.08 CDCl3
76.83 CDCl3
56.28
53.75
49.05
43.20
40.04
39.57
39.55
36.50
36.45
36.28
35.78
31.26
28.07
28.04
27.97
24.64
24.51
23.88
22.87
22.62
21.94
18.79
11.92
HN
H
HO
74
f1 (ppm)

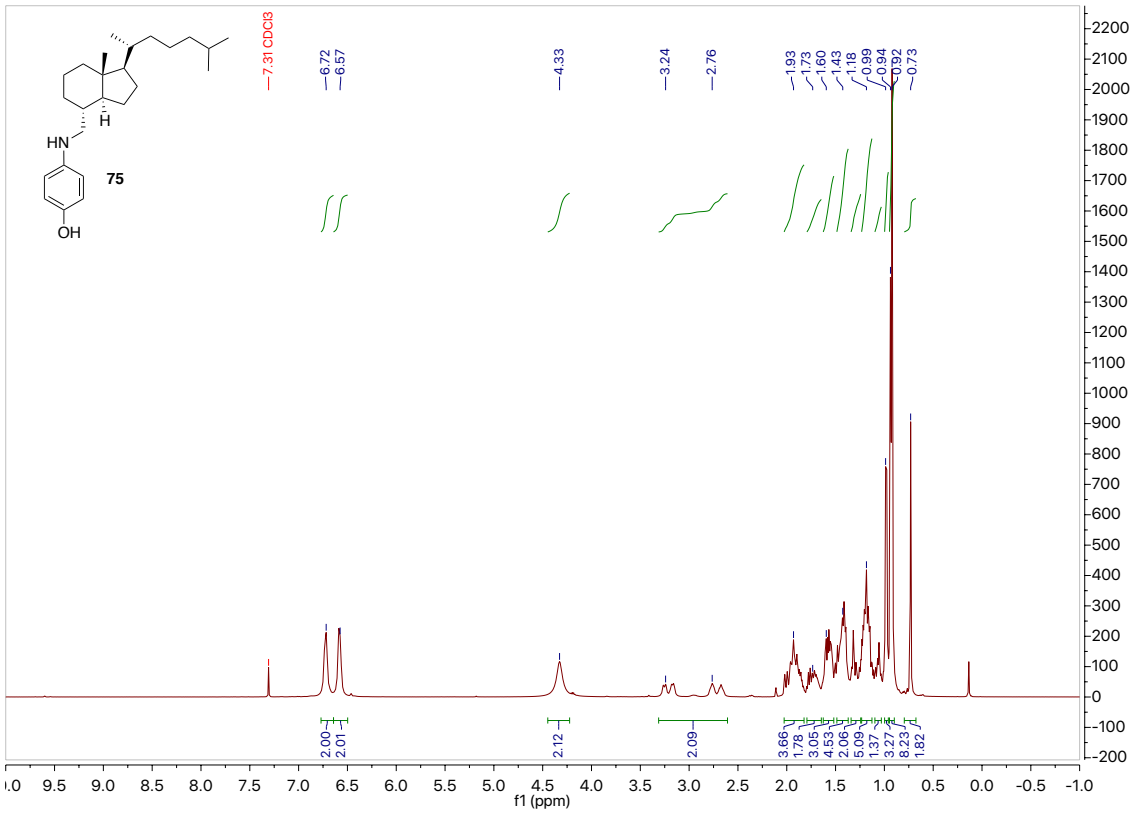
7.31 CDCl3
6.72
6.57
4.33
3.24
2.76
1.93
1.73
1.60
1.43
1.18
0.99
0.94
0.92
0.73
HN
H
OH
75
2.00
2.01
2.12
2.09
3.66
1.78
3.05
4.53
2.06
5.09
1.37
3.27
8.23
1.82
f1 (ppm)

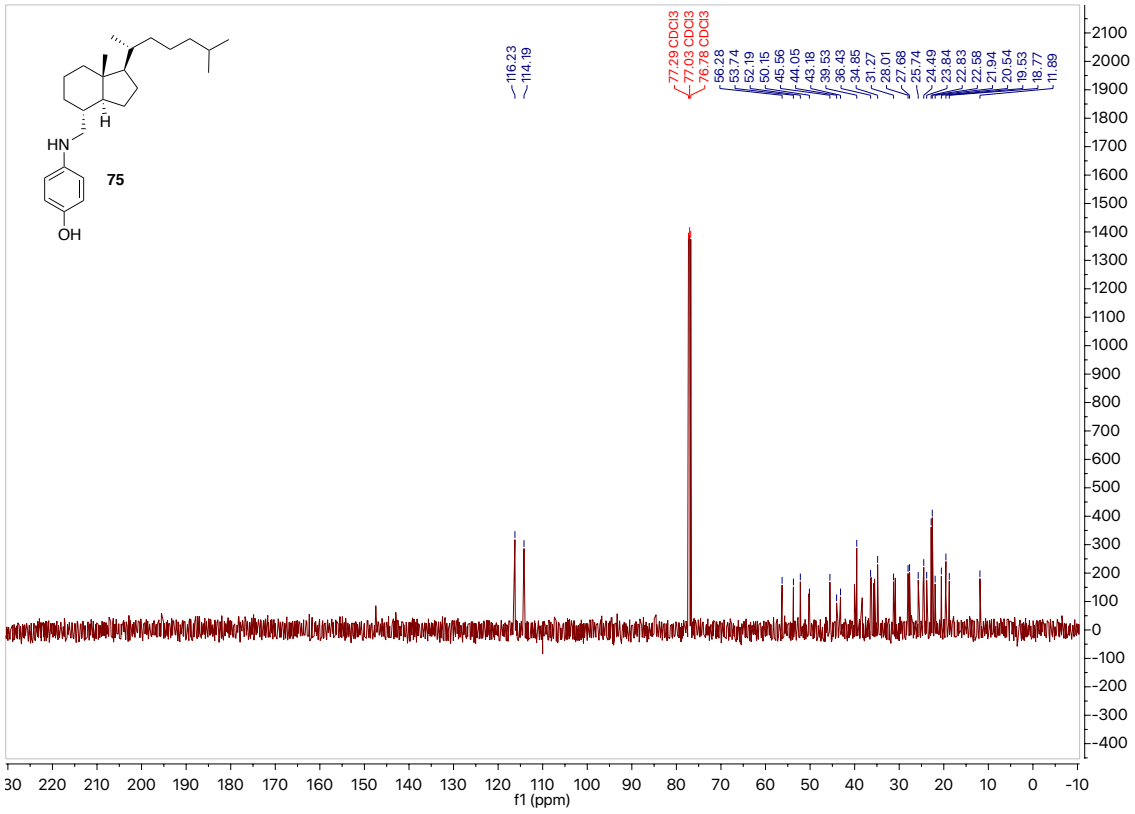
116.23
114.19
77.29 CDCl3
77.03 CDCl3
76.78 CDCl3
56.28
53.74
52.19
50.15
45.56
44.05
43.18
39.53
36.43
34.85
31.27
28.01
27.68
25.74
24.49
23.84
22.83
22.58
21.94
20.54
19.53
18.77
11.89
HN
H
OH
75
f1 (ppm)

c. C-25 Functionalized Analogues

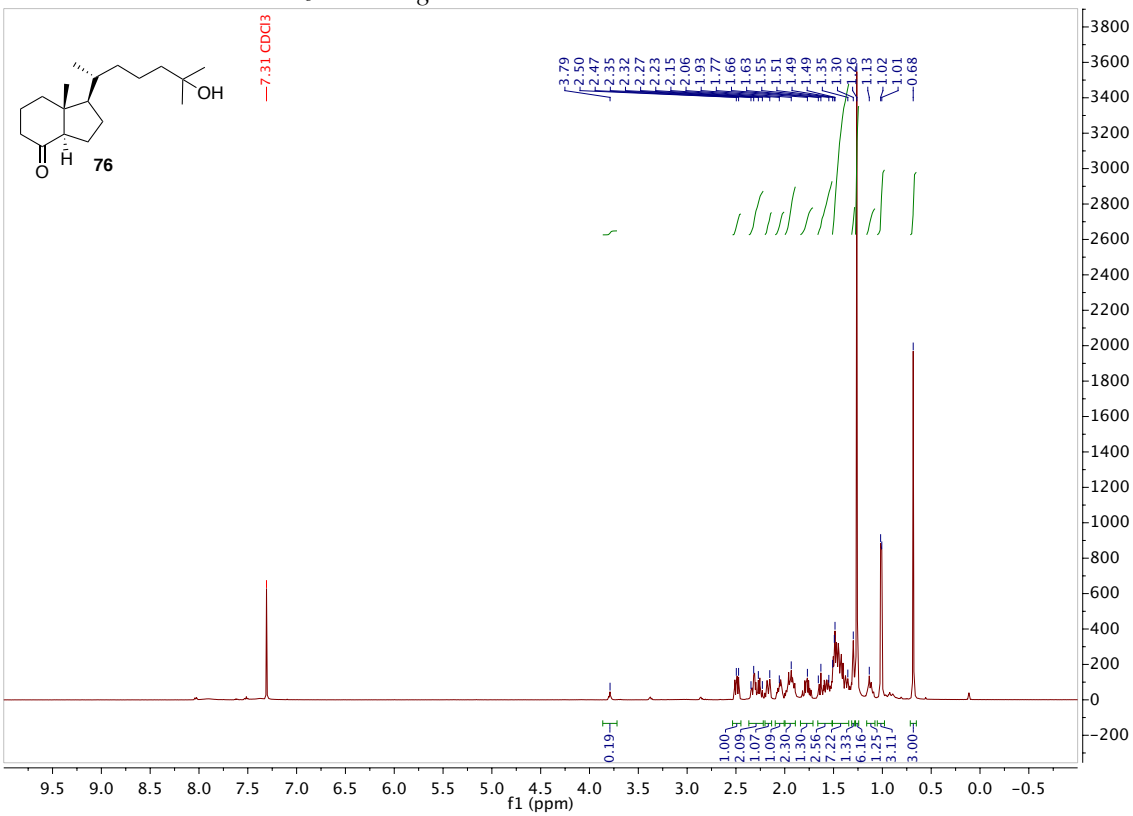

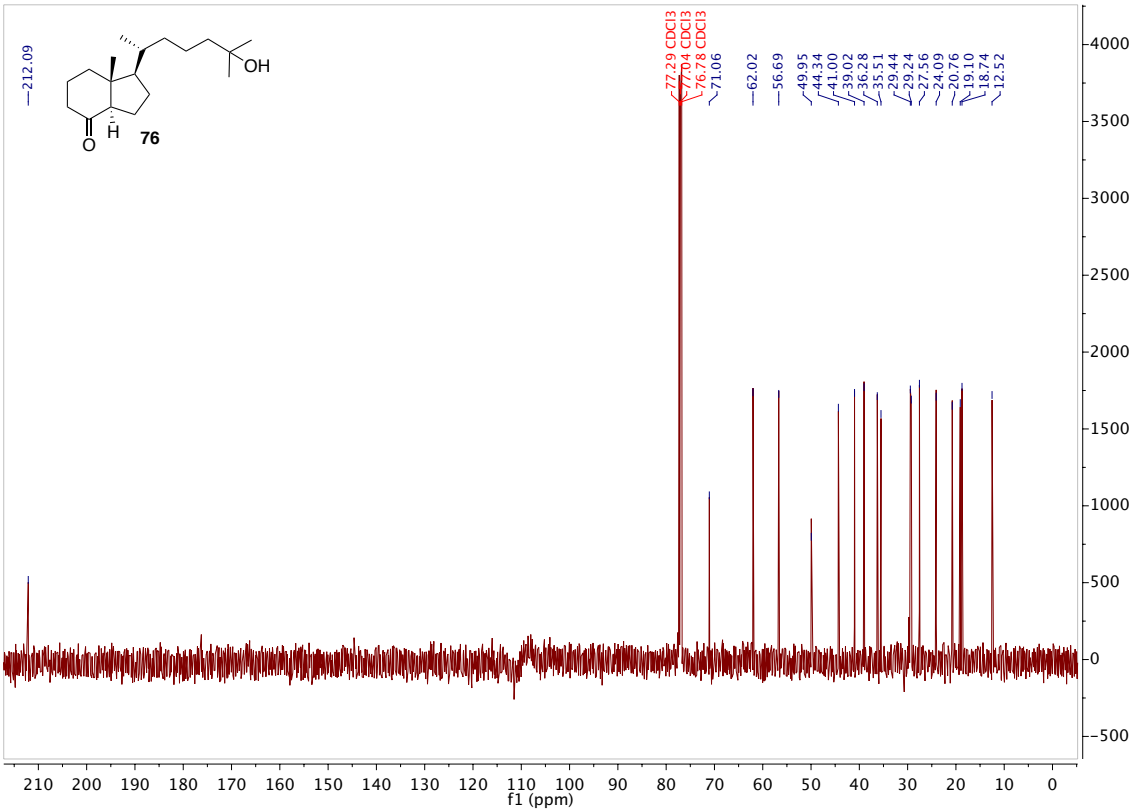

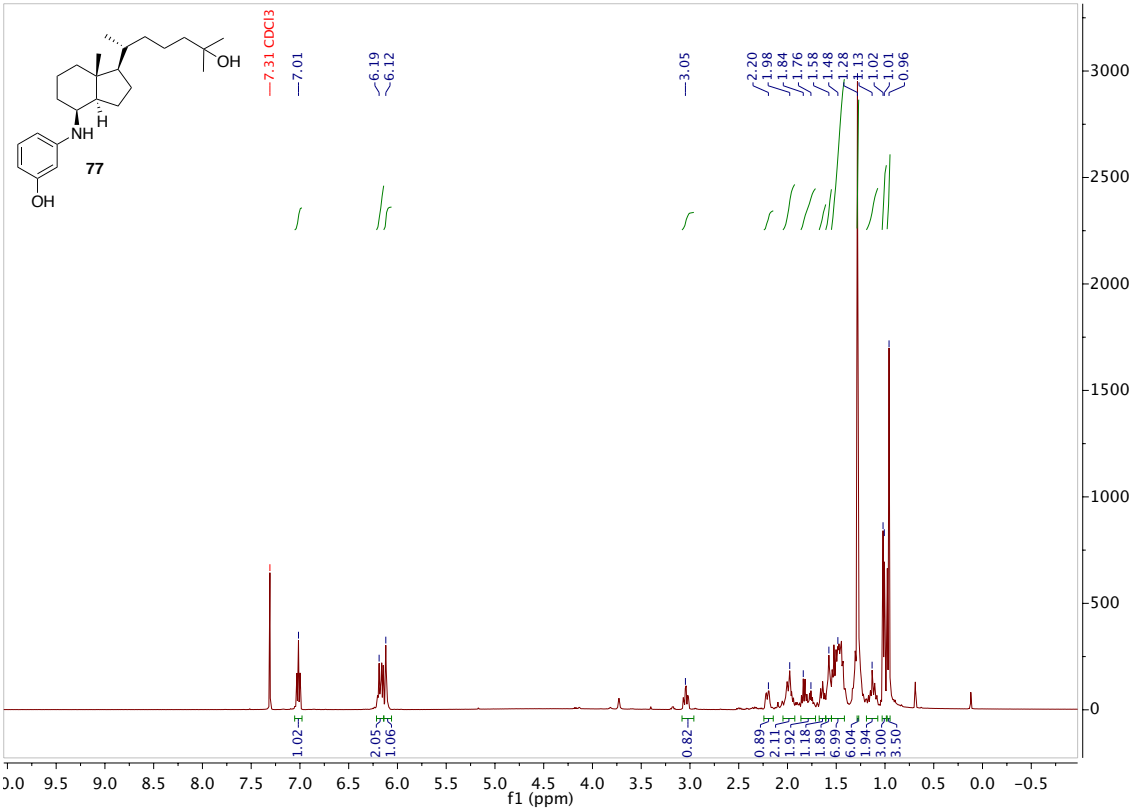
77
OH
NH
H
OH
7.31 CDCl3
7.01
6.19
6.12
3.05
2.20
1.98
1.84
1.76
1.58
1.48
1.28
1.13
1.02
1.01
0.96
1.02
2.05
1.06
0.82
0.89
2.11
1.92
1.18
1.89
6.99
6.04
1.94
3.00
3.50
f1 (ppm)

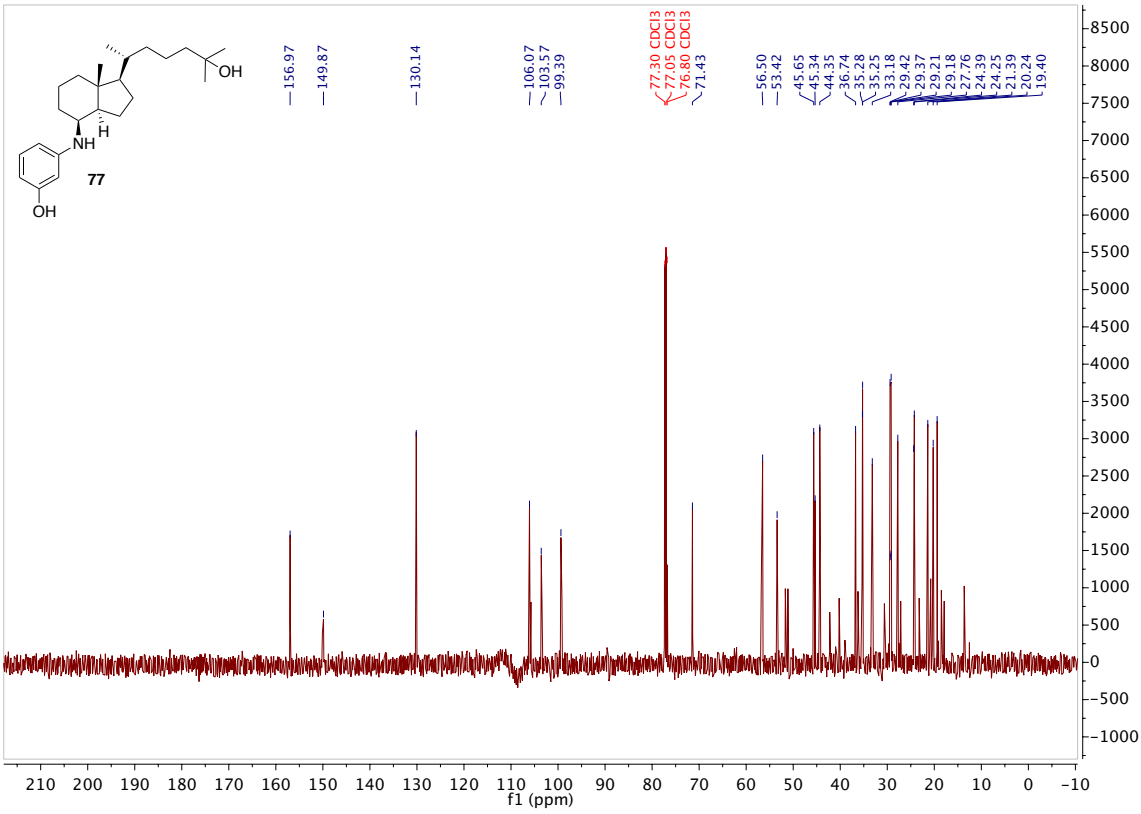
77
OH
NH
H
OH
156.97
149.87
130.14
106.07
103.57
99.39
77.30 CDCl3
77.05 CDCl3
76.80 CDCl3
71.43
56.50
53.42
45.65
45.34
44.35
36.74
35.28
35.25
33.18
29.42
29.37
29.21
29.18
27.76
24.39
24.25
21.39
20.24
19.40
f1 (ppm)

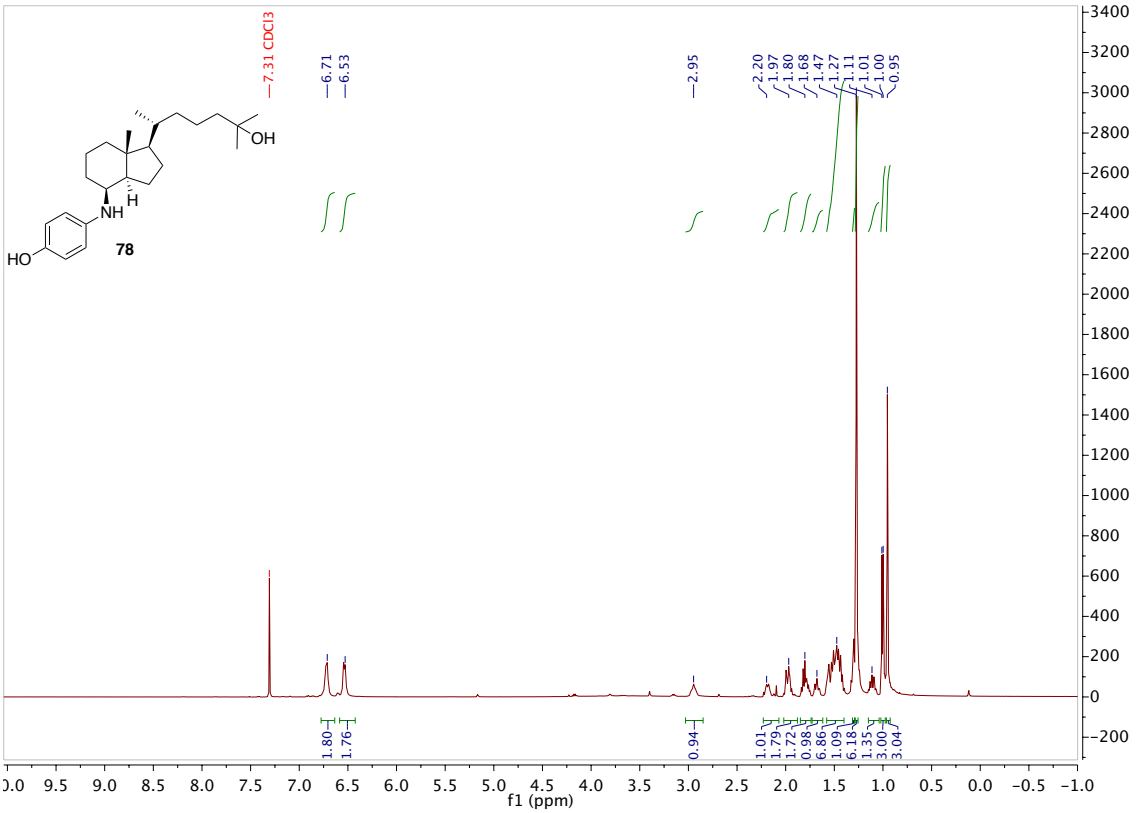
7.31 CDCl3
6.71
6.53
2.95
2.20
1.97
1.80
1.68
1.47
1.27
1.11
1.01
1.00
0.95
OH
NH
H
HO
78
1.80
1.76
0.94
1.01
1.79
1.72
0.98
6.86
1.09
6.18
1.35
3.00
3.04
f1 (ppm)

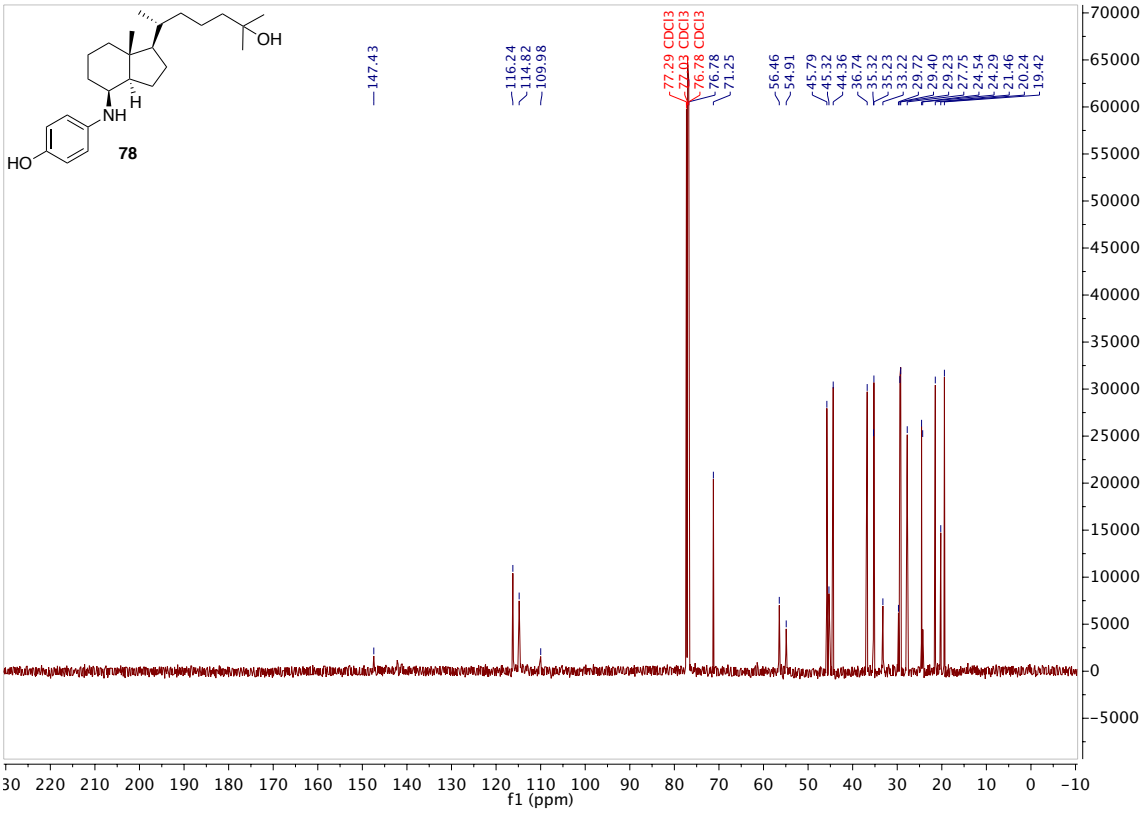
147.43
116.24
114.82
109.98
77.29 CDCl3
77.03 CDCl3
76.78 CDCl3
76.78
71.25
56.46
54.91
45.79
45.32
44.36
36.74
35.32
35.23
33.22
29.72
29.40
29.23
27.75
24.54
24.29
21.46
20.24
19.42
OH
NH
H
HO
78
f1 (ppm)

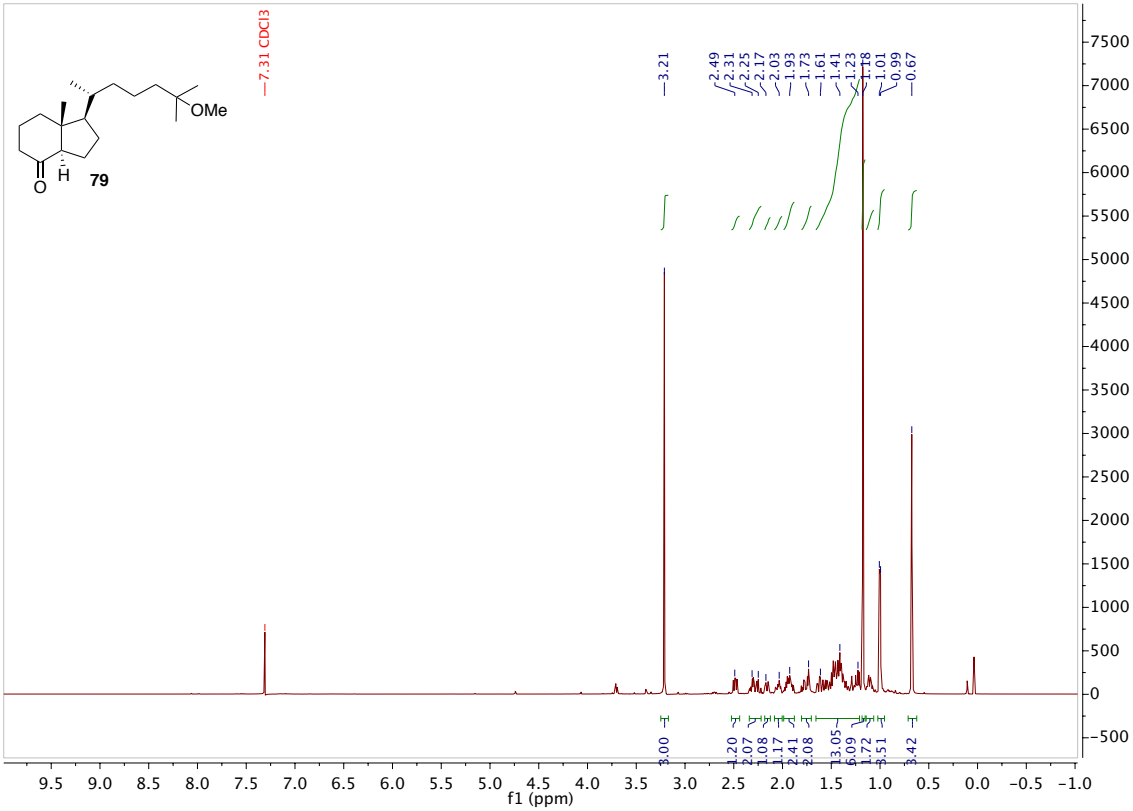
7.31 CDCl3
3.21
2.49
2.31
2.25
2.17
2.03
1.93
1.73
1.61
1.41
1.23
1.18
1.01
0.99
0.67
OMe
H
O
79
3.00
1.20
2.07
1.08
1.17
2.41
2.08
13.05
6.09
1.72
3.51
3.42
f1 (ppm)

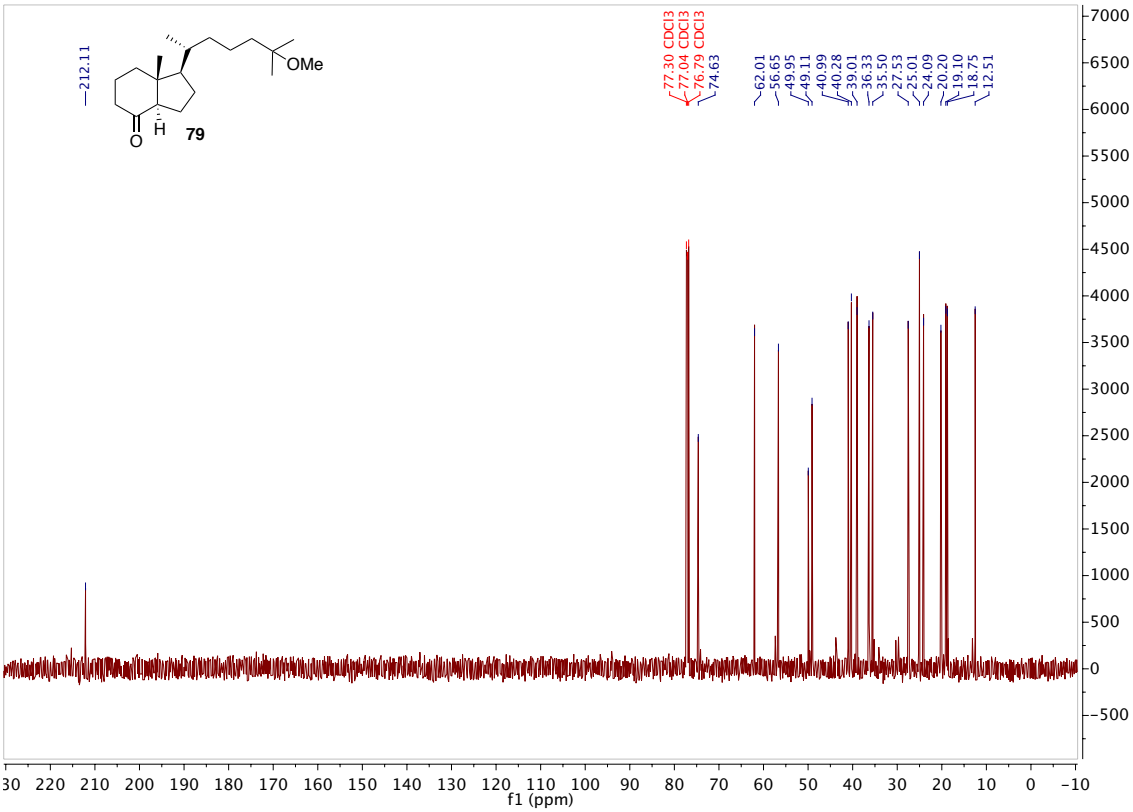
212.11
77.30 CDCl3
77.04 CDCl3
76.79 CDCl3
74.63
62.01
56.65
49.95
49.11
40.99
40.28
39.01
36.33
35.50
27.53
25.01
24.09
20.20
19.10
18.75
12.51
OMe
H
O
79
f1 (ppm)

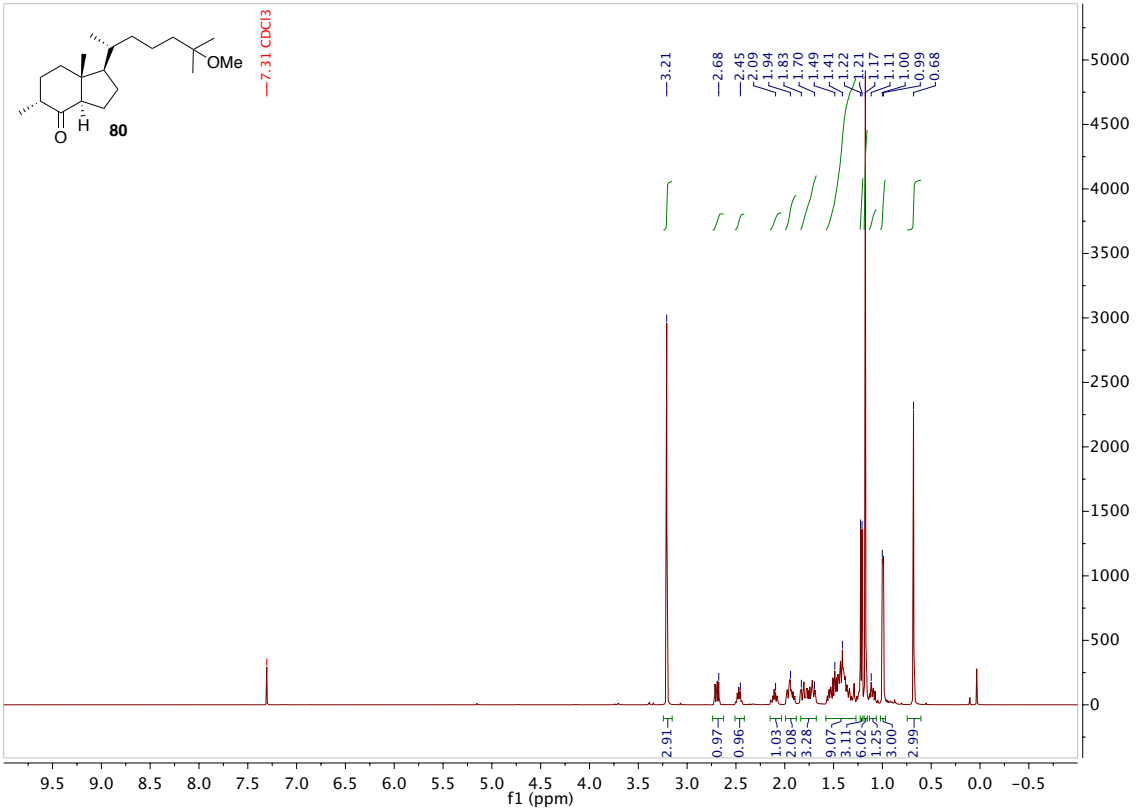
OMe
H
O
80
7.31 CDCl3
3.21
2.68
2.45
2.09
1.94
1.83
1.70
1.49
1.41
1.22
1.21
1.17
1.11
1.00
0.99
0.68
2.91
0.97
0.96
1.03
2.08
3.28
9.07
3.11
6.02
1.25
3.00
2.99
f1 (ppm)

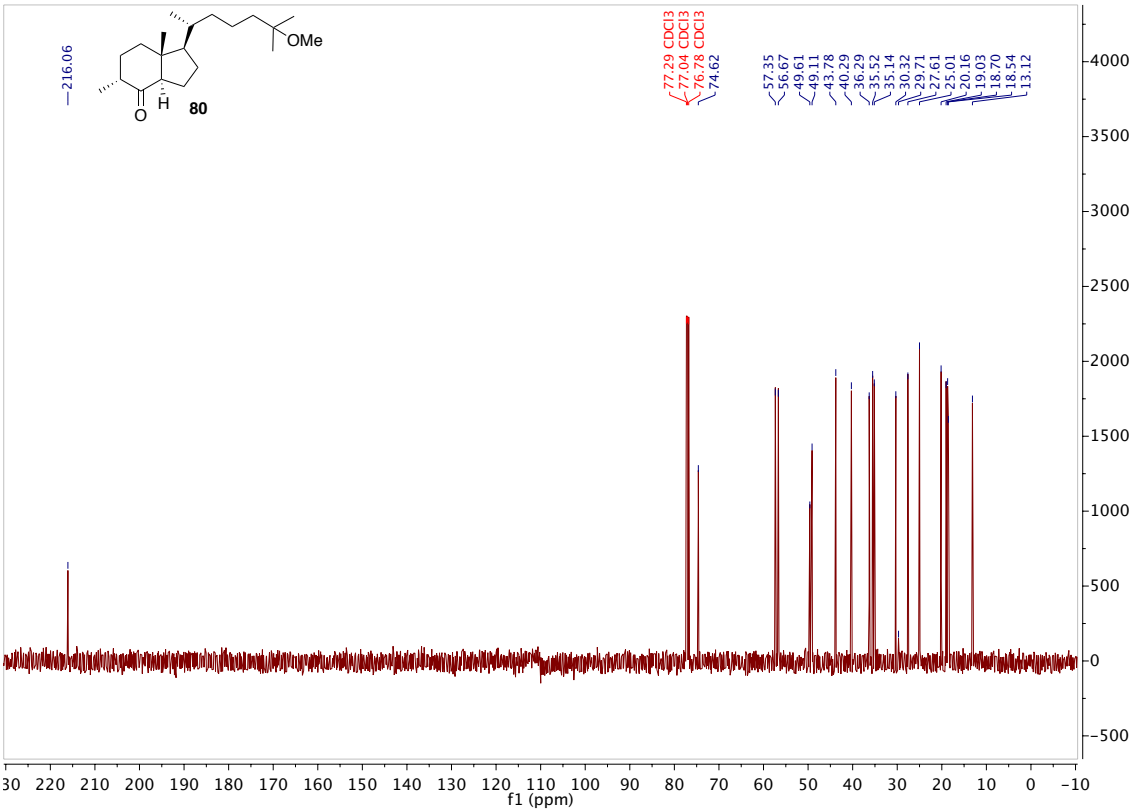
OMe
H
O
80
216.06
77.29 CDCl3
77.04 CDCl3
76.78 CDCl3
74.62
57.35
56.67
49.61
49.11
43.78
40.29
36.29
35.52
35.14
30.32
29.71
27.61
25.01
20.16
19.03
18.70
18.54
13.12
f1 (ppm)

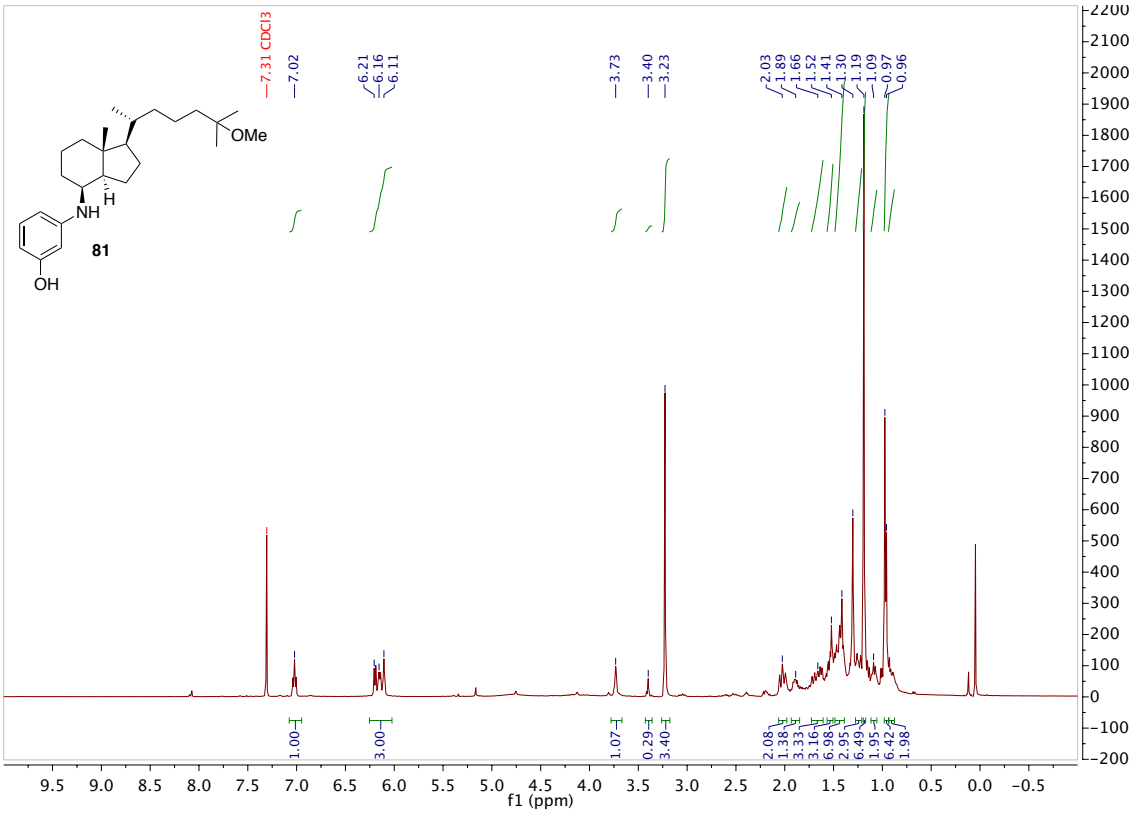
7.31 CDCl3
7.02
6.21
6.16
6.11
3.73
3.40
3.23
2.03
1.89
1.66
1.52
1.41
1.30
1.19
1.09
0.97
0.96
OMe
NH
H
OH
81
1.00
3.00
1.07
0.29
3.40
2.08
1.38
3.33
3.16
6.98
2.95
6.49
1.95
6.42
1.98
f1 (ppm)

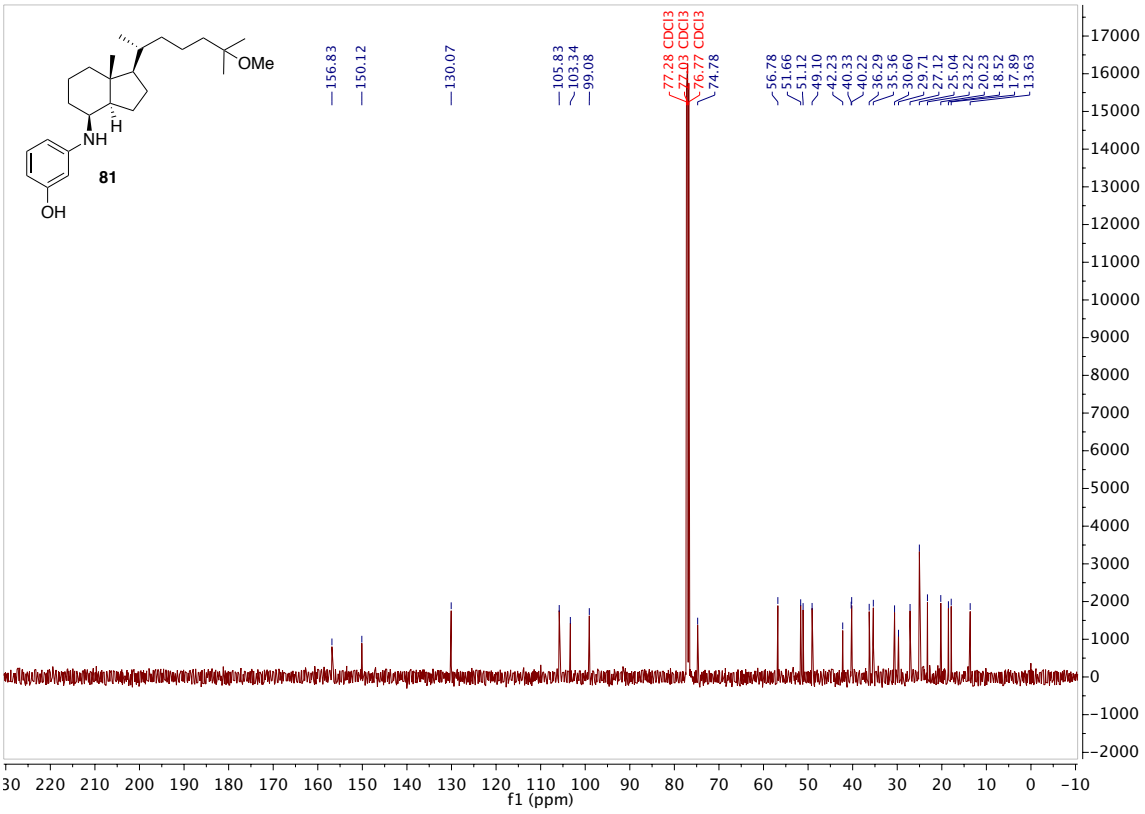
OMe
NH
H
OH
81
156.83
150.12
130.07
105.83
103.34
99.08
77.28 CDCl3
77.03 CDCl3
76.77 CDCl3
74.78
56.78
51.66
51.12
49.10
42.23
40.33
40.22
36.29
35.36
30.60
29.71
27.12
25.04
23.22
20.23
18.52
17.89
13.63
f1 (ppm)

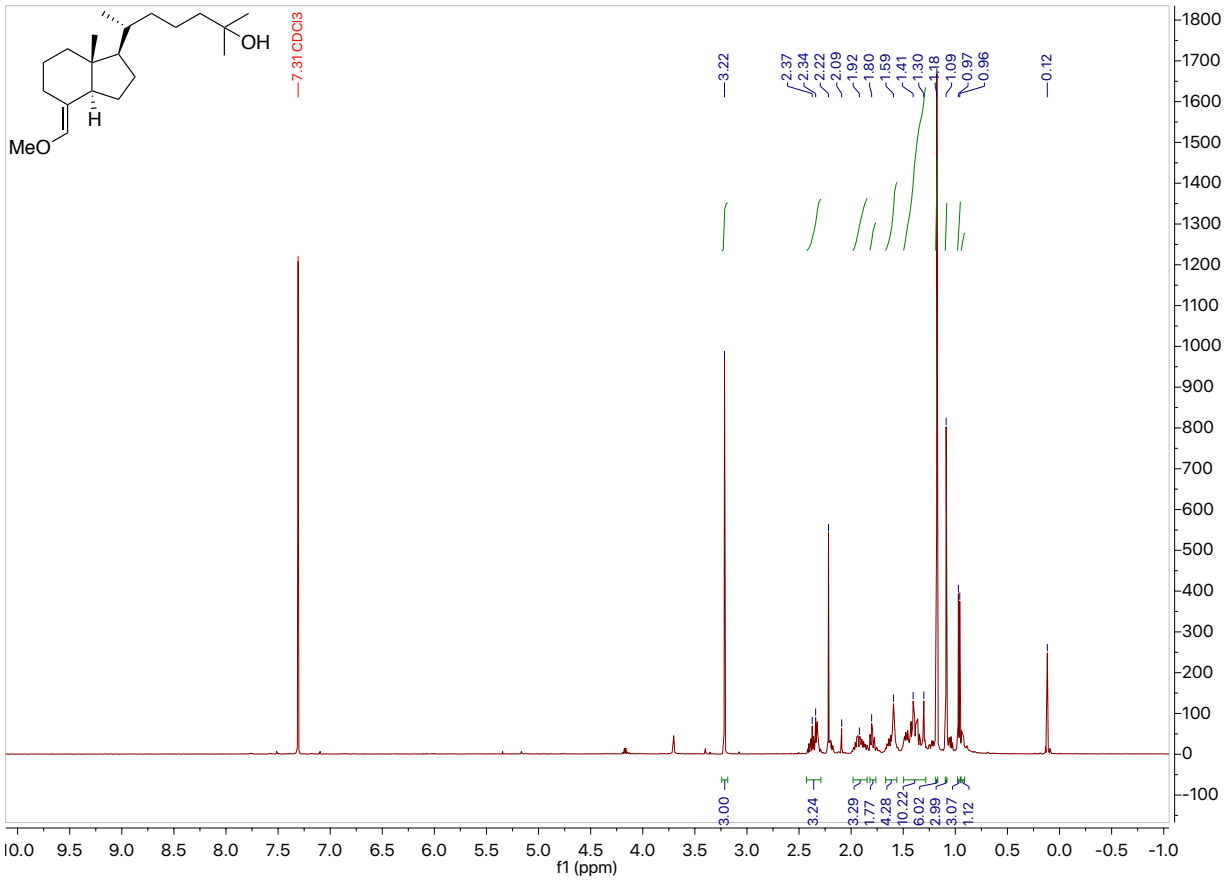
OH
H
MeO
7.31 CDCl3
3.22
2.37
2.34
2.22
2.09
1.92
1.80
1.59
1.41
1.30
1.18
1.09
0.97
0.96
0.12
3.00
3.24
3.29
1.77
4.28
10.22
6.02
2.99
3.07
1.12
f1 (ppm)

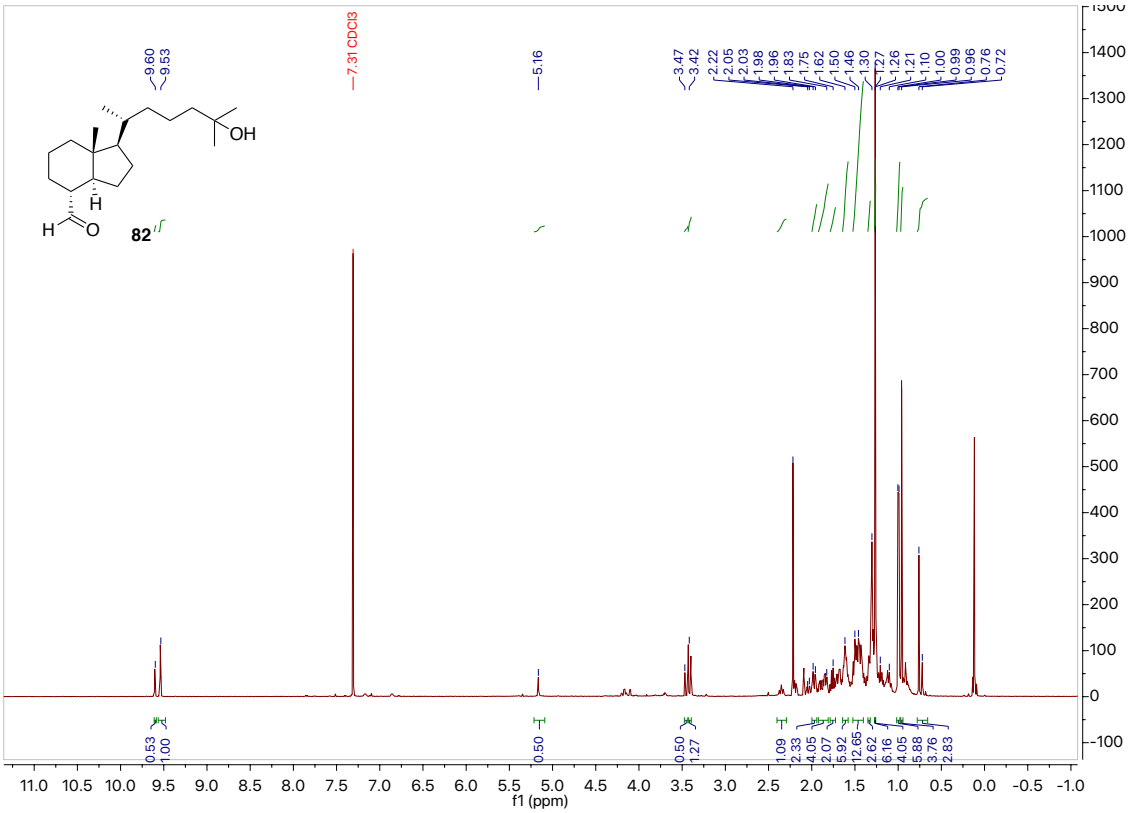
9.60
9.53
7.31 CDCl3
5.16
3.47
3.42
2.22
2.05
2.03
1.98
1.96
1.83
1.75
1.62
1.50
1.46
1.30
1.27
1.26
1.21
1.10
1.00
0.99
0.96
0.76
0.72
OH
H
H
O
82
0.53
1.00
0.50
0.50
1.27
1.09
2.33
4.05
2.07
5.92
12.65
2.62
6.16
4.05
5.88
3.76
2.83
f1 (ppm)

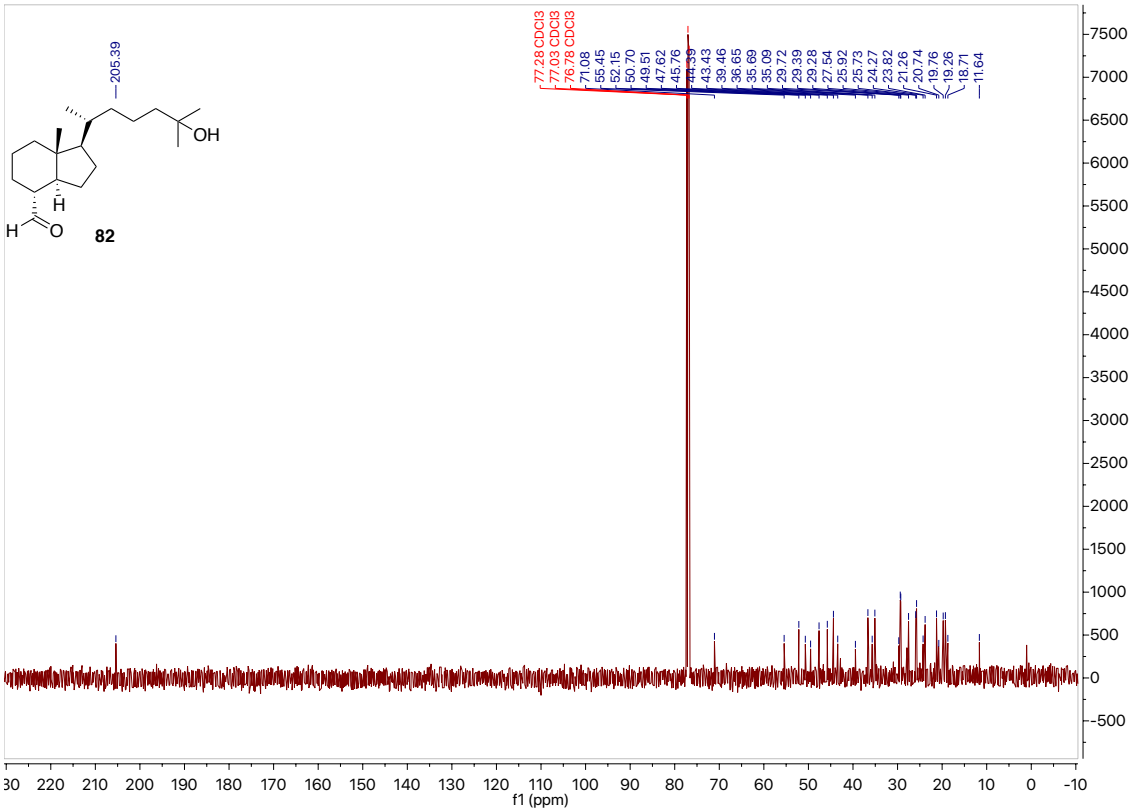
205.39
77.28 CDCl3
77.03 CDCl3
76.78 CDCl3
71.08
55.45
52.15
50.70
49.51
47.62
45.76
44.39
43.43
39.46
36.65
35.69
35.09
29.72
29.39
29.28
27.54
25.92
25.73
24.27
23.82
21.26
20.74
19.76
19.26
18.71
11.64
OH
H
H
O
82
f1 (ppm)

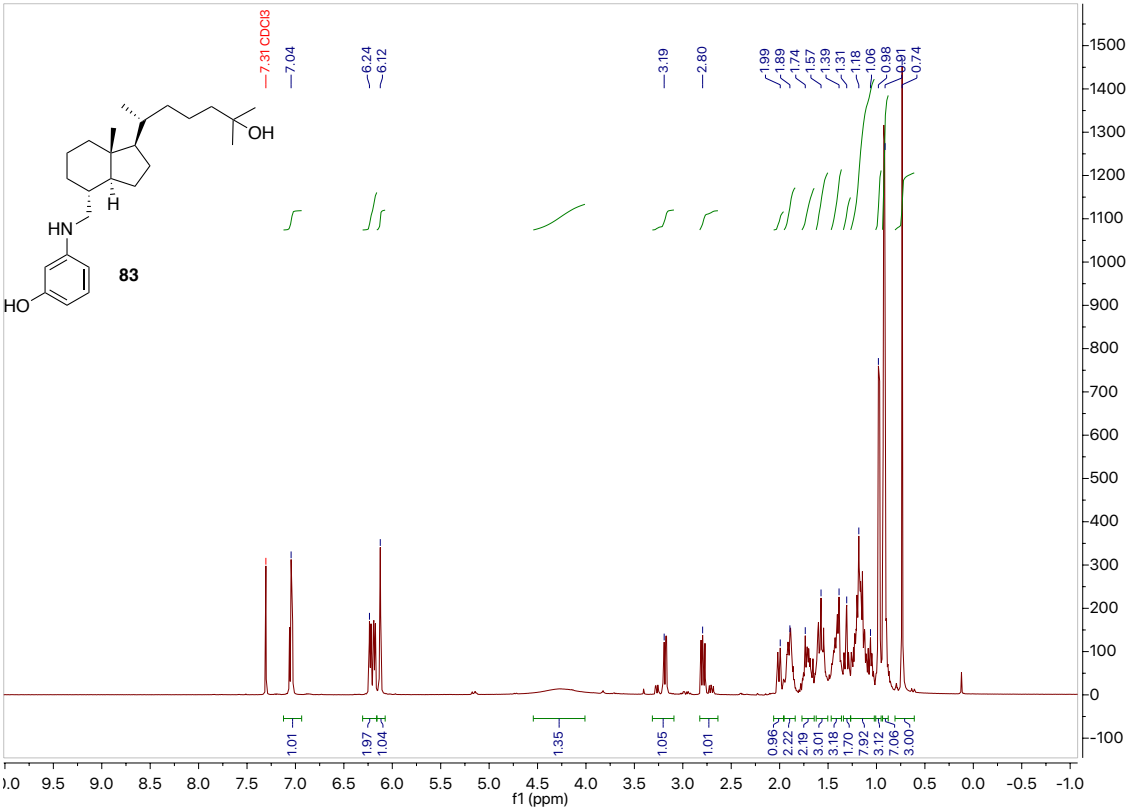
7.31 CDCl3
7.04
6.24
6.12
3.19
2.80
1.99
1.89
1.74
1.57
1.39
1.31
1.18
1.06
0.98
0.91
0.74
OH
H
HN
HO
83
1.01
1.97
1.04
1.35
1.05
1.01
0.96
2.22
2.19
3.01
3.18
1.70
7.92
3.12
7.06
3.00
f1 (ppm)

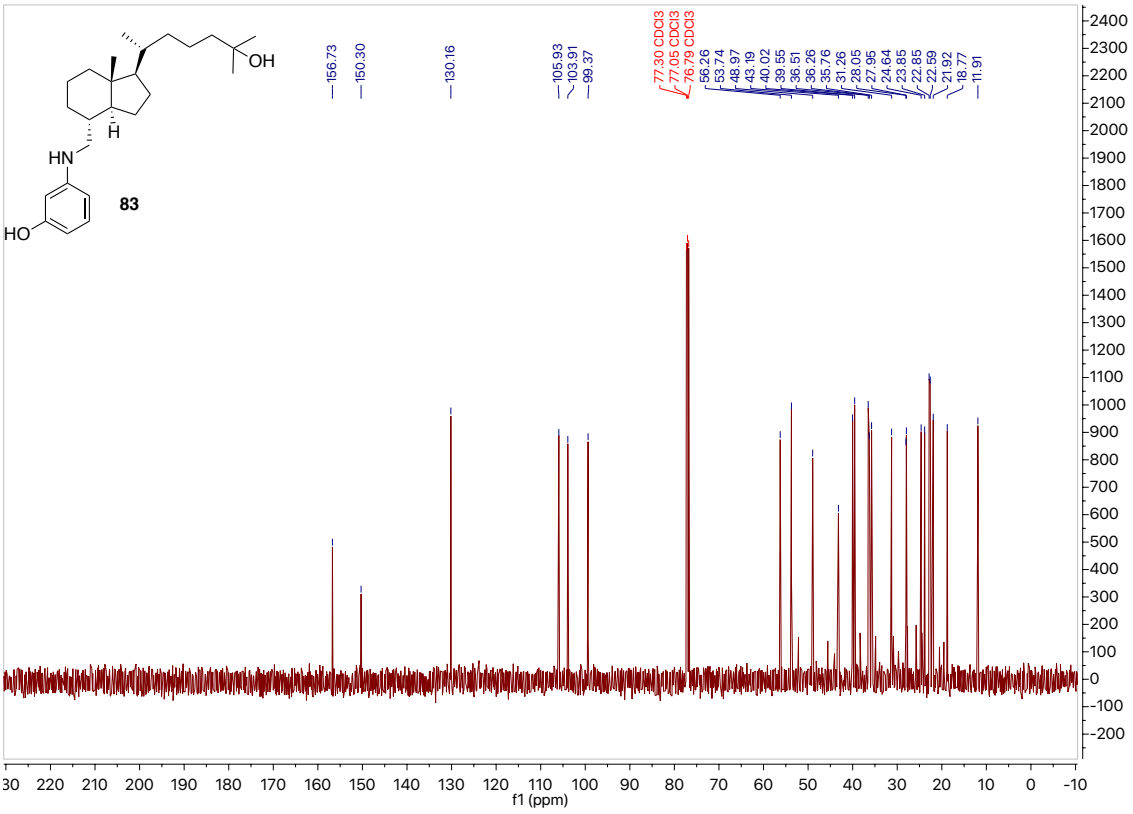
156.73
150.30
130.16
105.93
103.91
99.37
77.30 CDCl3
77.05 CDCl3
76.79 CDCl3
56.26
53.74
48.97
43.19
40.02
39.55
36.51
36.26
35.76
31.26
28.05
27.95
24.64
23.85
22.85
22.59
21.92
18.77
11.91
OH
H
HN
HO
83
f1 (ppm)

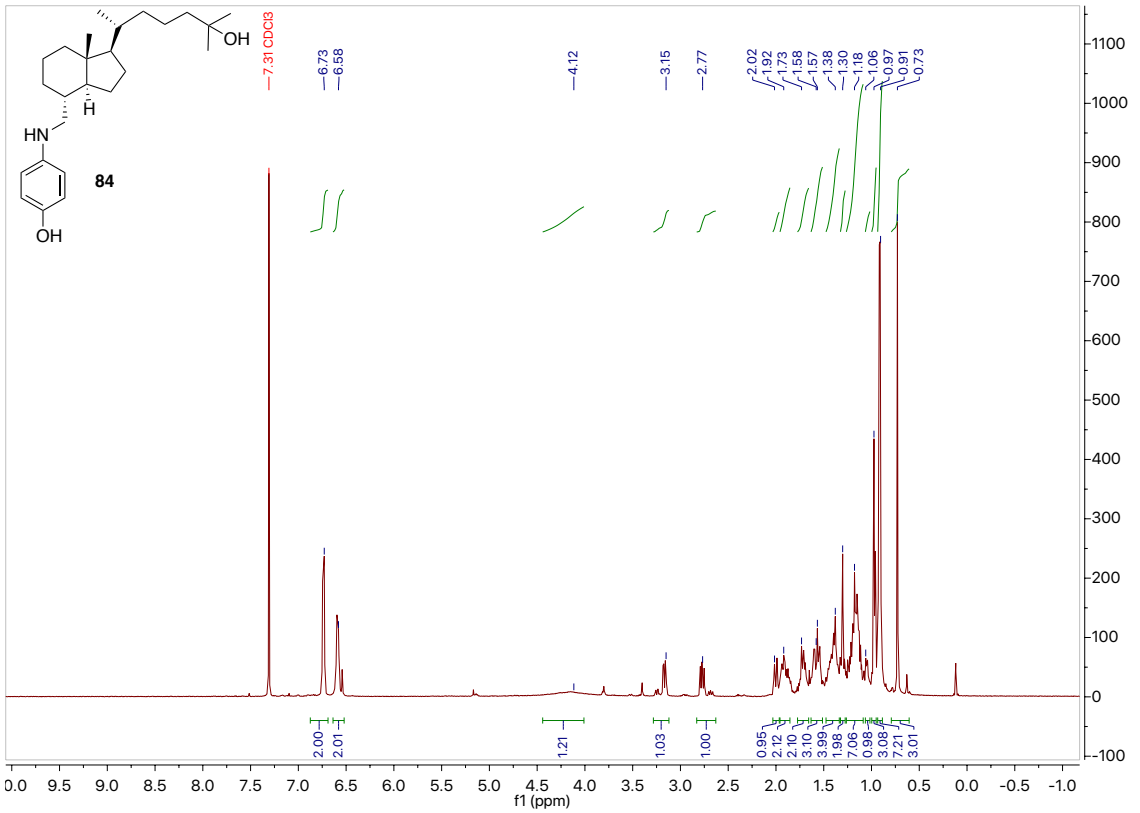
OH
H
HN
OH
84
7.31 CDCl3
6.73
6.58
4.12
3.15
2.77
2.02
1.92
1.73
1.58
1.57
1.38
1.30
1.18
1.06
0.97
0.91
0.73
2.00
2.01
1.21
1.03
1.00
0.95
2.12
2.10
3.10
3.99
1.98
7.06
0.98
3.08
7.21
3.01
f1 (ppm)

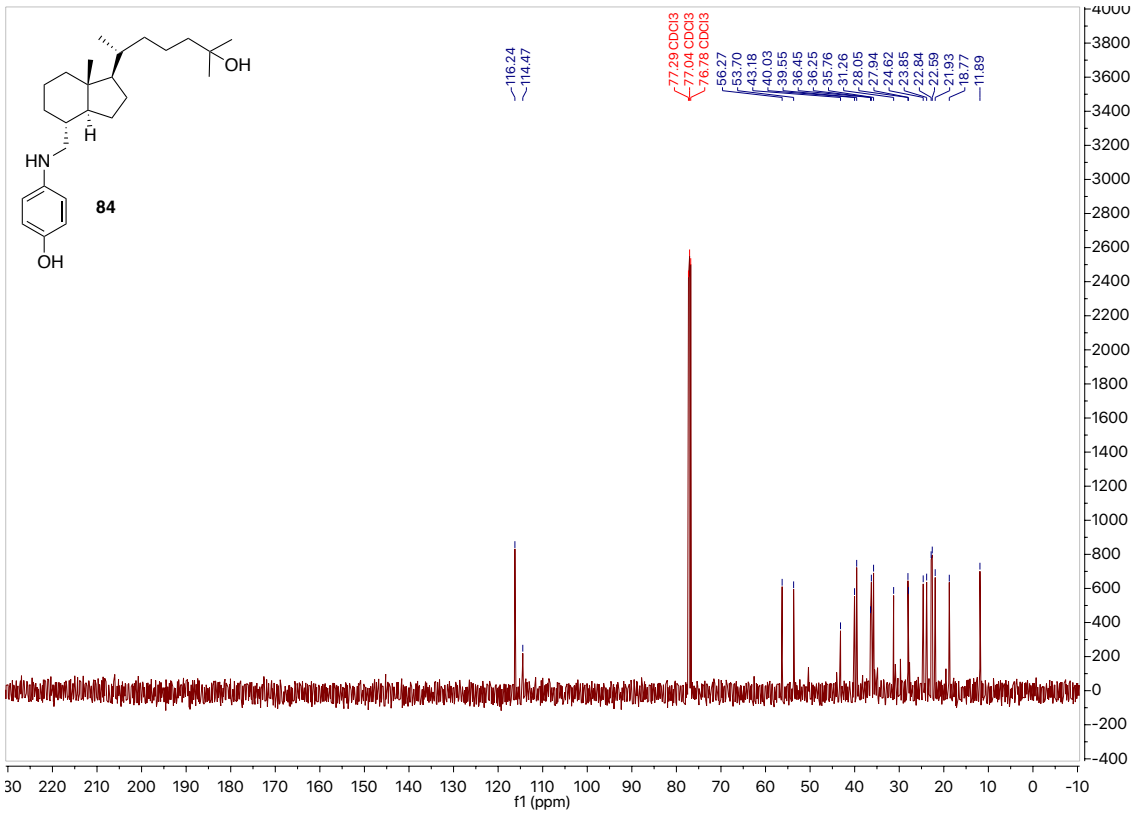
OH
H
HN
OH
84
116.24
114.47
77.29 CDCl3
77.04 CDCl3
76.78 CDCl3
56.27
53.70
43.18
40.03
39.55
36.45
36.25
35.76
31.26
28.05
27.94
24.62
23.85
22.84
22.59
21.93
18.77
11.89
f1 (ppm)

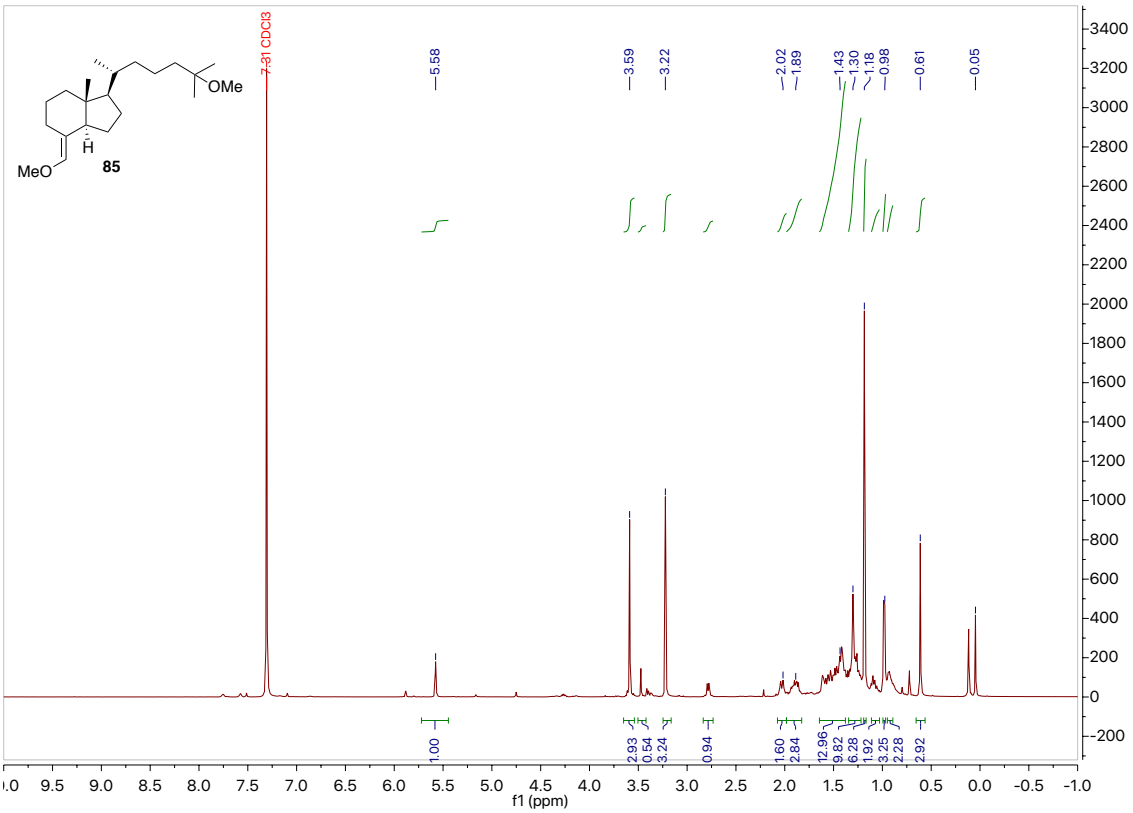
OMe
MeO
H
85
7.31 CDCl3
5.58
3.59
3.22
2.02
1.89
1.43
1.30
1.18
0.98
0.61
0.05
1.00
2.93
0.54
3.24
0.94
1.60
2.84
12.96
9.82
6.28
1.92
3.25
2.28
2.92
f1 (ppm)

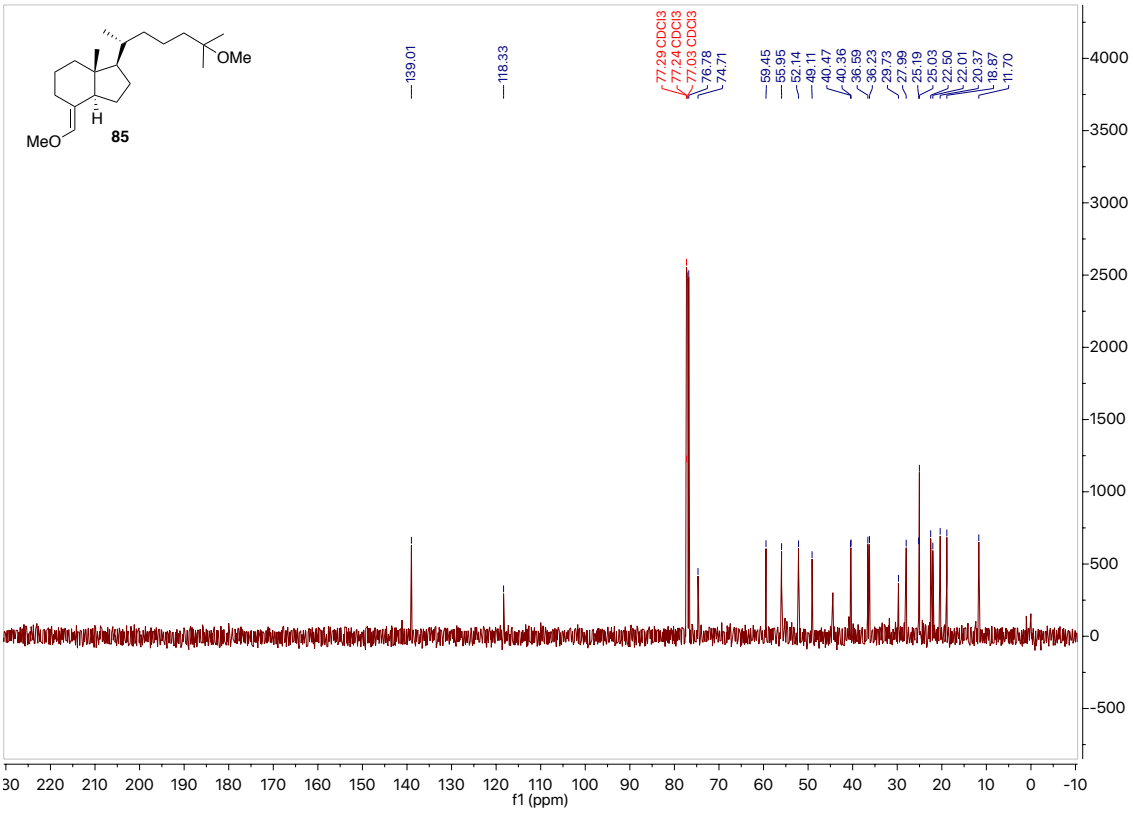
OMe
MeO
H
85
139.01
118.33
77.29 CDCl3
77.24 CDCl3
77.03 CDCl3
76.78
74.71
59.45
55.95
52.14
49.11
40.47
40.36
36.59
36.23
29.73
27.99
25.19
25.03
22.50
22.01
20.37
18.87
11.70
f1 (ppm)

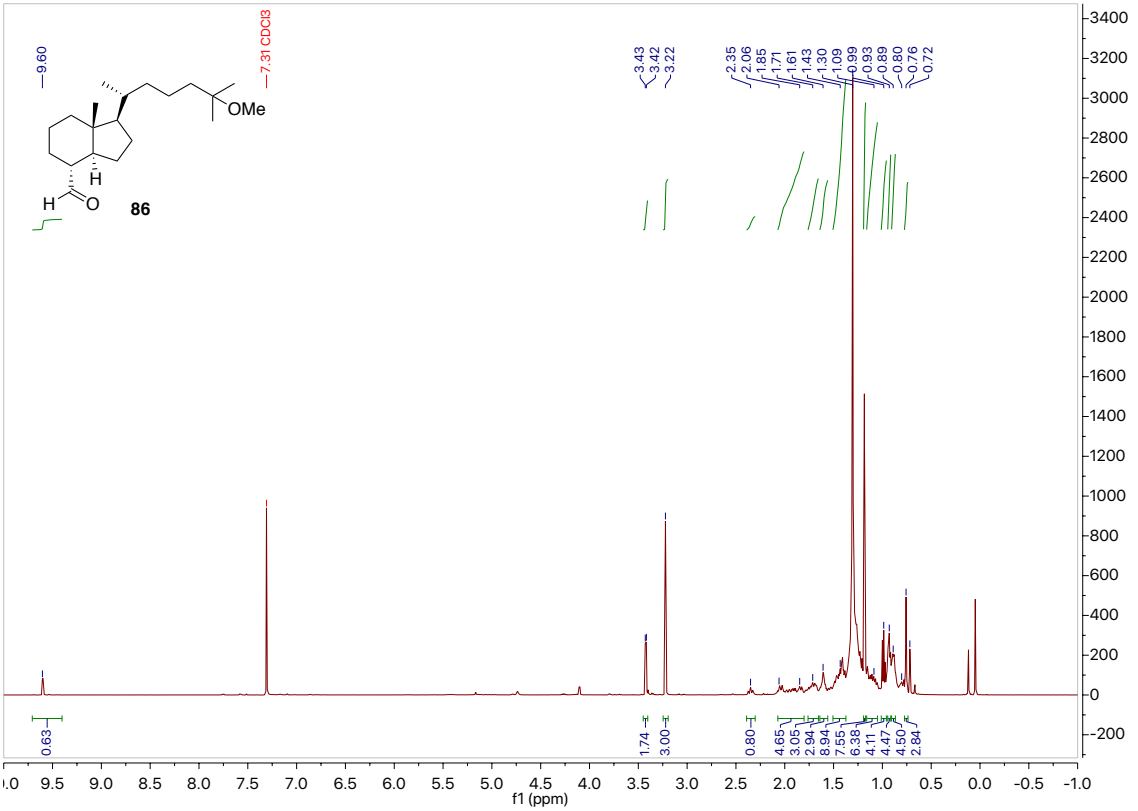
9.60
7.31 CDCl3
OMe
H
H
O
86
3.43
3.42
3.22
2.35
2.06
1.85
1.71
1.61
1.43
1.30
1.09
0.99
0.93
0.89
0.80
0.76
0.72
0.63
1.74
3.00
0.80
4.65
3.05
2.94
8.94
7.55
6.38
4.11
4.47
4.50
2.84
f1 (ppm)

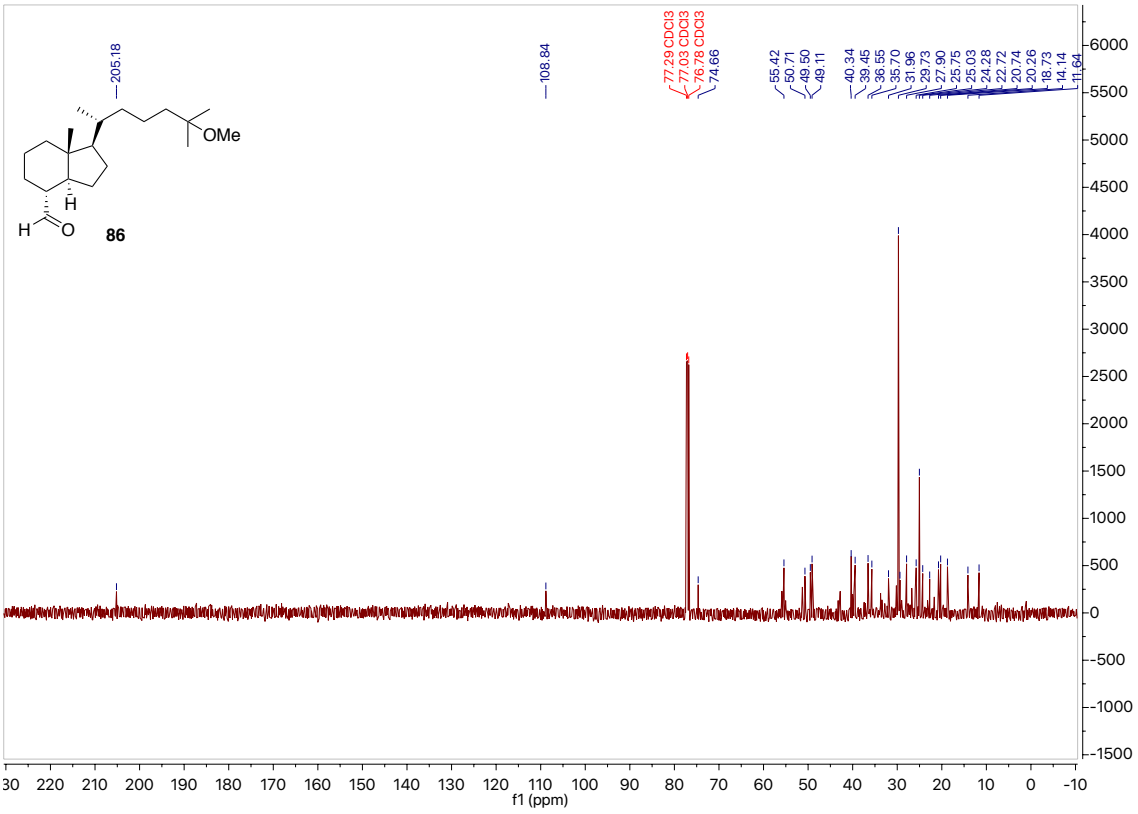
205.18
OMe
H
H
O
86
108.84
77.29 CDCl3
77.03 CDCl3
76.78 CDCl3
74.66
55.42
50.71
49.50
49.11
40.34
39.45
36.55
35.70
31.96
29.73
27.90
25.75
25.03
24.28
22.72
20.74
20.26
18.73
14.14
11.64
f1 (ppm)

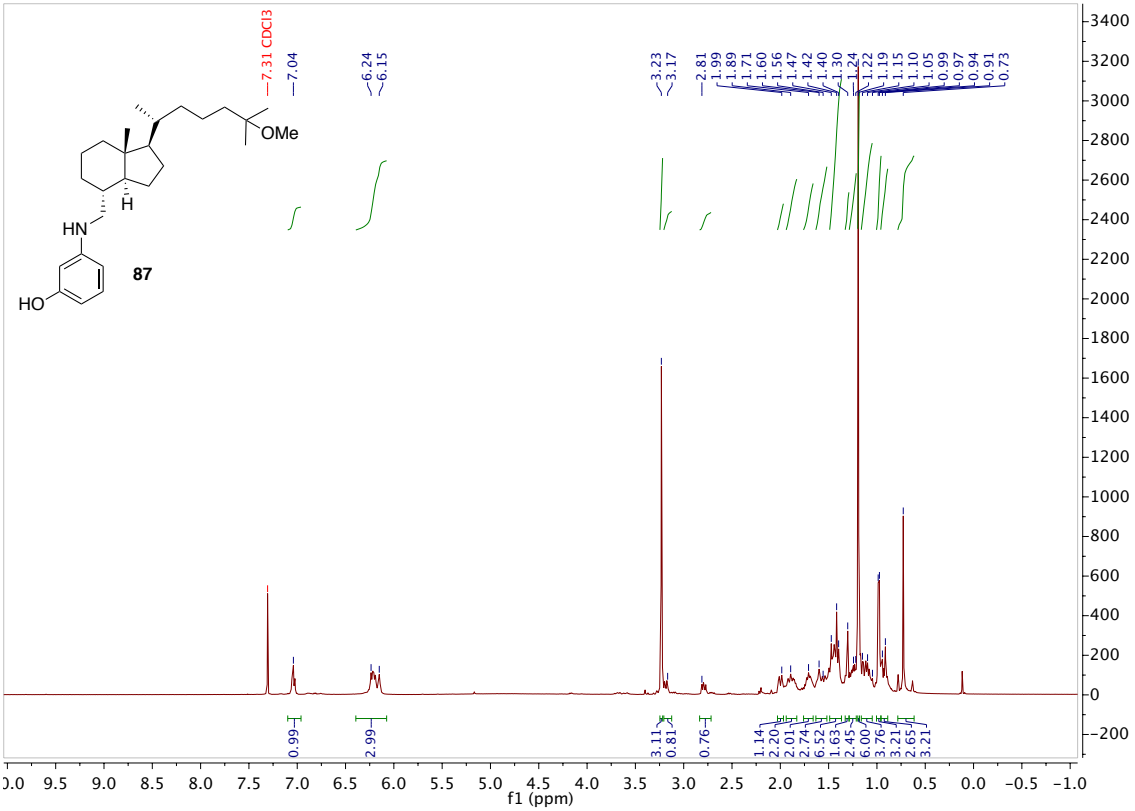
7.31 CDCl3
7.04
6.24
6.15
3.23
3.17
2.81
1.99
1.89
1.71
1.60
1.56
1.47
1.42
1.40
1.30
1.24
1.22
1.19
1.15
1.10
1.05
0.99
0.97
0.94
0.91
0.73
OMe
H
HN
HO
87
0.99
2.99
3.11
0.81
0.76
1.14
2.20
2.01
2.74
6.52
1.63
2.45
6.00
3.76
3.21
2.65
3.21
f1 (ppm)

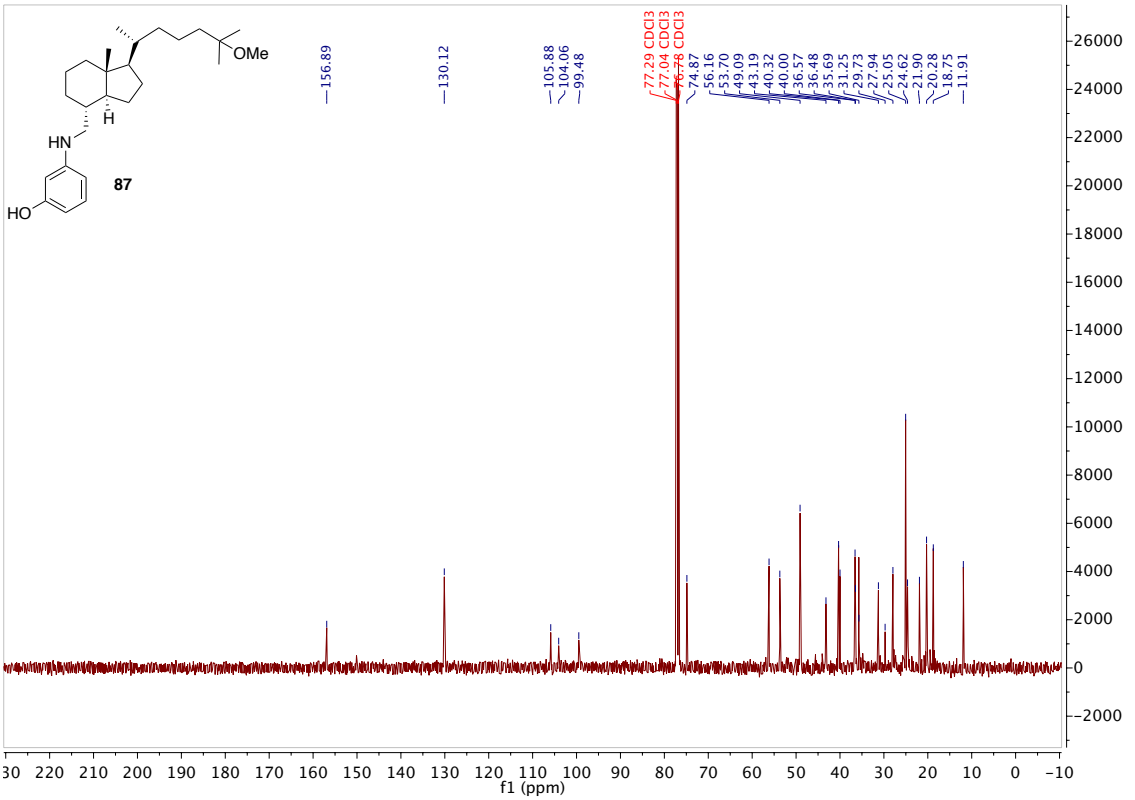
OMe
H
HN
HO
87
156.89
130.12
105.88
104.06
99.48
77.29 CDCl3
77.04 CDCl3
76.78 CDCl3
74.87
56.16
53.70
49.09
43.19
40.32
40.00
36.57
36.48
35.69
31.25
29.73
27.94
25.05
24.62
21.90
20.28
18.75
11.91
f1 (ppm)

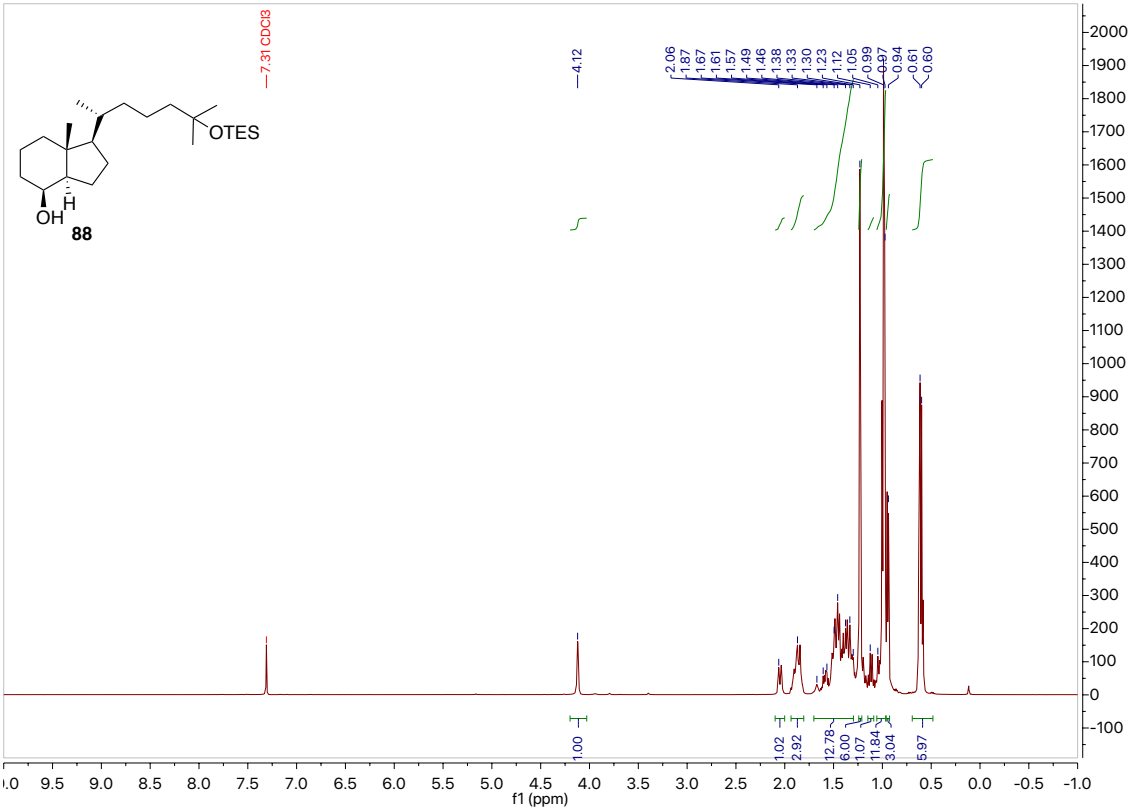
OTES
OH
H
88
7.31 CDCl3
4.12
2.06
1.87
1.67
1.61
1.57
1.49
1.46
1.38
1.33
1.30
1.23
1.12
1.05
0.99
0.97
0.94
0.61
0.60
1.00
1.02
2.92
12.78
6.00
1.07
11.84
3.04
5.97
f1 (ppm)

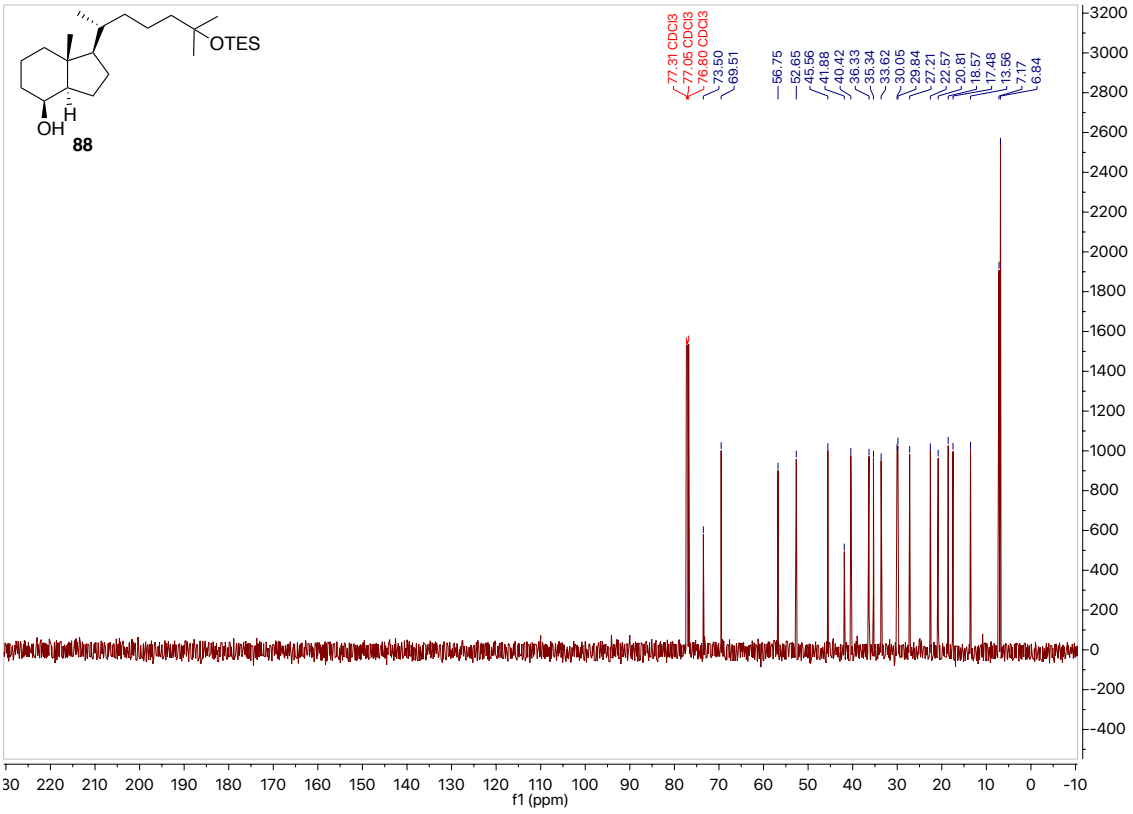
OTES
OH
H
88
77.31 CDCl3
77.05 CDCl3
76.80 CDCl3
73.50
69.51
56.75
52.65
45.56
41.88
40.42
36.33
35.34
33.62
30.05
29.84
27.21
22.57
20.81
18.57
17.48
13.56
7.17
6.84
f1 (ppm)

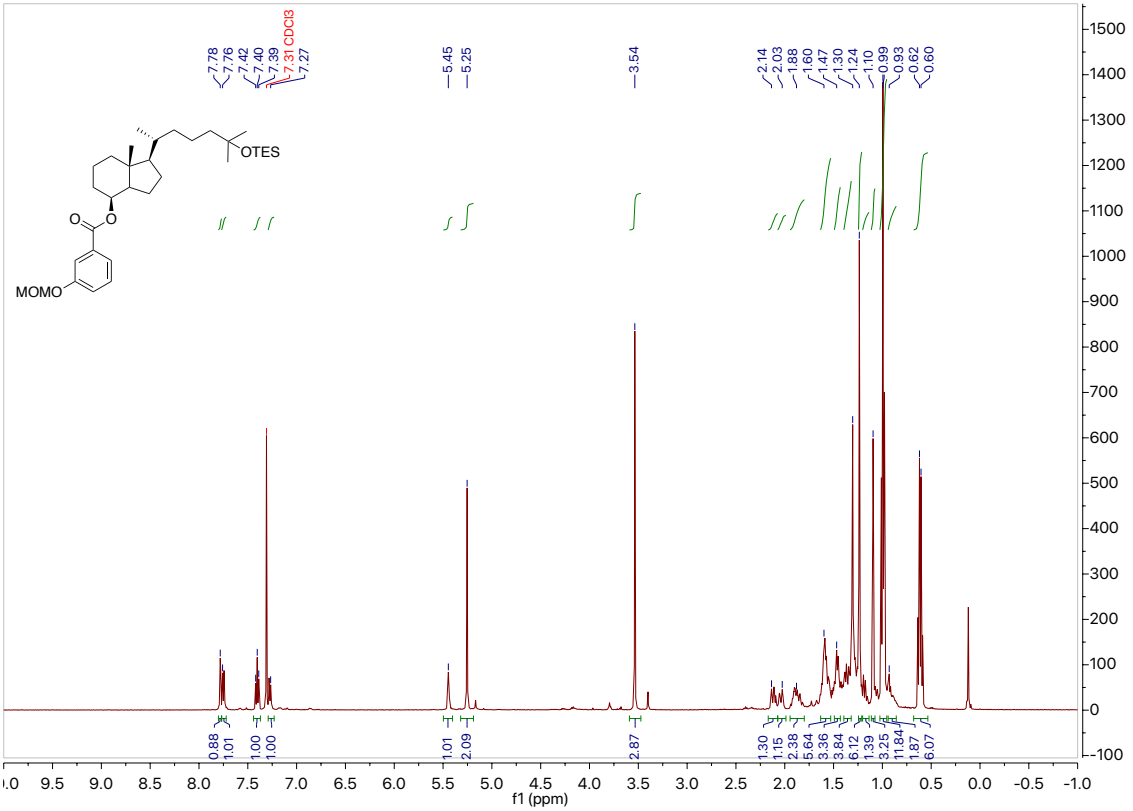
7.78
7.76
7.42
7.40
7.39
7.31 CDCl3
7.27
5.45
5.25
3.54
2.14
2.03
1.88
1.60
1.47
1.30
1.24
1.10
0.99
0.93
0.62
0.60
OTES
O
O
MOMO
0.88
1.01
1.00
1.00
1.01
2.09
2.87
1.30
1.15
2.38
5.64
3.36
3.84
6.12
1.39
3.25
11.84
1.87
6.07
f1 (ppm)

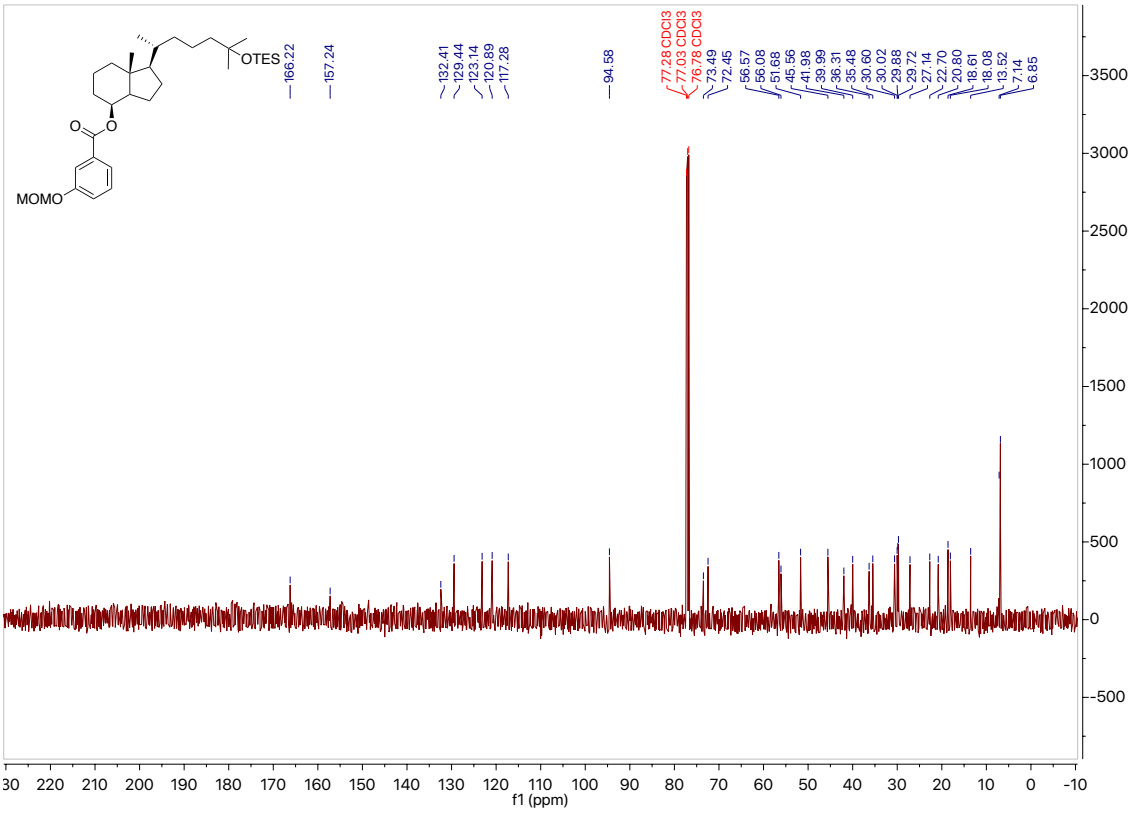
OTES
O
O
MOMO
166.22
157.24
132.41
129.44
123.14
120.89
117.28
94.58
77.28 CDCl3
77.03 CDCl3
76.78 CDCl3
73.49
72.45
56.57
56.08
51.68
45.56
41.98
39.99
36.31
35.48
30.60
30.02
29.88
29.72
27.14
22.70
20.80
18.61
18.08
13.52
7.14
6.85
f1 (ppm)

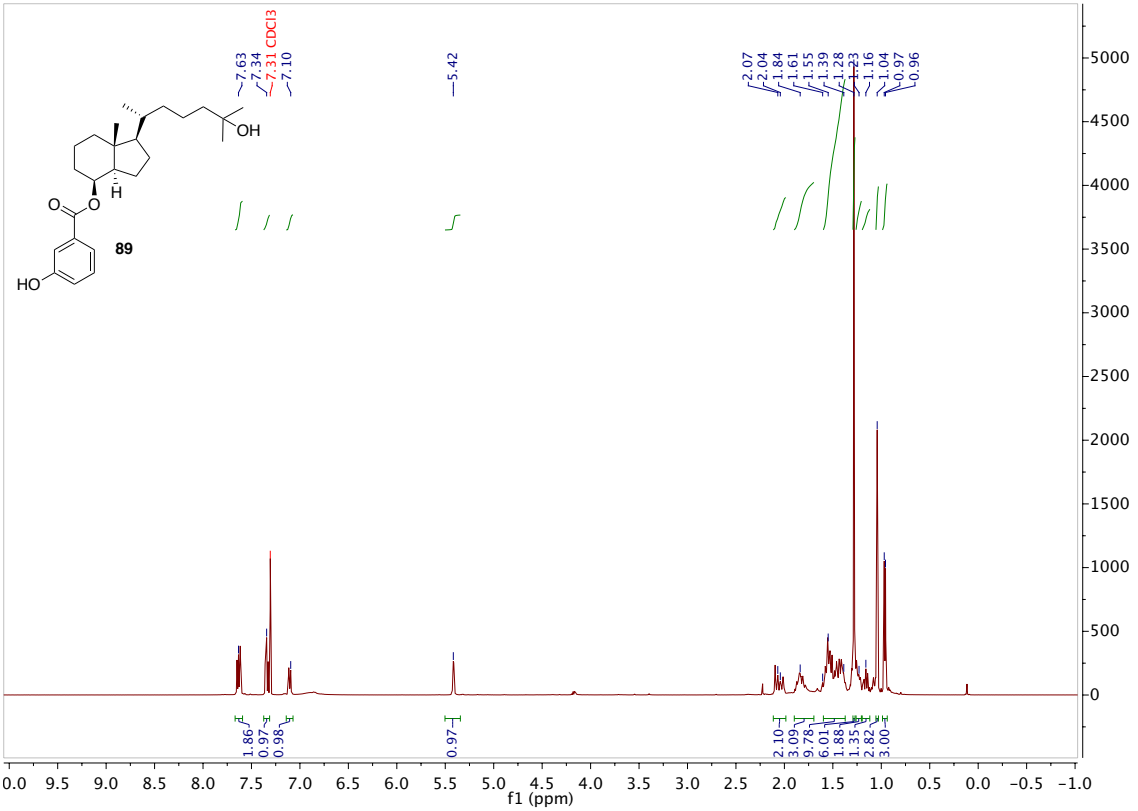
7.63
7.34
7.31 CDCl3
7.10
5.42
2.07
2.04
1.84
1.61
1.55
1.39
1.28
1.23
1.16
1.04
0.97
0.96
OH
O
O
H
HO
89
1.86
0.97
0.98
0.97
2.10
3.09
9.78
6.01
1.88
1.35
2.82
3.00
f1 (ppm)

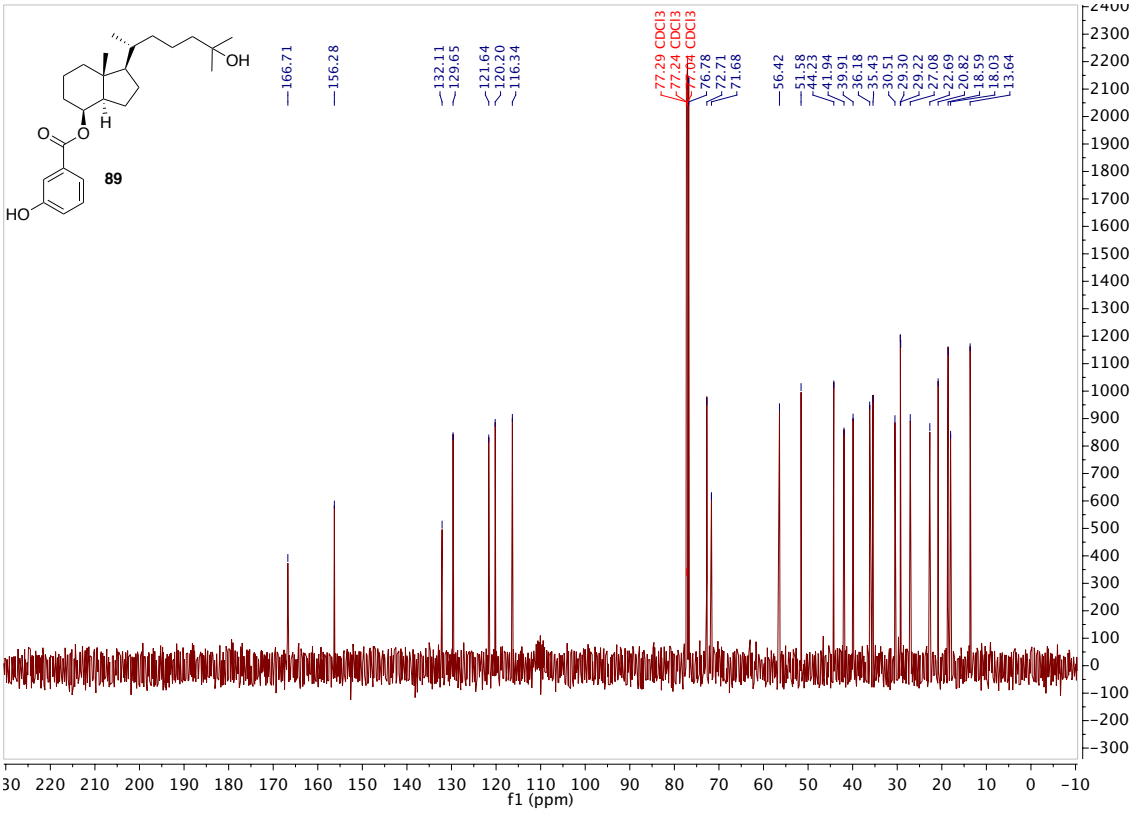
166.71
156.28
132.11
129.65
121.64
120.20
116.34
77.29 CDCl3
77.24 CDCl3
77.04 CDCl3
76.78
72.71
71.68
56.42
51.58
44.23
41.94
39.91
36.18
35.43
30.51
29.30
29.22
27.08
22.69
20.82
18.59
18.03
13.64
OH
O
O
H
HO
89
f1 (ppm)

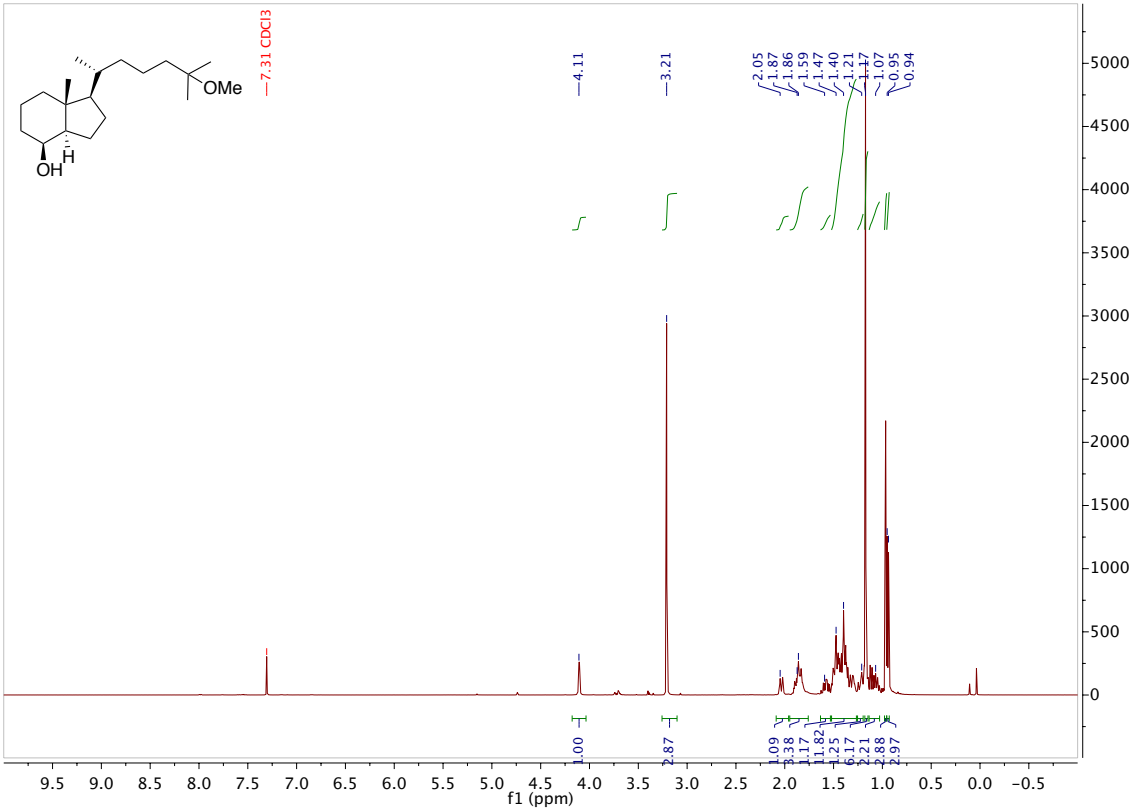
OMe
OH
H
7.31 CDCl3
4.11
3.21
2.05
1.87
1.86
1.59
1.47
1.40
1.21
1.17
1.07
0.95
0.94
1.00
2.87
1.09
3.38
1.17
11.82
1.25
6.17
2.21
2.88
2.97
f1 (ppm)

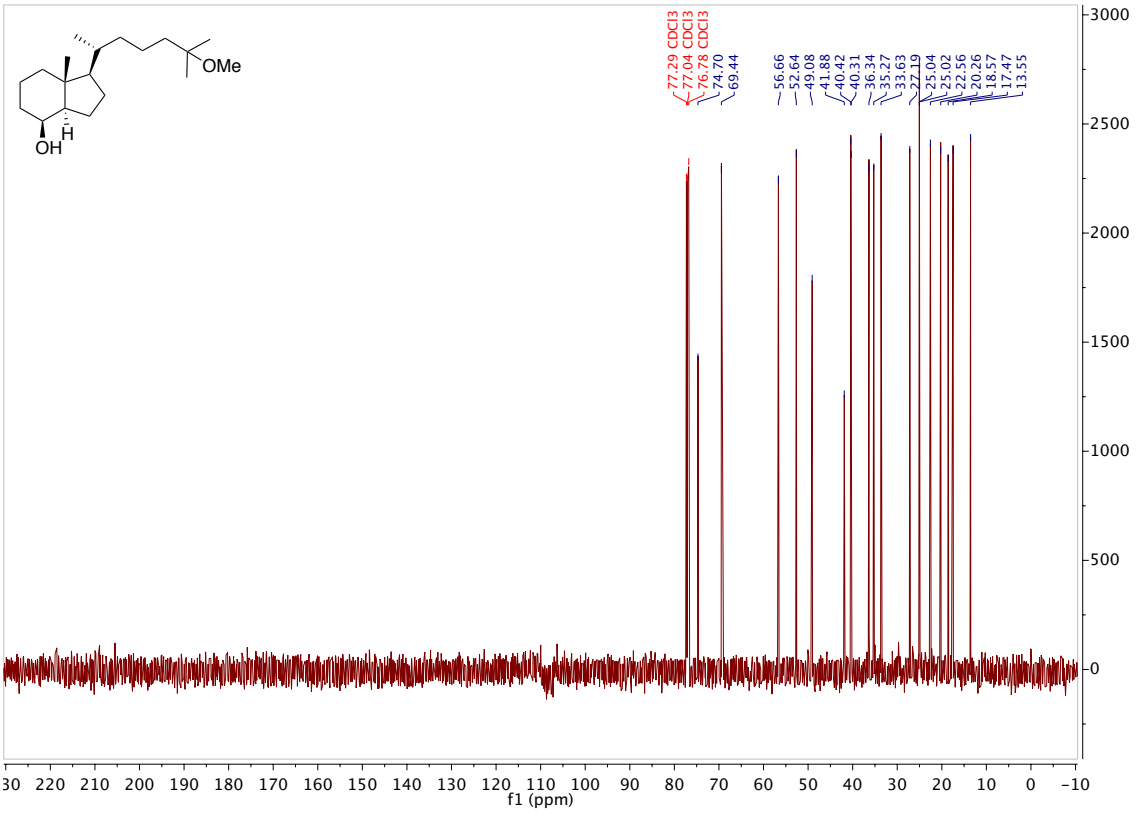
OMe
OH
H
77.29 CDCl3
77.04 CDCl3
76.78 CDCl3
74.70
69.44
56.66
52.64
49.08
41.88
40.42
40.31
36.34
35.27
33.63
22.19
25.04
25.02
22.56
20.26
18.57
17.47
13.55
f1 (ppm)

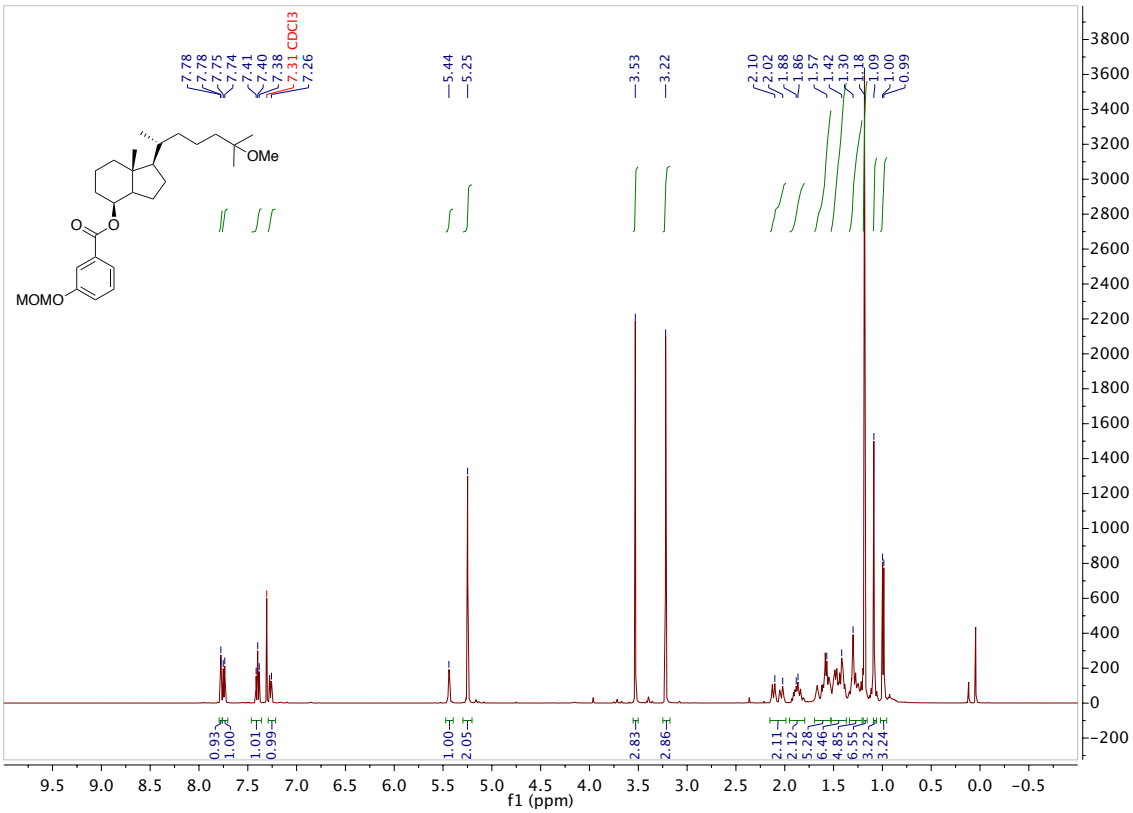
7.78
7.78
7.75
7.74
7.41
7.40
7.38
7.31 CDCl3
7.26
5.44
5.25
3.53
3.22
2.10
2.02
1.88
1.86
1.57
1.42
1.30
1.18
1.09
1.00
0.99
OMe
O
O
MOMO
0.93
1.00
1.01
0.99
1.00
2.05
2.83
2.86
2.11
2.12
5.28
6.46
4.85
6.55
3.22
3.24
f1 (ppm)

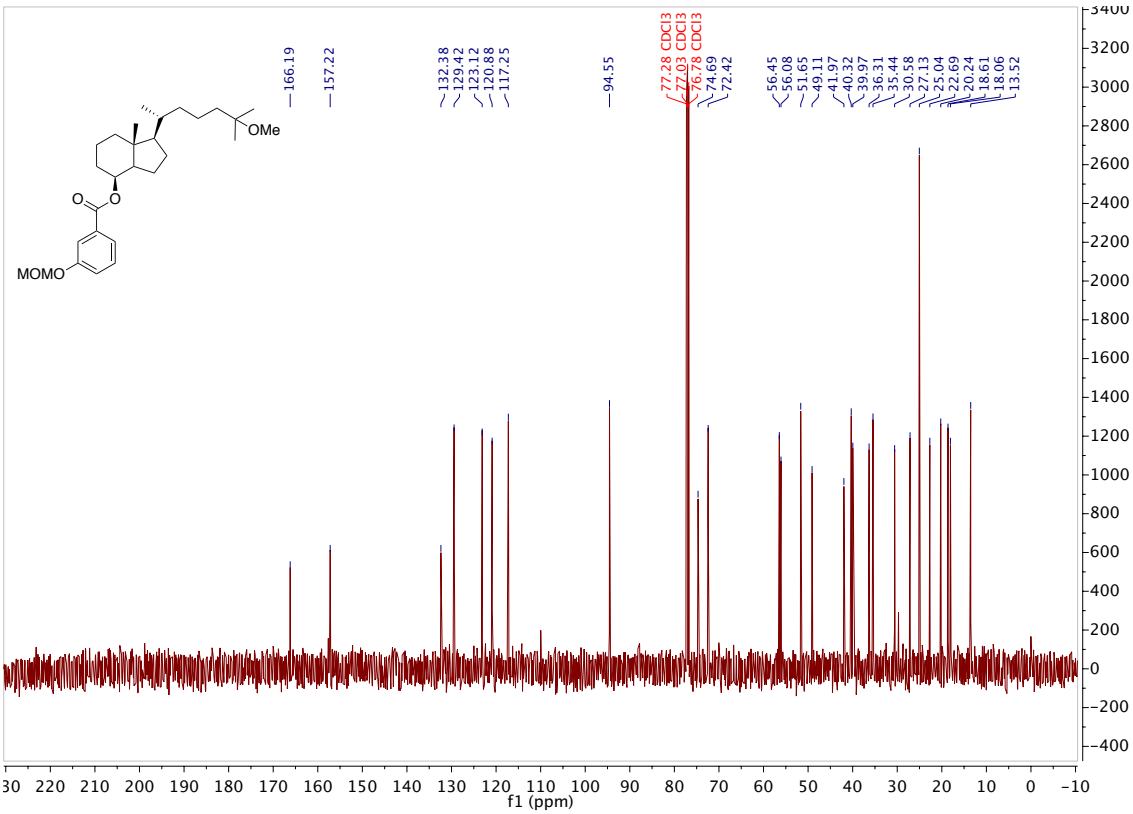
166.19
157.22
132.38
129.42
123.12
120.88
117.25
94.55
77.28 CDCl3
77.03 CDCl3
76.78 CDCl3
74.69
72.42
56.45
56.08
51.65
49.11
41.97
40.32
39.97
36.31
35.44
30.58
27.13
25.04
22.69
20.24
18.61
18.06
13.52
OMe
O
O
MOMO
f1 (ppm)

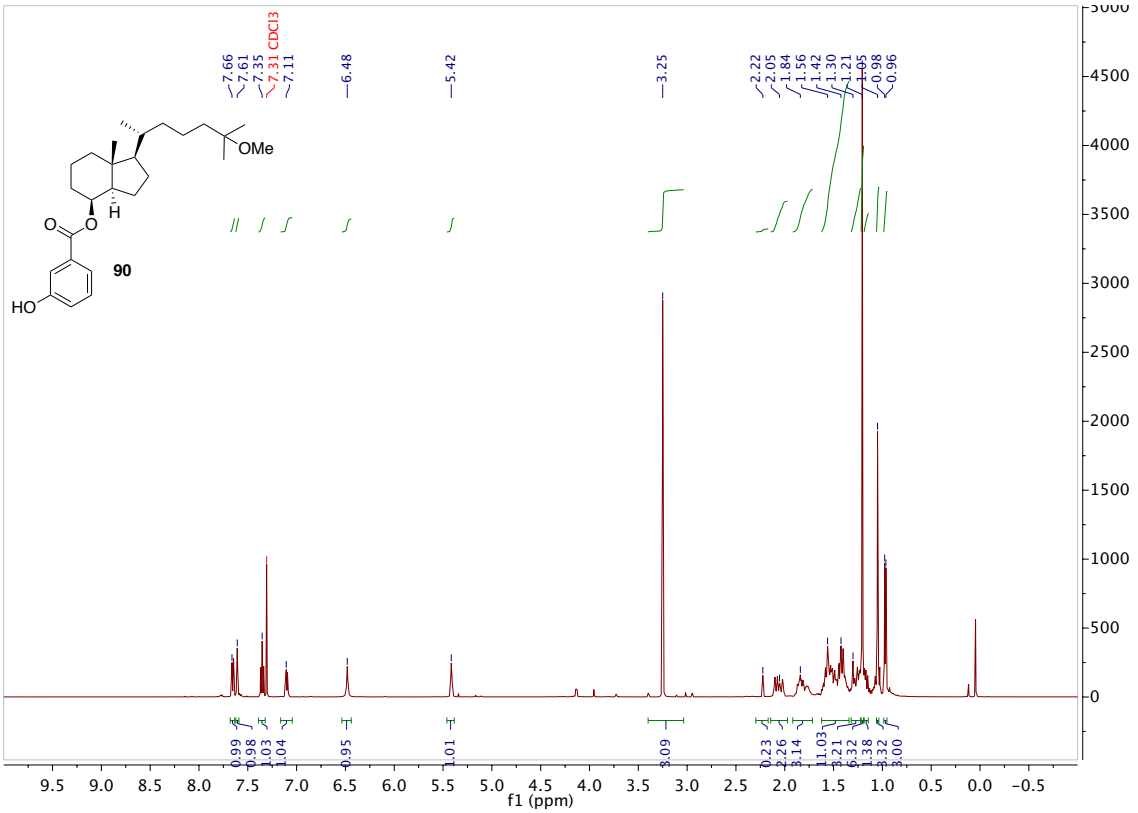
7.66
7.61
7.35
7.31 CDCl3
7.11
6.48
5.42
3.25
2.22
2.05
1.84
1.56
1.42
1.30
1.21
1.05
0.98
0.96
OMe
H
O
O
90
HO
0.99
0.98
1.03
1.04
0.95
1.01
3.09
0.23
2.26
3.14
11.03
3.21
6.32
1.38
3.32
3.00
f1 (ppm)

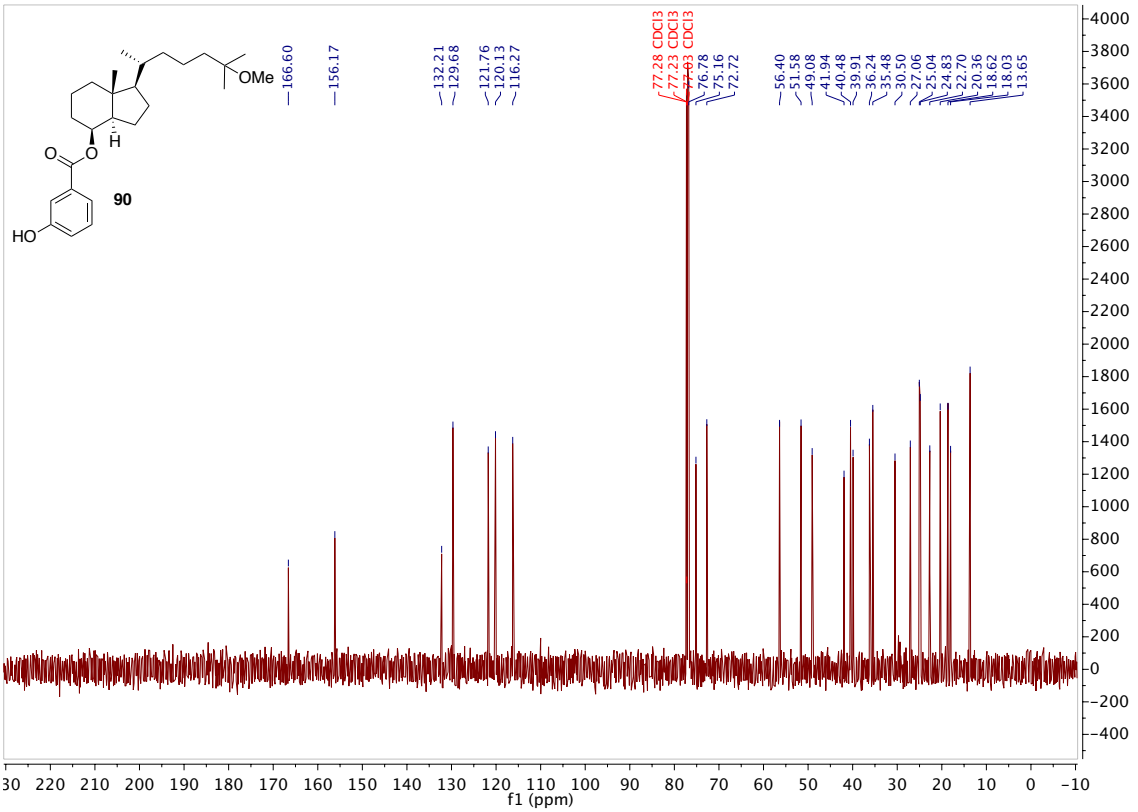
166.60
156.17
132.21
129.68
121.76
120.13
116.27
77.28 CDCl3
77.23 CDCl3
77.03 CDCl3
76.78
75.16
72.72
56.40
51.58
49.08
41.94
40.48
39.91
36.24
35.48
30.50
27.06
25.04
24.83
22.70
20.36
18.62
18.03
13.65
OMe
H
O
O
90
HO
f1 (ppm)